Development of Improved MPPT Methodologies for Grid Integration of Wind-PV Hybrid Distributed Generation System

Thesis submitted by
Boni Satya Varun Sai

DOCTOR OF PHILOSOPHY (Engineering)

Department of Electrical Engineering
Faculty Council of Engineering & Technology
Jadavpur University
Kolkata, India
2023

Development of Improved MPPT Methodologies for Grid Integration of Wind-PV Hybrid Distributed Generation System

By
Boni Satya Varun Sai

A thesis submitted for fulfillment of the requirement for the degree of Doctor of Philosophy (Engineering) in the Faculty of Engineering &Technology, Jadavpur University

Under the Supervision of
Dr. Debashis Chatterjee,
Professor, EE Dept., Jadavpur University

Department of Electrical Engineering
Faculty Council of Engineering & Technology
Jadavpur University
Kolkata, India
2023

Jadavpur University
Kolkata-70003, India

INDEX NO. 83/19/E

1. **Title of the thesis** — **Development of improved MPPT methodologies for Grid integration of Wind-PV hybrid distributed generation system**

2. **Name, Designation & Institution of Supervisor/s** — **Dr. Debashis Chatterjee**
   Professor
   Department of Electrical Engineering Jadavpur University, Kolkata, India

3. **List of Publications**

I. journal publications:

[J1]. **BSV Sai**, D. Chatterjee et al., "A dummy peak elimination based MPPT technique for PV generation under partial shading condition," **IET Renew. Power Gener.**, 2021, 15:2438–2451.

[J2]. **BSV Sai**, D. Chatterjee et al., "Inter-harmonics mitigation for PV based Converters Using INHARE MPPT Algorithm," **IETE Journal of research**, **Taylor & Francis**, 2022.

[J3]. **BSV Sai**, D. Chatterjee et al., "An SSM-PSO Based MPPT Scheme for Wind driven DFIG system," **IEEE Access**, 2022.

[J4]. **BSV Sai**, D. Chatterjee et al., "An Improved Weather Adaptable P&O MPPT Technique Under Varying Irradiation Condition," **ISA Transactions**, **Elsevier**, 2023.

[J5]. **BSV Sai**, D. Chatterjee, "An Accurate MPPT Technique under Partial Shading Conditions Using PV Panel Operating Characteristics," **IEEE**, 2023. (Submitted to journal)

[J6]. **BSV Sai**, D. Chatterjee, "A Fast-Global Peak Estimation Technique for Photovoltaic System Under Partial Shading Situation," **IEEE**, 2023. (Submitted to journal)

[J7]. **BSV Sai**, D. Chatterjee, "An Improved MPPT Technique for Grid Integration of Hybrid Photovoltaic-Battery- DFIG based WECS," **Elsevier**, 2023. (Submitted to journal)

II. Book Chapter publications:

[B1]. **BSV Sai**, D. Chatterjee et al., "A Sensor-Based Improved MPPT Technique Under Partial Shading Condition," **Advances in Thermofluids and Renewable Energy Select Proceedings of TFRE 2020**, NIT Arunachal Pradesh, India, 2020.

III. Conference publications:

[C1]. **BSV Sai**, D. Chatterjee et al., "An Improved Maximum Power Point Tracking Scheme Without Memory Unit," **2020 IEEE International Conference on Renewable Energy Integration into Smart Grids: A Multidisciplinary Approach to Technology Modelling and Simulation (ICREISG)**, Odisha, India, 2020.

[C2]. **BSV Sai**, D. Chatterjee et al., "An Improved MPPT Technique Under Partial Shading Condition Using Simple P&O Algorithm," **2020 IEEE International Conference on Computational Intelligence for Smart Power System and Sustainable Energy (CISPSSE)**, Odisha, 2020.

Faculty of Engineering & Technology
Jadavpur University

Statement of Originality

I **Boni Satya Varun Sai** registered on **27. 05. 2019** do hereby declare that this thesis entitled "**Development of improved MPPT methodologies for Grid integration of Wind-PV hybrid distributed generation system**," contains literature survey and original research work done by the undersigned candidate as a part of Doctoral studies.

All information in this thesis have been obtained and presented in accordance with existing academic rules and ethical conduct. I declare that, as required by these rules and conduct, I have fully cited and referred all materials and results that are not original to this work.

I also declare that I have checked this thesis as per the "Policy on Anti Plagiarism, Jadavpur University, 2019", and the level of similarity as checked by iThenticate software is **2%**.

Signature of Candidate: B.S Varun sai

Date: 23-11-2023

Professor
Electrical Engineering Department
JADAVPUR UNIVERSITY
Kolkata-700 032

23-11-2023

Certified by the Supervisor (Signature with date, seal)

Faculty of Engineering & Technology
Jadavpur University

Certificate from the Supervisor

This is to certify that the thesis entitled "**Development of improved MPPT methodologies for Grid integration of Wind-PV hybrid distributed generation system**," submitted by Mr. Boni Satya Varun Sai, who got his name registered on 27th May 2019, for the award of Ph. D. (Engg.) degree of Jadavpur University, is absolutely based upon his own work under the supervision of Prof. (Dr.) Debashis Chatterjee and that neither his thesis nor any part of the thesis has been submitted for any degree/diploma or any other academic award anywhere before.

Professor
Electrical Engineering Department
JADAVPUR UNIVERSITY
Kolkata-700 032

23-11-2023

………………………………………………..
Signature of the supervisor with date & seal

Acknowledgement

Since from Ph.D. registration to till this work the kind of guidance, constructive discussion and criticism by supervisor Prof. (Dr.) Debashis Chatterjee of Electrical Engineering Department, Jadavpur University, enriched author with knowledge and helps to reach at this stage of research work. It is an opportunity of the author to express immense respect to the supervisor for every possible help offered throughout the research journey.

The author is grateful to the Head of Electrical Engineering Department, Jadavpur University, for providing research opportunity. Author also would like to thank and Doctoral Committee members of Electrical Engineering Department, Jadavpur University, for their kind support and concern regarding my academic requirements.

Author expresses his heartfelt gratitude to Prof. (Dr.) Saad Mekhilef, Fellow IEEE, of power Electronics and Renewable Energy Research Laboratory, Department of Electrical Engineering, University of Malaya, Kuala Lumpur, Malaysia and Electrical Engineering Department, School of Science, Computing and Engineering Technologies, Swinburne University of Technology, Hawthorn, Victoria, Australia for his valuable suggestions and critical comments in developing PV and Wind MPPT schemes. His comments for improving writing and technicality of research articles immensely helped in progress.

Author expresses his sincere gratitude to Dr. Addy Wahyudie, Member IEEE, of Department of Electrical Engineering, United Arab Emirates University, Al Ain, United Arab Emirates for his valuable financial support in developing wind MPPT. This work would not been possible without active support of senior scholar and friend Mr. Sarang A. Khadtare, Mr. Subhendu Bikash Santra, Ms. Rupali Mohanty, Mr. Mukul Anand and Mr. Anagha Bhattacharya.

Author would like to express his heartfelt gratitude to my wife Ms. Navudu Tanuja and Ms. Boni Sri Surya Mounika for their support to complete the work. Author also want to express his sincere respect to his parents Boni Chinna Rao and Boni Satyavathi for their inseparable support and prayers. They are the persons who show me the joy of intellectual pursuit ever since I was a child. I thank them for sincerely bringing up me with care and love.

Finally, author would like to thank all who have encouraged to continue research work.

Department of Electrical Engineering
Jadavpur University, Kolkata

Boni Satya Varun Sai

Dedication

This thesis is dedicated to my beloved wife and parents.

Table of Contents

R_q	Parallel resistance
I_{po}	Solar cell current
di	Diode
I_{ph}	Solar cell photocurrent
V_{po}	Solar cell output voltage
R_e	Series resistance
I_{sat}	Saturation current
A	Diode ideal factor
q	Charge
n_s	Number of series connected PV cells
Te	Temperature
V_p	Open circuit voltage
I_{sh}	Short circuit current
Te_r	Temperature at STC
$I_{sh,r}$	Short circuit current at STC
g_r	Irradiance at STC
g	Irradiation
a	Irradiation correction factor of V_p
α	Temperature constant of I_{sh}
$V_{p,r}$	Open circuit voltage at STC
P_{max}, P_r	MPP power
V_{max}, V_r	MPP Voltage
I_{max}, I_r	MPP Current
K_m, K_n	Constants
$V_r\|_{series}$	MPP Voltage for series configuration
$I_r\|_{series}$	MPP Current for series configuration
$P_r\|_{series}$	MPP power for series configuration
$V_r\|_{parallel}$	MPP Voltage for parallel configuration
$I_r\|_{parallel}$	MPP Current for parallel configuration
$P_r\|_{parallel}$	MPP power for parallel configuration

K_p, K_I	PI controller gain values
C, $C_{parallel}$, C_{series}	Constants
$k_p\|_{op}, k_I\|_{op}$	PI controller gain values for single panel
$\left(k_p\|_{op}\right)_{series}, \left(k_I\|_{op}\right)_{series}$	PI controller gain values for series configuration
$\left(k_p\|_{op}\right)_{parallel}, \left(k_I\|_{op}\right)_{parallel}$	PI controller gain values for parallel configuration
$P_{\max}\|_{STC}$	Actual MPP power
$P_r\|_{op}$	Maximum power at operating condition.
L_{bi}	Inductance
C_{bo}	Output capacitance
C_{bi}	Input capacitance
P&O	Perturb and Observe
WA-P&O	Weather Adaptable Perturb and Observe
CV	Constant voltage
ARV	Adaptive Reference Voltage
STC	Standard testing condition
MP&O	Modified P&O
PWM	Pulse width modulation
MPPT	Maximum power point tracking
P-V	Power-voltage
I-V	Current-voltage
PV	Photovoltaic
FGPE	Fast-global peak estimation
S-P	Series- Parallel
ANN	Artificial neural network
CS	Cuckoo search
DPE	Dummy Peak Elimination
D_e	Diode
I_Q	Photo current
R_{sr}	Series resistance
R_{pr}	Parallel resistance
I_{LP}	Solar panel current

V_{LP}	Solar panel voltage
KVL	Kirchhoff's Voltage Law
G	Irradiation
T	Temperature
N_s	Number of series connected solar cells
A	Diode ideal factor
a	Irradiation correction factor
T_r	Temperature reference
$I_{sc,r}$	I_{sc} at STC
G_r	Irradiation at STC
$V_{ov,r}$	V_{ov} at STC.
P_{mpp}	MPP power
V_{mpp}	MPP voltage
I_{mpp}	MPP current
α	Temperature coefficient of I_{sc}
β	Temperature coefficient of V_{ov}
L_{ip}	Inductance
C_{ip} & C_o	Input & output capacitances
I	IGBT
Pa_i	i^{th} parallel string
$G_j\|_{pa_i}$	Irradiance of j^{th} panel in i^{th} parallel string
$G_1\|_{pa_1}, G_2\|_{pa_1}, G_3\|_{pa_1}$	Irradiances of first parallel string
$G_1\|_{pa_2}, G_2\|_{pa_2}, G_3\|_{pa_2}$	Irradiances of second parallel string
V_1, V_2, V_3	Voltages
I_1, I_2, I_3	Currents
max	Maximum
PS	Partial shading
SB	Slope based
ANN	Artificial neural network
EA-P&O	Enhanced adaptive P&O
CS	Cuckoo search
D_e	Diode
I_Q	Photo current

OCC or V_{ov}	Open circuit voltage
SCC or I_{sc}	Short circuit current
Q	Elementary Charge
I_{sa}	Saturation current
STC	Standard testing condition
M	Number of series connected panels
N	Number of parallel strings
DFIG	Doubly fed induction generator
SSM-ABC	Searching space minimization-based artificial bee colony
WECS	Wind energy conversion system
IARV	Improved adaptive reference voltage
MPP	Maximum power point
HRES	Hybrid renewable energy system
PSO	Particle swarm optimization
BPSO	Binary particle swarm optimization
PMSG	Permanent magnet synchronous generator
RPO-FOSMC	Robust Perturbation Observer based Fractional Order Sliding Mode Controller
GGWO	Grouped grey wolf optimizer
LS-P&O	Large step perturb and observe
SS-P&O	Small step perturb and observe
FLC-A	Adaptive feedback linearization controller
CS	Cuckoo search
ABC	Artificial bee colony
RSC	Rotor side converter
GSC	Grid side converter
I_p	Photo current
d	Diode
I_{PV}	Solar panel output current
P_{PV}	Solar panel output power
R_{se}	Series resistance
R_{pa}	Parallel resistance

V_{PV}	Solar panel voltage
S, S_a, S_b	Switching pulse to converter
WT	Wind turbine
P_{WT}	Wind turbine power
V_{BAT}	Battery voltage
I_{BAT}	Battery current
I_{BAT}^*	Reference battery current
P_{BAT}	Battery power
BES	Battery energy storage
P_{Grid}	Grid power
I_{gabc}	Grid current
V_{gabc}	Grid voltage
V_{abcs}, I_{abcs}	Stator voltage and current
V_{abcr}	Rotor voltage
P_m	Mechanical power
W_m	Rotor speed
W_m^*	Reference rotor speed
V_{dc}	DC-link voltage
G	Irradiation
T	Temperature
V_W	Wind speed
R_f	Resistance
L_f	Inductance
p	Pole pair
R_s	Stator resistance
R_r	Rotor resistance
$L_{\sigma s}$	Stator leakage inductance
L_m	Magnetizing inductance
$L_{\sigma r}$	Rotor leakage inductance
u	Turns ratio
R	Blade radius
ρ	Air density
D	Damping Coefficient

H_m	Inertia constant
λ_{opt}	Optimal Tip speed ration
C_{p_max}	Maximum power coefficient
C_1-C_7	Unknown coefficients
I_{sho}	Short Circuit Current
V_{ope}	Open Circuit Voltage
α	Temperature coefficient of I_{sho}
T_β	Temperature coefficient of V_{ope}
C_{Bat}	Rated battery capacity
A	Curve fitting factor
k	Boltzmann constant
q	Electron charge
I_o	Saturation current of diode
$I_{sho,ref}$	Short circuit current at STC
$V_{ope,ref}$	Open circuit voltage at STC
T_{ref}	Temperature at STC condition
G_{ref}	Irradiation at STC
a	irradiation correction factor of V_{ope}
I_M	MPP current
V_M	MPP voltage
P_M	MPP power
β	Pitch angle
ρ	Air density
C_p	Power coefficient of a wind turbine
A_r	Swept area
λ	Tip speed ratio
$V_{ds}, V_{qs}, V_{dr}, V_{qr}$	dq components of stator voltages and rotor voltages
$\psi_{ds}, \psi_{qs}, \psi_{dr}, \psi_{qr}$	dq components of stator flux and rotor flux
i_r	Rotor current
ω_r	Rotor speed
ω_s	Synchronous speed
T_{em}	Electromagnetic torque
$i_{ds}, i_{qs}, i_{dr}, i_{qr}$	dq components of stator and rotor currents

ψ_s	Stator flux
ψ_r	Rotor flux
PI	Proportional-integral controller
S-P	Series- Parallel configuration
a, b, K_1, K_2, $\in$, γ	constants
1S	Single panel
$\left(V_M\vert_{1S}\right)_G$	MPP voltage for 1S configuration at irradiation G
$\left(V_M\vert_{24S-2P}\right)_G$	MPP voltage for 24S-2P configuration at irradiation G
$\left(V_M\vert_{1S}\right)_{STC}$	MPP voltage for 1S configuration at STC
$\left(V_{ope}\vert_{1S}\right)_{STC}$	Open circuit voltage for 1S configuration at STC
$\left(I_M\vert_{1S}\right)_G$	MPP current for 1S configuration at irradiation G
$\left(I_M\vert_{24S-2P}\right)_G$	MPP current for 24S-2P configuration at irradiation G
$\left(I_M\vert_{1S}\right)_{STC}$	MPP current for 1S configuration at STC
$\left(I_{sho}\vert_{1S}\right)_{STC}$	Short circuit current for 1S configuration at STC
MRAS	Model reference adaptive system
Np	Number of bees
$\omega_{\max}$	Maximum rotor speed
FFT	Fast Fourier Transform
$\omega_{\min}$	Minimum rotor speed
ω_{opt}	Optimum rotor speed
X_{hi}	Food source position with high nectar amount
SSM-PSO	Searching space minimization-based particle swarm optimization

***Abbreviations/Symbols appearing in this thesis other than the mentioned ones are defined in the respective contexts.**

List of Tables

INTRODUCTION

1.1 HYBRID RENEWABLE ENERGY SYSTEM

The WECS and PV systems shares the major share of renewable energy production in modern world [1.1]. The WECS and PV energy are continuously varying due to the weather dependent nature. Due to this, the alone operation of PV and WECS systems does not guarantee the continuous supply to the consumer. Therefore, it is profitable to operate the wind and PV combination for reliable supply of power [1.2]. Also, the combined energy from these sources can supply the power to large number of loads. Due to the advancement in technologies, two or many renewable energy sources are operated as HRES [1.3]. The PV-wind system is further integrated with energy storage systems like the battery, fuel cell etc., in delivering the efficient power supply to the customers [1.4, 1.5].

The HRES are operated in grid and standalone mode. In grid mode, the PV, wind and battery collectively operate to feed the load. If there is a power deficiency, the load will draw the power from AC grid. The standalone mode is employed in meeting the load requirement of remote areas. Under the temporary unavailability of grid, the grid mode can be treated as standalone. In HRES, the output characteristics of solar and wind are non-linear in nature. Therefore, proper control strategies are required for tracking the maximum power for PV and wind systems [1.6].

The classifications and architecture of HRES are represented in [1.7]. The general schemes of converter in HRES are classified into AC-coupled HRES, DC-coupled HRES and Mixed-structure HRES [1.8]. Fig. 1.1, represents the DC-coupled HRES system. This system consists of PV system, WECS and battery coupled together with DC-bus. Also, on the other side, a single DC-AC converter is employed in feeding the load. In case of DC-coupled HRES, the MPPT scheme for PV system is applied at DC-DC converter, while for DFIG system it is applied at AC-DC or RSC [1.9]. The battery is connected to DC-bus through a bi-directional DC-DC converter. Fig. 1.2 denotes the AC-coupled HRES, where the PV, wind and battery systems are connected to common AC-bus through individual DC-AC converters. Also, for controlling the wind and PV power, MPPT schemes are employed. There is mixed HRES, in which displays advantages of the both AC and DC coupled schemes [1.10].

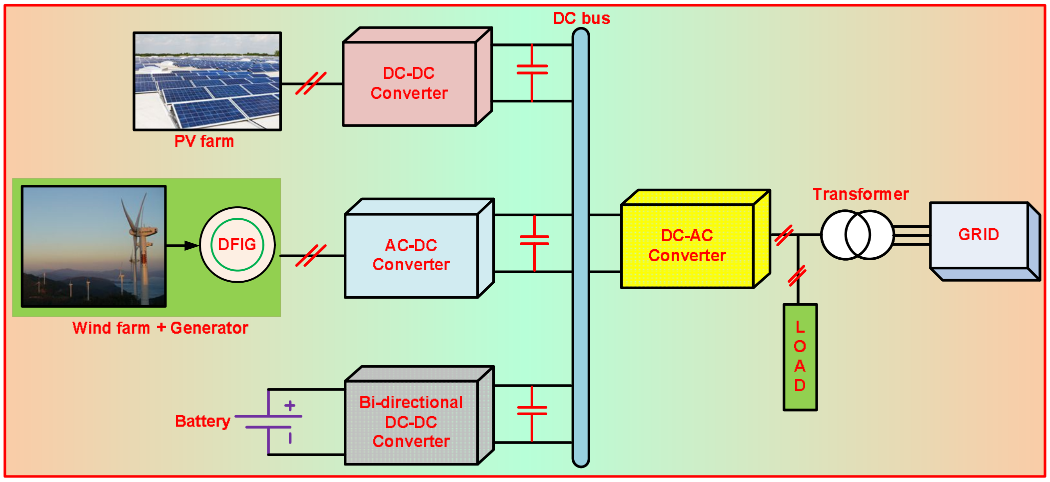

Fig. 1.1. DC coupled HRES system

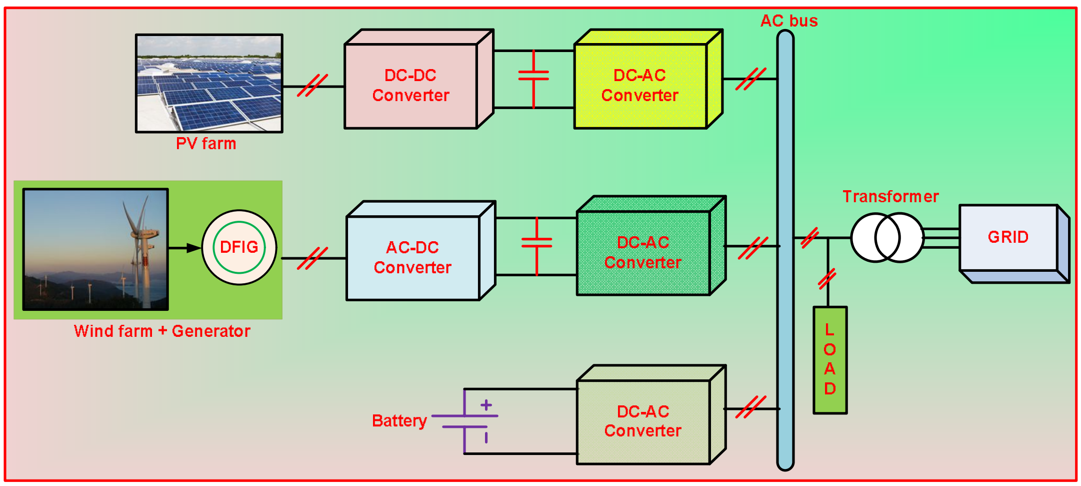

Fig. 1.2. AC coupled HRES system

A PSO-BPSO Technique, Particle Swarm Optimization Algorithm and Two-Stage Optimization are employed in sizing of the HRES [1.11-1.13]. Along with the sizing, the economic assessment of the HRES implementation is defined in [1.14]. The wind/PV along with battery/supercapacitor-based systems are defined in [1.15, 1.16]. The HRES can be operated in grid connected and standalone modes. It is observed that most of the HRES are operated in the standalone mode. In [1.17], there is system established for the standalone microgrid operation. The power quality improvement of the standalone hybrid energy system is proposed in [1.18]. Sensitivity analysis of a standalone hybrid system for the rural healthcare facility is represented in [1.19]. The grid connected HRES are discussed in [1.20]. From [1.21-1.23], it can be observed that the MPPT schemes plays a key role in the operating characteristics of the system. Also, it is known that, MPPT schemes plays key role in producing inter-harmonics into grid [1.24]. Therefore, it is recommended to employ the MPPT schemes in PV and wind systems such that, the system will result in lower settling time and near zero steady state oscillations. In this research work, improved MPPT techniques has been proposed for wind and PV systems to display the desired characteristics.

1.2 PV BASED SYSTEMS

PV energy is one of the most focused and well-established renewable energy sources among all others due to its hefty availability and relatively simpler control strategies [1.25]. With high establishment cost till date, the activity of solar modules under MPPT condition is essential for greatest utilization of accessible power. The adaptability in development and precision in delivering performance characteristics of solar cell encourages the single diode model as the most utilized one for Photovoltaic cell construction [1.26]. Because, the power generated by single solar panel is lower, a noteworthy number of PV panels are to be associated either in series or parallel configurations etc., for any PV power generation system. In spite of the fact that the PV panels are placed on open space to receive direct irradiation, various obstructions e.g., passing of clouds, shadows, dust particles on boards and bird's left-overs etc., prevent the availability of uniform irradiance everywhere throughout all the panels.

1.2.1 UNIFORM SHADING CASE

To better utilize available PV panel power different MPPT schemes regulate the switching pulses for the power electronic converter [1.27-1.28]. The available MPPT techniques are broadly categorized into conventional and advanced MPPT schemes. Where artificial neural network (ANN), fuzzy logic-based and optimization-based algorithms comes under the advanced type. Generally, in uniform shading cases, ANN and Fuzzy based schemes are not recommended for MPPT, as they are very complex while coming to hardware implementation. But, the PI tuning-based MPPT schemes with the application of ANN and Fuzzy based techniques produce better dynamic characteristics, which is helpful in reducing the inter-harmonics. At the same time, they result in the disadvantage of a higher settling time in reaching maximum power point (MPP) [1.29]. Because of their simple structure and easy hardware implementation, conventional MPPT algorithms are most generally used in industries. In conventional MPPT schemes, Perturb and Observe (P&O) method is the utmost straightforward, effective one with good tracking efficiency [1.30-1.32]. Besides being advantageous, the P&O algorithm has limitations in detecting sudden changes in irradiations, resulting in power fluctuations. Modified Perturb and observe scheme (MP&O) is the developed version of P&O with an additional current component. It displays negligible drift along with commendable tracking efficiency under a sudden change in irradiation levels [1.33].

Constant Voltage (CV) MPPT requires a single sensor for tracking maximum power; it is more economical related to available MPPT techniques [1.34-1.35]. But CV algorithm is insensitive to irradiation and temperature, resulting in low tracking efficiency. Adaptive reference voltage (ARV) MPPT is the improved form of CV, in which irradiation and temperature sensors are required in the MPPT process. ARV MPPT has the disadvantage of requiring a huge memory for the processing unit, resulting in higher installation costs [1.36]. The PV-boost converter arrangement with MPPT provides DC output, requires an inverter to feed ac loads. Normally, three-Phase voltage source Pulse width modulated (PWM) inverters with low output voltage harmonics are extensively used for feeding ac loads [1.37]. Out of the available PWM methods, sinusoidal pulse width modulation (SPWM) is extensively employed for its simpler control structure and easier implementation [1.38].

The PV-based inverters with oscillating input and non-ideal switching, can lead to the generation of harmonics into the system [1.39], the harmonic cushioning techniques are already available to counter this issue [1.40-1.42]. Along with harmonic content, it is observed that Inter-harmonics is also induced in the PV-grid integration system. Inter-harmonics have a similar effect to harmonics, but some of the impacts, like flickering, can be higher in inter-harmonics. Due to the unwanted triggering, inter-harmonics, isolates the load from PV system, leading to discontinuity in supplying the load. These Interharmonics are mainly caused by the MPPT schemes employed in the system. The inter harmonic modelling and analysis of the grid-connected solar system is already done, the role of MPPT in Inter-harmonics are also analyzed in [1.24]. The Mitigation of Inter-harmonics is still a burning research topic for modern researchers.

Although very few pieces of literature exist in the reduction of Inter-harmonics for PV-grid integrated systems, most of the presented schemes do not address the MPPT efficiency and drifts due to sudden changes in irradiation. [1.43] and [1.44] are the literature available for the reduction of Interharmonics with modification in MPPT under low power conditions. Interharmonics are observed under a more moderate power condition because, under quiet power operation, the inter harmonic components become comparable with the fundamental frequency component [1.43]. In [1.43], under more moderate power conditions, it is observed that CV MPPT reduces the lower-order Inter-harmonics considerably under uniform irradiation cases. But it fails to explain maintaining maximum efficiency and the case of a sudden change in irradiation. In [1.44], inter harmonic mitigation is done by controlling the sampling rate of P&O MPPT. Even though [1.44] can mitigate the interharmonics, it results in fluctuations under sudden change irradiation due to the weather insensitive nature of P&O. So, under a sudden change in irradiation case, [1.44] fails to mitigate the inter-harmonics. Inter-harmonic mitigation for wind energy system has been demonstrated in [1.45], while multiple harmonic eliminations for the multilevel inverter is described in [1.46], as recent advancement in this area. However, all these works do not address the inter harmonic elimination for PV-based systems.

A learning-based hill climbing (L-HC) algorithm has been implemented in [1.47], for the accurate harmonic supportive control schemes. In [1.48], a self-tuned perturb and observe (SPO) has been developed for quick maximum power point tracking. A Learning-based Incremental Conductance (LIC) has been introduced in [1.49-1.50] to avoid the drawbacks of incremental conductance (InC) algorithm. A Learning-based Perturb and Observe (LPO) maximum power point tracking (MPPT) algorithm has been introduced in [1.51] to avoid the inherent disadvantages in the P&O scheme. Even though L-HC, SPO, LIC and LPO displays better performance characteristics compared to traditional P&O algorithm, they have the common disadvantage of atmosphere insensitivity. Moreover, squirrel search algorithm [1.52], Improved Differential Evolution-based MPPT Algorithm [1.53], Modified Butterfly Optimization Algorithm [1.54] and Most Valuable Player Algorithm [1.55] are introduced for better MPPT process, but they are very difficult to implement while coming to real time situation [1.56-1.57].

1.2.2 PARTIAL SHADING CASE

Since, uniform irradiation results in a single peak for the overall configuration, tracking of maximum power is easier [1.58, 1.59]. On the other hand, the PS situation leads to multiple peaks both in the Power-Voltage (P-V) and Current-Voltage (I-V) characteristics of the cascaded PV panels, resulting in difficulty to track maximum power. Boost converter is chosen commonly as an intermediate power conditioner in PV system due to its simple structure, cost compatibility and flexible control schemes with non-invertible output voltage [1.60, 1.61]. Under PS case, the conventional MPPT schemes results in lesser efficiency. The mostly used traditional MPPT technique is Perturb and Observe (P&O) algorithm, which has a limitation in identifying global maximum point under PS condition. Similarly, other conventional MPPT schemes like Hill Climbing (HC) method, Incremental conductance (IC) method etc., are also inefficient in tracking power at global maximum under PS condition [1.62]. For effective tracking of global maximum under shading case, numerous optimization-based algorithms are introduced to improve efficiency, reduction of cost and complexity [1.63,1.64]. Execution of these optimization-algorithms is subjected to numerous adjustable parameters e.g., population size, the number of iterations, acceleration and tuning off parameters etc., [1.65].

Under PS condition, global maximum tracking based on artificial vision is presented recently, in which web cam is utilized to recognize the shading pattern. Even though this method shows improved characteristics, the implementation cost can be high due to high end hardware requirement with higher computational compatibility [1.66]. Beside this, it is also mentioned that, low-cost camera can be used for tracking purpose, but it may lead to precision error. Maximum power point scanning (MPPS) technique is the one wherein group selection optimizer along with P&O is utilized for tracking global maximum, where the research to be carried out in controlled voltage source for improved performance [1.67]. Fusion firefly algorithm (FFA) is able to show the improved MPPT characteristics with moderate difficulty in the algorithm [1.68]. Using optical isolation mechanism, PS MPPT can be successfully implemented with low cost and fast tracking [1.69]. An Artificial Neural network-based system is also developed for shading pattern detection to generate particular reference voltage to track global peak power, but precision initialization routine is necessary for successful hardware implementation [1.70].

Particle swarm optimization (PSO) and cuckoo search (CS) algorithms are the most normally employed optimization techniques in tracking global maximum under shading environment [1.71, 1.72]. The CS search algorithm displays better performance characteristics compared to PSO [1.73, 1.74]. In [1.75], an enhanced Adaptive P&O (EA-P&O) MPPT is proposed where the scanning is done to measure the region of convergence for global maximum. This work avoids the inability of P&O in detecting MPP under PS scenario. But the scanning takes considerable time, resulting in inferior dynamic response of system. In [1.76], an accurate MPPT to detect PS occurrence is determined in which, based on the shading pattern detection, it is observed whether the system is under PS condition or uniform irradiation condition. If the PS condition occurs PSO comes into picture, while for uniform irradiation P&O is considered. This leads to high complexity with poor dynamic response of the system for practical implementation under PS condition. Moreover, recent studies reveal that, MPPT techniques with low dynamic response employed in the PV systems are one of the major reasons behind the introduction of interharmonics into the system. So, a MPPT scheme with good tracking efficiency, easy real time implementation and good dynamics is strongly required [1.24]. However, all these schemes discussed have the major difficulty of high computational requirement for the processor with low dynamic performance, which restricts these to be efficiently used for MPPT schemes under PS condition.

1.3 WIND ENERGY CONVERSION SYSTEMS

Wind power is most promising because of its abundant accessibility and pollution less nature compared to the other available renewable sources. The usage of wind energy for the residential purpose, leads to energy independence [1.77]. Irrespective of the size, the energy-producing wind turbine system contains different sections; they are the portion experiencing the wind force, tower, speed controlling apparatus and electrical generator. Generally, for WECS, any of the fixed or variable speed turbines are employed [1.78].

Due to its flexibility in operating at above-rated speeds, doubly fed induction generator (DFIG) is mostly considered for wind power generation. Moreover, DFIG has the advantages of variable speed and constant frequency operation, low mechanical tension, maximum power capturing ability, decoupled active or reactive power governance, etc. Also, the expenditure required for static power converters in DFIG is lower than that of permanent magnet synchronous generator (PMSG) [1.79]. These advantages in DFIG are due to the control schemes used in the back-to-back converters. Therefore, the process used in controlling back-to-back converters proves to display a vital role for the operating characteristics in DFIG. Because of its flexibility in the real power and reactive power decoupled control, vector control strategy is frequently employed in DFIG systems [1.80].

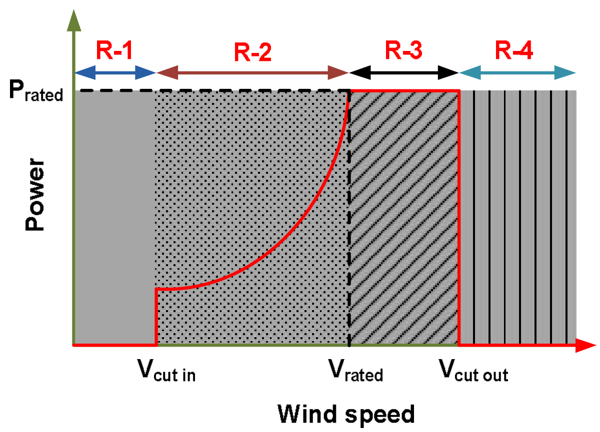

Fig. 1.3. Different operating areas for wind turbine

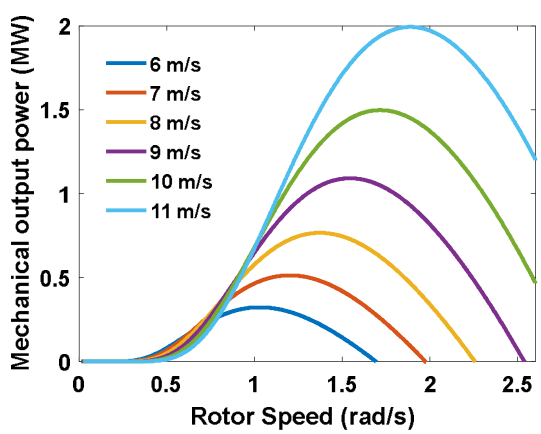

Fig. 1.4. Power-speed characteristics at various wind speeds

The working range for variable speed WECS is primarily divided into four regions, Region-1 (R-1), R-2, R-3, and R-4, as represented in Fig. 1.3. In R-1 and R-4, DFIG is not in the operating state, owing to safety measurements. In R-2, DFIG operates in MPP tracking zone, where the system is operated under below rated speeds. In R-3, DFIG operates in pitch controlling region, where the pitch controller is employed to reduce the stress over the wind turbines for above rated speeds [1.81]. As shown in Fig. 1.4, DFIG displays non-linear mechanical power and rotor speed characteristics. So, in DFIG, MPPT methods are employed for the efficient operation of the system. In MPP tracking, Perturb and Observe (P&O) scheme is considered to be prevalent because of its easy structure and flexible real-time operation. But, P&O displays fluctuation in output power characteristics under variation in speed situations and fails to track maximum power efficiently. P&O scheme operates with a small step and large step changes in rotor speed, where small step-change results in more settling time and less steady-state error [1.82]. With large steps, operation in P&O results in less settling time but more oscillation over a steady state. Many optimization-based schemes have already been available for tracking maximum power with improved dynamic characteristics compared to the P&O scheme.

A novel Robust Perturbation Observer based Fractional Order Sliding Mode Controller (RPO-FOSMC) has been proposed for tracking peak power [1.83]. RPO-FOSMC can display the improved dynamics compared to conventional MPPT schemes but results in the fluctuations of output power under a sudden change in speed cases. In [1.84], four sectors operation-based P&O scheme is implemented for faster tracking of peak power. The [1.84], displays a faster tracking response but undergoes more settling time compared to the large step P&O scheme. In [1.85], a fixed-time control scheme is used for MPP tracking in the DFIG system. In this method, aerodynamic torque is estimated without employing speed sensors with the help of a fixed-time observer. The Grouped grey wolf optimizer (GGWO) is employed to detect MPPT and improving fault ride-through capability for DFIG [1.86]. But the work should be expanded in grid side controller (GSC) side to operate the GGWO with the entire DFIG system.

An artificial Neural Network Controller (ANNC) assisted mechanical speed control is employed with a robust MPPT controller for studying wind power generation with respect to wind disturbances [1.87]. The novel fuzzy logic sensorless maximum power point tracking (FLC-MPPT) method for WECS is implemented by downsizing the pulse width modulation (PWM) back to back converters compared to conventional schemes by 40% [1.88]. Quantum parallel multi-layer Monte Carlo optimization algorithm, Archimedes optimization algorithm and Techno-economic optimization-based schemes are the few recently introduced optimization schemes in tracking maximum power [1.89-1.91]. A nonlinear maximum power point tracking scheme is introduced where the adaptive backstepping control method is employed for stable operation at speed disturbances and parametric uncertainties [1.92]. Estimation based enhanced maximum energy extraction scheme has been introduced for the MPPT case in DFIG, where it possesses the major advantage of easy real-time implementation [1.93]. For a DC-based DFIG system, MPPT is done by employing a coordinated adaptive feedback linearization controller (FLC-A) based on a flux observer [1.94].

Even though optimization-based schemes display better-operating characteristics, the settling time is longer. Particle swarm optimization (PSO) is simpler to implement in real-time atmosphere due to its less mathematical formulation [1.95]. PSO and cuckoo search (CS) algorithms are the most commonly used approaches for MPPT in wind and PV generation [1.96-1.98]. Even though CS shows -operating properties than PSO, the latter is simpler while coming to real-time implementation [1.99]. Even though PSO is simpler, the development has to be done regarding the limitation of searching space, leading to lower settling time [1.100].

1.4 MOTIVATION OF THE THESIS

The main motivation of the thesis is the high requirement of improved MPPT methodologies for reducing inter-harmonics in the HRES. Coming to PV, it can be mentioned that conventional MPPT are used for tracking MPP in uniform shading case. P&O scheme is most prominently considered for MPPT among conventional MPPT schemes. P&O has the major disadvantage of drift under sudden change in irradiation. This may lead to the injection of inter-harmonics in the grid [1.24]. CV based MPPT scheme and P&O with sampling rate control are used to reduce inter-harmonics in the grid connected systems. But CV has the major disadvantage of low MPP tracking efficiency under lower irradiation levels [1.37].

ARV MPPT scheme is advantageous compared to CV scheme. ARV method requires huge processing memory unit for tracking MPP. Even though advanced MPPT schemes like ANN, optimization etc., can be helpful in tracking the MPP under both uniform and partial shading cases, they are difficult to implement in real time situation. In case of partial shading, scanning based MPPT schemes are introduced. They are capable of easy real time implementation and same time they take larger settling time in reaching MPP. Therefore, there is a high requirement of the MPPT method which can reduce the inter-harmonics along with maintaining good tracking efficiency and better dynamic characteristics. Also, the MPPT schemes must be easily implemented with already available hardware.

In WECS, P&O scheme is mostly considered for MPP tracking. The SS-P&O scheme results in the lower steady state oscillation. Same time, SS-P&O results in higher tracking time in detecting MPP. Even though LS-P&O scheme employed results in lower settling time, it results in the higher steady state oscillations over the steady state [1.82]. PSO and CS algorithms are most commonly used optimization-based schemes for tracking MPP [1.99]. Even though CS algorithm displays lower settling time compared to PSO, PSO is easier to implement in real time situation [1.100]. By observing the outcomes of recently introduced MPPT schemes in WECS, it is observed that there is a high requirement of an algorithm which displays lower settling time, near zero steady state oscillations and easy real time implementation. Beside this, the MPPT schemes must be successful in reducing the inter-harmonic content in to the grid.

From the recent advancements in HRES, it is noted that the MPPT schemes in wind and PV systems plays a key role in the operating characteristics of the system. Also, it is noted that, there is high a requirement of MPPT systems which can reduce the inter-harmonic content into the grid. This vacuum in research has led the author to develop a thesis related to improved MPPT schemes in HRES.

1.5 OBJECTIVE OF THESIS

The thesis objective based on research has been presented as below. The proposed MPPT scheme under uniform shading and partial shading cases in PV system are developed to track the MPP with low settling time and near zero steady state error. It is also able to display the better operating characteristics without usage of any memory unit. The MPPT schemes are made weather sensitive to avoid the fluctuation under sudden change in irradiation. Also, the proposed MPPT scheme in partial shading situation is made easier to implement in real time situation compared to other existing MPPT schemes.

The wind MPPT is proposed to address the improved MPPT characteristics. The proposed schemes mainly address to reduce the settling time, steady state oscillations and fluctuations under sudden change in wind speed. Moreover, the proposed wind MPPT scheme can be implemented successfully using already available hardware. Correspondingly, PV, wind turbine driven DFIG and battery are operated coordinatively to provide reliable supply to customer.

1.6 THESIS ORGANIZATION

The organization of thesis is presented as below;

Chapter 1 gives an introduction regarding the contextual of research work that highlights on some of the technical literature survey under the heading of the literature assessment and summarizes into research motivation and objective trailed by introduction on existing MPPT schemes. Finally, it ends up with thesis organization.

Chapter 2 introduces an inter-harmonic mitigation MPPT algorithm for PV based Converters. This is followed by a description on the working of the proposed scheme in MATLAB & simulink. This chapter ends up with validation of the topology with results on laboratory prototype.

Chapter 3 presents an improved weather adaptable P&O MPPT technique under varying irradiation condition. The proposed scheme is able to describe the tracking speed and fluctuations under sudden change in irradiation. Also, the PI control gain adjustment with variation in irradiation is described successfully. This is followed by a description on the working of the proposed scheme in MATLAB & simulink. This chapter ends up with validation of the topology with results on laboratory prototype.

Chapter 4 has three subparts, where first subpart (**A4)** introduces a dummy peak elimination based MPPT technique for PV generation under partial shading condition. Detailed mathematical modeling, controlling methodology for finding the nearest point to global MPP is discussed. Moreover, the derived peak point is used as an initial point for P&O MPPT scheme in tracking MPP. This is followed by a description on the working of the proposed scheme in MATLAB & simulink. This chapter ends up with validation of the topology with results on laboratory prototype.

Second subpart **(B4)** introduces A Fast-Global Peak Estimation Technique for Photovoltaic System Under Partial Shading Situation. The expanded mathematical formulation of dummy peak elimination MPPT scheme for series-parallel configurations are discussed here. This is followed by a description on the working of the proposed scheme in MATLAB & simulink. This chapter ends up with validation of the topology with results on laboratory prototype.

Third subpart **(C4)** presents an Accurate MPPT Technique under Partial Shading Conditions Using PV Panel Operating Characteristics. The modelling of near global peak detection using sensors is presented here. The detection of global MPP by using slopes of individual solar panels are formulated. It has been developed using MATLAB & simulink and also a low scale laboratory prototype has been developed to validate the topology.

Chapter 5 introduces an SSM-PSO Based MPPT Scheme for Wind driven DFIG system. The searching space minimization for tracking MPP has been addressed with anemometer. The mathematical modeling, controlling methodology for formulating PSO in MPPT is discussed in this chapter. This is followed by a description on the working of the proposed scheme in MATLAB & simulink.

Chapter 6 introduces a proposed HRES system with the proposed SSM-ABC and IARV methods for Wind driven DFIG and PV systems respectively. The mathematical modeling, controlling methodology for formulating SSM-ABC and IARV methods in MPPT are discussed in this chapter. This is followed by a description on the working of the proposed scheme in MATLAB & simulink. This chapter ends up with validation of the topology with results on laboratory prototype.

Finally, **chapter 7** summarizes and concludes the effort of this research and provides a stance for works to carry out in future.

References:

[1.1] Gajewski, P and Krzysztof, P, “Control of the Hybrid Renewable Energy System with Wind Turbine,” Photovoltaic Panels and Battery Energy Storage. Energies 2021, 14, 1595.

[1.2] G. B. Arjun Kumar and Shivashankar, “Optimal power point tracking of solar and wind energy in a hybrid wind solar energy system,” International Journal of Energy and Environmental Engineering, 2021.

[1.3] Can Wan, Weiting Qian, Changfei Zhao, Yonghua Song and Guangya Yang, “Probabilistic Forecasting Based Sizing and Control of Hybrid Energy Storage for Wind Power Smoothing,” IEEE transactions on sustainable energy, vol. 12, no. 4, october 2021.

[1.4] Unnikrishnan Raveendran Nair, Monika Sandelic, Ariya Sangwongwanich, Tomislav, D, IEEE, Ramon Costa-Castelló and Frede Blaabjerg, “Grid Congestion Mitigation and Battery Degradation Minimisation Using Model Predictive Control in PV-Based Microgrid,” IEEE transactions on energy conversion, vol. 36, no. 2, June, 2021.

[1.5] Pranoy Roy, Jiangbiao He, Tiefu Zhao and Yash Veer Singh, “Recent Advances of Wind-Solar Hybrid Renewable Energy Systems for Power Generation: A Review,” IEEE open journal of the industrial electronics society, 2022.

[1.6] Boualam Benlahbib, Noureddine Bouarroudj, Saad Mekhilef, Dahbi Abdeldjalil, Thameur Abdelkrim, Farid Bouchafaa and Abelkader lakhdari, “Experimental investigation of power management and control of a PV/wind/fuel cell/battery hybrid energy system microgrid,” international journal of hydrogen energy,45, 2020, 2911-29122.

[1.7] Rashid Al Badwawi, Mohammad Abusara and Tapas Mallick, “A Review of Hybrid Solar PV and Wind Energy System, Smart Science,” 2015, 3:3, 127-138,

[1.8] Mohamed, H.A., Khattab, H.A., Mobarka, A., Morsy, G.A., “Design, control and performance analysis of DC-DC boost converter for stand-alone PV system,” In Proceedings of the 2016 Eighteenth International Middle East Power Systems Conference (MEPCON), Cairo, Egypt, 27–29 December 2016; pp. 101–106.

[1.9] Liyong, Y.; Peie, Y.; Zhenguo, C.; Zhigang, C.; Zhengxi, L, “A novel control strategy of power converter used to direct driven permanent magnet wind power generation system,” In Proceedings of the 2009 2nd International Conference on Power Electronics and Intelligent Transportation System (PEITS), Shenzhen, China, 19–20 December 2009; Volume 1, pp. 456–459.

[1.10] Villalva, M.G.; Gazoli, J.R.; Filho, E.R, “Comprehensive approach to modelling and simulation of photovoltaic arrays,” IEEE Trans. Power Electron. 2009, 24, 1198–1208.

[1.11] O. Llerena-Pizarro, N. Proenza-Perez, C. Tuna and J. Luz, “A PSO-BPSO Technique for Hybrid Power Generation System Sizing,” IEEE Latin America Transactions, Vol. 18, No. 8, August 2020.

[1.12] Jon Martinez-Rico, Ekaitz Zulueta, Ismael Ruiz de Argandoña, Unai Fernandez-Gamiz and Mikel Armendia, “Multi-objective Optimization of Production Scheduling Using Particle Swarm Optimization Algorithm for Hybrid Renewable Power Plants with Battery Energy Storage System,” Journal of Modern Power Systems and Clean Energy, Vol. 9, No. 2, March 2021.

[1.13] Jonglak Pahasa and Issarachai Ngamroo, “Two-Stage Optimization Based on SOC Control of SMES Installed in Hybrid Wind/PV System for Stabilizing Voltage and Power Fluctuations,” IEEE Transactions On Applied Superconductivity, Vol. 31, No. 8, November 2021.

[1.14] Kumar D and Tewary T., “Techno-economic assessment and optimization of a standalone residential hybrid energy system for sustainable energy utilization,” Int J Energy Res. 2021;1–20.

[1.15] Tingna Shi1, Haitian Lu, Yanfei Cao, Xinmin Li, Changliang Xia, “Supercapacitor/battery hybrid energy storage unit for brushless DC motor operation,” IET Electr. Power Appl., 2020, Vol. 14 Iss. 4, pp. 597-604.

[1.16] Tareq Salameh, Mohammad Ali Abdelkareem, A.G. Olabi, Enas Taha Sayed, Monadhil Al-Chaderchi and Hegazy Rezk, “Integrated standalone hybrid solar PV, fuel cell and diesel generator power system for battery or supercapacitor storage systems in Khorfakkan, United Arab Emirates,” international journal of hydrogen energy, 46, 2021, 6014-6027.

[1.17] Juma, M.I., Mwinyiwiwa, B.M.M. Msigwa, C.J and Mushi, A.T., “Design of a Hybrid Energy System with Energy Storage for Standalone DC Microgrid Application,” Energies, 2021, 14, 5994.

[1.18] Soufiane Marmouh, Mohamed Boutoubat and Lakhdar Mokrani, “Performance and power quality improvement based on DC-bus voltage regulation of a stand-alone hybrid energy system,” Electric Power Systems Research 163 (2018) 73–84.

[1.19] Jamiu O. Oladigbolu, Yusuf A. Al-Turki and Lanre Olatomiwa, “Comparative study and sensitivity analysis of a standalone hybrid energy system for electrification of rural healthcare facility in Nigeria,” Alexandria Engineering Journal (2021) 60, 5547–5565.

[1.20] Sudip Bhattacharyya, S. Puchalapalli and Bhim Singh, “Operation of Grid Connected PV-Battery-Wind Driven DFIG Based System,” IEEE Transactions on Industry Applications, 2022.

[1.21] Simone Vanti, Prabhat Ranjan Bana, Salvatore D’Arco and Mohammad Amin, “Single-Stage Grid-Connected PV System with Finite Control Set Model Predictive Control and an Improved

Maximum Power Point Tracking," IEEE Transactions on Sustainable Energy, Vol. 13, No. 2, April 2022.

[1.22] Priyadarshi N, Padmanaban S, Bhaskar MS, Blaabjerg F and Holm-Nielsen JB, "An improved hybrid PV-wind power system with MPPT for water pumping applications," Int Trans Electr Energ Syst. 2020, 30, e12210.

[1.23] Ratnakar Babu Bollipo, Suresh Mikkili, and Praveen Kumar Bonthagorla, "Hybrid, Optimal, Intelligent and Classical PV MPPT Techniques: A Review," CSEE Journal of Power and Energy Systems, Vol. 7, No. 1, January 2021.

[1.24] Ariya Sangwongwanich, Yongheng Yang, Dezso Sera, Hamid Soltani, and Frede Blaabjerg, "Analysis and Modeling of Interharmonics From Grid-Connected Photovoltaic Systems," IEEE Transactions on Power Electronics, Vol. 33, No. 10, October 2018.

[1.25] Ku Ding, XinGao Bian, HaiHao Liu, and Tao Peng.: 'A MATLAB-Simulink-Based PV Module Model and Its Application under Conditions of Non uniform Irradiance', IEEE Trans. On ENERGY Conv. vol. 27, no. 4, Dec.2012.

[1.26] Hitesh K. Mehta, Himanshu Warke, Kaushik Kukadiya and Ashish K. Panchal.: 'Accurate Expressions for Single-Diode-Model Solar Cell Parameterization', IEEE journal of Photovolt., vol. 9, no. 3, May 2019.

[1.27] M.A. Danandeh and S.M. Mousavi G, "Comparative and comprehensive review of maximum power point tracking methods for PV cells," Renewable and Sustainable Energy Reviews, Vol. 82, Part 3, Feb. 2018, Pages 2743-2767.

[1.28] Mingxuan Mao, Lichuang Cui, Qianjin Zhang, Ke Guo, Lin Zhou and Han Huang, "Classification and summarization of solar photovoltaic MPPT techniques: A review based on traditional and intelligent control strategies," Energy Reports Volume 6, Nov. 2020, Pages 1312-1327.

[1.29] M. A. G. de Brito, L. Galotto, L. P. Sampaio, G. A. e Melo, and C. A. Canesin, "Evaluation of the main MPPT techniques for photovoltaic applications," IEEE Trans. Ind. Electron., vol. 60, no. 3, pp. 1156–1167, Mar. 2013.

[1.30] Jyotirmaya Sahoo, Susovon Samanta and Shamik Bhattacharyya, "Adaptive PID Controller with P&O MPPT Algorithm for Photovoltaic System," IETE Journal of Research, 2018.

[1.31] Hafsa Abouadane, Abderrahim Fakkar, Dezso Sera, Abderezak Lashab, Sergiu Spataru and Tamas Kerekes, "Multiple-Power-Sample Based P&O MPPT for Fast-Changing Irradiance Conditions for a Simple Implementation," IEEE Journal of Photovoltaics, Vol.10, Iss. 5, Sept. 2020.

[1.32] Shun-Chung Wang, Hung-Yu Pai, Guan-Jhu Chen, and Yi-Hwa Liu, "A Fast and Efficient Maximum Power Tracking Combining Simplified State Estimation With Adaptive Perturb and Observe," IEEE Access, Vol. 8, 2020.

[1.33] Jyri Kivimaki, Sergei Kolesnik, Moshe Sitbon, Teuvo Suntio and Alon Kuperman, “Design Guidelines for Multiloop Perturbative Maximum Power Point Tracking Algorithms,” IEEE Trans. on Power Electron., vol. 33, no. 2, Feb., 2018.

[1.34] Muralidhar Killi and Susovon samanta, “Modified Perturb and Observe MPPT Algorithm for Drift Avoidance in Photovoltaic Systems,” IEEE Tans. Ind. Electron, VOL. 62, NO. 9, Sep.2015.

[1.35] Vibhu Jately, Somesh Bhattacharya, Brian Azzopardi, Antoine Montgareuil, Jyoti Joshi, and Sudha Arora, “Voltage and Current Reference Based MPPT Under Rapidly Changing Irradiance and Load Resistance,” IEEE Trans. On Energy Conv., Vol. 36, No. 3, Sept. 2021.

[1.36] Shengqing, L., Fujun, L., Jian, Z. et al., “An improved MPPT control strategy based on incremental conductance method,” Soft Comput 24, 6039–6046, 2020.

[1.37] Mohamed Lasheen, Ali Kamel Abdel Rahman, Mazen Abdel-Salam and Shinichi Ookawara, “Adaptive reference voltage-based MPPT technique for PV application,” IET Renew, Power Gener., 2017, Vol. 11 lss. 5, PP. 715-722.

[1.38] Yee-Pien Yang and Ming-Tsan Peng, “A Surface-Mounted Permanent-Magnet Motor With Sinusoidal Pulsewidth-Modulation-Shaped Magnets,” IEEE Trans. on Magnetics, Volu.55, Issue: 1, Jan. 2019.

[1.39] Hanyang Yu, Bin Chen, Wenxi Yao and Zhengyu Lu, “Hybrid Seven-Level Converter Based on T-Type Converter and H-Bridge Cascaded Under SPWM and SVM,” IEEE Trans. on Power Electron., Vol. 33, Jan. 2018.

[1.40] Anh Tuan Nguyen, Sang-Wook Ryu, Abd Ur Rehman, Han Ho Choi And Jin-Woo Jung, “Improved Continuous Control Set Model Predictive Control for Three-Phase CVCF Inverters: Fuzzy Logic Approach,” IEEE Access, VOL. 9, 2021.

[1.41] Malay Bhunia, Bidyadhar Subudhi, and Pravat Kumar Ray, “Design and Real-Time Implementation of Cascaded Model Reference Adaptive Controllers for a Three-Phase Grid-Connected PV System,” IEEE Journal of Photovoltaics, Vol. 11, No. 5, September 2021.

[1.42] Vineetha Ravichandran, Sarah K. Rönnberg and Math H.J. Bollen, “Interharmonics in PV systems: a review of analysis and estimation methods; considerations for selection of an apt method,” IET Renew. Power Gener., 2019, Vol. 13 Iss. 12, pp. 2023-2032.

[1.43] Ariya Sangwongwonich, Yongheng Yang, Dezso sera, Hamid Soltni and Frede Blaabjerg, “Interharmonics from grid connected PV systems: Mechanism and Mitigation,” IEEE 3rd international future energy electronics conference and ECCE Asia (IFEEC 2017-ECCE).

[1.44] Ariya Sangwongwonich and Frede Blaabjerg, “Mitigation of Interharmonics in PV Systems with Maximum Power Point Tracking Modification,” IEEE Trans. Power electron, VOL.34, NO. 9, 2019.

[1.45] Mostefa, Abdelkader, Houari Merabet Boulouiha, Ahmed Allali, and Mouloud Denai, “Mitigation of harmonics and inter-harmonics with LVRT and HVRT enhancement in grid-connected wind energy systems using genetic algorithm-optimized PWM and fuzzy adaptive PID control," Journal of Renewable and Sustainable Energy 13, no. 2 (2021): 026302.

[1.46] Ahmad, Salman, Irfan Khan, Atif Iqbal, and Syed Rahman," A Novel Pulse Width Amplitude Modulation for Elimination of Multiple Harmonics In Asymmetrical Multilevel Inverter," In 2021 IEEE Texas Power and Energy Conference (TPEC), pp. 1-6. IEEE, 2021.

[1.47] Nishant Kumar, Bhim Singh, Jihong Wang and Bijaya Ketan Panigrahi, "A Framework of L-HC and AM-MKF for Accurate Harmonic Supportive Control Schemes," IEEE Trans. on circuits and systems–I: regular research works, 2020.

[1.48] Nishant Kumar, Bhim Singh and Bijaya Ketan Panigrahi, "Integration of Solar PV with Low-Voltage Weak Grid System: using Maximize-M Kalman Filter and Self-tuned P&O Algorithm," IEEE Transactions on Industrial Electronics, 2018.

[1.49] Nishant Kumar, Bhim Singh, Bijaya Ketan Panigrahi and L. Xu, "Leaky Least Logarithmic Absolute Difference Based Control Algorithm and Learning Based InC MPPT Technique for Grid Integrated PV System," IEEE Transactions on Industrial Electronics, 2018.

[1.50] Nishant Kumar, Bhim Singh, Bijaya Ketan Panigrahi, Chandan Chakraborty, Hiralal Murlidhar Suryawanshi and Vishal Verma, Member IEEE, "Integration of Solar PV with Low-Voltage Weak Grid System: Using Normalized Laplacian Kernel Adaptive Kalman Filter and Learning Based InC Algorithm," IEEE Transactions on Power Electronics, 2019.

[1.51] Nishant Kumar, Bhim Singh and Bijaya Ketan Panigrahi, "LLMLF Based Control Approach and LPO MPPT Technique for Improving Performance of a Multifunctional Three-Phase Two-Stage Grid Integrated PV System," IEEE Transactions on Sustainable Energy, 2019.

[1.52] Dalila Fares, Mohamed Fathi, Immad Shams and Saad Mekhilef, "A novel global MPPT technique based on squirrel search algorithm for PV module under partial shading conditions," Energy Conversion and Management, 230, 2021, 113773.

[1.53] Kok Soon Tey, Saad Mekhilef, Mehdi Seyedmahmoudian, Ben Horan, Amanullah Than Oo, and Alex Stojcevski, "Improved Differential Evolution-based MPPT Algorithm using SEPIC for PV Systems under Partial Shading Conditions and Load Variation," IEEE Transactions on Industrial Informatics, 2018.

[1.54] Immad Shams, Saad Mekhilef, and Kok Soon Tey, "Maximum Power Point Tracking using Modified Butterfly Optimization Algorithm for Partial Shading, Uniform Shading and Fast Varying Load Conditions," IEEE Transactions on Power Electronics, 2020.

[1.55] Imran Pervez, Immad Shams, Saad Mekhilef, Adil Sarwar, Mohd Tariq, and Basem Alamri, "Most Valuable Player Algorithm based Maximum Power Point Tracking for a Partially Shaded PV Generation System," IEEE Transactions on Sustainable Energy, Vol. 12, No. 4, October 2021.

[1.56] Ratnakar Babu Bollipo, Suresh Mikkili and Praveen Kumar Bonthagorla, "Hybrid, Optimal, Intelligent and Classical PV MPPT Techniques: A Review," CSEE Journal of Power and Energy Systems, Vol. 7, No. 1, January 2021.

[1.57] Ratnakar Babu Bollipo, Suresh Mikkili and Praveen Kumar Bonthagorla, "Critical Review on PV MPPT Techniques: Classical, Intelligent and Optimisation," IET Renew. Power Gener., 2020, Vol. 14 Iss. 9, pp. 1433-1452.

[1.58] H. Patel and V. Agarwal.: 'MATLAB-based modeling to study the effects of partial shading on PV array characteristics', IEEE Trans. Energy Con. vol. 23, no. 1, pp. 302–310, Mar. 2008.

[1.59] Jieming Ma, Xinyu Pan, Ka Lok Man, Xingshuo Li, Huiqing Wen and Tiew On Ting.: 'Detection and Assessment of Partial Shading Scenarios on Photovoltaic Strings', IEEE Trans. on Ind. Applications, VOL. 54, NO. 6, NOV./DEC. 2018.

[1.60] Sanjeev Kumar Pandey, Sanjaykumar Limaji Patil and Shrivijay B. Phadke.: 'PWM-Based Adaptive Sliding-Mode Control for Boost DC–DC Converters', IEEE Trans. on Ind. Electron., vol. 65, no. 6, June 2018.

[1.61] Mohamad Reza Banaei and Sajad Ghabeli Sani.: 'Analysis and Implementation of a New SEPIC-Based Single-Switch Buck–Boost DC–DC Converter with Continuous Input Current', IEEE Trans. on Power Electron., vol. 33, no. 12, Dec. 2018.

[1.62] Indu Rani Balasubramanian, Saravana Ilango Ganesan and Nagamani Chilakapati.: 'Impact of partial shading on the output power of PV systems under partial shading conditions', IET Power Electron., 2014, Vol. 7, Iss. 3, pp. 657–666

[1.63] Amit Kumer Podder, Naruttam Kumar Roy and Hemanshu Roy Pota.: 'MPPT methods for solar PV systems: a critical review based on tracking nature', IET Renew. Power Gener., 2019, Vol. 13 Iss. 10, pp. 1615-1632.

[1.64] Adeel Feroz Mirza, Qiang Ling, M. Yaqoob Javed and Majad Mansoor.: 'Novel MPPT techniques for photovoltaic systems under uniform irradiance and Partial shading', Solar Energy 184 (2019) 628–648.

[1.65] Majad Mansoor, Adeel Feroz Mirza, Qiang Ling and M. Yaqoob Javed.: 'Novel Grass Hopper optimization based MPPT of PV systems for complex partial shading conditions', Solar Energy 198 (2020) 499–518.

[1.66] Aranzazu D. Martin, Jesus R. Vazquez and J.M. Cano.: 'MPPT in PV systems under partial shading conditions using artificial vision', Electric Power Systems Research 162 (2018) 89–98.

[1.67] B. Y. Lin, L. Wang and Q. H. Wu.: 'Maximum Power Point Scanning for PV Systems under Various Partial Shading Conditions', IEEE Trans. on Sustainable Energy, 2020.

[1.68] Yu-Pei Huang, Ming-Yi Huang and Cheng-En Ye.: 'A Fusion Firefly Algorithm with Simplified Propagation for Photovoltaic MPPT under Partial Shading Conditions', IEEE Trans. on Sustainable Energy, 2020.

[1.69] Ali F. Murtaza and Riaz Ahmad.: 'Optical isolation mechanism based MPPT for PV array under partial shading condition', Solar Energy 185 (2019) 516–524.

[1.70] Venkata Reddy Kota and Muralidhar Nayak Bhukya.: 'A novel global MPP tracking scheme based on shading pattern identification using artificial neural networks for photovoltaic power generation during partial shaded condition', IET Renew. Power Gener., 2019, Vol. 13 Iss. 10, pp. 1647-1659.

[1.71] Hong Li, Duo Yang, Wenzhe Su, Jinhu Lu and Xinghuo Yu.: 'An Overall Distribution Particle Swarm Optimization MPPT Algorithm for Photovoltaic System Under Partial Shading', IEEE Trans. on Ind. Electron., VOL. 66, NO. 1, JAN 2019.

[1.72] Neeraj Priyadarshi, Sanjeevikumar Padmanaban, Jens Bo Holm-Nielsen, Frede Blaabjerg and Mahajan Sagar Bhaskar.: 'An Experimental Estimation of Hybrid ANFIS–PSO-Based MPPT for PV Grid Integration Under Fluctuating Sun Irradiance', IEEE Systems Journal, 2019.

[1.73] Thanikanti Sudhakar Babu, J. Prasanth Ram, Tomislav Dragicevic, Masafumi Miyatake, Frede Blaabjerg and Natarajan Rajasekar.: 'Particle Swarm Optimization Based Solar PV Array Reconfiguration of the Maximum Power Extraction Under Partial Shading Conditions', IEEE Trans. on Sustainable Energy, VOL. 9, NO. 1, JAN 2018.

[1.74] Dimas Aji Nugraha, K. L. Lian and Suwarno.: 'A Novel MPPT Method Based on Cuckoo Search Algorithm and Golden Section Search Algorithm for Partially Shaded PV System', canadian journal of electrical and computer engineering, vol. 42, no. 3, summer 2019.

[1.75] Jubaer Ahmed and Zainal Salam.: 'An Enhanced Adaptive P&O MPPT for Fast and Efficient Tracking Under Varying Environmental Conditions', IEEE Trans. ON SUSTAINABLE ENERGY, VOL. 9, NO. 3, JULY 2018.

[1.76] Jubaer Ahmed and Zainal Salam.: 'An Accurate Method for MPPT to Detect the Partial Shading Occurrence in a PV System', IEEE Trans. ON INDUSTRIAL INFORMATICS, VOL. 13, NO. 5, OCTOBER 2017.

[1.77] Abdellatif Kasbi and Abderrafii Rahali, "Adaptive FOPI Controller Based on The Fuzzy Supervisory for Wind Power Conversion System Equipped by A Doubly Fed Induction Generator," Int Trans Electr Energ Syst. 2021, e12923. https://doi.org/10.1002/2050-7038.12923

[1.78] Gonzalo Abad, Jesu´s Lo´pez, Miguel A. Rodrı´guez, Luis Marroyo and Grzegorz Iwanski, "Doubly Fed Induction Machine Modeling and Control for Wind Energy Generation," IEEE Press and John Wiley & Sons Ltd, 2011.

[1.79] Nishad Mendis, Kashem M. Muttaqi, Saad Sayeef and Sarath Perera, "Standalone Operation of Wind Turbine-Based Variable Speed Generators with Maximum Power Extraction Capability," IEEE Trans. Energy Convers., Vol. 27, No. 4, Dec.2012.

[1.80] Krishna S. Patel & Vijay H. Makwana, "Modified Control Technique of DFIG for Power Quality Improvement," IETE Journal of Education, 2021, 62:1,44-54.

[1.81] Fariba Fateh, Warren N. White and Don Gruenbacher, "A Maximum Power Tracking Technique for Grid-Connected DFIG-Based Wind Turbines," IEEE J Emerg Select Top Power Electron, VOL. 3, NO. 4, DEC. 2015.

[1.82] Mousa HHH, Youssef A-R, Mohamed EEM, "Study of robust adaptive step-sizes P&O MPPT algorithm for high-inertia WT with direct-driven multiphase PMSG," Int Trans Electr Energ Syst., 2019, 29: e12090. https://doi.org/10.1002/2050-7038.12090

[1.83] Ali Darvish Falehi, "An innovative optimal RPO-FOSMC based on multi-objective grasshopper optimization algorithm for DFIG-based wind turbine to augment MPPT and FRT capabilities," Chaos, Solitons and Fractals 130, 2020, 109407.

[1.84] Abdel-Raheem Youssef, Ahmed I.M. Ali, Mahmoud S.R. Saeed and Essam E.M. Mohamed, "Advanced multi-sector P&O maximum power point tracking technique for wind energy conversion system," Electrical Power and Energy Systems, 107, 2019, 89–97.

[1.85] Jie Wang and Didi Bo, "Adaptive fixed-time sensorless maximum power point tracking control scheme for DFIG wind energy conversion system," Int J Electr Power Energy Syst., 135, 2022, 107424.

[1.86] Bo Yang, Xiaoshun Zhang, Tao Yu, Hongchun Shu and Zihao Fang, "Grouped grey wolf optimizer for maximum power point tracking of doubly-fed induction generator-based wind turbine," Energy Conversion and Management, 133, 2017, 427–443.

[1.87] Hamid Chojaa, Aziz Derouich, Seif Eddine Chehaidia, Othmane Zamzoum, Mohammed Taoussi and Hasnae Elouatouat, "Integral sliding mode control for DFIG based WECS with MPPT based on artificial neural network under a real wind profile," Energy Reports, 7, 2021, 4809–4824.

[1.88] K. Belmokhtar, M.L. Doumbia and K. Agbossou, "Novel fuzzy logic based sensorless maximum power point tracking strategy for wind turbine systems driven DFIG (doubly-fed induction generator)," Energy, 76, 2014, 679e693.

[1.89] Kunlun Han, Tianwei Huang and Linfei Yin, "Quantum parallel multi-layer Monte Carlo optimization algorithm for controller parameters optimization of doubly-fed induction generator-based wind turbines," Applied Soft Computing, 112, 2021, 107813.

[1.90] Ahmed Fathy, Abdullah G. Alharbi, Sulaiman Alshammari and Hany M. Hasanien, "Archimedes optimization algorithm based maximum power point tracker for wind energy generation system," Ain Shams Engineering Journal, 2021.

[1.91] Jeroen D.M. De Kooning, Arash E. Samani, Simon De Zutter, Jeroen De Maeyer and Lieven Vandevelde, "Techno-economic optimisation of small wind turbines using co-design on a parametrised model," Sustainable Energy Technologies and Assessments, 45, 2021, 101165.

[1.92] Mohammad Mahdi Rezaei, "A nonlinear maximum power point tracking technique for DFIG-based wind energy conversion systems," Engineering Science and Technology, an International Journal, 21, 2018, 901–908.

[1.93] Ganesh P. Prajapat, N. Senroy and I.N. Kar, “Estimation based enhanced maximum energy extraction scheme for DFIG-wind turbine systems,” Sustainable Energy, Grids and Networks, 26, 2021, 100419.

[1.94] Yuliang Sun, Shaomin Yan, Bin Cai, YuqiangWu and Zhongcai Zhang, “MPPT Adaptive Controller of DC-based DFIG in Resistances Uncertainty,” International Journal of Control, Automation and Systems, 19(8), 2021, 2734-2746.

[1.95] James Kennedy and Russell Eberhart, “Particle Swarm Optimization,” IEEE, 1995.

[1.96] Salmi Hassan, Badri Abdelmajid, Zegrari Mourad, Sahel Aicha and Baghdad Abdennaceur, “PSO-Backstepping controller of a grid connected DFIG based wind turbine,” International Journal of Electrical and Computer Engineering (IJECE), Vol. 10, No. 1, Feb. 2020, pp. 856-867.

[1.97] Masafumi Miyatake, Mummadi Veerachary, Fuhito Toriumi, Nobuhiko Fujii and Hideyoshi Ko, “Maximum Power Point Tracking of Multiple Photovoltaic Arrays: A PSO Approach,” IEEE Trans On Aerospace and Electronic Systems, Vol. 47, No. 1, Jan. 2011.

[1.98] B. Srikanth Goud, P. Srinivasa Varma, B. Loveswara Rao, M. Sai Krishna Reddy, A. Pandian and Ch. Rami Reddy, “Cuckoo Search Optimization based MPPT for Integrated DFIG-Wind Energy System,” IEEE International Conference on Decision Aid Sciences and Application (DASA), 2020.

[1.99] Kashif Ishaque, Zainal Salam, Muhammad Amjad, and Saad Mekhilef, “An Improved Particle Swarm Optimization (PSO)–Based MPPT for PV With Reduced Steady-State Oscillation,” IEEE Trans. Power Electron., Vol. 27, No. 8, Aug. 2012.

[1.100] Kinattingal Sundareswaran, Peddapati Sankar, P. S. R. Nayak, Sishaj P. Simon, and Sankaran Palani, “Enhanced Energy Output from a PV System Under Partial Shaded Conditions Through Artificial Bee Colony,” IEEE Trans. Sustain. Energy, Vol. 6, No. 1, Jan. 2015.

INTER-HARMONICS AND ITS MITIGATION TECHNIQUES

2.1 INTRODUCTION

The harmonics are further classified into inter-harmonics, which are the non-integer multiples of the fundamental operating frequency. The inter-harmonic reduction with respect to MPPT efficiency is proved to be a burning research topic at present. Since the reduction of inter-harmonics ultimately to reduction in power efficiency. Therefore, in this work major focus is drawn towards reducing inter-harmonics along with better MPP tracking efficiency.

The single diode model is the frequently employed approach for solar cell construction with considerable accuracy [2.1-2.2]. Under uniform irradiation and sudden change in irradiation cases, solar panel exhibits non-linear electrical characteristics [2.3-2.4]. A boost converter is the most commonly used power electronic converter in the PV generation because of its easy topology, lower cost, and excellent maximum power point (MPP) tracking efficiency [2.5-2.7].

To better utilize available PV panel power different MPPT schemes regulate the switching pulses for the power electronic converter [2.8-2.10]. The available MPPT techniques are broadly categorized into conventional and advanced MPPT schemes [2.11]. In conventional MPPT schemes, Perturb and Observe (P&O) method is the utmost straightforward, effective one with good tracking efficiency [2.12-2.14]. Modified Perturb and observe scheme (MP&O) is the developed version of P&O with an additional current component [2.15].

Constant Voltage (CV) MPPT requires a single sensor for tracking maximum power; it is more economical related to available MPPT techniques [2.16-2.18]. Out of the available PWM methods, sinusoidal pulse width modulation (SPWM) is extensively employed for its simpler control structure and easier implementation [2.19-2.20].

The PV-based inverters with oscillating input and non-ideal switching, can lead to the generation of harmonics into the system [2.21-2.24]. The inter harmonic modelling and analysis of the grid-connected solar system is already done, the role of MPPT in Inter-harmonics are also analyzed in [2.25]. The Mitigation of Inter-harmonics is still a burning research topic for modern researchers.

Although very few pieces of literature exist in the reduction of Inter-harmonics for PV-grid integrated systems, most of the presented schemes do not address the MPPT efficiency and drifts due to sudden changes in irradiation. [2.26] and [2.27] are the literature available for the reduction of Interharmonics with modification in MPPT under low power conditions. Inter-harmonic mitigation for wind energy system has been demonstrated in [2.28-2.29]. However, all these works do not address the inter harmonic elimination for PV-based systems. Many MPPT schemes [2.34-2.41] are introduced for better MPPT process, but they are very difficult to implement while coming to real time situation [2.42-2.43].

In this research work, INHARE MPPT is proposed; it displays improved dynamic characteristics compared to P&O and CV-based MPPT schemes. Unlike P&O, INHARE MPPT scheme avoids drift due to sudden changes in irradiation because of its weather-sensitive nature. The proposed scheme avoids the inefficiency problem in CV-based schemes under the inter-harmonic elimination process. The proposed INHARE scheme is easy to implement in real-time, as it does not require memory for tracking maximum power points like [2.18].

The INter-HARmonic-Elimination (INHARE) MPPT algorithm has been established to remove the drawbacks of the existing schemes [2.26] & [2.27]. The INHARE algorithm is able to reduce the inter-harmonics, along with maintaining good tracking efficiency, unlike [2.26], where the latter fails at maintaining maximum efficiency at lower irradiation cases. Compared with [2.27], the proposed INHARE displays better drift avoidance along with inter-harmonic reduction due to its weather-sensitive nature. The proposed INHARE MPPT scheme tends to reduce the inter-harmonics by improving the dynamics of the input to the inverter from the solar panel. The proposed scheme reduces the settling time, oscillating behaviour over the steady state, and drift due to sudden change in irradiation in the input of the inverter, leading to inter-harmonic reduction.

2.2 SCHEMSES BEHIND DEVELOPING INHARE MPPT SCHEME

2.2.1 P&O based MPPT schemes

The method of tracking the peak power developed in the solar panel is termed MPPT. It is achieved by controlling the pulse widths of the converter switches to make the load impedance on par with the input impedance of the solar panel.

2.2.1.1 Conventional Perturb and Observe (P&O) Algorithm: P&O is a conventional method, which is mostly known for its simple structure and secure real-time implementation with lower cost [2.12-2.13]. This method requires the solar panel current and voltage as inputs to the MPPT block for tracking maximum power point (MPP). In P&O, solar panel power is derived after multiplying the current and voltage followed by variation in the duty cycle. Comparing old and new calculated powers is used to track the MPP.

2.2.1.2 Modified Perturb and Observe (MP&O) Algorithm: In the MP&O algorithm, drift avoidance with an abrupt variation in insolation is addressed with the SEPIC converter [2.15]. Even though the single-ended primary-inductance converter (SEPIC) converter displays better tracking properties, it results in the major disadvantage of power loss due to extra components in its circuit. So, in this research work, drift avoidance is treated with a boost converter. The sudden drift in tracking maximum power is neglected by introducing the additional current component into the standard P&O scheme, as displayed in Fig. 2.1.

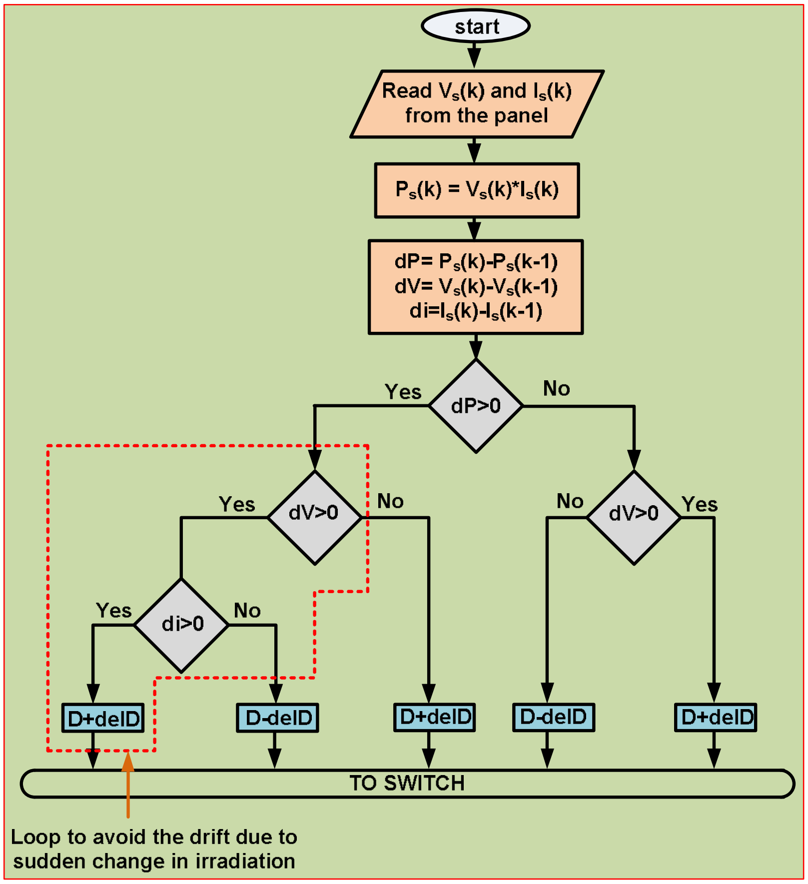

Fig. 2.1. Flow chart for Modified Perturb and Observe (MP&O) algorithm.

The power drift can be more in the P&O method compared to the MP&O scheme. The voltage relation of boost converter can be formulated as [2.18],

$$V_{out} = \left(\frac{1}{1-D}\right)V_s \tag{2.1}$$

Where D is duty cycle, V_s is solar panel voltage V_{out} is the output voltage. It is already known fact that the efficiency is calculated as a ratio of output and input power. It is known that the efficiency (η) of converter is [2.15],

$$\eta = \frac{V_{out} I_{out}}{V_s I_s} \tag{2.2}$$

Where I_{out} is output current and I_s is solar panel current. By substituting (2.1) in (2.2), the conversion efficiency is derived as,

$$\eta = \frac{V_{out} I_{out}}{V_s^2 / R_{in}} = \left[\frac{V_{out}}{V_s}\right]^2 \frac{R_{in}}{R_{load}} = \left[\frac{1}{1-D}\right]^2 \frac{R_{in}}{R_{load}} \tag{2.3}$$

Where R_{in} denotes the overall resistance of the converter experienced by the solar panel and R_{load} is load resistance. Rearranging (2.3),

$$R_{in} = \eta(1-D)^2 R_{load} \tag{2.4}$$

From (2.4), it can be concluded that R_{in} varies with the change in the duty cycle (*D*), which indirectly implies that the maximum power transfer point can be obtained, where the load impedance equals the source impedance. The V_s and I_s can be related as,

$$I_s = \frac{V_s}{\eta R_{load}(1-D)^2} \tag{2.5}$$

Basic equation for the solar cell modelling can be formulated as [2.2],

$$I_s = I_{sc} - I_o\left[e^{\frac{V_s}{a*v_{th}}} - 1\right] - \frac{V_s + R_{se}I_s}{R_{pa}} \tag{2.6}$$

Where I_{sc} is short-circuited current of the solar panel, *a* is the ideal diode factor, V_{th} is the thermal voltage, R_{se} is the series resistance of the single diode solar cell model, I_o is diode saturation current and R_{pa} is the parallel resistance of single diode solar cell model. Relieving I_s from (2.5) into (2.6) and by employing first-order expansion of Taylor's series, (2.6) becomes,

$$V_s \frac{1}{\eta R_{load}(1-D)^2} = I_{sc} - I_o\frac{V_s}{a*v_{th}} - \frac{V_s}{R_{pa}} - \frac{R_{se}}{R_{pa}}\frac{V_s}{\eta R_{load}(1-D)^2} \tag{2.7}$$

Shortening (2.7) by means (2.5), the equations for PV panel voltage and current are derived as,

$$V_s = \frac{I_{sc}}{\frac{1}{\eta R_{load}(1-D)^2}\left[1+\frac{R_{se}}{R_{pa}}\right] + \frac{I_o}{a*v_{th}} + \frac{1}{R_{pa}}} \tag{2.8}$$

$$I_s = \frac{1}{\eta R_{load}(1-D)^2}\frac{I_{sc}}{\frac{1}{\eta R_{load}(1-D)^2}\left[1+\frac{R_{se}}{R_{pa}}\right] + \frac{I_o}{a*v_{th}} + \frac{1}{R_{pa}}} \tag{2.9}$$

Where Short circuit current (I_{sc}) at an irradiance (*Ir*) can be shown in terms of short circuit current at standard test condition (STC) is,

$$I_{sc} = \left[I_{sc,ref} + K_I \Delta T_e\right]\frac{Ir}{Ir_{ref}} \tag{2.10}$$

Where is K_I short-circuit temperature coefficient, Ir_{ref} is nominal irradiance, $\Delta T_e = T - T_{no}$ (T, T_{no} are actual and nominal temperatures) and $I_{sc,ref}$ is short circuit current at nominal condition. By substituting (2.10) in (2.8) and (2.9) and then by taking derivatives of V_s and I_s in regard to irradiance, the resultant equations are,

$$\frac{dV_s}{dIr} = \frac{\left(I_{sc,ref} + K_I \Delta T_e\right)\frac{1}{Ir_{ref}} + K_I \frac{Ir}{Ir_{ref}}\frac{dT}{dIr}}{\frac{1}{\eta R_{load}(1-D)^2}\left[1+\frac{R_{se}}{R_{pa}}\right] + \frac{I_o}{a*v_{th}} + \frac{1}{R_{pa}}} \quad (2.11)$$

$$\frac{dI_s}{dIr} = \frac{1}{\eta R_{load}(1-D)^2}\frac{\left(I_{sc,ref} + K_I \Delta T_e\right)\frac{1}{Ir_{ref}} + K_I \frac{Ir}{Ir_{ref}}\frac{dT}{dIr}}{\frac{1}{\eta R_{load}(1-D)^2}\left[1+\frac{R_{se}}{R_{pa}}\right] + \frac{I_o}{a*v_{th}} + \frac{1}{R_{pa}}} \quad (2.12)$$

$$\frac{dV_s}{dIr} = \frac{\left(I_{sc,ref} + K_I \Delta T_e\right)\frac{1}{Ir_{ref}}}{\frac{1}{\eta R_{load}(1-D)^2}\left[1+\frac{R_{se}}{R_{pa}}\right] + \frac{I_o}{a*v_{th}} + \frac{1}{R_{pa}}} \quad (2.13)$$

$$\frac{dI_s}{dIr} = \frac{1}{\eta R_{load}(1-D)^2}\frac{\left(I_{sc,ref} + K_I \Delta T_e\right)\frac{1}{Ir_{ref}}}{\frac{1}{\eta R_{load}(1-D)^2}\left[1+\frac{R_{se}}{R_{pa}}\right] + \frac{I_o}{a*v_{th}} + \frac{1}{R_{pa}}} \quad (2.14)$$

From (2.11) and (2.12), dT/dIr is a positive value, as the rate of temperature change is proportional to the variation in irradiance. In the proposed system, sudden change in irradiation is addressed with constant temperature value, so the value can be considered zero. Therefore, (2.11) and (2.12) become (2.13) and (2.14). From (2.13) and (2.14), both dV_s/dIr and dI_s/dIr will be positive as all other constants are positive. Therefore, the conditions $dV_s/dIr > 0$ and $dI_s/dIr > 0$ are valid with the situation of sudden change in irradiation [2.15]. Hence, the drift due to sudden change in irradiation can be avoided by introducing ΔI term into the P&O algorithm. Except for the drift avoidance, remaining all operating characteristics of P&O and MP&O are almost the same.

2.2.2 CV-based MPPT schemes

The MPPT algorithm should be implemented such that the generation of lower-order Inter-harmonics are to be reduced. Although the Constant Voltage (CV) algorithm in [2.26] reduces Inter-harmonics, the same is not preferable due to its insensitivity to irradiation and temperature.

CV MPPT fails at lower irradiation levels and displays better tracking characteristics at greater insolation levels [2.18]. The CV MPPT topology is represented in Fig. 2.2, where reference voltage (V_{ref}) is equal to $K_1 \times V_{oc}$, V_{oc} is the open-circuit voltage at STC and K_1 ranges from 0.7 to 0.8.

The adaptive reference voltage (ARV) MPPT is the developed form of the CV. In ARV MPPT, two sensors (irradiation and temperature) and a memory unit are employed to produce reference voltage [2.18]. For the different values of irradiations and temperatures, the voltages at which maximum power point is seen are deposited in memory, and in the future, they are employed as reference voltages. This reference voltage is related to the solar panel voltage, and the difference is given to the PI controller to produce the respective gate pulse for converter switching.

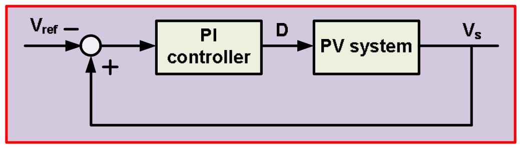

Fig. 2.2. Block diagram for Constant Voltage (CV) algorithm (v_{ref} is reference voltage).

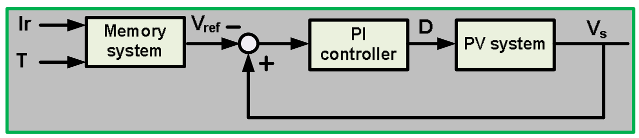

Fig. 2.3. Block diagram for the ARV MPPT scheme.

The PI controller mainly operates to improve the system's dynamics and make the oscillation over a steady-state almost equal to zero. The outline schematic figure of ARV MPPT is represented in Fig. 2.3, it has the disadvantage of requiring a large memory capacity of the processor resulting in higher cost and processing time.

2.2.3 Maximum Power Point Tracking Effects

For Inter-harmonic reduction, lower output ripple and faster tracking are required. Besides this, drift due to change in irradiation should be eliminated. By adjusting stepping size in duty cycle/voltage (*delD/delV*), both settling time and ripple can be varied in P&O and MP&O as,

1. An Increase in *delD/delV* results in less settling time (fast-tracking) but more ripple.
2. A decrease in *delD/delV* results in more settling time (slow tracking) but less ripple.

Ultimately, it can be observed that none of the above cases will result in Inter-harmonics reduction with good dynamic characteristics. Moreover, increasing MPPT sampling frequency (f_{MPPT}) can improve the tracking performance, but the same is not preferred due to the dynamic of the DC-link voltage controller. For the instance of varied irradiation under constant temperature, P&O MPPT shows drift in the tracking path leading to the fluctuation in output. This drift results in the introduction of Inter-harmonics into the system. Many studies revealed that MPPT in PV-inverter combination plays a vital role in the Inter-harmonic injection into the load and the grid [2.25].

The Inter-harmonic elimination issue is addressed with CV MPPT and P&O with sampling rate control; it is observed that lower-order Inter-harmonics content is decreased considerably under more moderate power operation [2.26-2.27]. The main drawbacks with [2.26] & [2.27] are their inefficiency in MPPT tracking under lower irradiation conditions and oscillation under a sudden change in irradiation. ARV MPPT can reduce Inter-harmonics more effectively and also can maintain excellent tracking efficiency at all available irradiation conditions. Still, the same is not preferable due to the requirement of large memory processing units, leading to enormous processing cost. INHARE MPPT overcomes the drawbacks of P&O-based and CV-based MPPT schemes. INHARE scheme can reduce Interharmonics by maintaining excellent tracking efficiency at all available irradiation cases.

Moreover, INHARE MPPT is economical since there is no requirement of the memory unit, unlike ARV MPPT.

2.3 PROPOSED INHARE MPPT SCHEME

2.3.1 Proposed System Block Diagram

In the present research work, the proposed Inter-HARmonic-Elimination technique has been termed as INHARE algorithm. Fig. 2.4, denotes the overall block diagram for the proposed system. Since the proposed scheme is more related to the MPPT scheme, inverter control is not much discussed in the proposed work. In the proposed system, the dc-link voltage and load current are controlled similar to that of [2.30], [2.31], and [2.25]. The proposed INHARE MPPT system's design specifications are represented in Table-2.1, where R_{Load} is load resistance, L_{Load} is load inductance, R_{DS} is drain-source resistance and V_{GS} is gate-source voltage. The proposed MPPT algorithm is derived using P&O-based and CV-based algorithms. INHARE is proposed to address the Inter-harmonic issue by decreasing ripple, settling time and, eliminating the drifting problem due to sudden changes in irradiation, and maintaining MPPT efficiency.

Even though ARV MPPT is advantageous compared to Perturb and observe (P&O), modified P&O (MP&O), and constant voltage (CV) MPPT schemes, it has the major disadvantage of requiring a huge processing memory unit. Moreover, the system should underdo difficult initial work in storing maximum power point (MPP) voltage values all over the day. With the change in configuration of the system, the initial work is to be carried out again; this makes the system complex while coming to real-time situations. The proposed INHARE MPPT, sensed irradiation, and temperature values of a single solar panel are sufficient to track maximum power. Even if the system is expanded into a larger farm of series-connected solar panels, as shown in Fig. 2.4, single irradiation and temperature sensors are sufficient in tracking MPP. This itself makes INHARE MPPT simpler while coming to hardware implementation.

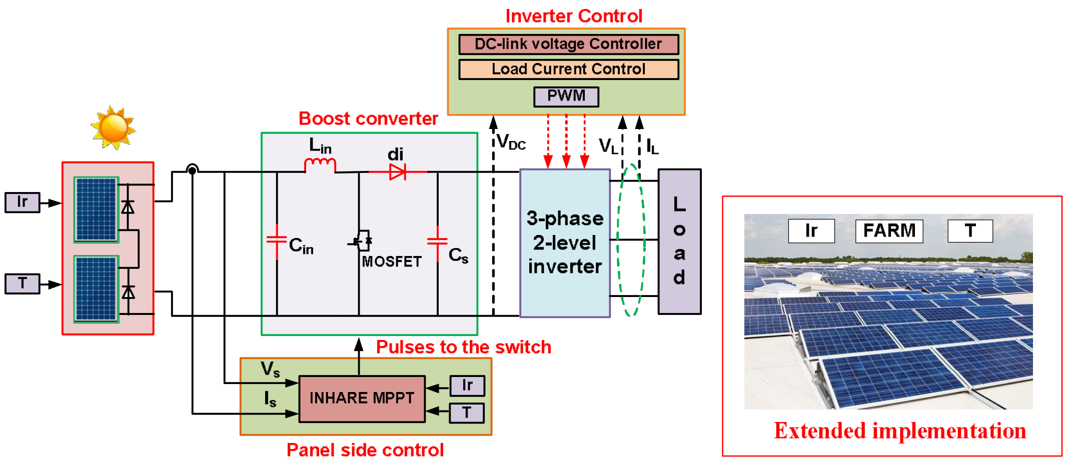

Fig. 2.4. Block diagram of the overall proposed PV standalone system along with extended implementation (*L_{in}* is inductance, *C_{in}* is input capacitor, *di* is a diode, *C_s* is the output capacitor, , *Ir* is irradiance, *T* is temperature, V_L is load voltage, V_{DC} is dc-link voltage and I_L is loaded current and *PWM*-Sinusoidal Pulse Width Modulation)

Table 2.1. Design specifications of standalone PV system

Load	
R_{Load}	25 ohms
L_{Load}	1.5 mH
Boost Converter	
L_{in}	1.371 mH
C_{in}	10 μF
C_s	83.583 μF
Switching frequency (f_{sw})	25 kHz
Inverter	
K2611 (MOSFET)	11A,900V, R_{DS} (on) (Max1.10Ω) @ V_{GS}=10V

The change in temperature leads to an increase in the inter-harmonics content, as there is a fluctuation in output tracking characteristics [2.32]. Since the proposed INter-HARmonic-Elimination (INHARE) algorithm is atmosphere sensitive, it overcomes the case of sudden temperature change. The temperature variation is very minute compared to irradiation changes in real-time. Therefore, in the proposed system, sudden change in irradiation at constant temperature is considered for the MPPT process.

Because of the influence on dc-link voltage, the time varying loads (arc furnace, etc.) are one reason behind inter-harmonics generation. The proposed INHARE MPPT is established to effectively mitigate inter-harmonics related to MPPT compared to few existing schemes. But, similar to [2.27], the proposed work primarily addresses the inter-harmonics production due to MPPT.

2.3.2 Flow Chart for Proposed INHARE MPPT Scheme

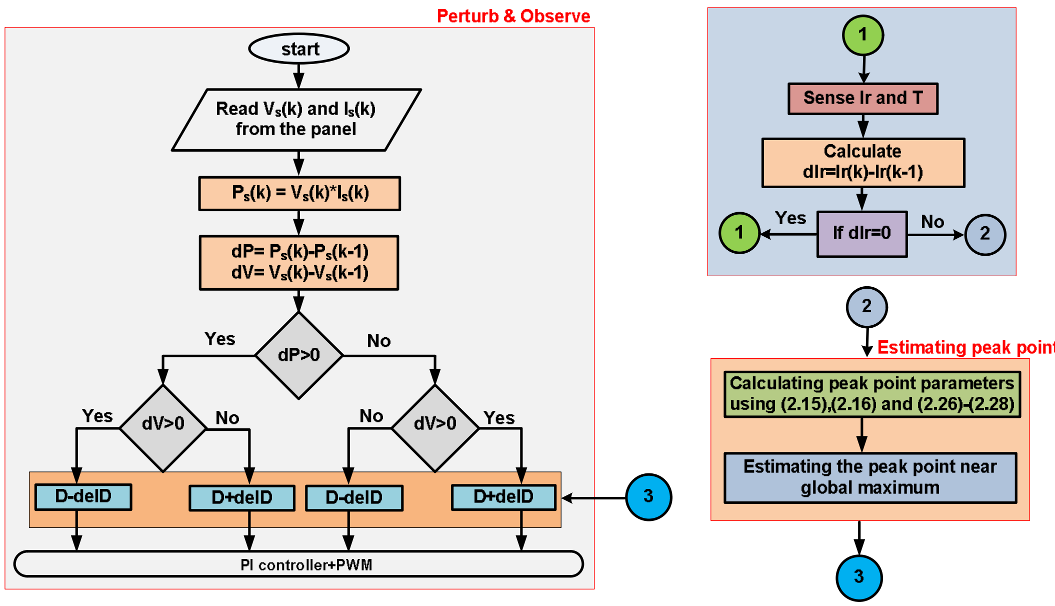

Fig. 2.5. Flow chart for proposed INHARE MPPT algorithm

In Fig. 2.5, the schematic flow chart of the proposed INHARE MPPT is presented. The major difference between INHARE and existing P&O and CV based algorithms is the estimating peak point loop, as shown in Fig. 2.5. In this Proposed INHARE MPPT, the tracking error is given as an input to the PI controller in generating the duty cycle for switching.

2.3.2.1 Settling time and ripple control

$$I_{sc} = I_{sc,ref}\left[1+\alpha\left(T-T_{ref}\right)\right]\frac{Ir}{Ir_{ref}} \quad (2.15)$$

$$V_{oc} = V_{oc,ref}\left[1+a\times\ln\frac{Ir}{Ir_{ref}}+\beta\left(T-T_{ref}\right)\right] \quad (2.16)$$

The short-circuit current and open-circuit voltage are calculated as a function of irradiance and temperature, using (2.15) and (2.16). Where T_{ref} is the temperature at STC and $V_{oc,ref}$ open-circuit voltage at STC condition. Whereas the peak point, voltage (V_m), current (I_m) and power (P_m) respectively are calculated using,

$$V_m = K_2 * V_{oc} \quad (2.17)$$

$$I_m = K_3 * I_{sc} \quad (2.18)$$

$$P_m = V_m * I_m \tag{2.19}$$

From (2.17) and (2.18), the unknown values K_2 and K_3 are calculated as,

$$K_2 = \left.\frac{V_{\mathrm{m}}}{V_{oc}}\right|_{STC} \tag{2.20}$$

$$k_3 = \left.\frac{I_{\mathrm{m}}}{I_{sc}}\right|_{STC} \tag{2.21}$$

The MPP is determined near the peak point using the outcomes from (2.15)-(2.21). This estimated maximum peak is employed as the initial point for P&O in tracking Maximum power. This results in reducing the response time of the overall system.

In INHARE MPPT, proportional and integral (PI) controller reduces the settling time and ripple content. Increasing the proportional gain (K_p) will reduce the rise time, it is capable of reducing the steady-state error (e_{ss}) but will not make it completely zero and also, there is an increase in overshoot. Increasing integrator gain (K_I) has the advantage of making e_{ss} almost equal to zero, but it will increase the settling time and overshoot of the system. So K_p and K_I gains are adjusted such that the system will have the required settling time and ripple content.

2.3.2.2 Drift control

In INHARE algorithm, there is no deflection in the tracking path during a sudden change in irradiation, this can be explained with Fig. 2.6. Let the maximum power point (MPP) voltage be the one where the maximum power is seen. For an abrupt variation in irradiation at a constant temperature, the tracking point 1 shift to point 2. In the case of the P&O MPPT scheme, when the change in power and voltage is positive, the tracking decreases in the duty cycle, resulting in moving away from the MPP voltage line to point 3. While coming to the INHARE, the new peak point 2 is compared with the estimated peak point generated by sensing irradiation and temperature, making it track towards point 4, which is nearer MPP voltage [2.15]. Including the reduction in fluctuation, PI controller makes it settle faster in case of a sudden change in irradiation, making the proposed scheme more effective than MP&O.

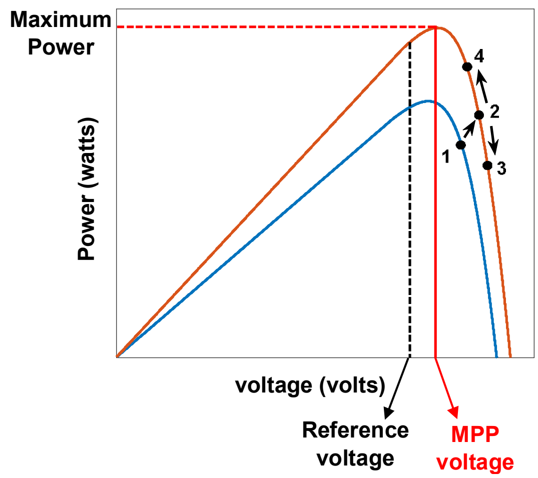

Fig. 2.6. Drift avoidance during a sudden change in irradiation

2.3.3 Proposed INHARE algorithm for series configuration

Table-2.2 displays the manufacturer specifications for the solar panel construction. Fig. 2.7 represents PV modules' P-V & I-V characteristics for various insolation levels at a standard testing condition (STC) temperature of 25^{0}C. From Fig. 2.7, the maximum power (P_m) seen for each irradiance and also the respective current (I_m) and voltage (V_m) at which this power is observed are formed in Table-2.3.

In the proposed system, the 2S configuration is operated with two sets. For set 1, 2S configuration is assumed to be operated under irradiation levels of 144 W/m^2. Similarly, for set 2, 2S configuration is assumed to be operated under irradiation levels of 253 W/m^2. For considered set 1, output characteristics are represented in Fig. 2.8a. By comparing the peak values of voltage (V_p) and current (I_p) of Fig. 2.8a with Table-2.3 characteristics, it is derived that,

$$V_p\big|_{2S*144} \approx 2*V_m\big|_{144} \tag{2.22}$$

$$I_p\big|_{2S*144} \approx I_m\big|_{144} \tag{2.23}$$

Where $V_p\big|_{2S*144}$ is peak voltage for 2S configuration at 144 W/m^2, $V_m\big|_{144}$ is peak voltage for single panel configuration at 144 W/m^2, $I_p\big|_{2S*144}$ is peak current for 2S configuration at 144 W/m^2 and $I_m\big|_{144}$ is peak voltage for single panel configuration at 144 W/m^2. Similarly, by comparing the peak values of Fig. 8b with Table-2.3 characteristics, it is derived that,

$$V_p\big|_{2S*253} \approx 2*V_m\big|_{253} \tag{2.24}$$

$$I_p\big|_{2S*253} \approx I_m\big|_{253} \tag{2.25}$$

Where $V_p|_{2S*253}$ is peak voltage for 2S configuration at 253 W/m^2, $V_m|_{253}$ is peak voltage for single panel configuration at 253 W/m^2, $I_p|_{2S*253}$ is peak current for 2S configuration at 253 W/m^2 and $I_m|_{253}$ is peak voltage for single panel configuration at 253 W/m^2. By observing (2.22)-(2.25), it is formulated that, peak characteristic of series configuration can be derived as,

$$V_p = N * K_2 * V_{oc} \tag{2.26}$$

$$I_p = K_3 * I_{sc} \tag{2.27}$$

$$P_p = V_p * I_p \tag{2.28}$$

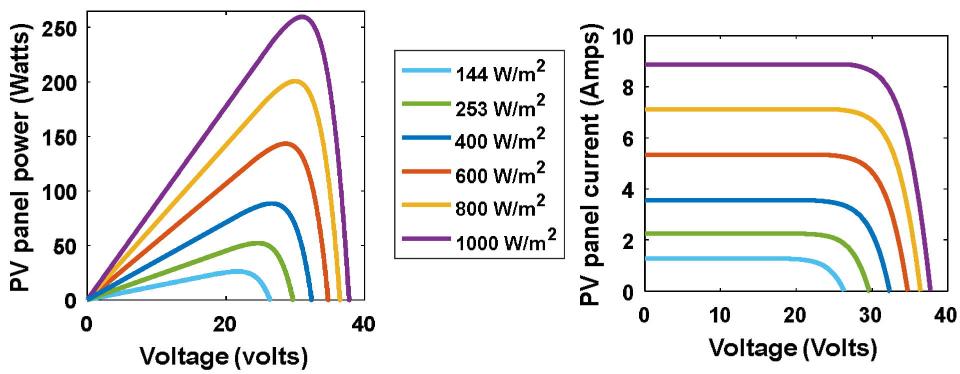

Fig. 2.7. P-V and I-V characteristics for a single solar panel

Where P_p is peak power and N is the number of series-connected modules. By using (2.22)-(2.28), the peak values of set 1&2 cases are compared with actual peak values as represented in Table-2.4. It is derived from Table-2.4 that, by employing the proposed INHARE algorithm, the estimation of peak point can be done with precision. This, initial estimated peak point is used as a reference point for P&O to start tracking, resulting in a lower settling time.

2.4 SIMULATION OUTPUTS AND DISCUSSIONS

2.4.1 MPPT comparison between CV, ARV and proposed INHARE

For observing the comparison of INHARE MPPT with CV and ARV, the proposed system is operated for the step-up change from set 1 to set 2 and step-down change from set 2 to set 1. Moreover, both these step changes are applied at the time period of 0.62 sec. From Fig. 2.9a and 2.9b, it is noted that, the INHARE algorithm has similar convergence speed compared to CV MPPT. But, coming to lower irradiation cases, proposed scheme displays better MPP tracking efficiency over CV MPPT. Also, the INHARE MPPT scheme is easy real-time implementable compared to the ARV MPPT scheme, as it does not require any memory unit to track maximum power.

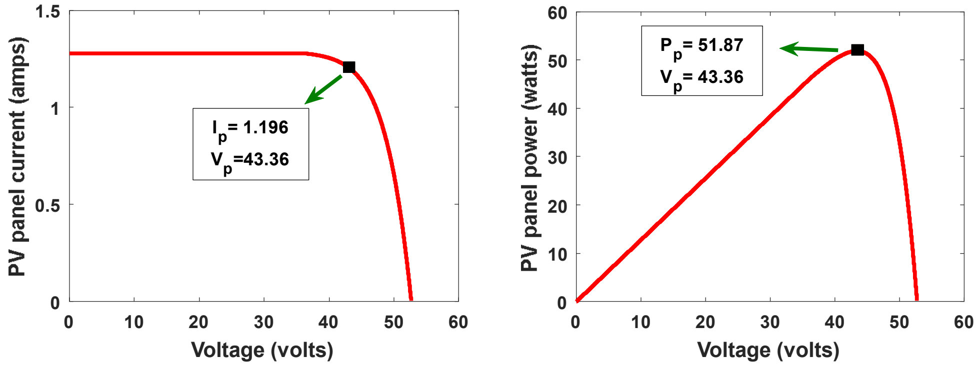

a

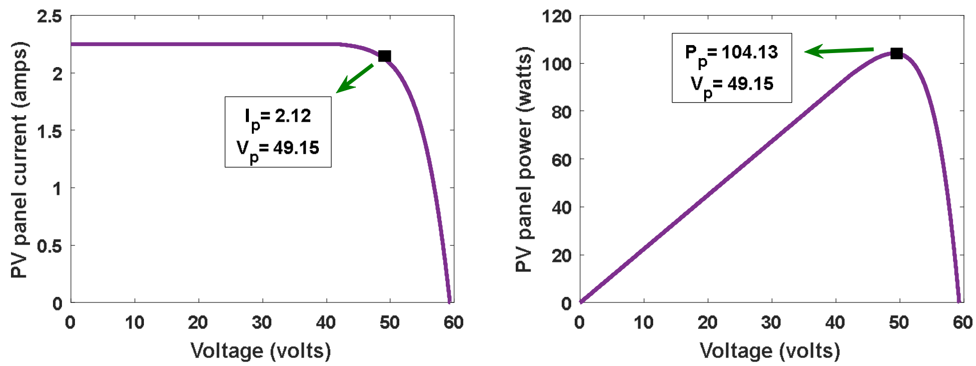

b

Fig. 2.8. P-V and I-V characteristics of considered sets of 2S configuration patterns (a. Set 1 and b. Set 2)

2.4.2 MPPT comparison between proposed INHARE, P&O and MP&O

Table 2.2. Electrical characteristics of PV module of 260 watts

VARIABLE	QUANTITY
Maximum power at MPPT	260 watts
Voltage at MPPT	30.88 volts
Current at MPPT	8.42 amps
Short Circuit Current	8.98 amps
Open Circuit Voltage	37.75 volts
Temperature coefficient of short circuit current	0.04%/^{0}C
Temperature coefficient of open circuit voltage	-0.325%/^{0}C

For observing the comparison of INHARE MPPT with P&O and MP&O, the proposed system is operated for the step-up change from set 1 to set 2 and step-down change from set 2 to set 1. Moreover, both these step changes are applied at the time period of 0.62 sec. It is known that the drift phenomenon is a major issue under step-up variation compared with step-down change

[2.15]. From Fig. 2.10a, it can be noted that the P&O scheme undergoes more drift in power than MP&O and INHARE MPPT schemes.

Table 2.3. I_m, V_m and P_m for 1S-configuration

IRRADIATION (W/m²)	TEMPARATURE (°c)	I_m (Amps)	V_m (Volts)	P_m (Volts)
144	25	1.1960	21.6834	25.9334
253	25	2.1184	24.5779	52.0658
400	25	3.3654	26.8291	90.2904
600	25	5.0635	28.6911	145.2768
800	25	6.7626	29.8940	202.1601
1000	25	8.4625	30.7235	259.999

Table 2.4. Comparison of actual and calculated peak values at different irradiation cases

Set	I_p (Amps)		V_p (Volts)		P_p (Watts)	
	Actual	estimated	Actual	estimated	Actual	estimated
1	1.196	1.196	43.36	43.3668	51.87	51.867
2	2.12	2.1184	49.15	49.1558	104.13	104.132

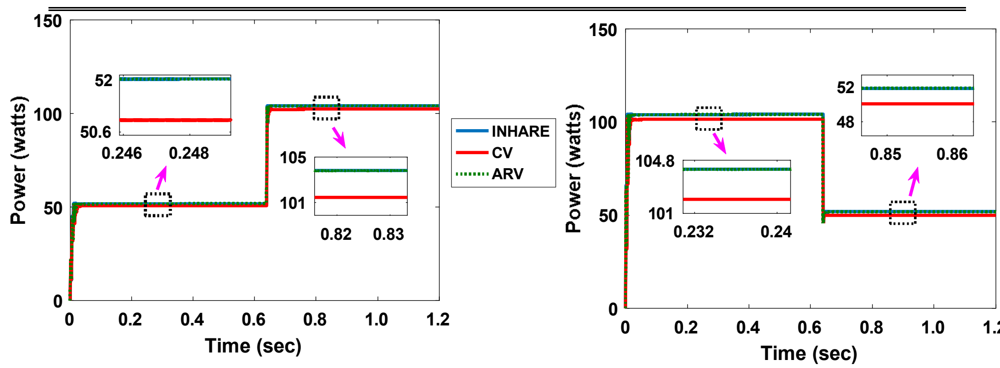

a b

Fig. 2.9. Comparison of MPP tracking between CV, ARV and INHARE (a. Step-up and b. Step-down)

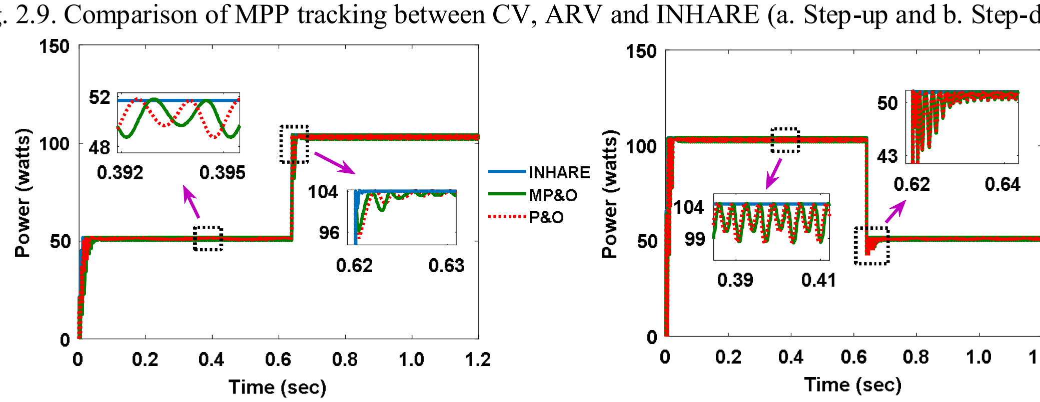

a b

Fig. 2.10. Comparison of MPP tracking between P&O, MP&O and INHARE (a. Step-up and b. Step-down)

Leaving the drift avoidance, the operating characteristics between P&O and MP&O are almost the same. From Fig. 2.10b, it can be noted that the INHARE MPPT scheme converges faster (14.38ms) than P&O (26.17ms) and MP&O (26.16ms) schemes.

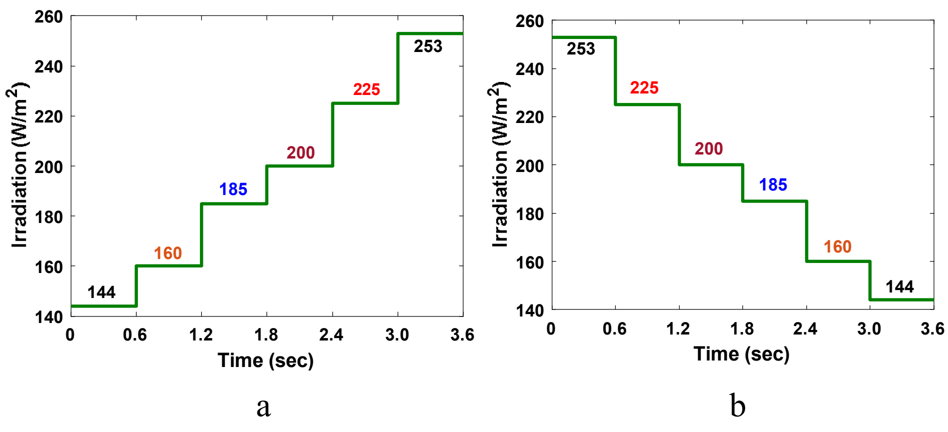

Fig. 2.11. Five-step variations in irradiation levels (a. Step-up and b. Step-down)

2.4.3 Interharmonic elimination Using INHARE MPPT Algorithm

Even though CV and ARV MPPT are able to reduce the inter-harmonics, they have the disadvantages of low tracking efficiency and more significant processing memory requirement, respectively. Therefore, inter-harmonic elimination with INHARE MPPT is compared with P&O-based schemes.

2.4.3.1 Step up variation in irradiance

The inter harmonic elimination using INHARE is observed for step-up and step-down variation in irradiation levels. Since the inter harmonic content is considered to be the fundamental component under low power conditions, the proposed system is operated at lower irradiation cases.

The set 1 irradiation results in the 10% of rated power (52 Watts), and set 2 produces 20% of rated power (104 Watts), respectively. In the case of step-up variation in irradiance, the inter-harmonic elimination is examined for single step-up (set 1 to set 2) and five step-up (set 1 to set 2) cases. Five step-up change in irradiation from set 1 to set 2 is shown in Fig. 2.11a. For observing the inter-harmonic elimination, P&O and MP&O are operated at the step voltages (V_{step}) and sampling frequency (f_{MPPT}) of 1.2V and 20Hz, respectively. At the same time, INHARE MPPT algorithm is operated at the different voltage step voltage changes of 1.2V and 0.6V and different MPPT sampling frequencies of 20Hz and 16Hz. The single step-up variation with V_{step} and f_{MPPT} of 1.2V and 20Hz in P&O, MP&O, and INHARE schemes, display DC-link voltage under steady states and load current waveforms, as shown in Fig. 2.12a, 2.12b, and 2.12c.

Similarly, For the operating cases, V_{step} and f_{MPPT} of 1.2V and 16Hz, DC-link voltages under steady-state and load current waveforms for INHARE, are represented in Fig. 2.12d. Finally, For the operating cases, V_{step} and f_{MPPT} of 0.6V and 16Hz, DC-link voltages, and load current waveforms for INHARE cases are represented in Fig. 2.12e. Five step-up cases also display similar operating characteristics to that of single-step cases.

FFT analysis is employed by employing load currents in step-up cases, and %fundamental components at different sampling rates and step voltages are represented in Table-2.5 and Table-2.6. By employing Table-2.5 and Table-2.6, the %Fundamental components vs Frequency plot is represented in Fig. 2.13. As, the fundamental component is of 100%, representing it in plot makes it difficult to identify inter harmonic components. So, the 50Hz component is represented like a straight dotted line in inter-harmonics representation. From Fig. 2.13, it can be observed that, the proposed INHARE algorithm with low step voltage (V_{step}=0.6V) and sampling frequency (f_{MPPT}=16Hz) displays lower interharmonic content. From Table-2.5, it can be noted that MP&O displays lower interharmonic content than P&O. While, INHARE MPPT is able to nearly reduce the average inter-harmonic content in a single step-up variation by 23.54% compared to P&O based scheme for V_{step}=1.2V and f_{MPPT}=20Hz combination.

Moreover, with the further variation in step voltages and sampling rates, INHARE MPPT displays, more reduction in inter-harmonics. With the change in sampling rate to 16Hz, inter-harmonic content is further reduced by 34.33%. Finally, with a change in both step voltage and sampling rate values, to 0.6V and 16Hz, inter-harmonic content is reduced by 45.58%. Similar to Table-2.5, from Table-2.6, it can be noted that MP&O and INHARE schemes show better interharmonic reduction than P&O-based schemes.

2.4.3.2 Step down variation in irradiance

In case of step-down variation in irradiance, the inter-harmonic elimination is examined for single step-down (set 2 to set 1) and five step-down (set 2 to set 1) cases.

Five step-down change in irradiation from set 2 to set 1 is shown in Fig. 2.11b. For observing the inter-harmonic elimination, P&O and MP&O are operated at the step voltages (V_{step}) and sampling frequency (f_{MPPT}) of 1.2V and 20Hz respectively. Whereas, INHARE MPPT algorithm is operated at the different voltage step voltage changes, 1.2V and 0.6V and different MPPT sampling frequencies of 20Hz and 16Hz.

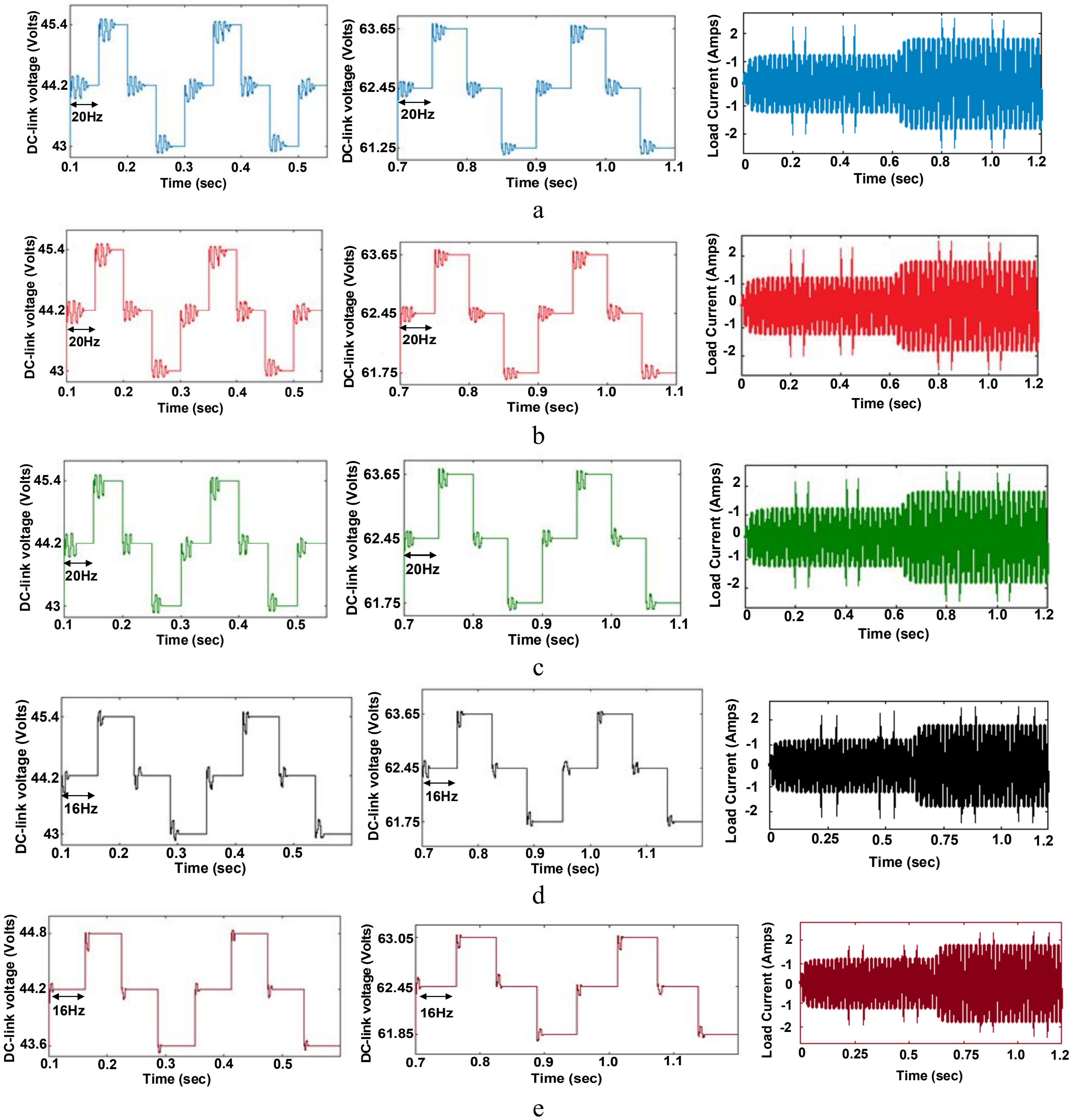

Fig. 2.12. DC-link voltage and load current with single step-up variation in irradiation levels (a. P&O, b. MP&O, c. INHARE, d. INHARE (16Hz, 1.2V) and e. INHARE (16Hz, 0.6V)).

Table 2.5. % Fundamental component of interharmonics of load current for single step-up case

F (Hz)	P&O	MP&O	INHARE 1.2V 16Hz	INHARE 0.6V 16Hz	INHARE 1.2V 20Hz	F (Hz)	P&O	MP&O	INHARE 1.2V 16Hz	INHARE 0.6V 16Hz	INHARE 1.2V 20Hz
0	0.09	0.08	0.05	0.01	0.15	51.72	4.49	4.48	4.2	4.1	4.28
1.72	0.15	0.15	0.09	0.03	0.19	53.45	1.99	1.92	1.28	1.18	1.36
3.45	0.18	0.17	0.1	0.005	0.2	55.17	1.82	1.81	1.39	1.29	1.47
5.17	0.17	0.16	0.1	0.005	0.2	56.89	1.77	1.72	1.1	1	1.18
6.89	0.2	0.18	0.11	0.01	0.21	58.62	1.32	1.29	0.84	0.74	0.92
8.62	0.2	0.19	0.12	0.02	0.22	60.34	1.5	1.46	0.92	0.82	1
10.34	0.23	0.22	0.12	0.02	0.22	62.06	1.09	1.06	0.62	0.52	0.7
12.07	0.23	0.23	0.14	0.04	0.24	63.79	1.29	1.15	0.77	0.67	0.85
13.79	0.27	0.25	0.14	0.04	0.24	65.52	0.95	0.94	0.51	0.41	0.59
15.52	0.29	0.28	0.17	0.07	0.27	67.24	1.11	1.07	0.65	0.55	0.73
17.24	0.32	0.3	0.16	0.06	0.26	68.97	0.86	0.84	0.45	0.35	0.55
18.97	0.35	0.34	0.21	0.11	0.31	70.69	0.96	0.93	0.56	0.46	0.66
20.69	0.37	0.35	0.18	0.08	0.28	71.41	0.79	0.77	0.41	0.31	0.51
22.41	0.43	0.42	0.26	0.16	0.36	74.14	0.85	0.82	0.49	0.39	0.59
24.14	0.42	0.4	0.21	0.11	0.31	75.86	0.73	0.71	0.38	0.28	0.48
25.86	0.53	0.51	0.32	0.22	0.42	77.58	0.75	0.73	0.43	0.33	0.53
27.59	0.49	0.47	0.24	0.14	0.34	79.31	0.68	0.66	0.36	0.26	0.46
29.31	0.66	0.64	0.39	0.29	0.49	81.03	0.67	0.66	0.38	0.28	0.48
31.03	0.56	0.54	0.28	0.18	0.38	82.76	0.64	0.62	0.34	0.24	0.44
32.76	0.82	0.78	0.49	0.39	0.59	84.48	0.61	0.6	0.34	0.24	0.44
34.48	0.66	0.65	0.35	0.25	0.45	86.21	0.6	0.58	0.32	0.22	0.42
36.21	1.02	0.98	0.62	0.52	0.72	87.93	0.56	0.55	0.31	0.21	0.41
37.93	0.8	0.78	0.45	0.35	0.53	89.66	0.56	0.55	0.3	0.2	0.4
39.66	1.26	1.23	0.78	0.68	0.86	91.38	0.52	0.51	0.28	0.18	0.38
41.38	1.03	1.01	0.67	0.57	0.75	93.1	0.53	0.51	0.29	0.19	0.39
43.01	1.59	1.53	0.99	0.89	1.07	94.83	0.49	0.48	0.26	0.16	0.36
44.83	1.53	1.52	1.23	1.13	1.31	96.55	0.5	0.49	0.27	0.17	0.37
46.55	1.89	1.83	1.21	1.11	1.29	98.28	0.46	0.45	0.25	0.15	0.35
48.28	4.19	4.18	4.03	3.93	4.11	100	0.47	0.46	0.26	0.16	0.36
						Average	0.871	0.848	0.572	0.474	0.666

Table 2.6. % Fundamental component of interharmonics of load current for five step-up case

F (Hz)	P&O	MP&O	INHARE 1.2V 16Hz	INHARE 0.6V 16Hz	INHARE 1.2V 20Hz	F (Hz)	P&O	MP&O	INHARE 1.2V 16Hz	INHARE 0.6V 16Hz	INHARE 1.2V 20Hz
0	0.42	0.42	0.25	0.15	0.35	51.72	3.32	3.27	2.66	2.56	2.74
1.72	0.85	0.85	0.5	0.4	0.6	53.45	2.47	2.44	1.63	1.53	1.71
3.45	0.86	0.85	0.5	0.4	0.6	55.17	2.14	2.07	1.31	1.21	1.39
5.17	0.87	0.86	0.5	0.4	0.6	56.89	1.95	1.91	1.12	1.02	1.2
6.89	0.87	0.86	0.51	0.41	0.61	58.62	1.76	1.72	0.98	0.88	1.06
8.62	0.88	0.87	0.51	0.41	0.61	60.34	1.6	1.55	0.85	0.75	0.93
10.34	0.89	0.84	0.52	0.42	0.62	62.06	1.44	1.4	0.77	0.67	0.85
12.07	0.91	0.9	0.53	0.43	0.63	63.79	1.32	1.3	0.7	0.6	0.78
13.79	0.93	0.92	0.53	0.43	0.63	65.52	1.19	1.16	0.63	0.53	0.71
15.52	0.97	0.96	0.55	0.45	0.65	67.24	1.1	1.07	0.58	0.48	0.66
17.24	0.99	0.97	0.56	0.46	0.66	68.97	1.01	0.99	0.53	0.43	0.61
18.97	1.02	1	0.57	0.47	0.67	70.69	0.94	0.92	0.49	0.39	0.57
20.69	1.05	1.04	0.59	0.49	0.69	71.41	0.87	0.85	0.45	0.35	0.53
22.41	1.09	1.07	0.61	0.51	0.71	74.14	0.81	0.8	0.42	0.32	0.5
24.14	1.13	1.1	0.63	0.53	0.73	75.86	0.74	0.73	0.39	0.29	0.47
25.86	1.19	1.17	0.65	0.55	0.75	77.58	0.7	0.69	0.37	0.27	0.45
27.59	1.24	1.21	0.68	0.58	0.78	79.31	0.65	0.64	0.34	0.24	0.42
29.31	1.3	1.27	0.71	0.61	0.81	81.03	0.61	0.6	0.33	0.23	0.41
31.03	1.37	1.34	0.75	0.65	0.85	82.76	0.57	0.56	0.31	0.21	0.41
32.76	1.45	1.42	0.8	0.7	0.9	84.48	0.54	0.54	0.29	0.19	0.39
34.48	1.53	1.49	0.85	0.75	0.95	86.21	0.51	0.5	0.28	0.18	0.38
36.21	1.65	1.62	0.9	0.8	1	87.93	0.47	0.47	0.26	0.16	0.36
37.93	1.75	1.71	0.97	0.87	1.07	89.66	0.45	0.44	0.25	0.15	0.35
39.66	1.87	1.81	1.02	0.92	1.12	91.38	0.42	0.42	0.24	0.14	0.34
41.38	2.05	2	1.18	1.08	1.28	93.1	0.4	0.4	0.23	0.13	0.33
43.01	2.22	2.17	1.31	1.21	1.39	94.83	0.38	0.38	0.22	0.12	0.32
44.83	2.39	2.32	1.49	1.39	1.57	96.55	0.36	0.35	0.21	0.11	0.31
46.55	2.72	2.68	1.82	1.72	1.9	98.28	0.34	0.34	0.2	0.1	0.3
48.28	3.58	3.53	2.86	2.76	2.94	100	0.32	0.32	0.19	0.09	0.29
						Average	1.197	1.174	0.708	0.608	0.801

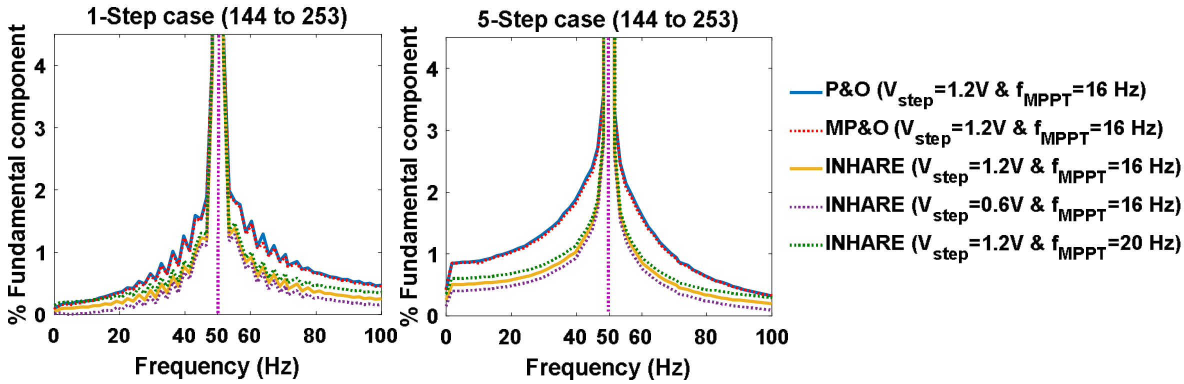

Fig. 2.13. % Fundamental frequency components vs frequency for step-up cases.

The single step-down variation with considered V_{step} and f_{MPPT} combinations in P&O, MP&O and INHARE schemes displays DC-link voltage under steady states and load current waveforms, as shown in Fig. 2.14a, 2.14b, 2.14c, 2.14d and 2.14e. Five-step down variations in irradiation steps display similar operating characteristics to a single-step down case.

FFT analysis is employed by employing load currents in step-down cases, and %fundamental components at different sampling rates and step voltages are represented in Table-2.7 and Table-2.8. By employing Table-2.7 and Table-2.8, the % Fundamental components vs Frequency plot is represented in Fig. 15.

From Fig. 2.15, it can be observed that, the proposed INHARE algorithm with low step voltage (V_{step}=0.6V) and sampling frequency (f_{MPPT}=16Hz) displays lower interharmonic content. From Table-2.7, it can be noted that, INHARE displays reduced inter-harmonic content compared to P&O and MP&O schemes for single step-down cases since it is already known that the drift phenomenon shows negligible effect [2.15].

So, it can be seen that MP&O and P&O displays almost similar inter-harmonic content in step-down cases. The proposed INHARE MPPT is able to nearly reduce the average inter-harmonic content in single step-down variation by 18.34% compared to P&O based scheme for V_{step}=1.2V and f_{MPPT}=20Hz combination.

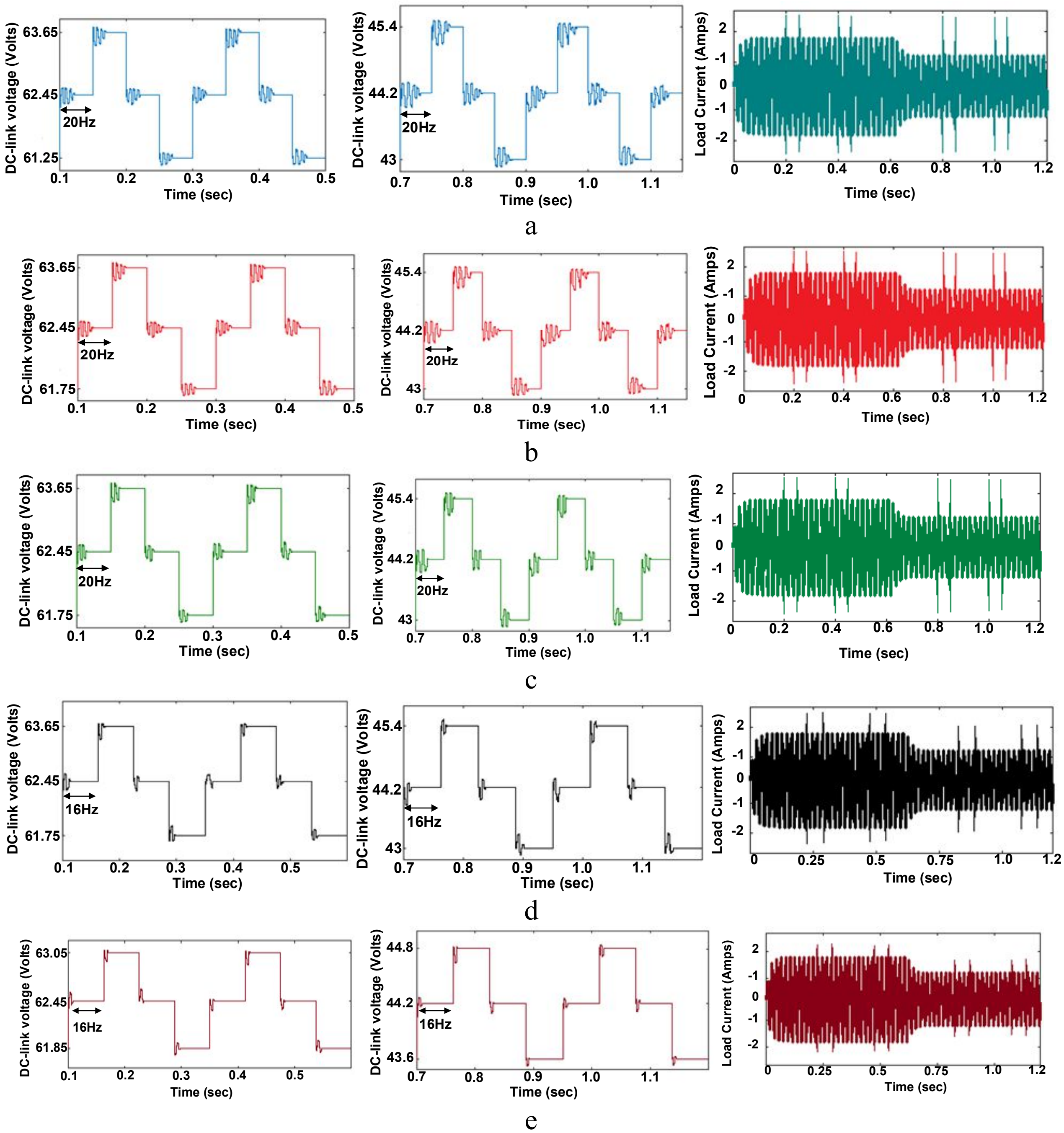

Fig. 2.14. DC-link voltage and load current with single step-down variation in irradiation levels (a. P&O, b. MP&O, c. INHARE, d. INHARE (16Hz, 1.2V) and e. INHARE (16Hz, 0.6V)).

Moreover, with the further variation in step voltages and sampling rates, INHARE MPPT displays more reduction in inter-harmonics. With the change in sampling rate to 16Hz, inter-harmonic content is further reduced by 34.69%. Finally, with a change in step voltage and sampling rate values, to 0.6V and 16Hz, inter-harmonic content is reduced by 48.01%. Similar to Table-2.7, from Table-2.8, it can be noted that MP&O and INHARE schemes show better interharmonic reduction under five step-down cases than the P&O scheme.

Table 2.7. % Fundamental component of interharmonics of load current for single step-down case

F (Hz)	P&O	MP&O	INHARE 1.2V 16Hz	INHARE 0.6V 16Hz	INHARE 1.2V 20Hz	F (Hz)	P&O	MP&O	INHARE 1.2V 16Hz	INHARE 0.6V 16Hz	INHARE 1.2V 20Hz
0	0.07	0.07	0.04	0.01	0.14	51.72	4.48	4.48	4.18	4.08	4.38
1.72	0.13	0.13	0.08	0.03	0.18	53.45	1.98	1.98	1.26	1.16	1.46
3.45	0.16	0.16	0.09	0.007	0.19	55.17	1.81	1.81	1.37	1.27	1.57
5.17	0.15	0.15	0.09	0.007	0.19	56.89	1.76	1.76	1.08	0.98	1.28
6.89	0.18	0.18	0.1	0.009	0.2	58.62	1.31	1.31	0.82	0.72	1.02
8.62	0.18	0.18	0.11	0.01	0.21	60.34	1.49	1.49	0.9	0.7	1.1
10.34	0.21	0.21	0.11	0.01	0.21	62.06	1.08	1.08	0.6	0.4	0.8
12.07	0.21	0.21	0.13	0.03	0.23	63.79	1.28	1.28	0.75	0.55	0.95
13.79	0.25	0.25	0.13	0.03	0.23	65.52	0.94	0.94	0.49	0.29	0.69
15.52	0.27	0.27	0.16	0.06	0.26	67.24	1.1	1.1	0.63	0.43	0.83
17.24	0.3	0.3	0.15	0.05	0.25	68.97	0.85	0.85	0.43	0.23	0.63
18.97	0.33	0.33	0.2	0.1	0.3	70.69	0.95	0.95	0.54	0.34	0.64
20.69	0.35	0.35	0.17	0.07	0.27	71.41	0.78	0.78	0.4	0.2	0.5
22.41	0.41	0.41	0.25	0.15	0.35	74.14	0.84	0.84	0.48	0.28	0.58
24.14	0.4	0.4	0.2	0.1	0.3	75.86	0.72	0.72	0.37	0.17	0.47
25.86	0.51	0.51	0.31	0.21	0.41	77.58	0.74	0.74	0.42	0.32	0.52
27.59	0.47	0.47	0.23	0.13	0.33	79.31	0.67	0.67	0.35	0.25	0.45
29.31	0.64	0.64	0.38	0.28	0.58	81.03	0.66	0.66	0.37	0.27	0.47
31.03	0.54	0.54	0.27	0.17	0.47	82.76	0.63	0.63	0.33	0.23	0.43
32.76	0.8	0.8	0.48	0.38	0.68	84.48	0.6	0.6	0.33	0.23	0.43
34.48	0.64	0.64	0.34	0.24	0.54	86.21	0.59	0.59	0.31	0.21	0.41
36.21	1	1	0.61	0.51	0.81	87.93	0.55	0.55	0.3	0.2	0.4
37.93	0.78	0.78	0.44	0.34	0.64	89.66	0.55	0.55	0.29	0.19	0.39
39.66	1.24	1.25	0.77	0.67	0.97	91.38	0.51	0.51	0.27	0.17	0.37
41.38	1.01	1.02	0.66	0.56	0.86	93.1	0.52	0.52	0.28	0.18	0.38
43.01	1.57	1.58	0.98	0.88	1.18	94.83	0.48	0.48	0.25	0.15	0.35
44.83	1.51	1.52	1.21	1.11	1.41	96.55	0.49	0.49	0.26	0.16	0.36
46.55	1.87	1.88	1.19	1.09	1.39	98.28	0.45	0.45	0.24	0.14	0.34
48.28	4.17	4.18	4.01	3.91	4.21	100	0.46	0.46	0.25	0.15	0.35
						Average	0.856	0.856	0.559	0.445	0.699

2.5 HARDWARE SETUP AND DISCUSSIONS

Fig. 2.16, represents the experimental setup for the proposed INHARE algorithm, where two 260W solar panels are connected in a series configuration to feed the load. Halogen lamps are used to create artificial irradiance in the lab atmosphere, where a rheostat is used to vary the irradiation levels.

Table 2.8. % Fundamental component of interharmonics of load current for five step-down case

F (Hz)	P&O	MP&O	INHARE 1.2V 16Hz	INHARE 0.6V 16Hz	INHARE 1.2V 20Hz	F (Hz)	P&O	MP&O	INHARE 1.2V 16Hz	INHARE 0.6V 16Hz	INHARE 1.2V 20Hz
0	0.4	0.4	0.24	0.14	0.34	51.72	3.31	3.31	2.64	2.54	2.71
1.72	0.83	0.83	0.49	0.39	0.59	53.45	2.46	2.46	1.61	1.51	1.68
3.45	0.84	0.84	0.49	0.39	0.59	55.17	2.13	2.13	1.3	1.19	1.37
5.17	0.85	0.85	0.49	0.39	0.59	56.89	1.94	1.94	1.11	1	1.18
6.89	0.85	0.85	0.5	0.4	0.6	58.62	1.75	1.75	0.97	0.87	1.04
8.62	0.86	0.86	0.5	0.4	0.6	60.34	1.59	1.59	0.84	0.74	0.91
10.34	0.87	0.87	0.51	0.41	0.61	62.06	1.43	1.43	0.76	0.66	0.83
12.07	0.89	0.89	0.52	0.42	0.62	63.79	1.31	1.31	0.69	0.59	0.76
13.79	0.91	0.91	0.52	0.42	0.62	65.52	1.18	1.18	0.62	0.52	0.69
15.52	0.95	0.95	0.54	0.44	0.64	67.24	1.09	1.09	0.57	0.47	0.64
17.24	0.97	0.97	0.55	0.45	0.65	68.97	1	1	0.52	0.42	0.59
18.97	1	1	0.56	0.46	0.66	70.69	0.93	0.93	0.48	0.38	0.56
20.69	1.03	1.038	0.58	0.48	0.68	71.41	0.86	0.86	0.44	0.34	0.52
22.41	1.07	1.078	0.6	0.5	0.7	74.14	0.8	0.8	0.41	0.31	0.49
24.14	1.11	1.118	0.62	0.52	0.72	75.86	0.73	0.73	0.38	0.28	0.46
25.86	1.17	1.178	0.64	0.54	0.74	77.58	0.69	0.69	0.36	0.26	0.44
27.59	1.22	1.228	0.67	0.57	0.77	79.31	0.64	0.64	0.33	0.23	0.41
29.31	1.28	1.288	0.7	0.6	0.8	81.03	0.6	0.6	0.32	0.22	0.4
31.03	1.35	1.358	0.74	0.64	0.84	82.76	0.56	0.56	0.3	0.2	0.38
32.76	1.43	1.438	0.78	0.69	0.88	84.48	0.53	0.53	0.28	0.18	0.36
34.48	1.51	1.51	0.83	0.73	0.93	86.21	0.5	0.5	0.27	0.17	0.35
36.21	1.63	1.63	0.88	0.78	0.98	87.93	0.46	0.46	0.25	0.15	0.33
37.93	1.73	1.73	0.95	0.85	1.05	89.66	0.44	0.44	0.24	0.14	0.32
39.66	1.85	1.85	1	0.9	1.07	91.38	0.41	0.408	0.23	0.13	0.31
41.38	2.03	2.03	1.16	1.06	1.23	93.1	0.39	0.388	0.22	0.12	0.32
43.01	2.2	2.2	1.29	1.19	1.36	94.83	0.37	0.368	0.21	0.11	0.31
44.83	2.37	2.37	1.47	1.37	1.54	96.55	0.35	0.348	0.2	0.1	0.3
46.55	2.7	2.7	1.8	1.7	1.87	98.28	0.33	0.328	0.19	0.09	0.29
48.28	3.56	3.56	2.84	2.74	2.91	100	0.31	0.308	0.18	0.08	0.28
						Average	1.182	1.182	0.696	0.596	0.783

A pyranometer and LM35 are employed to sense the irradiation and temperature as an equivalent voltage reference. Since the output voltage reference of irradiation and temperature sensors are of lower voltage values, an amplifier circuit is employed to reduce noise in output waveforms. A three-phase two-level inverter is constructed using K2611 N-channel MOSFET, where the latter is mounted on a heat sink. Along with the proposed MPPT scheme, inverter control is also programmed into a micro-controller. The inverter output is associated with a three-phase-load. The sensed constraints such as irradiance, temperature, voltage, and current are given as input to the PIC18F452 controller, where the microcontroller programming is done using a PC interface. For the respective sensed input parameters, the PIC 18F452 controller generates a gate pulse in the range of 5V.

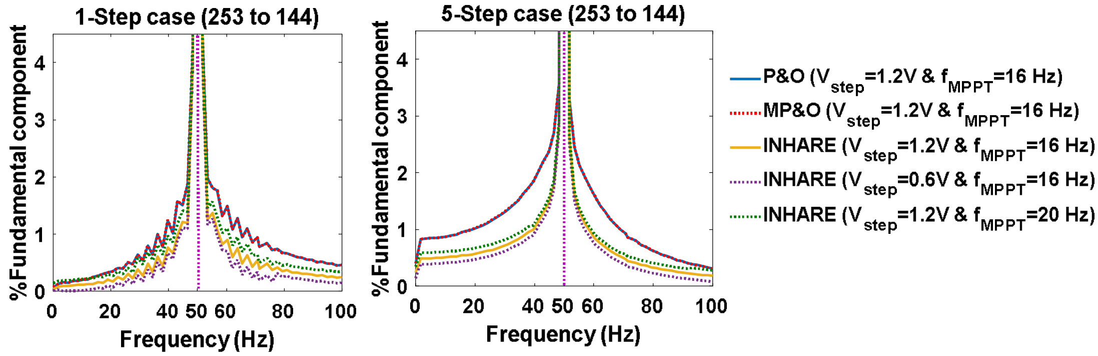

Fig. 2.15. % Fundamental frequency components vs frequency for step-down cases

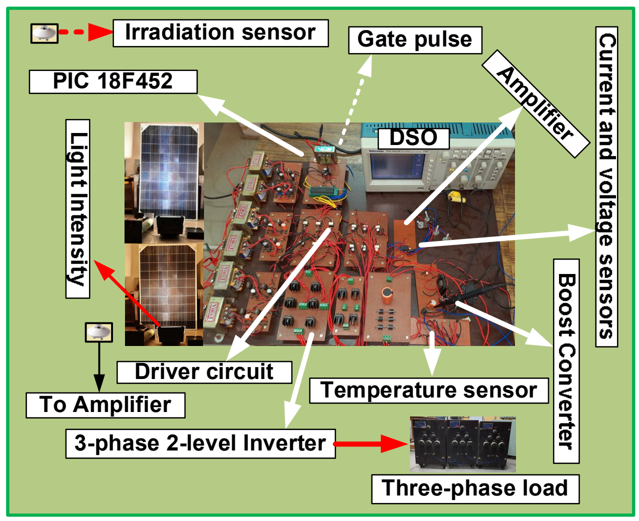

Fig. 2.16. Hardware design for proposed INHARE MPPT

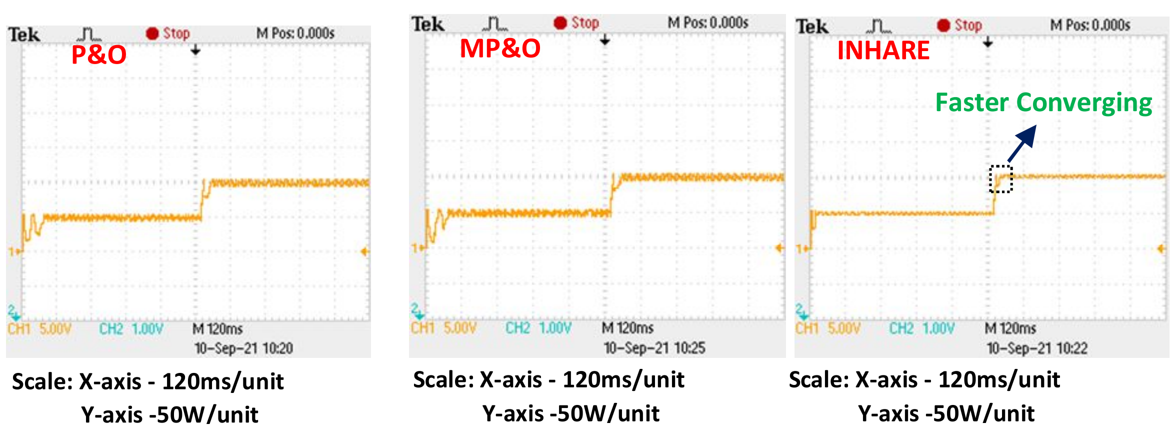

Fig. 2.17. PV panel power for different MPPT schemes

Table 2.9. Efficiency and convergence time comparison of INHARE MPPT scheme with existing schemes

Properties	P&O		MP&O		INHARE	
	Set 1	Set 2	Set 1	Set 2	Set 1	Set 2
Efficiency (%)	98.47	98.5	98.15	98.23	99.08	99.05
Convergence time (ms)	26.2		26.18		14.4	

Since the 5V level is not sufficient to trigger the MOSFET gate of the boost converter, a TLP250H topology is employed to enhance the voltage level of the triggering pulse. The hardware components required for designing the proposed system are represented in Table-2.1.

The proposed system is operated for the single step-up of variation in the considered irradiation sets, set 1 to set 2. The tracked PV panel power with P&O-based schemes and INHARE MPPT are represented in Fig. 2.17. From this, INHARE MPPT displays better MPP tracking efficiency at all possible irradiation cases. Also, by observing the operating characteristics of INHARE and P&O-based schemes, the tracking efficiency and converging time (At step change) are represented in Table-2.9. From Table-2.9, it can be observed that leaving drift avoidance, P&O and MP&O algorithms display similar operating characteristics.

In the case of step-up variation in irradiance, the inter-harmonic elimination is examined for the single step-up (set 1 to set 2) case. For observing the inter-harmonic elimination, P&O and MP&O are operated at the step voltages (V_{step}) and sampling frequency (f_{MPPT}) of 1.2V and 20Hz, respectively.

Whereas INHARE MPPT algorithm is operated at the different voltage step voltage changes, 1.2V and 0.6V, and different MPPT sampling frequencies of 20Hz and 16Hz, respectively. For the different operating cases, DC-link voltage under steady-state, load current waveforms, and FFT analysis with P&O, MP&O, and INHARE cases of single step-up variation is represented in Fig. 2.18a, 2.18b, 2.18c, 2.18d, and 2.18e.

From Fig. 2.18, it can be observed that the proposed INHARE MPPT scheme displays better harmonic reduction compared to P&O-based schemes. Also, it can be noted that the INHARE MPPT with low step voltages and sampling frequencies display lower inter-harmonic content to all the other cases. Overall, it can be observed that, the INHARE MPPT of V_{step}=0.6V and f_{MPPT}=16Hz displays lower inter-harmonic content compared to other cases.

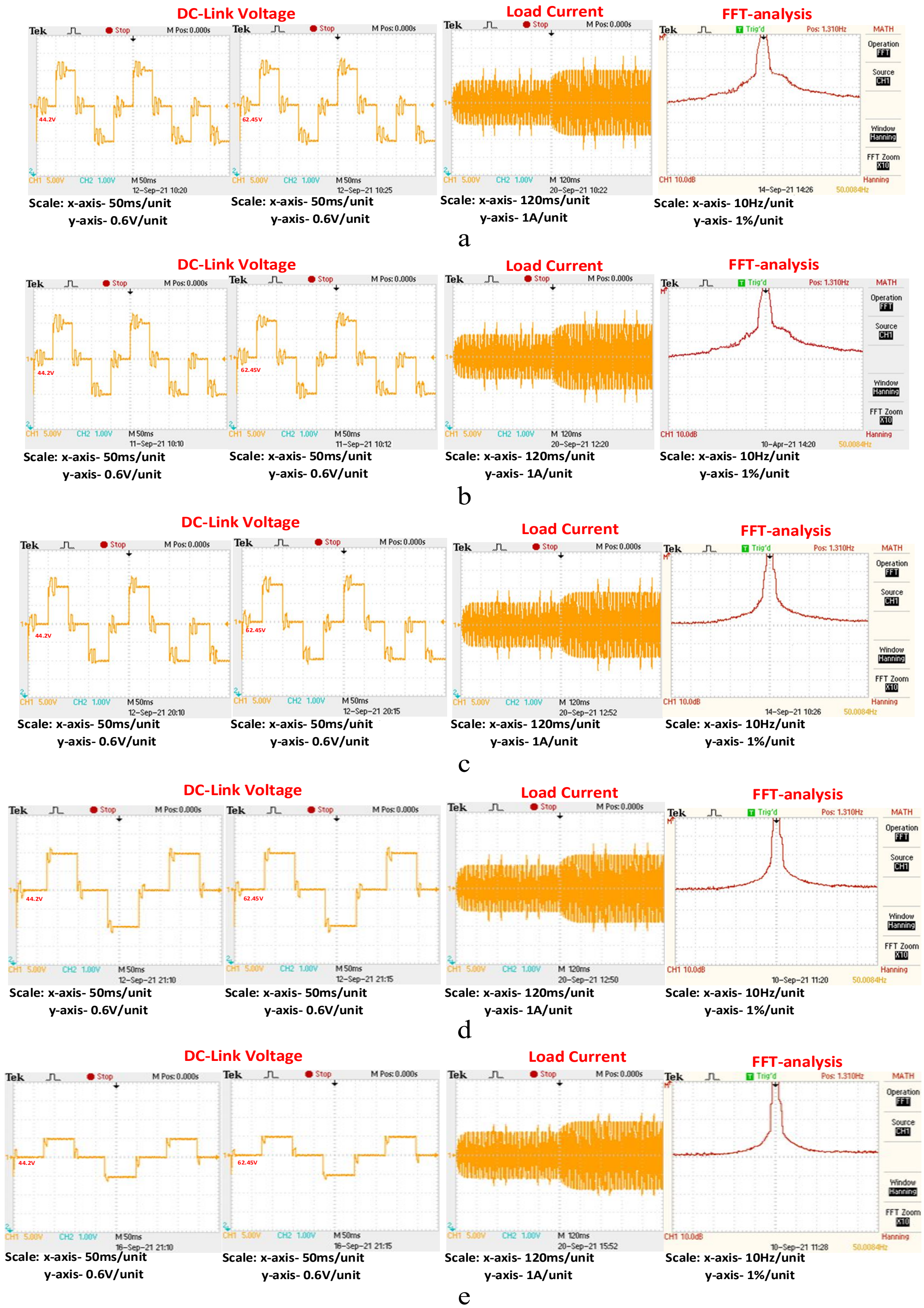

Fig. 2.18. DC-link voltage, load current and FFT analysis with single step-up variation in irradiation levels (a. P&O, b. MP&O, c. INHARE, d. INHARE (16Hz, 1.2V) and e. INHARE (16Hz, 0.6V)).

Table-2.10, represents the comparison of the proposed INHARE MPPT scheme with available MPPT schemes. From Table-2.10, it can be observed that, the proposed INHARE algorithm results in better dynamic characteristics with lower inter harmonic content.

Table 2.10. Overall comparison of INHARE MPPT scheme with existing schemes

MPPT	Convergence speed	Complexity	Efficiency	Ripple	Memory unit required	Inter-harmonic content
P&O	Varies	Simple	High	High	No	High
[2.27]	Medium	Medium	Medium	High	No	Medium
Incremental cond.	Varies	Complex	High	High	No	High
[2.26]	Faster	simple	Low	High	No	Medium
Short- circuit current	Medium	simple	Low	High	No	Medium
Modified P&O	Varies	simple	High	High	No	High
ARV	Faster	Medium	High	Medium	Yes	Medium
Proposed INHARE	Faster	simple	High	Low	No	Low

2.6 CONCLUSION

In this research work an INHARE MPPT algorithm is implemented for inter-harmonic elimination.

(1) The proposed INHARE MPPT scheme displays better tracking efficiency comparing to CV MPPT under lower irradiation levels. Also, it displays interharmonic-elimination similar to that of CV MPPT.

(2) Due to the weather-sensitive nature, the proposed scheme displays low drift in PV panel power under sudden change in irradiation compared to [2.27].

(3) Unlike ARV MPPT, INHARE method does not require memory unit for tracking. So, proposed scheme is more preferred compared to ARV method for MPPT purpose.

(4) Compared to PI tuning-based optimization schemes, the proposed scheme can be developed easily with already available hardware.

(5) The proposed INHARE MPPT scheme displays an improvement in the average tracking efficiency (99.07%) compared to P&O and MP&O schemes.

(6) INHARE algorithm is able to detect the nearest location to MPP, with a change in irradiation, resulting in lower settling time. The convergence time of INHARE MPPT scheme is faster (14.4ms) compared to MP&O and P&O schemes.

(7) Finally, compared to P&O-based MPPT schemes, the proposed INHARE MPPT scheme displays effective interharmonic elimination irrespective of the step up/down changes with different voltage steps and sampling frequency changes.

(8) The proposed scheme can be extended for larger PV farms, where a single irradiation and temperature sensors are sufficient in successfully tracking maximum power.

Related Publication:

- **BSV Sai**, D. Chatterjee et al., "Inter-harmonics mitigation for PV based Converters Using INHARE MPPT Algorithm," **IETE Journal of research**, **Taylor & Francis**, 2022.

References:

[2.1] Ku Ding, XinGao Bian, HaiHao Liu, and Tao Peng, "A MATLAB-Simulink-Based PV Module Model and Its Application under Conditions of Non uniform Irradiance," IEEE Trans. On ENERGY Conv. vol. 27, no. 4, Dec.2012.

[2.2] M.Piliougine, R.A. Guejia-Burbano, G. Petrone, F.J. Sánchez-Pacheco, L. Mora López and M. Sidrach-de-Cardona, "Parameters extraction of single diode model for degraded photovoltaic modules," Renewable Energy, Vol. 164, Feb. 2021, Pages 674-686.

[2.3] H. Patel and V. Agarwal, "MATLAB-based modeling to study the effects of partial shading on PV array characteristics," IEEE Trans. Energy Convers. vol. 23, no. 1, pp. 302–310, Mar. 2008.

[2.4] B.S.S. Ganesh Pardhu and Venkata Reddy Kota, "Radial movement optimization-based parameter extraction of double diode model of solar photovoltaic cell," Solar Energy Volume 213, 1 January 2021, Pages 312-327.

[2.5] Sanjeev Kumar Pandey, Sanjaykumar Limaji Patil and Shrivijay B. Phadke, "PWM-Based Adaptive Sliding-Mode Control for Boost DC–DC Converters," IEEE Trans. on Ind. Electron., vol. 65, no. 6, June 2018.

[2.6] Neeraj Priyadarshi, Mahajan Sagar Bhaskar, Sanjeevikumar Padmanaban, Frede Blaabjerg and Farooque Azam, "New CUK–SEPIC converter based photovoltaic power system with hybrid GSA–PSO algorithm employing MPPT for water pumping applications," IET Power Electron., 2020, Vol. 13 Iss. 13, pp. 2824-2830.

[2.7] Mohamad Reza Banaei and Sajad Ghabeli Sani, "Analysis and Implementation of a New SEPIC-Based Single-Switch Buck–Boost DC–DC Converter with Continuous Input Current," IEEE Trans. on Power Electron., vol. 33, no. 12, Dec. 2018.

[2.8] M.A. Danandeh and S.M. Mousavi G, "Comparative and comprehensive review of maximum power point tracking methods for PV cells," Renewable and Sustainable Energy Reviews, Vol. 82, Part 3, Feb. 2018, Pages 2743-2767.

[2.9] Mingxuan Mao, Lichuang Cui, Qianjin Zhang, Ke Guo, Lin Zhou and Han Huang, "Classification and summarization of solar photovoltaic MPPT techniques: A review based on traditional and intelligent control strategies," Energy Reports Volume 6, Nov. 2020, Pages 1312-1327.

[2.10] M. A. G. de Brito, L. Galotto, L. P. Sampaio, G. A. e Melo, and C. A. Canesin, “Evaluation of the main MPPT techniques for photovoltaic applications,” IEEE Trans. Ind. Electron., vol. 60, no. 3, pp. 1156–1167, Mar. 2013.

[2.11] Jyotirmaya Sahoo, Susovon Samanta and Shamik Bhattacharyya, “Adaptive PID Controller with P&O MPPT Algorithm for Photovoltaic System,” IETE Journal of Research, 2018.

[2.12] Hafsa Abouadane, Abderrahim Fakkar, Dezso Sera, Abderezak Lashab, Sergiu Spataru and Tamas Kerekes, “Multiple-Power-Sample Based P&O MPPT for Fast-Changing Irradiance Conditions for a Simple Implementation,” IEEE Journal of Photovoltaics, Vol.10, Iss. 5, Sept. 2020.

[2.13] Shun-Chung Wang, Hung-Yu Pai, Guan-Jhu Chen, and Yi-Hwa Liu, “A Fast and Efficient Maximum Power Tracking Combining Simplified State Estimation With Adaptive Perturb and Observe,” IEEE Access, Vol. 8, 2020.

[2.14] Jyri Kivimaki, Sergei Kolesnik, Moshe Sitbon, Teuvo Suntio and Alon Kuperman, “Design Guidelines for Multiloop Perturbative Maximum Power Point Tracking Algorithms,” IEEE Trans. on Power Electron., vol. 33, no. 2, Feb., 2018.

[2.15] Muralidhar Killi and Susovon samanta, “Modified Perturb and Observe MPPT Algorithm for Drift Avoidance in Photovoltaic Systems,” IEEE Tans. Ind. Electron, VOL. 62, NO. 9, Sep.2015.

[2.16] Vibhu Jately, Somesh Bhattacharya, Brian Azzopardi, Antoine Montgareuil, Jyoti Joshi, and Sudha Arora, “Voltage and Current Reference Based MPPT Under Rapidly Changing Irradiance and Load Resistance,” IEEE Trans. On Energy Conv., Vol. 36, No. 3, Sept. 2021.

[2.17] Shengqing, L., Fujun, L., Jian, Z. et al., “An improved MPPT control strategy based on incremental conductance method,” Soft Comput 24, 6039–6046, 2020.

[2.18] Mohamed Lasheen, Ali Kamel Abdel Rahman, Mazen Abdel-Salam and Shinichi Ookawara, “Adaptive reference voltage-based MPPT technique for PV application,” IET Renew, Power Gener., 2017, Vol. 11 lss. 5, PP. 715-722.

[2.19] Yee-Pien Yang and Ming-Tsan Peng, “A Surface-Mounted Permanent-Magnet Motor With Sinusoidal Pulsewidth-Modulation-Shaped Magnets,” IEEE Trans. on Magnetics, Volu.55, Issue: 1, Jan. 2019.

[2.20] Hanyang Yu, Bin Chen, Wenxi Yao and Zhengyu Lu, “Hybrid Seven-Level Converter Based on T-Type Converter and H-Bridge Cascaded Under SPWM and SVM,” IEEE Trans. on Power Electron., Vol. 33, Jan. 2018.

[2.21] Anh Tuan Nguyen, Sang-Wook Ryu, Abd Ur Rehman, Han Ho Choi And Jin-Woo Jung, “Improved Continuous Control Set Model Predictive Control for Three-Phase CVCF Inverters: Fuzzy Logic Approach,” IEEE Access, VOL. 9, 2021.

[2.22] Malay Bhunia, Bidyadhar Subudhi, and Pravat Kumar Ray, “Design and Real-Time Implementation of Cascaded Model Reference Adaptive Controllers for a Three-Phase Grid-Connected PV System,” IEEE Journal of Photovoltaics, Vol. 11, No. 5, September 2021.

[2.23] Vineetha Ravichandran, Sarah K. Rönnberg and Math H.J. Bollen, "Interharmonics in PV systems: a review of analysis and estimation methods; considerations for selection of an apt method," IET Renew. Power Gener., 2019, Vol. 13 Iss. 12, pp. 2023-2032.

[2.24] Y. Yang, K. Zhou, and F. Blaabjerg, "Current harmonics from single-phase grid-connected inverters - examination and suppression," IEEE J. Emerg. Sel. Top. Power Electron. vol. 4, no. 1, pp. 221–233, Mar. 2016.

[2.25] Ariya Sangwongwonich, Yongheng Yang, Dezso sera, Hamid Soltni and Frede Blaabjerg, "Analysis and Modelling of Interharmonics from Grid-connected Photovoltaic Systems," IEEE Trans. Power electron, VOL. PP, NO. 99, 2017.

[2.26] Ariya Sangwongwonich, Yongheng Yang, Dezso sera, Hamid Soltni and Frede Blaabjerg, "Interharmonics from grid connected PV systems: Mechanism and Mitigation," IEEE 3rd international future energy electronics conference and ECCE Asia (IFEEC 2017-ECCE).

[2.27] Ariya Sangwongwonich and Frede Blaabjerg, "Mitigation of Interharmonics in PV Systems with Maximum Power Point Tracking Modification," IEEE Trans. Power electron, VOL.34, NO. 9, 2019.

[2.28] Mostefa, Abdelkader, Houari Merabet Boulouiha, Ahmed Allali, and Mouloud Denai, "Mitigation of harmonics and inter-harmonics with LVRT and HVRT enhancement in grid-connected wind energy systems using genetic algorithm-optimized PWM and fuzzy adaptive PID control," Journal of Renewable and Sustainable Energy 13, no. 2 (2021): 026302.

[2.29] Ahmad, Salman, Irfan Khan, Atif Iqbal, and Syed Rahman," A Novel Pulse Width Amplitude Modulation for Elimination of Multiple Harmonics In Asymmetrical Multilevel Inverter," In 2021 IEEE Texas Power and Energy Conference (TPEC), pp. 1-6. IEEE, 2021.

[2.30] Ariya Sangwongwonich, Yongheng Yang and Frede Blaabjerg, "Sensorless Power Reserve Control Strategy for Two-Stage Grid-Connected PV Systems," IEEE Trans. Power electron, VOL., PP. NO. 99, 2017.

[2.31] M. Matsui, T. Kitano, D.-h. Xu, and Z.-q. Yang, "A new maximum photovoltaic power tracking control scheme based on power equilibrium at DC link," in Conf. Record 1999 IEEE Ind. Appl. Conf., 1999, pp. 804–809.

[2.32] David A. Elvira-Ortiz, Daniel Morinigo-Sotelo, Oscar Duque-Perez, Roque A. Osornio-Rios and Rene J. Romero-Troncoso, "Study of the harmonic and interharmonic content in electrical signals from photovoltaic generation and their relationship with environmental factors," J. Renewable Sustainable Energy 11, 043502 (2019); https://doi.org/10.1063/1.5094038.

[2.33] Nishant Kumar, Bhim Singh, Jihong Wang and Bijaya Ketan Panigrahi, "A Framework of L-HC and AM-MKF for Accurate Harmonic Supportive Control Schemes," IEEE Trans. on circuits and systems–I: regular research works, 2020.

[2.34] Nishant Kumar, Bhim Singh and Bijaya Ketan Panigrahi, "Integration of Solar PV with Low-Voltage Weak Grid System: using Maximize-M Kalman Filter and Self-tuned P&O Algorithm," IEEE Transactions on Industrial Electronics, 2018.

[2.35] Nishant Kumar, Bhim Singh, Bijaya Ketan Panigrahi and L. Xu, "Leaky Least Logarithmic Absolute Difference Based Control Algorithm and Learning Based InC MPPT Technique for Grid Integrated PV System," IEEE Transactions on Industrial Electronics, 2018.

[2.36] Nishant Kumar, Bhim Singh, Bijaya Ketan Panigrahi, Chandan Chakraborty, Hiralal Murlidhar Suryawanshi and Vishal Verma, Member IEEE, "Integration of Solar PV with Low-Voltage Weak Grid System: Using Normalized Laplacian Kernel Adaptive Kalman Filter and Learning Based InC Algorithm," IEEE Transactions on Power Electronics, 2019.

[2.37] Nishant Kumar, Bhim Singh and Bijaya Ketan Panigrahi, "LLMLF Based Control Approach and LPO MPPT Technique for Improving Performance of a Multifunctional Three-Phase Two-Stage Grid Integrated PV System," IEEE Transactions on Sustainable Energy, 2019.

[2.38] Dalila Fares, Mohamed Fathi, Immad Shams and Saad Mekhilef, "A novel global MPPT technique based on squirrel search algorithm for PV module under partial shading conditions," Energy Conversion and Management, 230, 2021, 113773.

[2.39] Kok Soon Tey, Saad Mekhilef, Mehdi Seyedmahmoudian, Ben Horan, Amanullah Than Oo, and Alex Stojcevski, "Improved Differential Evolution-based MPPT Algorithm using SEPIC for PV Systems under Partial Shading Conditions and Load Variation," IEEE Transactions on Industrial Informatics, 2018.

[2.40] Immad Shams, Saad Mekhilef, and Kok Soon Tey, "Maximum Power Point Tracking using Modified Butterfly Optimization Algorithm for Partial Shading, Uniform Shading and Fast Varying Load Conditions," IEEE Transactions on Power Electronics, 2020.

[2.41] Imran Pervez, Immad Shams, Saad Mekhilef, Adil Sarwar, Mohd Tariq, and Basem Alamri, "Most Valuable Player Algorithm based Maximum Power Point Tracking for a Partially Shaded PV Generation System," IEEE Transactions on Sustainable Energy, Vol. 12, No. 4, October 2021.

[2.42] Ratnakar Babu Bollipo, Suresh Mikkili and Praveen Kumar Bonthagorla, "Hybrid, Optimal, Intelligent and Classical PV MPPT Techniques: A Review," CSEE Journal of Power and Energy Systems, Vol. 7, No. 1, January 2021.

[2.43] Ratnakar Babu Bollipo, Suresh Mikkili and Praveen Kumar Bonthagorla, "Critical Review on PV MPPT Techniques: Classical, Intelligent and Optimisation," IET Renew. Power Gener., 2020, Vol. 14 Iss. 9, pp. 1433-1452.

IMPROVED MPPT TECHNIQUE UNDER VARYING IRRADIATION

3.1 INTRODUCTION

Photovoltaic (PV) system is the most considered energy source, since it offers continuous efficiency and savings even in the colder and cloudy climates [3.1]. Single diode model is most significant because of its simple structure along with better operation compared to double diode model in high efficiency PERL PV cells [3.2]. Boost converter is the most commonly used DC-DC converter in PV system for maintaing voltage requirement of load. It is chosen because of its simple structure and non-inverted output nature [3.3-3.5]. In P&O algorithm, the increase or decrease in the duty cycle or voltage step changes does not progress the overall operating characteristics of the system [3.6]. Along with this, P&O MPPT is insensitive to atmosphere, leads to fluctuations under sudden change in irradiation [3.7].

To avoid the steady state oscillation, adaptive PI controller-based P&O techniques are introduced, where PI controller is used to produce the signal related to tracking error and drives it as an input to PWM generator [3.8-3.10]. In [3.11], an adaptive PID controller-based scheme is introduced, in which a system is developed for auto-updating the K_P, K_I and K_D values. Except the advantage of no drift under sudden change in irradiation, all the operating characteristics are similar between P&O and MP&O [3.12].

In few adaptive PI based techniques, optimization-based systems and fuzzy logic-based methods are used to calculate the PI controller gain values [3.13-3.16]. Consant PI controller gain values under sudden change in irradiation results in the performance characteristics like maximum settling time and oscillation over steady state, at irradiation cases other than STC [3.17-3.20]. Different MPPT schemes for PV systems has been thoroughly discussed in [3.26], from which it can be noted that, the majority of optimization-based schemes are very complex for real time implementation. A novel musical chairs algorithm and an Improved Cuckoo Search Algorithm has been proposed for tracking maximum power for PV system in [3.27-3.28]. But the discussed schemes require more mathematical computation for the processor to track MPP. A slap swarm optimization-based scheme has been proposed in [3.29] which displays better tracking efficiency. On the other hand, it results in higher settling time and oscillations over the steady state operation while tracking maximum power.

The working principle of ARV based MPPT is similar to that of CV MPPT. In case of CV MPPT, investigators are divided into two categories, where first category deals with the fact that the MPP voltage of system is 80-90% of V_p at STC. The second category states that MPP voltage is 80-90% of V_p for each irradiation case [3.22-3.24]. Adaptive reference voltage MPPT is the developed version of CV MPPT, which addresses the disadvantages of both these categories and operates effectively for all possible irradiation cases without any disturbances in delivering power to load [3.25].

The proposed WA-P&O technique has suggested in this research work removes above mentioned problems and shows better results compared to the existing methods. The main features of the proposed technique are,

- High tracking efficiency.
- Quicker tracking response under abrupt change in irradiation.
- Self-updating PI controller tuning with less mathematical burden
- No fluctuation in output under the sudden change in irradiation.
- Single irradiation and temperature sensors are sufficient for tracking maximum power efficiently, irrespective of PV farm size.
- Implementation with already available hardware.

3.2 SOLAR CELL CONSTRUCTION

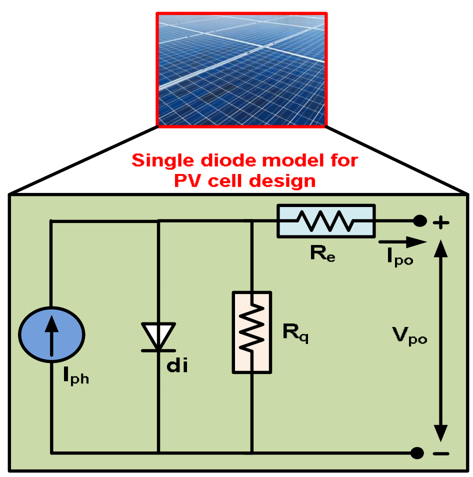

Fig. 3.1. PV cell configuration

Single diode model is widely employed in the mathematical implementation of practical solar cell, because of its simple structure and easy implementation in simulink atmosphere [3.2]. Solar cell is basically fabricated using p-n junction diodes, where the photo current generated is in terms with the solar insolation. Solar cell construction mainly depends on its mathematical implementation, the simplified design for solar cell involves a current source and a diode, parallel to each other. Moreover, to improve the accuracy of the system, series and parallel resistances are added in basic circuit. Single diode topology for PV cell is represented in Fig.3.1.

Table 3.1. Solar cell manufacturer data

VARIABLE	QUANTITY
MPP power (P_{max})	260 W
MPP Voltage (V_{max})	30.88 V
MPP Current (I_{max})	8.42 A
Short Circuit Current (I_{sh})	8.98 A
Open Circuit Voltage (V_p)	37.75 V
Temperature coefficient of I_{sh}	0.04%/^{0}C
Temperature coefficient of V_p	-0.325%/^{0}C

The relation among I_{po} and V_{po} is expressed as,

$$I_{po} = I_{ph} - I_{sat}\left(e^{\frac{q(V_{po}+R_e I_{po})}{n_s Ak*Te}} - 1 \right) - \frac{V_{po}+R_e I_{po}}{R_q} \tag{3.1}$$

The V_p and I_{sh} are expressed in terms of irradiance and temperature as [3.1],

$$I_{sh} = I_{sh,r}\left[1+\alpha\left(Te - Te_r\right)\right]\frac{g}{g_r} \tag{3.2}$$

$$V_p = V_{p,r}\left[1 + a \times \ln\frac{g}{g_r} + \beta\left(Te - Te_r\right)\right] \tag{3.3}$$

Whereas, the value of a is calculated using the practical implementation, in which the constant value is derived by operating the system for a particular irradiation and temperature levels [3.1]. The manufacturer data used for designing solar panel in MATLAB-Simulink atmosphere is represented in Table-3.1.

3.3 PROPOSED MPP DETECTION TECHNIQUE

3.3.1 Relation between MPP values for single panel, Series (S) and parallel (P) configurations

For observing the relation between MPP characteristics, the irradiation levels considered for different configurations are shown in Fig. 3.2. The proposed scheme is operated for 9 types of sets as shown in Fig. 3.2, where set 1, set 2 and set 3, are the single panel configurations with irradiation levels of 1000 W/m^2, 800 W/m^2 and 600 W/m^2 respectively. Similarly, set 4, set 5 and set 6, are the series (2S) configurations with irradiation levels of 1000 W/m^2, 800 W/m^2 and 600

W/m^2 respectively. Finally, set 7, set 8 and set 9, are the parallel (2P) configurations with irradiation levels of 1000 W/m^2, 800 W/m^2 and 600 W/m^2 respectively.

3.3.1.1 MPP values for single panel

By considering the manufacturer details as represented in Table-3.1, a model is developed in MATLAB environment to obtain power-voltage (P-V) and current-voltage (I-V) characteristics for single solar panel which is represented in Fig. 3.3. From Fig. 3.3a, MPP values of current, voltage and power for set 1 are I_1=8.4625A, V_1=30.7235V and P_1=259.999W. Similarly, from Fig. 3.3b, MPP values for set 2 are I_2=6.7626A, V_2=29.8940V and P_2=202.1601W. Finally, from Fig. 3.3c, MPP values for set 3 are I_3=5.0634A, V_3=28.6911V and P_3=145.2768W.

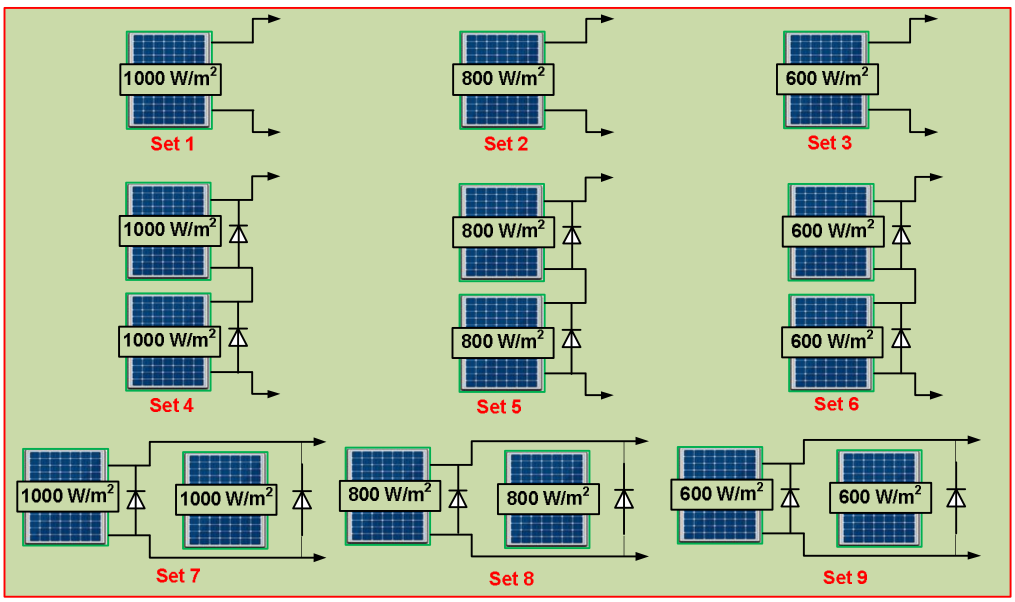

Fig. 3.2. Different patterns and configurations for proposed work

3.3.1.2 Relation between MPP values for single panel and series configuration

For the considered series configurations, output characteristics are represented in Fig. 3.4. From Fig. 3.4a, MPP values of current, voltage and power for set 4 are I_4=8.4603A, V_4=61.4795V and P_4=520.1378W. Similarly, from Fig. 3.4b, MPP values for set 5 are I_5=6.7635A, V_5=59.7802V and P_5=404.3252W. Finally, from Fig. 3.4c, MPP values for set 6 are I_6=5.064A, V_6=57.3765V and P_6=290.5574W. By observing the MPP values of single panel and series connected panels, the equations can be derived as (3.4)-(3.9).

$$V_4 \approx 2 * V_1 \tag{3.4}$$

$$I_4 \approx I_1 \tag{3.5}$$

$$V_5 \approx 2 * V_2 \tag{3.6}$$

$$I_5 \approx I_2 \tag{3.7}$$

$$V_6 \approx 2 * V_3 \tag{3.8}$$

$$I_6 \approx I_3 \tag{3.9}$$

3.3.1.3 Relation between MPP values for single panel and parallel configuration

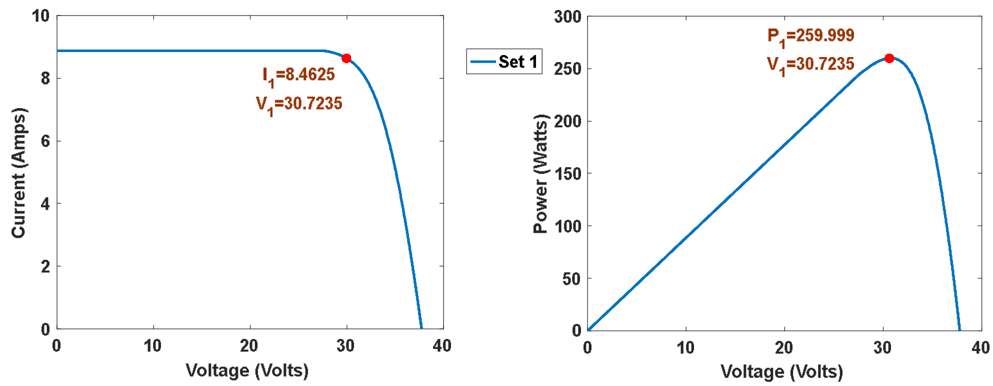

a

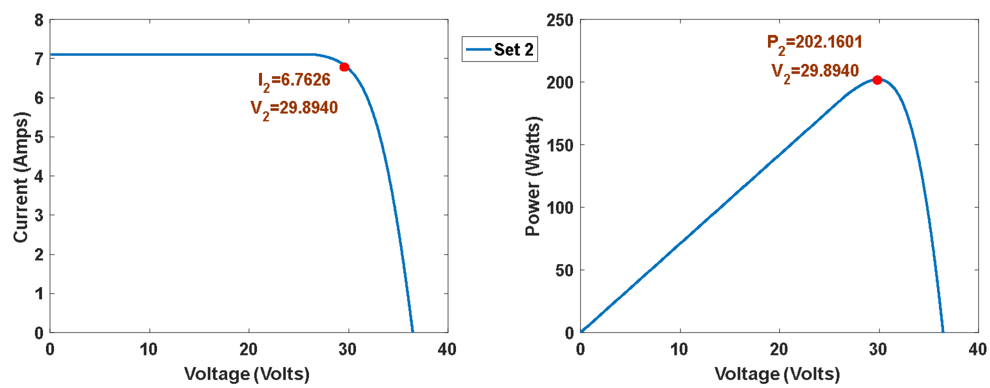

b

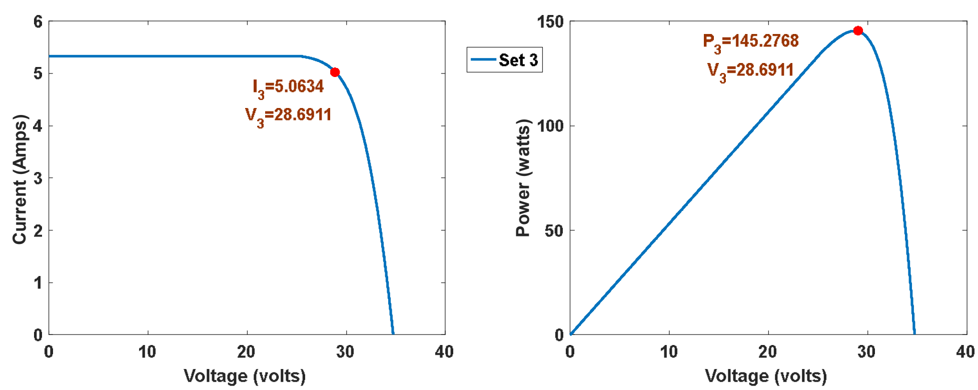

c

Fig. 3.3. I-V & P-V characteristics for single panel (a. Set 1, b. Set 2 & c. Set 3)

For the considered parallel configurations, output characteristics are represented in Fig. 3.5. From Fig. 3.5a, MPP values of current, voltage and power for set 7 are I_7=16.9001A, V_7=30.7756V and P_7=520.1116W. Similarly, from Fig. 3.5b, MPP values for set 8 are I_8=13.5365A, V_8=29.8679V and P_8=404.3077W. Finally, from Fig. 3.5c, MPP values for set 9 are I_9=10.1336A, V_9=28.6714V and P_9=290.5459W.

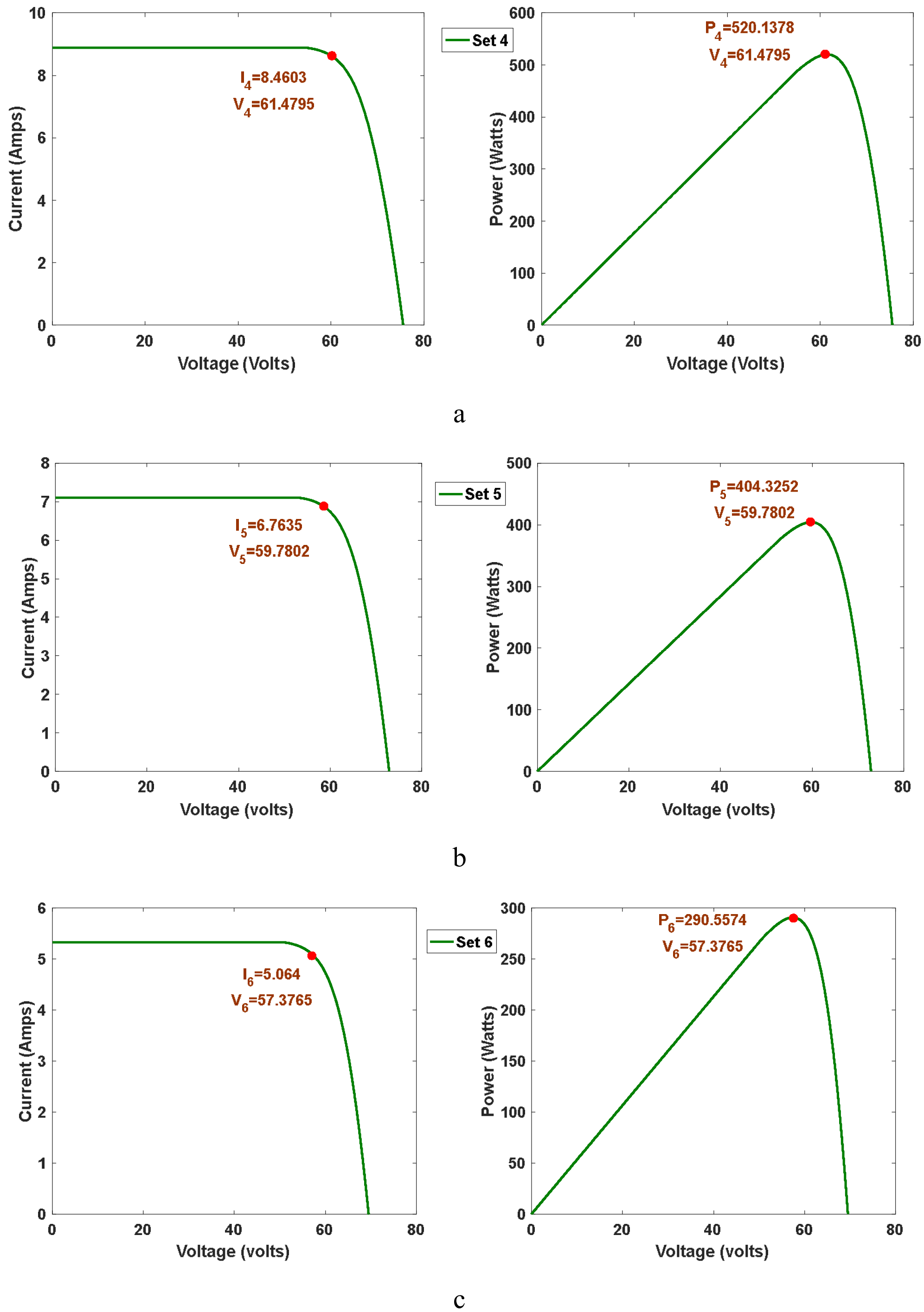

Fig. 3.4. I-V & P-V characteristics for series configurations (a. Set 4, b. Set 5 & c. Set 6)

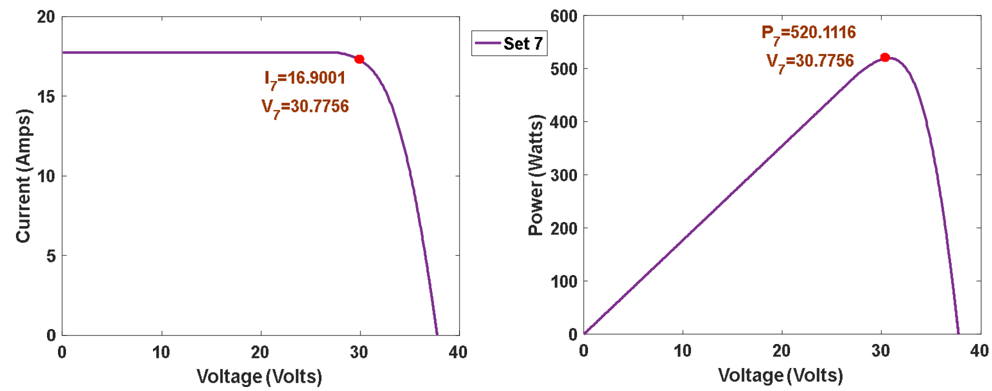

a

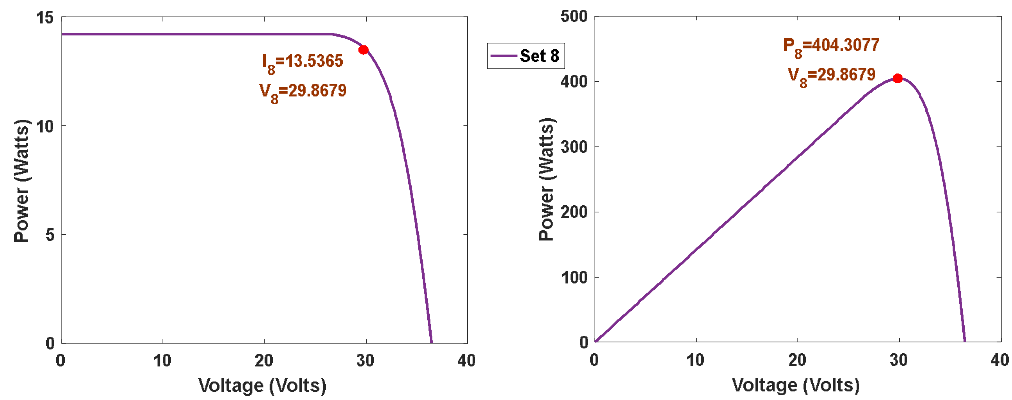

b

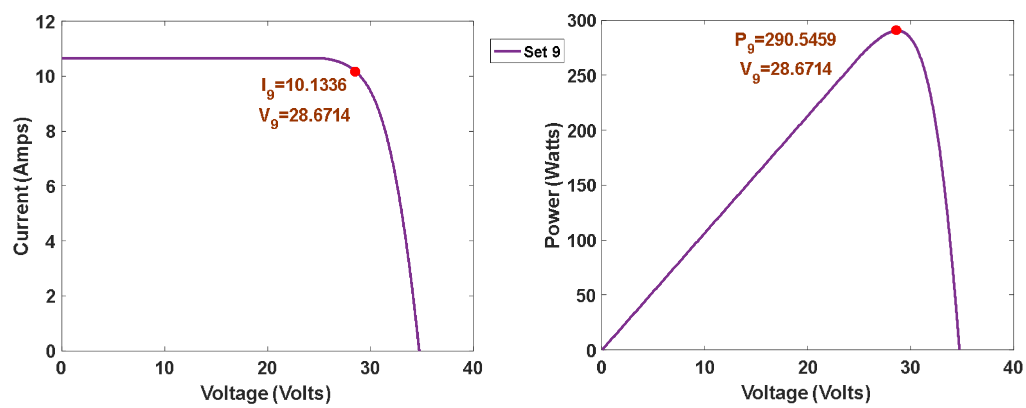

c

Fig. 3.5. I-V & P-V characteristics for parallel configurations (a. Set 7, b. Set 8 & c. Set 9)

By observing the MPP values of single panel and parallel connected panels, the equations can be is derived as,

$$V_7 \approx V_1 \tag{3.10}$$

$$I_7 \approx 2 * I_1 \tag{3.11}$$

$$V_8 \approx V_2 \tag{3.12}$$

$$I_8 \approx 2*I_2 \tag{3.13}$$

$$V_9 \approx V_3 \tag{3.14}$$

$$I_9 \approx 2*I_3 \tag{3.15}$$

3.3.2 MPP detection

By observing (3.4)-(3.15), it is confirmed that, MPP values of a single solar panel is sufficient in detecting the MPP values of series and parallel configurations. Therefore, by using the single panel MPP values as obtained in Fig. 3.3, the MPP values for series and parallel configurations can be evaluated.

3.3.2.1 Series Configuration

Using (3.4)-(3.5), the MPP values for set 4 are obtained as, I_4=8.4625A, V_4=61.447V and P_4=519.995W. Similarly, by employing (3.6)-(3.7), the MPP values for set 5 are obtained as, I_5=6.7626A, V_5=59.788V and P_5=404.3223W. Finally, by employing (3.8)-(3.9), the MPP values for set 6 are obtained as, I_6=5.0634A, V_6=57.3822V and P_6=290.5490W. The actual and calculated MPP values of series configurations are represented in Table-3.2.

Table 3.2. Comparison of actual and estimated MPP values of series configuration

Set	MPP voltage (V_{max}) (Volts)		MPP current (I_{max}) (Amps)		MPP power (P_{max}) (Watts)	
	actual	calculated	actual	calculated	actual	calculated
4	61.4795	61.447	8.4603	8.4625	520.1378	519.995
5	59.7802	59.788	6.7635	6.7626	404.3252	404.3223
6	57.3765	57.3822	5.064	5.0634	290.5574	290.5490

3.3.2.2 Parallel Configuration

By employing (3.10)-(3.11), the MPP values for set 7 are obtained as, I_7=8.4625A, V_7=61.447V and P_7=519.995W. Similarly, by employing (3.12)-(3.13), the MPP values for set 8 are obtained as, I_8=6.7626A, V_8=59.788V and P_8=404.3223W. Finally, by employing (3.14)-(3.15), the MPP values for set 9 are obtained as, I_9=5.0634A, V_9=57.3822V and P_9=290.5490W. The actual and calculated MPP values of parallel configurations are represented in Table-3.3.

Table 3.3. Comparison of actual and estimated MPP values of parallel configuration

Set	MPP voltage (V_{max}) (Volts)		MPP current (I_{max}) (Amps)		MPP power (P_{max}) (Watts)	
	actual	calculated	actual	calculated	actual	calculated
7	30.7756	30.7235	16.9001	16.925	520.116	519.995
8	29.8679	29.8940	13.5365	13.5252	404.3077	404.3223
9	28.6714	28.6911	10.1336	10.1268	290.5459	290.549

Overall, from Table-3.2 and Table-3.3, it is noted that, by using the MPP values of single solar panel MPP values for series and parallel configuration can be detected with precision.

3.4 PROPOSED WA-P&O MPPT SCHEME

3.4.1 Existing algorithms

The WA-P&O MPPT topology is derived by avoiding the disadvantages of the existing MPPT schemes like P&O, modified P&O, CV method, ARV method and [3.11]. Fig. 3.6a represents the flowchart for P&O MPPT scheme, where V_{po} and I_{po} are sensed for tracking MPP. With the sudden changes in irradiation, there is an abrupt variation in solar panel power, but in P&O case, as it is weather insensitive, it takes the abrupt power change, as a resultant of perturbation. This inconvenience results in drifting the MPP power under sudden changes in solar insolation.

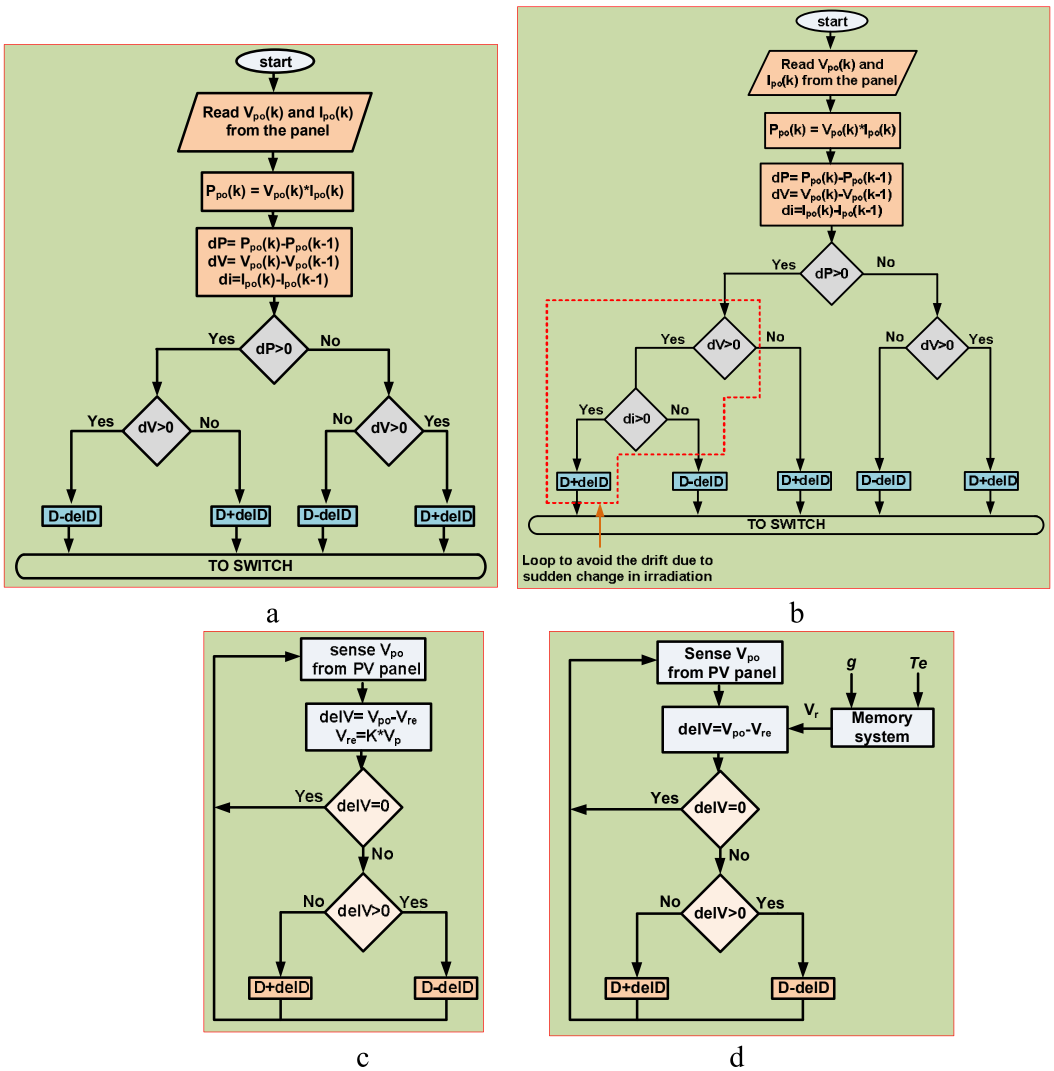

Fig. 3.6. Conventional MPPT algorithms (where V_{re} is reference voltage, K is a constant with variation of 80-90%)
a. P&O, b. MP&O, c. CV and d. ARV

Beside this, P&O results in considerable oscillation and settling time while tracking MPP [3.12]. To avoid this drifting problem in P&O, MP&O MPPT is introduced. Fig. 3.6b represents the modified P&O MPPT, where one extra current component is added in P&O MPPT to make it sensitive to atmosphere. This extra current component provides the ability to differentiate, whether the power change is because of tracking or irradiation variation. Except the avoidance of drift under sudden change in irradiation, MP&O operating properties are almost same like P&O MPPT.

The researches can be divided into two groups, where the first group deals with voltage-based MPPT schemes and other deal with current-based MPPT schemes. Both these schemes have the major advantage of requiring single sensor for MPPT. But they lead to the major disadvantage of low efficiency and irregularity in supplying to the load. In this proposed work, the voltage-based schemes have been employed in developing the topology for WA-P&O scheme.

Fig. 3.6c, represents the CV MPPT, where a single voltage sensor is sufficient for tracking MPP. CV MPPT is the most economical conventional MPPT algorithm related to other existing schemes [3.22]. In CV MPPT, solar panel voltage is compared with MPP voltage at STC in tracking maximum power. Since, the MPP voltages varies with change in irradiation, CV MPPT faces the major disadvantage of inefficiency in tracking maximum power at lower irradiation cases.

To overcome the inefficiency in CV MPPT, ARV MPPT is developed [3.25]. Fig. 3.6d represents the ARV MPPT algorithm, it has the major advantage of tracking the maximum power at all possible irradiation cases. In ARV MPPT, MPP voltages are stored in memory at all possible irradiation cases and later employed as reference voltages in tracking maximum power. Since ARV MPPT is irradiation sensitive, it avoids the drift due to abrupt variation in solar insolation. Although, ARV MPPT is advantageous comparing with CV, it results in the main drawback of huge processing memory requirement. Beside this, in ARV MPPT, PI controller gain values are calculated at STC and same values are used for all operating conditions, this results in poor dynamics under sudden change in irradiation case.

In [3.11], an adaptive PID controller-based P&O MPPT is introduced, in which controller gain values are updated with change in irradiation. This automatic updated PID controller mechanism improves the operating characteristics of the system at all possible irradiation cases. Even though, [3.11] is advantageous, it requires the feedback of perturbation power for each iteration, making it tedious to reach steady state. Beside this, [3.11] has the inability in detecting the cause for change in perturbation power, resulting in drift under abrupt change in irradiation. By observing the pros and cons of these MPPT schemes, the proposed WA-P&O MPPT is developed.

3.4.2 Proposed system

Fig. 3.7, represents the overall schematic diagram of proposed WA-P&O scheme. The proposed system comprises of a solar panel in coordination of DC-DC converter to feed the load. In the proposed system, PV panel voltage, current, irradiation and temperature are sensed and given as an input to WA-P&O MPPT scheme, to produce the respective pulse for triggering the DC-DC converter gate. The proposed system is operated for single, series and parallel solar panel configurations as shown in Fig. 3.7.

3.4.3 Proposed WA-P&O algorithm

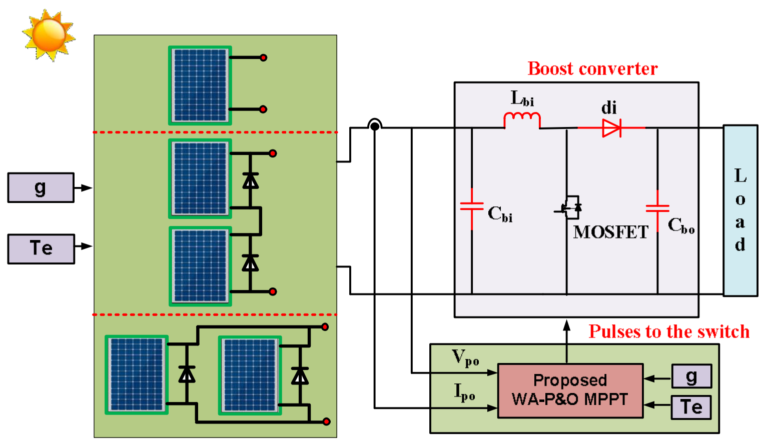

Fig. 3.7. Schematic diagram of proposed system

The algorithm for the WA-P&O scheme is represented in Fig. 3.8. The proposed algorithm consists of two major steps, they are estimating the MPP, K_P and K_I calculator.

3.4.3.1 Estimating the MPP

In the proposed WA-P&O scheme, nearest point to MPP is estimated and it is used as an initial point for starting P&O tracking. This results in the quick response leading to lower settling time.

3.4.3.1.1 single panel

The open circuit voltage and short circuit current of a single solar panel are derived by substituting, sensed irradiation and temperature values in (3.2) & (3.3). Using the derived V_p, I_{sh} values, the V_r, I_r and P_r at possible g and Te are calculated as,

$$V_r = K_m * V_p \big|_{(g,Te)} \tag{3.16}$$

$$I_r = K_n * I_{sh} \big|_{(g,Te)} \tag{3.17}$$

$$P_r = V_r * I_r \tag{3.18}$$

From (3.16) and (3.17), K_m and K_n are calculated as,

$$K_m = \frac{V_{max}}{V_p}\bigg|_{STC} \tag{3.19}$$

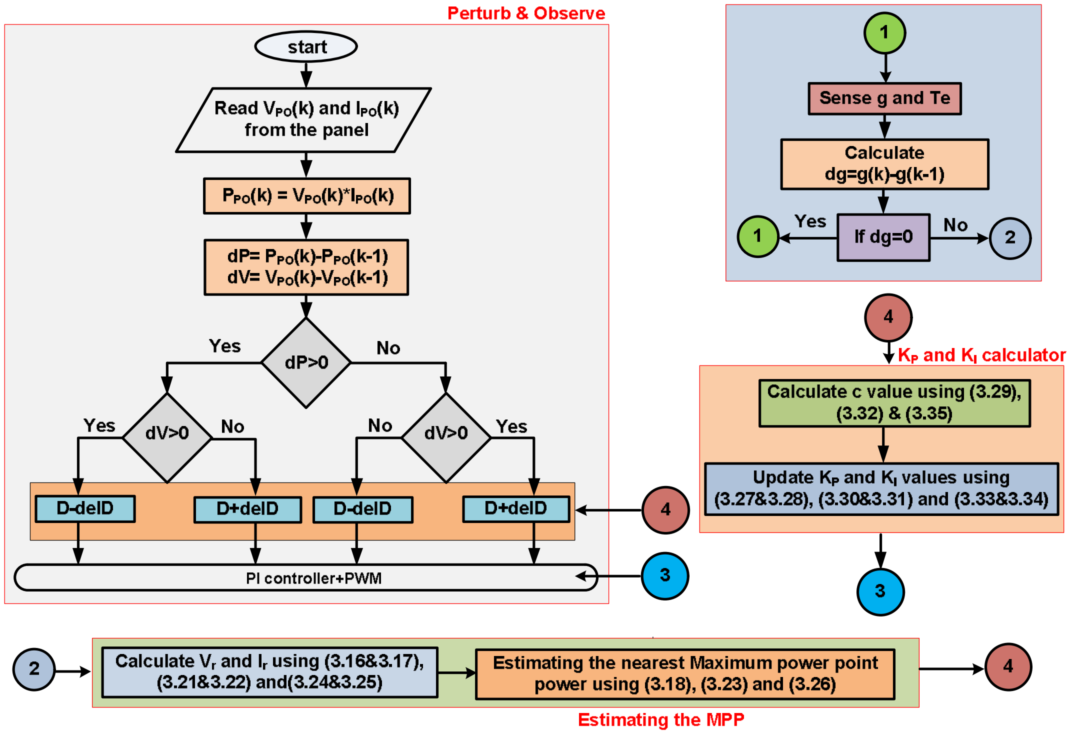

Fig. 3.8. Flowchart of proposed WA-P&O MPPT

$$k_n = \left.\frac{I_{\max}}{I_{sh}}\right|_{STC} \tag{3.20}$$

This estimated MPP point is use as a reference point, from where P&O starts tracking. This mechanism reduces the searching time for MPP detection, resulting in lower settling time.

3.4.3.1.2 Series configuration

By using (3.4)-(3.9), it can be observed that, MPP values of series configurations can be found using the MPP values of single solar panel. Therefore, by employing (3.16)-(3.20), the $V_r|_{series}$, $I_r|_{series}$ and $P_r|_{series}$ at all possible irradiation and temperature cases, for N number of series connected solar panels, are calculated as,

$$V_r|_{series} = N * V_r \tag{3.21}$$

$$I_r|_{series} = I_r \tag{3.22}$$

$$P_r|_{series} = V_r|_{series} * I_r|_{series} \tag{3.23}$$

3.4.3.1.3 Parallel configuration

By using (3.10)-(3.15), it can be observed that, MPP values of parallel configurations can be found using the MPP values of single solar panel. Therefore, by employing (3.16)-(3.20), the $V_r|_{parallel}$, $I_r|_{parallel}$ and $P_r|_{parallel}$ at all possible irradiation and temperature cases, for N number of parallel connected solar panels, are calculated as,

$$V_r|_{parallel} = V_r \tag{3.24}$$

$$I_r|_{parallel} = N * I_r \tag{3.25}$$

$$P_r|_{parallel} = V_r|_{parallel} * I_r|_{parallel} \tag{3.26}$$

3.4.3.2 K_P and K_I calculator

In ARV MPPT, PI controller gain values, K_p and K_I are calculated at STC and same values are employed for all other irradiation cases. This leads to effect the MPP tracking characteristics other than STC. In the proposed scheme, an automatic PI controller updating system is established to improve the MPPT response at all possible irradiation cases. The PI controller tuning in WA-P&O is similar to that of [3.11]. But, unlike [3.11], the WA-P&O method updates the K_p and K_I values at the instant of irradiation change without any delay as there is no perturbation of power is needed for calculating the control gains. Moreover, the proposed MPPT scheme does not require any optimization-based process in PI controller tuning resulting in low complexity and easy real time implementation. Overall, it is noted that, WA-P&O algorithm displays more advantages related to other existing adaptive PI & PID controller based MPPT schemes. In the proposed PI controller tuning process, K_p and K_I gain values are calculated initially by employing trial and error method at STC [3.25]. For the irradiation cases other than STC, PI controller gain values are updated as [3.11],

$$k_p|_{op} = k_p|_{STC} \times c \tag{3.27}$$

$$k_I|_{op} = k_I|_{STC} + c \tag{3.28}$$

From (3.27) and (3.28), c is calculated as (3.29),

$$c = \frac{P_{\max}|_{STC}}{P_r|_{op}} \tag{3.29}$$

Table. 3.4. Controller gain values at different irradiation levels for single solar panel

g (W/m^2)	Te (^{o}C)	K_p	K_I
800	25	1.2861	7.2861
600	25	1.7897	7.7897

For better clarification about updating PI controller gain values, single solar panel is considered. For the considered system, controller gain constants are calculated as K_p=1 and K_I=6 at STC, by using trial and error method [3.25]. The MPP power of single solar panel is calculated using (3.18), the obtained value is used as the operating MPP power in (3.29) to obtain c value. Further, the obtained c value is employed in updating PI controller gain values using (3.27)-

(3.28). By employing the proposed PI controller tuning, the values of gains at different irradiation levels for a single solar panel are represented in Table-3.4.

Similar kind of operation is employed for series and parallel configurations in tuning PI controller gain values. For series and parallel configurations, PI controller gain values are calculated using (3.30)-(3.32) and (3.33)-(3.35) respectively. Overall, the proposed system is having a simple auto PI tuning process compared to existing MPPT schemes, resulting in easy real time implementation.

$$\left(k_p\big|_{op}\right)_{series} = \left(k_p\big|_{STC}\right)_{series} \times c_{series} \tag{3.30}$$

$$\left(k_I\big|_{op}\right)_{series} = \left(k_I\big|_{STC}\right)_{series} + c_{series} \tag{3.31}$$

$$(c)_{series} = \left(\frac{P_{\max}\big|_{STC}}{P_r\big|_{op}}\right)_{series} \tag{3.32}$$

$$\left(k_p\big|_{op}\right)_{parallel} = \left(k_p\big|_{STC}\right)_{parallel} \times c_{parallel} \tag{3.33}$$

$$\left(k_I\big|_{op}\right)_{parallel} = \left(k_I\big|_{STC}\right)_{parallel} + c_{parallel} \tag{3.34}$$

$$(c)_{parallel} = \left(\frac{P_{\max}\big|_{STC}}{P_r\big|_{op}}\right)_{parallel} \tag{3.35}$$

3.5 SIMULATION RESULTS AND EXPLANATION

The proposed WA-P&O is implemented in MATLAB simulink atmosphere for the considered single panel, series and parallel configurations as shown in Fig. 3.2.

3.5.1 Single solar panel

For a single solar panel, various irradiation sets, set 1, set 2 and set 3 are considered as shown in Fig. 3.2. Further, single panel system is operated for single set and two step changes in sets cases.

3.5.1.1 Single set with no steps

For the set 1 of irradiation level 1000 W/m^2, the PV panel characteristics such as, voltage, current, power and duty cycle are represented in Fig. 3.9a, 3.9b, 3.9c & 3.9d, respectively. Similarly, for the set 2 and set 3 of 800 W/m^2 and 600 W/m^2, the tracked solar panel power is displayed in Fig. 3.9e & 3.9f. From Fig. 3.9, it is observed that, proposed WA-P&O scheme displays good dynamic characteristics of lower settling time (less than 10 ms) compared to [3.11], P&O and MP&O [3.12] schemes, with near zero steady state oscillations.

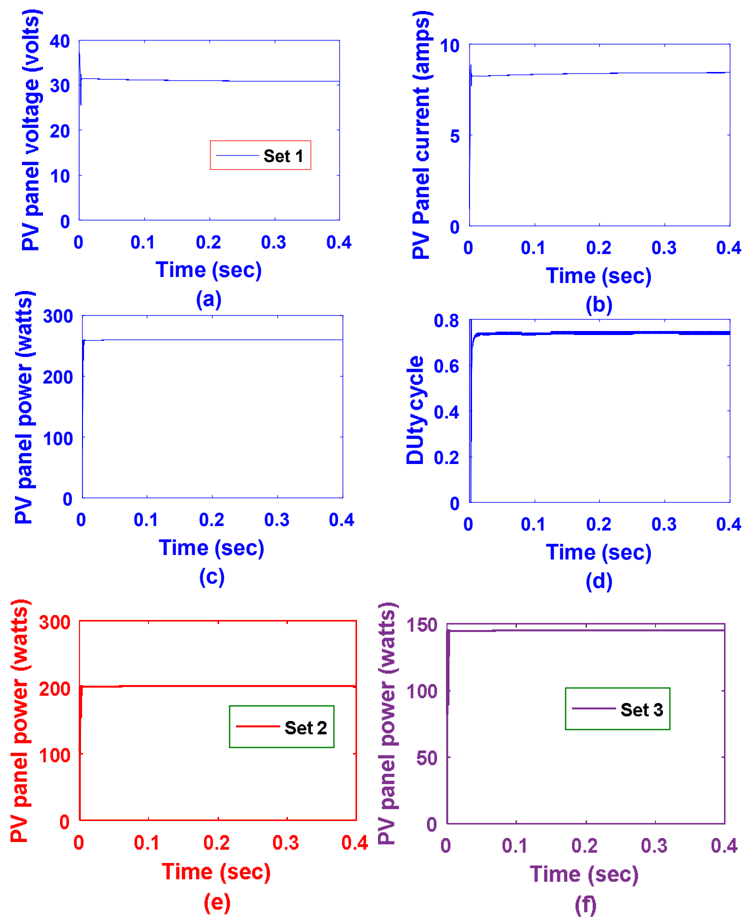

Fig. 3.9. PV panel characteristics for single panel

3.5.1.2 Two-step changes in single set

In this case, the proposed WA-P&O scheme is examined under the two steps variation of the considered sets. For the two-step up variation of set (3-2-1) at 200 ms & 400 ms, the PV panel voltage, current, power and duty cycle are represented in Fig. 3.10a, 3.10b, 3.10c & 3.10d, respectively. Similarly, for the two-step down variation of set (1-2-3) at 200 ms & 400 ms, the PV panel voltage, current, power and duty cycle are represented in Fig. 3.11a, 3.11b, 3.11c & 3.11d, respectively. From, Fig. 3.10 & 3.11, it can be noted that, irrespective of step-up and step-down changes in sets, the proposed WA-P&O displays smooth tracking with good dynamic characteristics compared to few existing MPPT schemes. From Fig. 3.10 & 3.11, it can be observed that, the proposed WA-P&O tracking displays improved MPPT efficiency compared to CV algorithm [3.25]. Moreover, due its weather sensitive nature, WA-P&O shows lower drift under sudden change in irradiation.

Overall, for the considered cases of single panel, PI controller gain values are updated along with irradiation variations, as shown in Table-3.4. This auto updating controller gains, results in the better operating characteristics compared to [3.11].

3.5.2 Series configuration

For series configuration, various irradiation sets, set 4, set 5 and set 6 are considered as represented in Fig. 3.2. Further, the series configuration system is executed for single set and two step changes in sets cases.

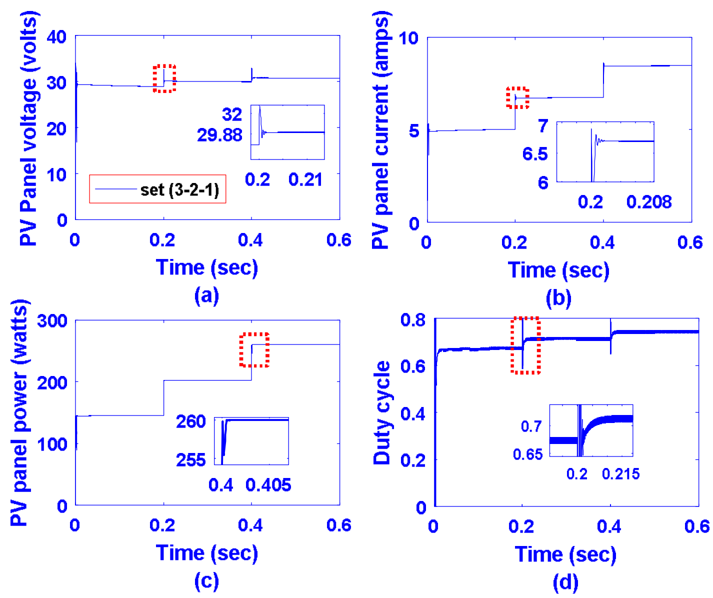

Fig. 3.10. PV panel characteristics for single panel under two-step up changes in sets

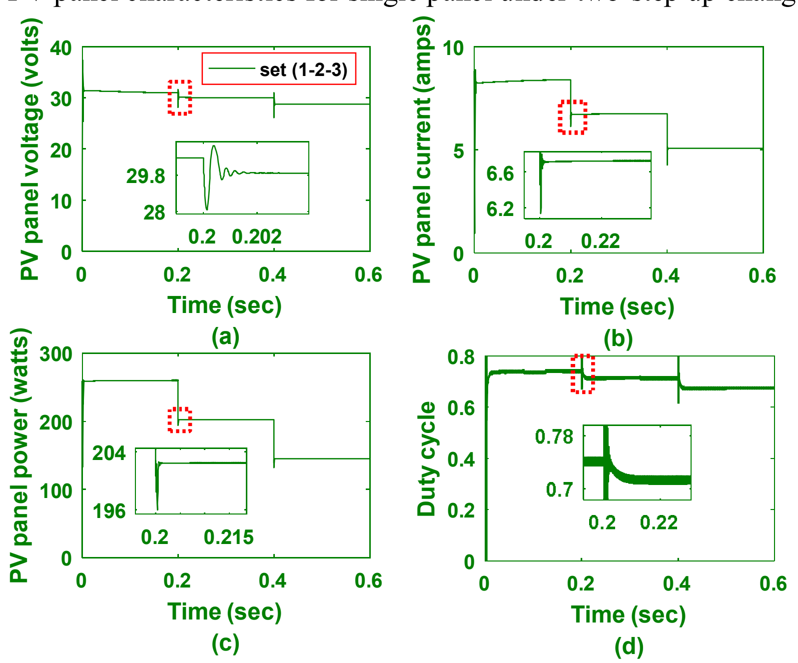

Fig. 3.11. PV panel characteristics for single panel under two step-down changes in sets

3.5.2.1 Single set with no step change

For the set 4 of irradiation level 1000 W/m^2, the PV panel characteristics such as, voltage, current, power and duty cycle are represented in Fig. 3.12a, 3.12b, 3.12c & 3.12d, respectively. Similarly, for the set 5 and set 6 of 800 W/m^2 and 600 W/m^2, the tracked solar panel power is displayed in Fig. 3.12e & 3.12f respectively.

3.5.2.2 Two-step changes in single set

In this case, the proposed WA-P&O scheme is examined under the two steps variation of the considered sets. For the two-step up changes of set (6-5-4) at 200 ms & 400 ms, the PV panel voltage, current, power and duty cycle are represented in Fig. 3.13a, 3.13b, 3.13c & 3.13d, respectively. Similarly, for the two-step down variation of set (4-5-6) at 200 ms & 400 ms, the PV panel voltage, current, power and duty cycle are represented in Fig. 3.14a, 3.14b, 3.14c & 3.14d respectively. Overall, From Fig. 3.12, 3.13 & 3.14, it can be observed that, series configuration of solar panels displays smooth operating characteristics with drift avoidance. The auto updating of PI controller gains for series configuration are done by using (3.30)-(3.32).

3.5.3 Parallel configuration

For parallel configuration, various irradiation sets, set 7, set 8 and set 9 are considered as represented in Fig. 3.2. Further, the parallel configuration system is operated for single set and two step changes in sets cases.

3.5.3.1 Single set with no step change

For the set 7 of irradiation level 1000 W/m^2, the PV panel characteristics such as, voltage, current, power and duty cycle are represented in Fig. 3.15a, 3.15b, 3.15c & 3.15d, respectively. Similarly, for the set 8 and set 9 of 800 W/m^2 and 600 W/m^2, the tracked solar panel power is displayed in Fig. 3.15e & 3.15f.

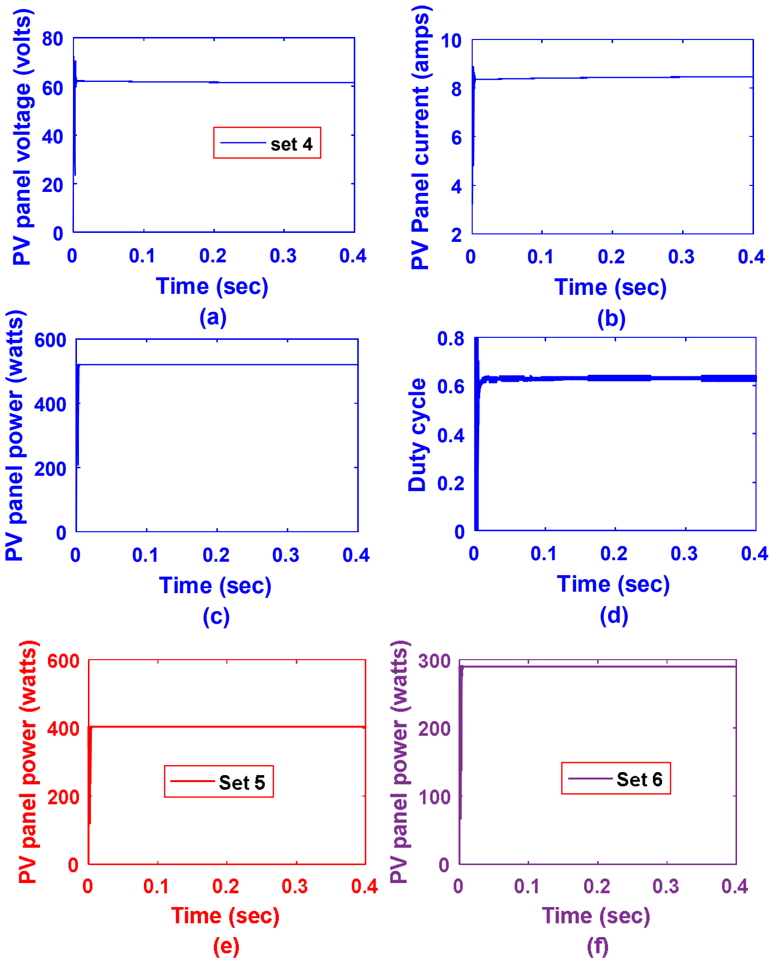

Fig. 3.12. PV panel characteristics for series configuration

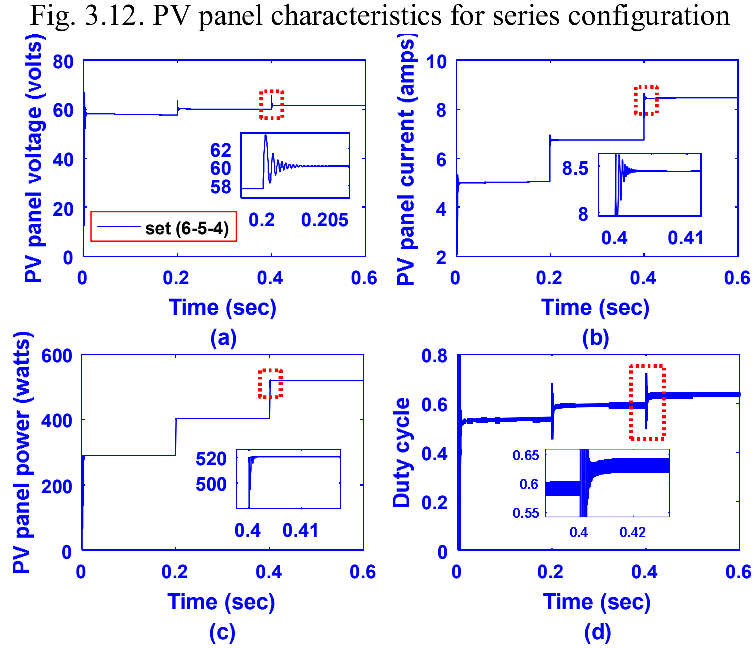

Fig. 3.13. PV panel characteristics for series configuration under two step-up changes in sets

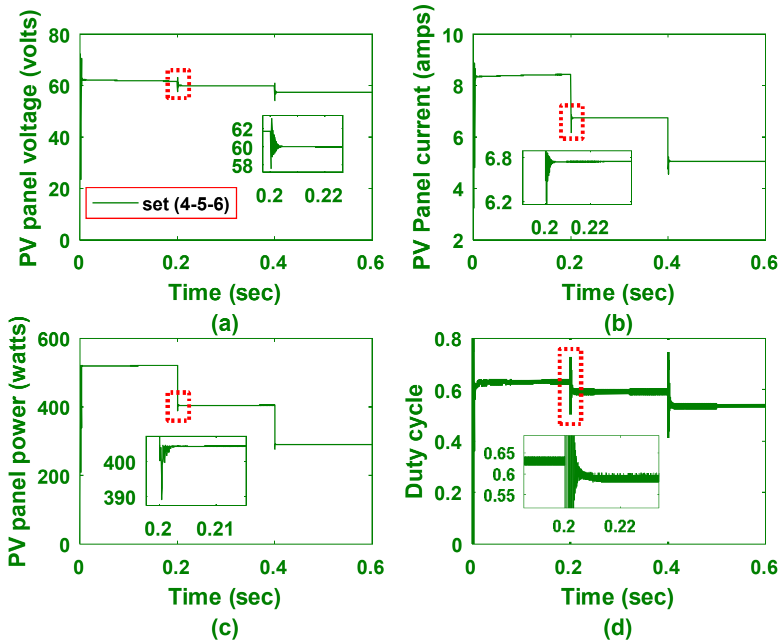

Fig. 3.14. PV panel characteristics series configuration under two-step down changes in sets

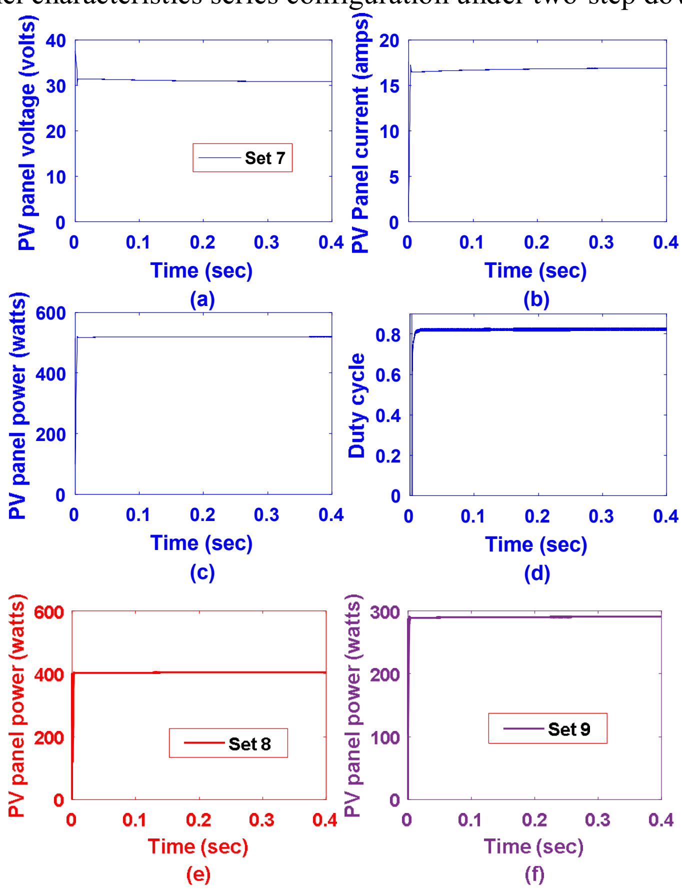

Fig. 3.15. PV panel characteristics for parallel configuration

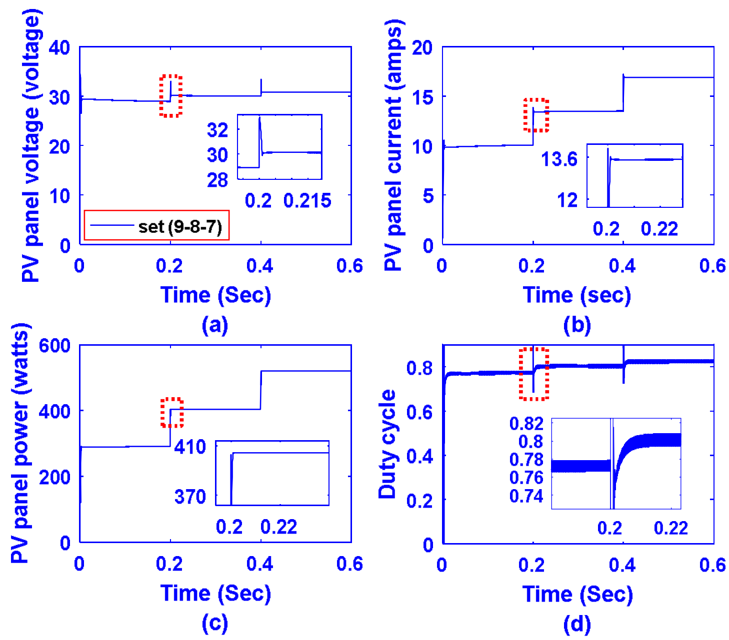

Fig. 3.16. PV panel characteristics for parallel configuration under two-step up changes in sets

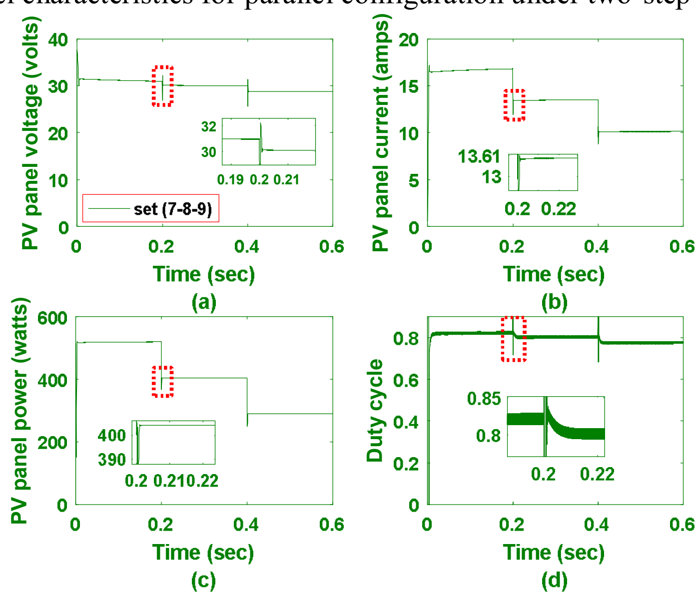

Fig. 3.17. PV panel characteristics for parallel configuration under two-step down changes in sets

3.5.3.2 Two-step changes in single set

In this case, the proposed WA-P&O scheme is examined under the two steps variation of the considered sets. For the two-step up changes of set (9-8-7) at 200 ms & 400 ms, the PV panel characteristics such as, voltage, current, power and duty cycle are represented in Fig. 3.16a, 3.16b, 3.16c & 3.16d, respectively. Similarly, for the two-step down variation of set (7-8-9) at 200 ms & 400 ms, the PV panel voltage, current, power and duty cycle are represented in Fig. 3.17a, 3.17b, 3.17c & 3.17d, respectively. Overall, From Fig. 3.15, 3.16 & 3.17, it can be observed that, parallel configuration of solar panels displays effective dynamic characteristics. The auto updating of PI controller gains for parallel configurations are done by using (3.33)-(3.35).

3.6 EXPERIMENTAL RESULTS

Fig. 3.18, represents the overall real time setup for the proposed system, where a 260-watt solar panels are employed as single panel, series and parallel configurations to feed the load. In laboratory, artificial insolation is established using halogen lamps, where the intensity of lamps can be varied using a rheostat. For sensing irradiation and temperature, pyranometer and LM35 are used. Along with this, voltage and current sensors are employed in detecting PV module voltage and current for the system. Here, a PIC 18F452 micro controller is employed, which is already automated with proposed algorithm and required PWM program using PC interface. Since the output of PIC controller is of level of 5V, a driver circuit is employed to trigger the K2611 of DC-DC converter. The hardware system is implemented for single panel, series and parallel configurations showed satisfactory results.

3.6.1 Single solar panel

For single solar panel, various irradiation sets, set 1, set 2 and set 3 are considered as represented in Fig. 3.2. Further, the single panel system is executed for single set and two step changes in sets cases.

For the set 1 of irradiation level 1000 W/m^2, the PV panel characteristics such as, voltage, current and power are represented in Fig. 3.19a, 3.19b & 3.19c, respectively. Similarly, for the set 2 and set 3 of 800 W/m^2 and 600 W/m^2, the tracked solar panel power is displayed in Fig. 3.19d & 3.19e.

The proposed WA-P&O scheme is examined under the two steps variation of the considered sets. For the two-step up variation of set (3-2-1) at 200 ms & 400 ms, the PV panel voltage, current and power are represented in Fig. 3.20a, 3.20b & 3.20c, respectively. Similarly, for the two-step down variation of set (1-2-3) at 200 ms & 400 ms, the PV panel voltage, current and power are represented in Fig. 3.21a, 3.21b & 3.21c, respectively.

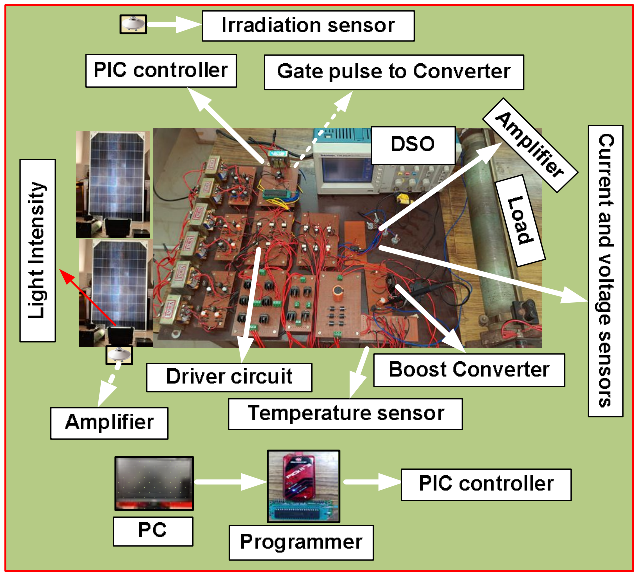

Fig. 3.18. Overall experimental setup for proposed system

3.6.2 Series configuration

For series configuration, various irradiation sets, set 4, set 5 and set 6 are considered as represented in Fig. 3.2. Further, the series configuration system is executed for single set and two step changes in sets cases.

For the set 4 of irradiation level 1000 W/m^2, the PV panel characteristics such as, voltage, current and power are represented in Fig. 3.22a, 3.22b & 3.22c, respectively. Similarly, for the set 5 and set 6 of 800 W/m^2 and 600 W/m^2, the tracked solar panel power is displayed in Fig. 3.22d & 3.22e.

For the two-step up variation of set (6-5-4) at 200 ms & 400 ms, the PV panel voltage, current and power are represented in Fig. 3.23a, 3.23b & 3.23c, respectively. Similarly, for the two-step down variation of set (4-5-6) at 200 ms & 400 ms, the PV panel voltage, current and power are represented in Fig. 3.24a, 3.24b & 3.24c, respectively.

3.6.3 Parallel configuration

For parallel configuration, various irradiation sets, set 7, set 8 and set 9 are considered as represented in Fig. 3.2. Further, the parallel configuration system is executed for single set and two step changes in sets cases.

For the set 7 of irradiation level 1000 W/m2, the PV panel characteristics such as, voltage, current and power are represented in Fig. 3.25a, 3.25b & 3.25c, respectively. Similarly, for the set 5 and set 6 of 800 W/m^2 and 600 W/m^2, the tracked solar panel power is displayed in Fig. 3.25d & 3.25e.

Scale : X-axis : 60ms/unit
Y-axis : 10V/unit

(a)

Scale : X-axis : 60ms/unit
Y-axis : 5A/unit

(b)

Scale : X-axis : 60ms/unit
Y-axis : 50W/unit

(c)

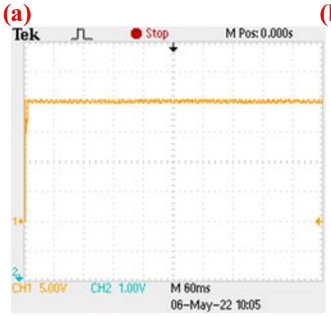

Scale : X-axis : 60ms/unit
Y-axis : 50W/unit

(d)

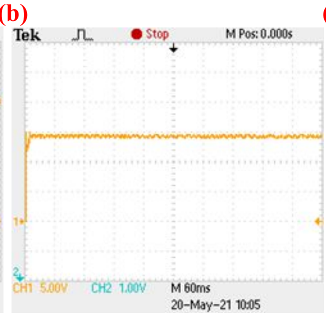

Scale : X-axis : 60ms/unit
Y-axis : 50W/unit

(e)

Fig. 3.19. PV panel characteristics for single panel

Scale : X-axis : 60ms/unit
Y-axis : 10V/unit

(a)

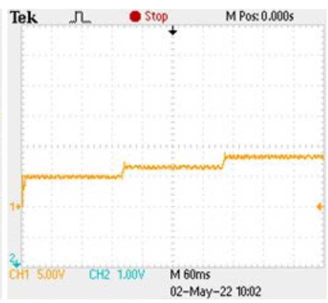

Scale : X-axis : 60ms/unit
Y-axis : 5A/unit

(b)

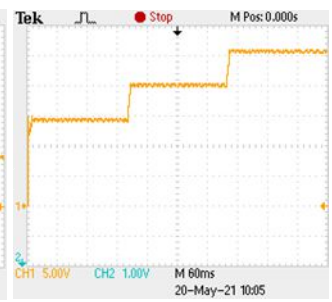

Scale : X-axis : 60ms/unit
Y-axis : 50W/unit

(c)

Fig. 3.20. PV panel characteristics for single panel under two step-up change in sets

Scale : X-axis : 60ms/unit
Y-axis : 10V/unit

(a)

Scale : X-axis : 60ms/unit
Y-axis : 5A/unit

(b)

Scale : X-axis : 60ms/unit
Y-axis : 50W/unit

(c)

Fig. 3.21. PV panel power for single panel under two step-down change in sets

Scale : X-axis : 60ms/unit
Y-axis : 20V/unit
(a)

Scale : X-axis : 60ms/unit
Y-axis : 5A/unit
(b)

Scale : X-axis : 60ms/unit
Y-axis : 100W/unit
(c)

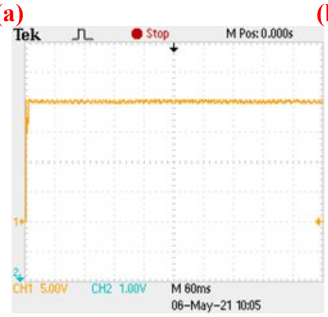

Scale : X-axis : 60ms/unit
Y-axis : 100W/unit
(d)

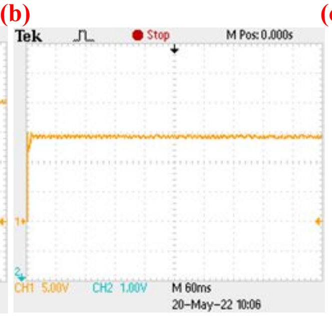

Scale : X-axis : 60ms/unit
Y-axis : 100W/unit
(e)

Fig. 3.22. PV panel characteristics for series configuration

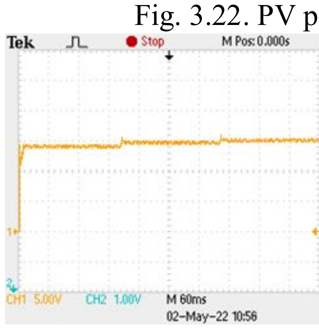

Scale : X-axis : 60ms/unit
Y-axis : 20V/unit
(a)

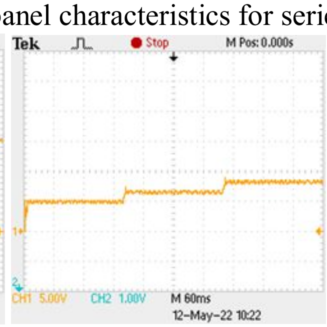

Scale : X-axis : 60ms/unit
Y-axis : 5A/unit
(b)

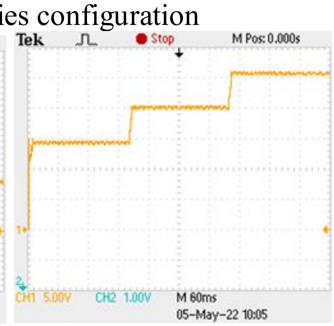

Scale : X-axis : 60ms/unit
Y-axis : 100W/unit
(c)

Fig. 3.23. PV panel characteristics for series configuration under two step-up change in sets

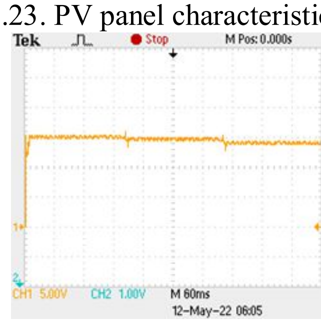

Scale : X-axis : 60ms/unit
Y-axis : 20V/unit
(a)

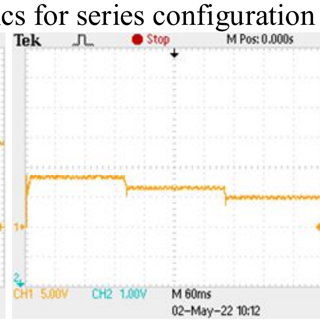

Scale : X-axis : 60ms/unit
Y-axis : 5A/unit
(b)

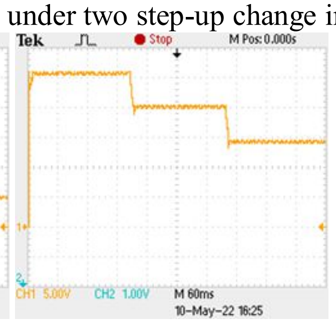

Scale : X-axis : 60ms/unit
Y-axis : 100W/unit
(c)

Fig. 3.24. PV panel characteristics for series configuration under two step-down change in sets

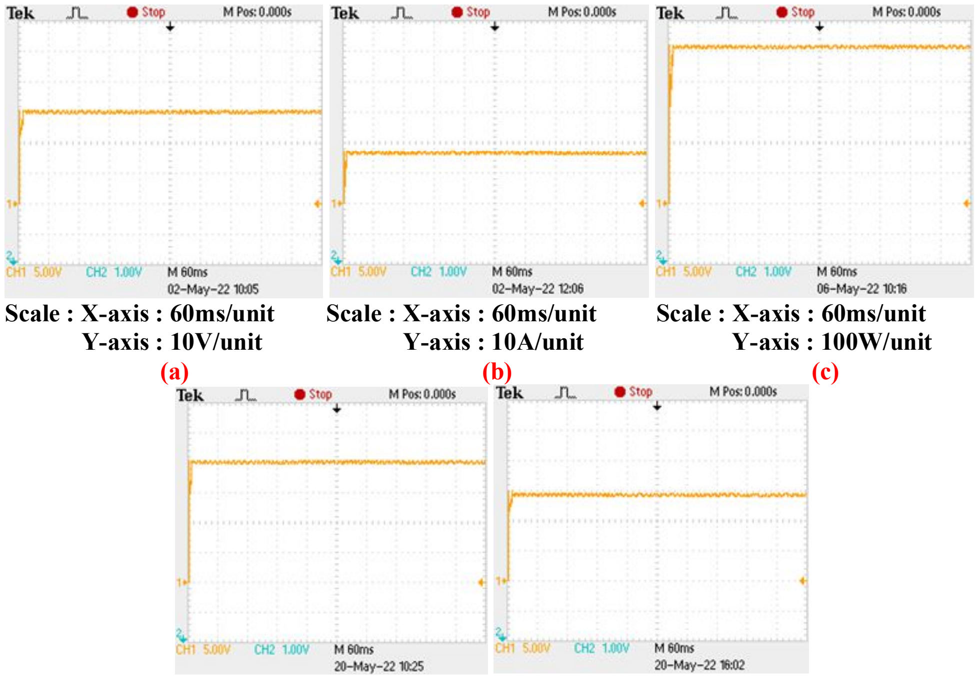

Scale : X-axis : 60ms/unit
Y-axis : 10V/unit
(a)

Scale : X-axis : 60ms/unit
Y-axis : 10A/unit
(b)

Scale : X-axis : 60ms/unit
Y-axis : 100W/unit
(c)

Scale : X-axis : 60ms/unit
Y-axis : 100W/unit
(d)

Scale : X-axis : 60ms/unit
Y-axis : 100W/unit
(e)

Fig. 3.25. PV panel characteristics for parallel configuration

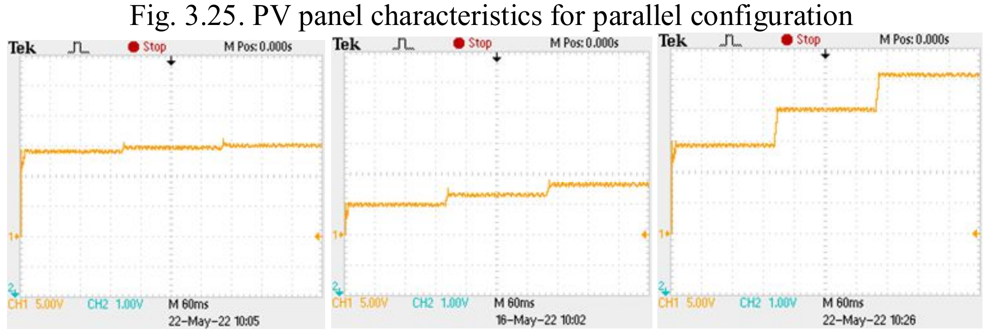

Scale : X-axis : 60ms/unit
Y-axis : 10V/unit
(a)

Scale : X-axis : 60ms/unit
Y-axis : 10A/unit
(b)

Scale : X-axis : 60ms/unit
Y-axis : 100W/unit
(c)

Fig. 3.26. PV panel power for parallel configuration under two step-up change in sets

Scale : X-axis : 60ms/unit
Y-axis : 10V/unit
(a)

Scale : X-axis : 60ms/unit
Y-axis : 10A/unit
(b)

Scale : X-axis : 60ms/unit
Y-axis : 100W/unit
(c)

Fig. 3.27. PV panel power for parallel configuration under two step-down change in sets

For the two-step up variation of set (9-8-7) at 200 ms & 400 ms, the PV panel voltage, current and power are represented in Fig. 3.26a, 3.26b & 3.26c, respectively. Similarly, for the two-step down variation of, set (7-8-9) at 200 ms & 400 ms, the PV panel voltage, current and power are represented in Fig. 3.27a, 3.27b & 3.27c, respectively.

Table 3.5. Comparison of Existing P&O based MPPT Techniques With WA-P&O MPPT

Algorithms	**Tracking Efficiency (%)**	**Settling time (ms)**
P&O	97.1	120
MP&O	98.2	100
[3.11]	99.1	500
WA-P&O	99.3	10

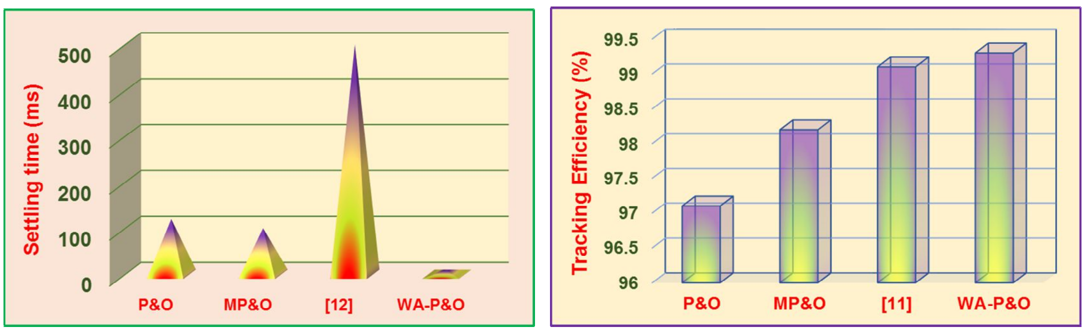

a b

Fig. 3.28. Comparison of the proposed WA-P&O scheme with the existing P&O based schemes (a) Settling time (b) Efficiency **Note:*[11]=[3.11] and *[12]=[3.12]**

Table 3.6. Comparison of Existing MPPT Techniques With WA-P&O MPPT (High-H, Medium-M And Low-L)

MPPT Schemes	**Complexity**	**Tracking efficiency**	**Response time**	**Drift exists**	**Memory unit**	**Steady state error**	**No. of sensors required**
P&O	L	H	H	Yes	No	H	2
Modified P&O	L	H	H	No	No	H	2
[3.11]	M	H	H	Yes	No	M	2
[3.13]-[3.16]	H	H	M	Yes	No	M	2
ARV	L	H	M	No	Yes	M	3
[3.27]	M	H	L	No	No	L	3
CV	L	L	M	No	No	M	1
[3.28]	M	H	M	No	No	L	3
[3.29]	H	H	M	No	No	H	2
Proposed WA-P&O	L	H	L	No	No	L	4

Overall, from Fig. 3.19 - Fig. 3.27, it is observed that, the proposed WA-P&O tracking displays improved dynamic characteristics compared to P&O and MP&O schemes [3.12]. Moreover, due to its weather sensitive nature, WA-P&O displays lower drift under sudden change in irradiation. Beside this, the auto updating controller gain system, results in the better operating characteristics compared to [3.25]. Moreover, the existing P&O based schemes are compared quantitively and statistically with the proposed WA-P&O scheme in the regard of settling time and efficiency as shown in Table-3.5 and Fig. 3.28a & 3.28b respectively. Table-3.6, represents the comparison of proposed WA-P&O scheme with few existing MPPT schemes. From Table-3.6, even though WA-P&O scheme requires two extra sensors, it displays improved MPPT characteristics compared to few existing conventional and adaptive PI & PID controller based MPPT schemes.

3.7 CONCLUSION

In this research work an improved WA-P&O scheme is suggested to avoid the disadvantages of existing conventional MPPT algorithms.

(1) The proposed method has improved characteristics over existing commonly used P&O based MPPT schemes in terms of lower settling time, negligible steady state error and avoidance of drift under sudden change in irradiation. The efficiency of P&O, MP&O and proposed WA-P&O are around 97.1%, 98.1% and 99.3%.

(2) The proposed scheme also has the advantage of high tracking time of 400ms under lower irradiation levels unlike CV-MPPT of 10ms.

(3) The existing ARV MPPT scheme requires huge processing memory, resulting in higher implementation cost. Moreover, the ARV method does not have any PI controller gain adjustment compared to proposed method.

(4) The Adaptive PI controller based MPPT schemes in [3.13]-[3.20] have the disadvantage of having higher mathematical burden to implement in real time compared to proposed WA-P&O scheme.

(5) The adaptive PID controller-based P&O method in [3.11] requires the continuous feedback of perturbation power for tuning purpose, resulting more drift with sudden change in solar insolation, compared to WA-P&O scheme. The settling time of [3.11] and proposed WA-P&O scheme are around, 500ms and 10ms respectively.

(6) The proposed WA-P&O method is compared with the existing schemes both experimentally and through simulation which provided improved results satisfying theoretical modelling.

Related Publication:

- **BSV Sai**, D. Chatterjee et al., "An Improved Weather Adaptable P&O MPPT Technique Under Varying Irradiation Condition," **ISA Transactions**, **Elsevier**, 2023. (Accepted)

References:

[3.1] Ku Ding, XinGao Bian, HaiHao Liu, and Tao Peng, "A MATLAB-Simulink-Based PV Module Model and Its Application under Conditions of Non uniform Irradiance," IEEE Trans. On ENERGY Conv. vol. 27, no. 4, Dec.2012.

[3.2] Hitesh K. Mehta, Himanshu Warke, Kaushik Kukadiya and Ashish K. Panchal, "Accurate Expressions for Single-Diode-Model Solar Cell Parameterization," *IEEE journal of Photovolt*., vol. 9, no. 3, May 2019.

[3.3] Sanjeev Kumar Pandey, Sanjaykumar Limaji Patil and Shrivijay B. Phadke, "PWM-Based Adaptive Sliding-Mode Control for Boost DC–DC Converters," *IEEE Trans. on Ind. Electron*., vol. 65, no. 6, June 2018.

[3.4] B. Lekshmi Sree and M.G. Umamaheswari, "A Hankel matrix reduced order SEPIC model for simplified voltage control optimization and MPPT," Solar Energy, Vol. 170, Aug. 2018, Page no. 280-292.

[3.5] R.B.A.Cunha, R.S.Inomoto, J.A.T.Altuna, F.F.Costa, S.G.Di Santo and A.J.Sguarezi Filho, "Constant switching frequency finite control set model predictive control applied to the boost converter of a photovoltaic system," Solar Energy, Vol. 189, 1 Sept. 2019, Page no. 57-66.

[3.6] Amit Kumer Podder, Naruttam Kumar Roy and Hemanshu Roy Pota, "MPPT methods for solar PV systems: a critical review based on tracking nature," *IET Renew. Power Gener*., 2019, Vol. 13 Iss. 10, pp. 1615-1632.

[3.7] Hegazy Rezk and Ali M. Eltamaly, "A comprehensive comparison of different MPPT techniques for photovoltaic systems," Solar Energy, Vol. 112, Feb. 2015, Page no.1-11.

[3.8] L. Piegari, and R. Rizzo, "Adaptive perturb and observe algorithm for photovoltaic maximum power point tracking," *IET Renew. Power Gener.*, Vol. 4, no. 4, pp. 317–28, Jul. 2010.

[3.9] A. K. Abdel salam, A. M. Massoud, S. Ahmed, and P. N. Enjeti, "High-performance adaptive perturb and observe MPPT technique for photovoltaic-based microgrids," *IEEE Trans. Power Electron.*, Vol. 26, no. 4, pp. 1010–21, Apr. 2011.

[3.10] Y. Jiang, J. A. A. Qahouq, and T. A. Haskew, "Adaptive step size with adaptive-perturbation-frequency digital MPPT controller for a single sensor photovoltaic solar system," *IEEE Trans. Power Electron.*, Vol. 28, no. 7, pp. 3195–205, Jul. 2013.

[3.11] Jyotirmaya Sahoo, Susovon Samanta and Shamik Bhattacharyya, "Adaptive PID Controller with P&O MPPT Algorithm for Photovoltaic System," IETE journal of research, Aug. 2018.

[3.12] Muralidhar Killi and Susovon samanta, “Modified Perturb and Observe MPPT Algorithm for Drift Avoidance in Photovoltaic Systems,” *IEEE Tans. Ind. Electron*, VOL. 62, NO. 9, Sep.2015.

[3.13] B. N. Alajmi, K. H. Ahmed, S. J. Finney, and B.W. Williams, “Fuzzy-logic-control approach of a modified hill-climbing method for maximum power point in microgrid standalone photovoltaic system,” *IEEE Trans. Power Electron.*, Vol. 26, no. 4, pp. 1022–30, Apr. 2011.

[3.14] A. S. Oshaba, E. S. Ali, and S. A. Elazin, “MPPT control design of PV system supplied SRM using BAT search algorithm,” *Sust. Energy Grids Netw.*, Vol. 2, pp. 51–60, 2015.

[3.15] N. Femia, G. Petrone, G. Spagnuolo, and M. Vitelli, “Optimization of perturb and observe maximum power point Tracking method,” *IEEE Trans. Power Electron.*, Vol. 20, no. 4, pp. 963–73, Jul. 2005.

[3.16] M. A. Elgendy, B. Zahawi, and D. J. Atkinson, “Assessment of perturb and observe MPPT algorithm implementation techniques for PV pumping applications,” *IEEE Trans. Sust. Energy*, Vol. 3, no. 1, pp. 21–33, Jan. 2012.

[3.17] W. Xiao, W. G. Dunford, P. R. Palmer, and A. Capel, “Application of centered differentiation and steepest descent to maximum power point tracking,” *IEEE Trans. Ind. Electron.*, Vol. 54, no. 5, pp. 2359–549, 2007.

[3.18] A. I. Dounis, P. Kofinas, C. Alafodimos, and D. Tseles, “Adaptive fuzzy gain scheduling PID controller for maximum power point tracking of photovoltaic system,” *Renew. Energy*, Vol. 60, pp. 204–14, Dec. 2013.

[3.19] Muhammad Arsalan, Ramsha Iftikhar, Iftikhar Ahmad, Ammar Hasan, K.Sabahat and A.Javeria, “MPPT for photovoltaic system using nonlinear backstepping controller with integral action,” Solar Energy, Vol. 170, Aug. 2018, Page no. 192-200.

[3.20] A. S. Oshaba, E. S. Ali, and S. A. Elazin, “PI controller design using ABC algorithm for MPPT of PV system suppling DC motor pump load,” *Neural Comput. Appl.*, Vol. 28, no. 2, pp. 353–64, 2017.

[3.21] Masoum, M.A., Dehbonei, H., Fuchs, E.F, “Theoretical and experimental analyses of photovoltaic systems with voltage and current-based maximum power-point tracking,” *IEEE Trans. Energy Convers.*, 2002, 17, (4), pp. 514–522

[3.22] Pandey, A., Dasgupta, N., Mukerjee, A.K., “A simple single-sensor MPPT solution,” *IEEE Trans. Power Electron.*, 2007, 22, (2), pp. 698–700

[3.23] Elgendy, M.A., Zahawi, B., Atkinson, D.J., "Comparison of directly connected and constant voltage controlled photovoltaic pumping systems," *IEEE Trans. Sustain. Energy*, 2010, **1**, (3), pp. 184–192.

[3.24] Aganah, K.A., Leedy, A.W., "A constant voltage maximum power point tracking method for solar powered systems," Proc. 43rd Southeastern Symp. System Theory, 2011, pp. 125–130.

[3.25] Mohamed Lasheen, Ali Kamel Abdel Rahman, Mazen Abdel-Salam and Shinichi Ookawara, "Adaptive reference voltage-based MPPT technique for PV application," *IET Renew, Power Gener*., 2017, Vol. 11 lss. 5, PP. 715-722.

[3.26] Ali M. Eltamaly, "Photovoltaic Maximum Power Point Trackers: An Overview." Advanced Technologies for Solar Photovoltaics Energy Systems (2021): 117-200.

[3.27] Ali M. Eltamaly, "A novel musical chairs algorithm applied for MPPT of PV systems," Renewable and Sustainable Energy Reviews, 146 (2021) 111135.

[3.28] Ali M. Eltamaly, "An Improved Cuckoo Search Algorithm for Maximum Power Point Tracking of Photovoltaic Systems under Partial Shading Conditions," Energies 2021, 14, 953.

[3.29] Mirza A, Mansoor M, Ling Q, Yin B, Javed M, "A Salp-Swarm Optimization based MPPT technique for harvesting maximum energy from PV systems under partial shading conditions.," Energy Convers Manag 2020, 209:112625.

MPPT TECHNIQUES UNDER PARTIAL SHADING CONDITION

A. Using Operating point (Series)

A4.1. INTRODUCTION

PV energy is one of the most focused and well-established renewable energy sources among all others due to its hefty availability and relatively simpler control strategies [A4.1-A4.2]. Since, uniform irradiation results in a single peak for the overall configuration, tracking of maximum power is easier [A4.3, A4.4]. On the other hand, the PS situation leads to multiple peaks both in the Power-Voltage (P-V) and Current-Voltage (I-V) characteristics of the cascaded PV panels, resulting in difficulty to track maximum power. Boost converter is chosen commonly as an intermediate power conditioner in PV system due to its simple structure and flexible control schemes with non-invertible output voltage [A4.5, A4.6]. Under PS case, the conventional MPPT schemes like Hill Climbing (HC) method, Incremental conductance (IC) method etc., are inefficient in tracking power at global maximum [A4.7]. For effective tracking of global maximum under shading case, numerous optimization-based algorithms are introduced to improve efficiency, reduction of cost and complexity [A4.8-A4.10].

Under PS condition, different optimization-based schemes are introduced for tracking global maximum [A4.11-A4.22]. However, all these schemes discussed have the major difficulty of high computational requirement for the processor with low dynamic performance, which restricts these to be efficiently used for MPPT schemes under PS condition.

In this research work, a Dummy Peak Elimination (DPE) based MPPT scheme is proposed which removes the disadvantages of the existing schemes. In the proposed scheme, all the peaks including the peak very close to global maxima for the combined P-V characteristic under PS condition are calculated based on the measured irradiance on each panel. The proposed algorithm uses P&O where the dummy peaks are eliminated and the peak nearest to the required global maxima becomes the initial search point for P&O. The initial estimation of the peak near the global maxima avoids the tendency of P&O to stick to any of the local peaks under PS condition. The proposed scheme uses simple control structure compared to any of the comparable existing schemes as it uses P&O along with dummy peak elimination algorithm. The proposed MPPT has better dynamic properties compared to existing schemes as the initial point is very near to the global maxima. Moreover, it is highly suitable for real time implementation with existing drive compatible hardware. The proposed algorithm is practically studied for 3S configuration under different shading patterns to justify the proposed theoretical concept.

The proposed Dummy Peak Elimination Based MPPT Technique can be implemented for series configuration with a greater number of parallel strings with different irradiations, but the approach is different, which will make the understanding of situation complex and can be a different work. Moreover, there are few irradiation sensors based MPPT schemes are available in research platform primarily handling series connected schemes. Out of which, the recent publication [A4.23], deals with series configuration. By keeping the research demand and developing improves methodologies, the present research article detailed more about series connected modules. The main advantageous features of the proposed DPE MPPT algorithm compared to available MPPT techniques are,

- accurate tracking
- good dynamic properties with low search time
- suitability for real time implementation with hardware having moderate computational facility
- economic viability with no requirement of high-end processing units including scanners etc.

A4.2. SOLAR MODULE MODEL

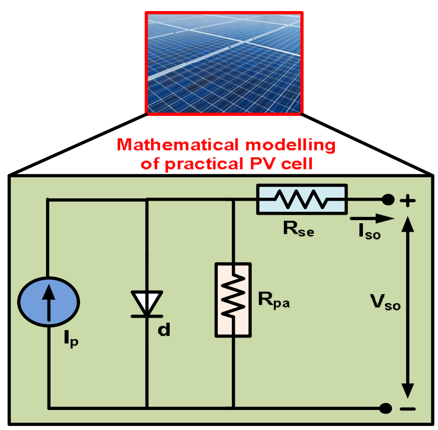

Fig. A4.1. Solar cell representation

Among the available designs for PV modelling, single diode model is prevalent due to its simple construction and precision in generating performance characteristics at par with practical PV cell [A4.2]. Fig. A4.1 represents the PV cell design using single diode model where I_p is photo current, d is diode, R_{se} is series resistance, R_{pa} is parallel resistance, I_{so} solar panel output current and V_{so} is solar panel voltage. The relation between I_{so} and V_{so} from Fig. A4.1 can be formulated as,

$$I_{so} = I_p - I_o\left(e^{\frac{q(V_{so}+R_{se}I_{so})}{AkT}} - 1\right) - \frac{V_{so} + R_{se}I_{so}}{R_{pa}} \tag{A4.1}$$

Where A is curve fitting factor, k is Boltzmann constant, q is electron charge, I_o is saturation current of diode and T is temperature. It is established that, short circuit current (I_s) and open circuit voltage (V_{op}) of solar cell are the functions of irradiation and temperature which can be represented as [A4.1],

$$I_s = I_{s,ref}\left[1 + \alpha\left(T - T_{ref}\right)\right]\frac{G}{G_{ref}} \tag{A4.2}$$

$$V_{op} = V_{op,ref}\left[1 + a \times \ln\frac{G}{G_{ref}} + \beta\left(T - T_{ref}\right)\right] \tag{A4.3}$$

Where $I_{s,ref}$ is short circuit current at STC, $V_{op,ref}$ is open circuit voltage at STC, T_{ref} is temperature at STC condition, G is irradiance, G_{ref} is irradiation at STC, α is temperature constant of I_s, β is temperature coefficient of V_{op} and a is irradiation correction factor of V_{op}.

Table A4.1. Photo Voltaic Module (TP250MBZ)

Variable	Quantity
MPP Power (P_m)	249 watts
MPP Voltage (V_m)	30 volts
MPP Current (I_m)	8.3 amps
Short Circuit Current (I_s)	8.83 amps
Open Circuit Voltage (V_{op})	36.8 volts
Temperature coefficient of I_s (α)	0.064%/^{0}C
Temperature coefficient of V_{op} (β)	-0.33%/^{0}C

Table-A4.1 represents the manufacturer data for different parameters of the PV panel used in the proposed work for simulation and experimentation. These parameters are utilized to develop single diode model in MATLAB/Simulink environment. Using single diode modelling, the output characteristics developed for the solar panel for different irradiation levels are shown in Fig. A4.2 (a) and (b). By using these curves, Maximum Power (P_m), Maxim Power Point (MPP) voltages and currents V_m and I_m, open circuit voltage (V_{op}) and short circuit current (I_s) for different irradiation levels and at constant STC temperature (25^{0}C) are attained and represented in Table-A4.2.

A4.3. THE PROPOSED PEAK DETECTION TECHNIQUE

The partial shading scenario in the proposed work mainly focuses on the method of [A4.23], where the panel is experiencing uniform irradiance throughout the module. The practical consideration of partial shading and real time situations are explained in this section.

A4.3.1 Dummy peak detection using P-V and I-V Relationship between individual and cascaded panel

The relation between I-V and P-V characteristics between individual and cascaded panels can be established by considering different shading patterns of individual panels under 3S configurations as shown in Fig. A4.3.

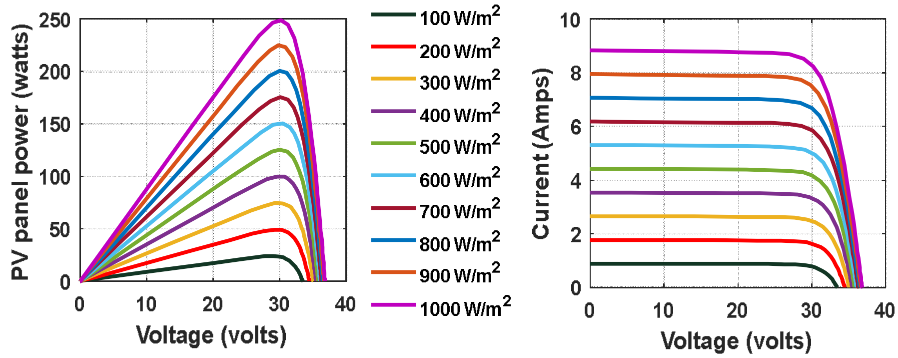

a b

Fig. A4.2. a. P-V Characteristics of Solar Panel for 1S configuration
b. I-V Characteristics of Solar Panel for 1S configuration

Table A4.2. Pm, Vm, Im, Vop and Is at different irradiation level

G (W/m^2)	P_m (Watts)	V_m (Volts)	I_m (Amps)	V_{op} (Volts)	I_s (Amps)
100	23.93	28.98	0.83	33.44	0.88
200	49.10	29.18	1.68	34.45	1.77
300	74.34	29.27	2.54	35.04	2.65
400	99.87	29.61	3.37	35.46	3.54
500	125.41	29.99	4.18	35.79	4.42
600	150.54	30.44	4.95	36.05	5.30
700	175.64	30.04	5.85	36.28	6.19
800	200.40	29.97	6.69	36.47	7.07
900	224.84	29.82	7.54	36.64	7.95
1000	249.1	30.01	8.3	36.79	8.83

The different combinations of the shading patterns can result in three peaks, two peaks or single peak in the combined P-V characteristic of the 3S configuration. For the first case Pa_1, the irradiation levels of individual panels considered are 1000 W/m^2, 800 W/m^2 and 600 W/m^2 respectively, which can result in three peaks in the overall P-V curve. Similarly, for the case Pa_2, the considered irradiation levels are 1000 W/m^2, 200 W/m^2 and 200 W/m^2 where two peaks will appear. On the other hand, for Pa_3, the irradiations for all the three panels are kept at 1000 W/m^2 and the overall P-V curve will show a single peak. For the considered shading patterns, the simulated P-V and I-V characteristics plots are displayed for the 3S configuration in Fig. A4.4. The simulated P-V and I-V characteristics for individual panels with 1S configuration under different irradiation levels are already shown in Fig. A4.2. From Fig. A4.2 and Fig. A4.4, it can be observed that I_s for individual 1S configured panel is in same line with 3S cascaded I-V plot for same irradiation. Thus, by observing the output characteristics, the relation to obtain MPP using individual panel characteristics with varying irradiation levels can be established for the proposed method.

It can be observed from Fig. A4.4a that, P-V and I-V curves display three peaks. The three panels are at irradiation levels of 1000 W/m^2, 800 W/m^2 and 600 W/m^2 respectively. The first peak occurs at V_1=28.22V, P_1=235.78W and I_1=8.36A, the second peak occurs at V_2=60.64V, P_2=415.04W and I_2=6.84A and the third peak occurs at V_3= 95.01V, P_3=492.67W and I_3=5.19A. From Table-A4.2, V_m and I_m for 1000 W/m^2 are 30.01V and 8.3A, for 800 W/m^2 the values are 29.97V and 6.69A and for 600 W/m^2 they are 30.44V and 4.95A respectively. As per the proposed methodology the peaks P_1 and P_2 can be considered as dummy peaks. So, by intently noticing these quantities, the relations for voltages and currents at different power peaks for cascaded and individual panels are developed as,

$$V_1 \approx (V_m)_{1000} \tag{A4.4}$$

$$V_2 \approx (V_m)_{1000} + (V_m)_{800} \tag{A4.5}$$

$$V_3 \approx (V_m)_{1000} + (V_m)_{800} + (V_m)_{600} \tag{A4.6}$$

Similarly,

$$I_1 \approx (I_m)_{1000} \tag{A4.7}$$

$$I_2 \approx (I_m)_{800} \tag{A4.8}$$

$$I_3 \approx (I_m)_{600} \tag{A4.9}$$

Here, V_1, V_2 and V_3 are voltages and I_1, I_2 and I_3 are the currents at the three peaks respectively. The numbers at the suffixes of (A4.4)-(A4.9) denotes the irradiation levels.

In the same manner, from Fig. A4.4b, the P-V curve displays two peaks. In this, the first peak is at V_1=28.20V, P_1=235.69W and I_1=8.36A. The second peak appears at V_2=59.19V, which is close to sum of V_m at 1000 W/m^2 and 200 W/m^2 and I_2=1.68A which is close to I_m at 200 W/m^2 as observed in Table-A4.2. Thus, the power at second peak is, P_2=V_2*I_2=99.44W. The third peak is at V_3= 94.94V, P_3=158.37W and I_3=1.67A. As the concept of dummy peak is developed on the basis of the local peak which appears on the combined P-V plot, the peaks P_2 and P_3 can be designated as dummy peaks. The dummy peak can fall on the same slope and may not be visible in the combined P-V characteristic of cascaded configuration. On the other hand, the dummy peaks can be also be visible in the combined P-V plot. In Fig A4.4b, the second and the third peaks are dummy peaks. The second peak at V_2=59.19V falls on the same slope with third peak at lower voltage, but at nearly same current of 1.68 A. On the other hand, here first and third peaks are visible, of which third one is a dummy peak. In this case also, the relation for voltages and currents at peaks for individual and cascaded panels can be developed as,

$$V_1 \approx (V_m)_{1000} \tag{A4.10}$$

$$V_2 \approx (V_m)_{1000} + (V_m)_{200} \quad \text{(A4.11)}$$

$$V_3 \approx (V_m)_{1000} + 2(V_m)_{200} \quad \text{(A4.12)}$$

Similarly,

$$I_1 \approx (I_m)_{1000} \quad \text{(A4.13)}$$

$$I_2 \approx (I_m)_{200} \quad \text{(A4.14)}$$

$$I_3 \approx (I_m)_{200} \quad \text{(A4.15)}$$

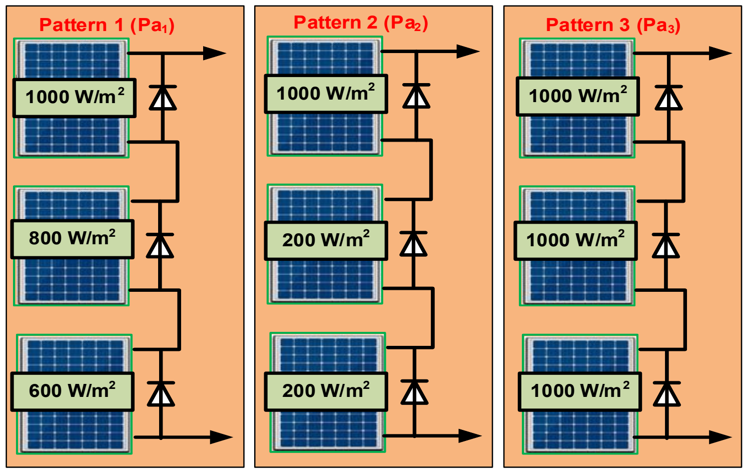

Fig. A4.3. Considered shading cases for 3S configuration at STC temperatures

Similarly, from Fig. A4.4c, the combined P-V curve displays single visible peak. Here, both the two dummy peaks appear on the same slope as that of the third peak. The first peak is at V_1=30.01V, I_1=8.3A, close to the corresponding V_m and I_m of 30.01V and 8.3A at 1000 W/m^2 for individual panels as observed in Table-A4.2. The power at this peak is $P_1=V_1*I_1$=249.1W. The second peak occurs at V_2=60.02V which is double to that of the V_m at 1000 W/m^2, I_2=8.3A which is I_m at 1000 W/m^2 and $P_2=V_2*I_2$=498.2W. The third peak occurs at V_3=90.25V, P_3=747.23W and I_3= 8.28A. So, by intently noticing these quantities, the relationships for voltages and currents at peaks are developed as,

$$V_1 \approx (V_m)_{1000} \quad \text{(A4.16)}$$

$$V_2 \approx 2(V_m)_{1000} \quad \text{(A4.17)}$$

$$V_3 \approx 3(V_m)_{1000} \quad \text{(A4.18)}$$

Similarly,

$$I_1 \approx (I_m)_{1000} \quad \text{(A4.19)}$$

$$I_2 \approx (I_m)_{1000} \quad \text{(A4.20)}$$

$$I_3 \approx (I_m)_{1000} \quad \text{(A4.21)}$$

In the expressions (A4.10)-(A4.21), the subscript numbers in voltage and current symbols indicate the irradiation level.

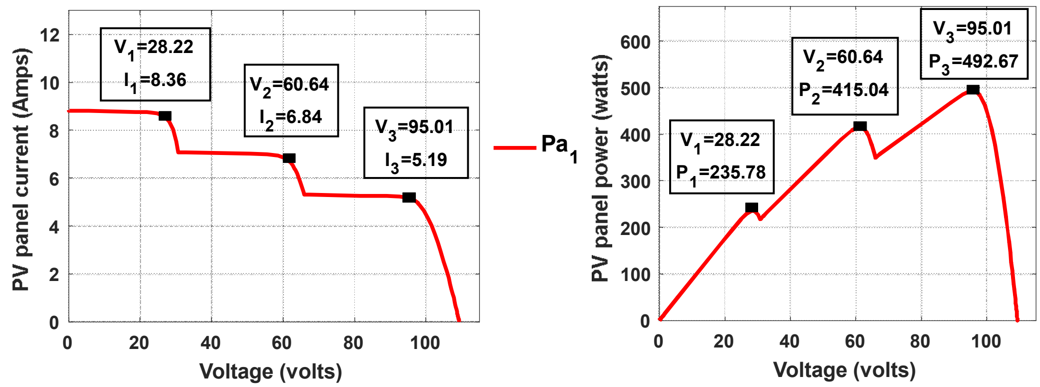

a

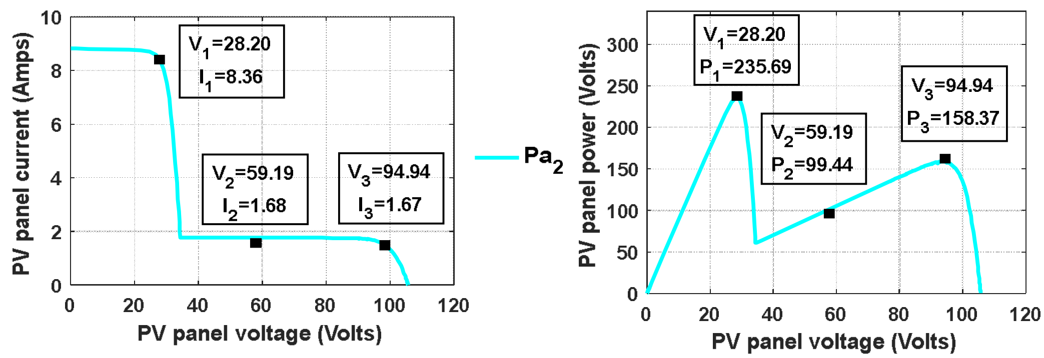

b

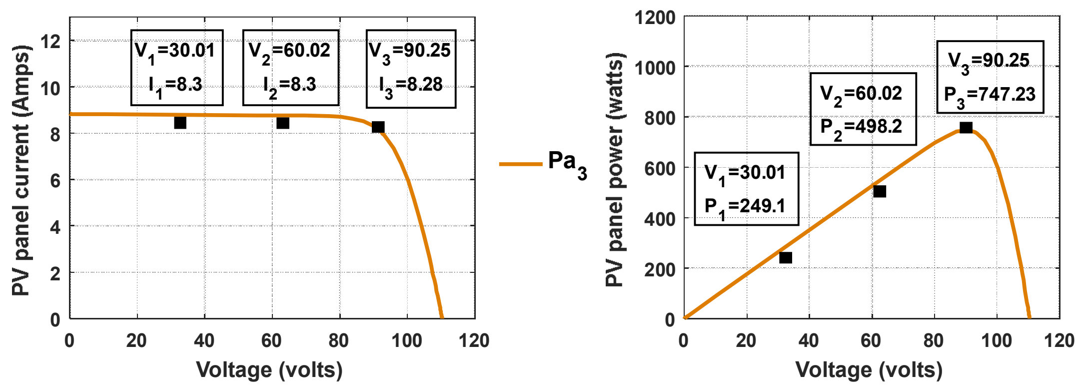

c

Fig. A4.4. I-V and P-V curves for shading patterns (a. Pa_1, b. Pa_2 and c. Pa_3)

A4.3.2 Proposed Global peak detection

By observing the I-V and P-V characteristics for cascaded and individual configurations of the PV array, it can be observed that, if V_m and I_m values for individual panels in the array are known for the given irradiation levels, it is possible to detect the nearest point to global maximum power. This can facilitate the P&O algorithm to have lower searching time for scanning the global maximum. Considering the case of Pa_1, the V_m and I_m values for individual panels from Table-A4.2 are,

- For panel under 1000 W/m^2, V_m=30.01V and I_m= 8.3A.

- For panel under 800 W/m^2, V_m= 29.97V and I_m=6.69A.
- For panel under 600 W/m^2, V_m=30.44V and I_m=4.95A.

By employing (A4.4)-(A4.9), V_1=30.01V, V_2=59.98V, V_3=90.42V, I_1=8.3A, I_2=6.69A and I_3=4.95A. Therefore, power at first peak is P_1= V_1*I_1 =249.1W, similarly power at second peak is P_2 = V_2*I_2 = 401.27W and power at third peak is P_3 = V_3*I_3 = 447.58W. From this, it can be detected that P_1 and P_2 are dummy peaks and the maximum power is near third peak at V_3=90.42V. So, if P&O is allowed to track from the voltage V_3=90.42V, the maximum power can be reached with very low search period.

Similarly, for Pa_2, the individual panels V_m and I_m values from Table-A4.2 are,

- For panel under 1000 W/m^2, V_m= 30.01V and I_m= 8.3A.
- For panels under 200 W/m^2, V_m=29.18V and I_m=1.68A.

By employing (A4.10)-(A4.15), V_1=30.01V, V_2=59.19V, V_3= 88.37V, I_1=8.3A, I_2=1.68A and I_3=1.68A. Therefore, approximate power at first peak is P_1=V_1*I_1=249.1W, at second peak is P_2=V_2*I_2=99.44W and at third peak is P_3=V_3*I_3=148.46W. From this, it can be observed that the second and third peaks are dummy and maximum power is near to voltage 30.01V.

In the same manner for Pa_3, the individual panels V_m and I_m values from Table-A4.2. are,

- All panels under 1000 W/m^2, V_m= 30.01V and I_m= 8.3A.

By employing (A4.16)-(A4.21), V_1=30.01V, V_2=60.02V, V_3= 90.03V, I_1=8.3A, I_2=8.3A and I_3=8.3A. Therefore, power at first peak is P_1=V_1*I_1=249.1W, at second peak is P_2=V_2*I_2=498.2W, at third peak is P_3=V_3*I_3=747.3W. From this, it can be observed that first two are dummy peaks and maximum power is near to voltage 90.03V. Table-A4.3 represents the comparison between actual V_m from model and calculated V_m through the proposed technique. Inspection of Table-A4.3 shows close conformity of V_m obtained through proposed calculation with those from actual model.

Table A4.3. Comparison of V_m for actual and calculated for considered shading patterns

Pattern	**V_m (actual) (Volts)**	**V_m (calculated) (Volts)**
Pa_1	95.01V	90.42V
Pa_2	28.20V	30.01V
Pa_3	90.25V	90.03V

A4.3.3 Practical implementation of proposed system

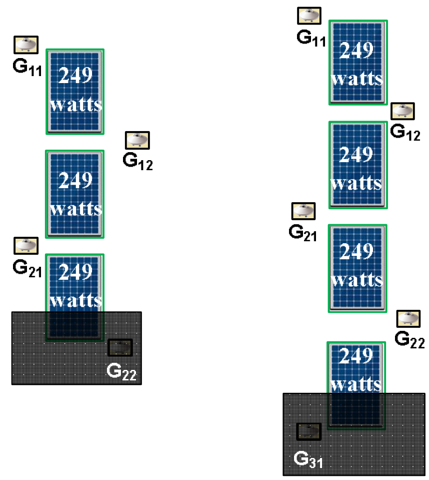

Fig. A4.5. Practical implementation of proposed system

Table A4.4. Calculated and actual values of V_m and P_m under partial shading conditions for different irradiation case

3S-configuration								
Panel 3 Shading	**Irradiance (W/m^2)**				**V_m (Volts)**		**P_m (watts)**	
	G_{11}	**G_{12}**	**G_{21}**	**G_{22}**	Actual	Proposed	Actual	Proposed
50-50%	150	250	350	750	82.82	88.96	144.62	149.45
66.7-33.3%	150	250	350	750	81.86	88.96	143.58	149.45
33.3-66.7%	150	250	350	750	82.69	88.96	145.47	149.45

4S-configuration									
Panel 4 Shading	**Irradiance (W/m^2)**					**V_m (Volts)**		**P_m (watts)**	
	G_{11}	**G_{12}**	**G_{21}**	**G_{22}**	**G_{31}**	Actual	Proposed	Actual	Proposed
50-50%	150	250	350	650	450	85.67	90.47	226.31	229.8
66.7-33.3%	150	250	350	650	450	86.75	90.47	227.02	229.8
33.3-66.7%	150	250	350	650	450	85.88	90.47	225.03	229.8

Table A4.5. Calculated and actual values of V_m and P_m under partial shading conditions for general case

3S-configuration								
Panel 3 Shading	**Irradiance (W/m^2)**				**V_m (Volts)**		**P_m (watts)**	
	G_{11}	**G_{12}**	**G_{21}**	**G_{22}**	Actual	Proposed	Actual	Proposed
50-50%	300	300	300	700	80.44	88.53	220.02	224.87
66.7-33.3%	300	300	300	700	79.12	88.53	224.15	224.87
33.3-66.7%	300	300	300	700	79.23	88.53	220.78	224.87

4S-configuration									
Panel 4 Shading	**Irradiance (W/m^2)**					**V_m (Volts)**		**P_m (watts)**	
	G_{11}	**G_{12}**	**G_{21}**	**G_{22}**	**G_{31}**	Actual	Proposed	Actual	Proposed
50-50%	300	300	300	300	700	113.12	117.79	296.58	299.17
66.7-33.3%	300	300	300	300	700	114.25	117.79	300.63	299.17
33.3-66.7%	300	300	300	300	700	114.04	117.79	296.92	299.17

It is assumed earlier that solar panels experience uniform shading throughout the panel as considered in [A4.23]. The practical implementation of the same can be carried out as shown in

Fig. A4.5, where partial shading within a panel is considered. In the proposed work, 3S and 4S configurations are considered where one of the panels is experiencing the shading.

The effective irradiation for any panel can be calculated after averaging the irradiations obtained by adjacent sensors to the panel.

For the proposed zig-zag type of sensor placement as shown in Fig. A4.5, the irradiation for individual panels can be calculated for 3S configuration as,

$$G_1 = \frac{G_{11} + G_{12}}{2} \quad \text{(A4.22)}$$

$$G_2 = \frac{G_{12} + G_{21}}{2} \quad \text{(A4.23)}$$

$$G_3 = \frac{G_{21} + G_{22}}{2} \quad \text{(A4.24)}$$

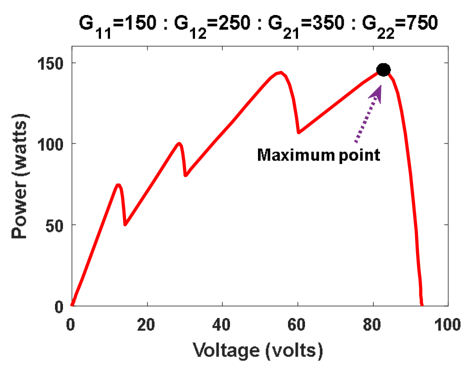

Fig. A4.6. P-V curve for 50-50% 3S configuration

Similarly, for 4 panels, the irradiation for each panel is calculated as,

$$G_1 = \frac{G_{11} + G_{12}}{2} \quad \text{(A4.25)}$$

$$G_2 = \frac{G_{12} + G_{21}}{2} \quad \text{(A4.26)}$$

$$G_3 = \frac{G_{21} + G_{22}}{2} \quad \text{(A4.27)}$$

$$G_4 = \frac{G_{22} + G_{31}}{2} \quad \text{(A4.28)}$$

Thus, in this case, the required number of irradiation sensors is N+1, with N being the number of panels. However, accuracy can be further improved with increased number of sensors effective per panel. Since the area of single panel is less, the considered configuration of N+1 sensor will give fairly accurate results. The accuracy can be further improved with a larger number of series connected panels. In the partial shading pattern three cases considered, where in one case 50% is shaded and 50% unshaded, in second case it is considered that 33.7% is unshaded and 66.7% shaded and for third cases it is 33.7% is shaded and 66.7% unshaded. For the case of, partial shading within the panel for 3S-configuration, of 50-50% shading with irradiation levels of G_{11}=

150 W/m^2, G_{12} = 250 W/m^2, G_{21}= 350 W/m^2 and G_{22} = 750 W/m^2, P-V curve is represented in Fig. A4.6.

In general, the irradiance sensed by the sensors are almost same except for the shaded panel. For the considered practical cases, the maximum power point voltage (V_m) and maximum power (P_m) for partially shaded and unshaded configurations are represented in Table-A4.4 and Table-A4.5. It can be observed that, calculated V_m with proposed averaging technique for partial shading within the panel almost nears the actual value.

A4.4. THE DUMMY PEAK ELIMINATION BASED MPPT TECHNIQUE

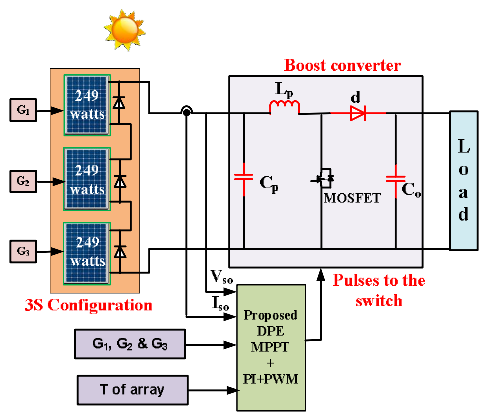

Fig. A4.7. Schematic figure for DPE MPPT

A4.4.1 Proposed System

The general schematic structure for the proposed work is represented in Fig. A4.7, where the boost converter is utilized in progressing PV panel voltage (V_{so}) in the degree of system requirement. The PV modules with 3S configuration are under the influence of irradiation levels of G_1, G_2 and G_3 at temperature (T). The boost converter circuit constraints such as, inductance (L_P) and capacitance (C_P, C_o) are formulated according to the system condition.

A4.4.2 Flow chart for proposed system

The schematic diagram for proposed DPE MPPT method is signified in Fig. A4.8. To explain the overall theme of proposed system, a pattern can be considered in which irradiation levels for the three panels under 3S configuration are G_1, G_2 and G_3 respectively. The overall flowchart can be explained with following steps.

STEP 1: Sensing parameters

For the proposed system, irradiation and temperature sensors are required for sensing the operating irradiation levels of individual panels and temperature of array for finding pattern change and dummy peak of the combinations under PS condition. Voltage and current sensors for the overall configuration are employed for tracking power using conventional P&O MPPT.

STEP 2: Dummy peak detection

In this step, based on the proposed concept developed in the preceding section, the sensed irradiation levels are arranged in decreasing order as $G_1 \geq G_2 \geq G_3$. By using the available irradiation levels and array temperature, I_s and V_{op} are calculated using (A4.2) and (A4.3). It can be observed from Table-A4.2 that the ratio of V_m to V_{op} is almost same for all considered irradiation levels. It can also be observed that the ratio of I_m to I_s are very close for all studied irradiation cases. The two ratios of V_m to V_{op} and I_m to I_s can be defined as K_1 and K_2 where,

$$K_1 = \left.\frac{I_m}{I_s}\right|_{STC} \quad \text{(A4.29)}$$

$$K_2 = \left.\frac{V_m}{V_{op}}\right|_{STC} \quad \text{(A4.30)}$$

Thus, based on the calculated I_s and V_{op} for each panel through (A4.2) and (A4.3), the individual panel voltages and currents V_m and I_m corresponding to maximum power for measured irradiation can be calculated as,

$$I_m(G_1) = K_1 * I_s(G_1) \quad \text{(A4.31)}$$

$$I_m(G_2) = K_1 * I_s(G_2) \quad \text{(A4.32)}$$

$$I_m(G_3) = K_1 * I_s(G_3) \quad \text{(A4.33)}$$

$$V_m(G_1) = K_2 * V_{op}(G_1) \quad \text{(A4.34)}$$

$$V_m(G_2) = K_2 * V_{op}(G_2) \quad \text{(A4.35)}$$

$$V_m(G_3) = K_2 * V_{op}(G_3) \quad \text{(A4.36)}$$

Using the calculated values of V_m and I_m through (A4.31)-(A4.36) for individual panels with measured shading patterns, the voltage and current values at every peak for the considered 3S configuration can be calculated as,

$$V_1 = V_m(G_1) \quad \text{(A4.37)}$$

$$V_2 = V_m(G_1) + V_m(G_2) \quad \text{(A4.38)}$$

$$V_3 = V_m(G_1) + V_m(G_2) + V_m(G_3) \quad \text{(A4.39)}$$

$$I_1 = I_m(G_1) \quad \text{(A4.40)}$$

$$I_2 = I_m(G_2) \quad \text{(A4.41)}$$

$$I_3 = I_m(G_3) \quad \text{(A4.42)}$$

Using (A4.37)-(A4.42), the peak powers calculated as,

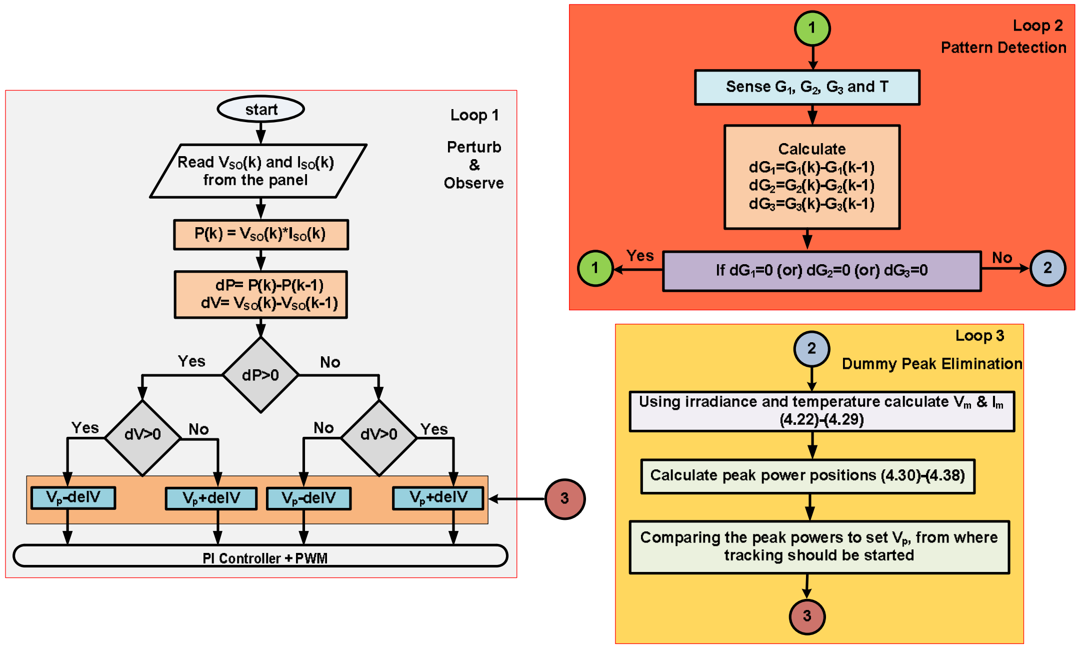

Fig. A4.8. Flow chart for proposed DPE MPPT

$$P_1=V_1*I_1 \tag{A4.43}$$

$$P_2=V_2*I_2 \tag{A4.44}$$

$$P_3=V_3*I_3 \tag{A4.45}$$

Comparing (A4.43)-(A4.45), the maximum power can be known and the respective voltage for that power can be taken as reference (V_p) for P&O MPPT algorithm for tracking global maximum power. The process is same for any possible pattern.

A4.4.3 Loop operation

As shown in Fig. A4.8, the proposed algorithm can be split into three separate loops. The first loop consists of standard P&O algorithm, the second loop is for pattern detection and the third loop is for dummy peak elimination. The maximum power tracking can be done initially and if there is a change in shading pattern, the same can be detected by employing loop 2 and it can finally activate loop 3 for dummy peak elimination by maximum peak point detection. The respective maximum peak point is used to set the reference voltage (V_p) from where the P&O starts its perturbation to track maximum power.

In proposed system, P&O with PI controller is employed to obtain the required dynamic characteristics with low settling time and zero steady state error of the system. Moreover, the initial point is estimated near to the global maximum, the time required for tracking maximum power is reduced. PI controller gain values are obtained using trial and error method [A4.24].

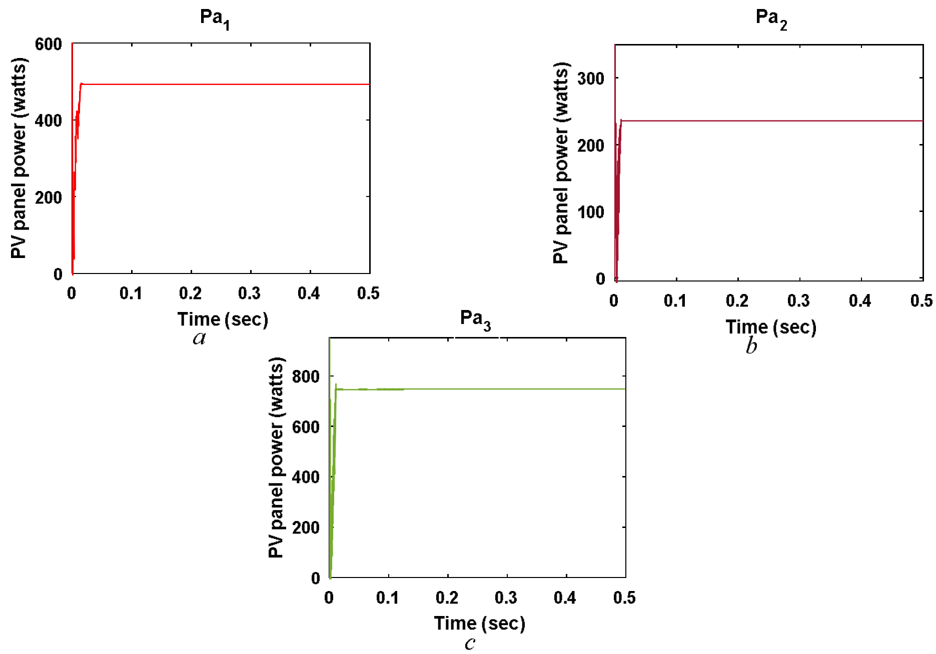

Fig. A4.9. PV panel power under Single pattern (a. Pa_1, b. Pa_2, c. Pa_3)

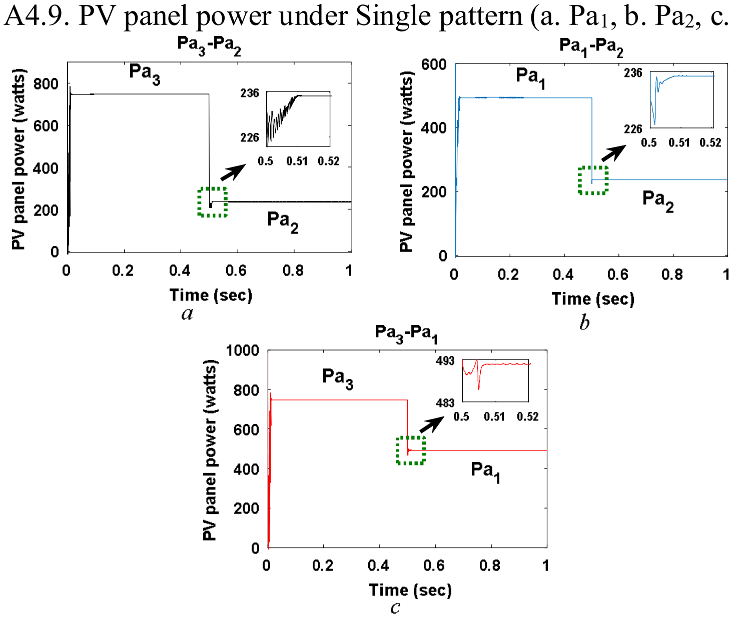

Fig. A4.10. PV panel power under single step change in patterns (a. Pa3-Pa2, b. Pa1-Pa2, c. Pa3-Pa1)

A4.5. SIMULATION RESULTS AND ANALYSIS

The simulation is carried out for similar situations given in [A4.23], where each solar panel experience a different irradiation with uniform isolation over panel surface. For the proposed system, simulation is carried out in MATLAB Simulink atmosphere for three following cases,

- Single pattern
- Single step change in patterns
- Multiple step change in patterns

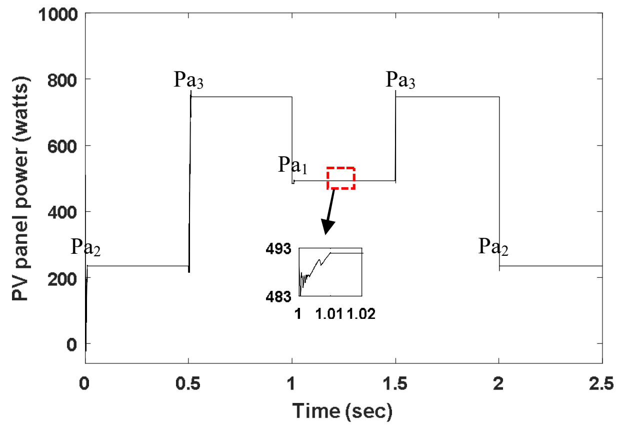

Fig.A4.11. PV panel power under multiple steps in patterns

A4.5.1 Single pattern

The term single pattern corresponds to any of the fixed pattern of shading e.g., Pa_1, Pa_2 or Pa_3 as indicated in Fig. A4.3.

The respective PV panel power obtained for each considered patterns by employing the proposed DPE MPPT. The simulation results for maximum power tracking for each of the patterns Pa_1, Pa_2 and Pa_3 are shown in Fig. A4.9(*a*), (*b*) and (*c*) correspondingly, showing that the proposed MPPT can successfully track the maximum power for all the considered patterns.

A4.5.2 Single Step change in patterns

In the second case of simulations with considered shading patterns in Fig. A4.3, a single step change between the patterns is applied and the results are observed. The step changes between the patterns considered are Pa_3-Pa_2, Pa_1-Pa_2 and Pa_3-Pa_1.

However, any other possible step changes also can be applied for test purpose. The step change is applied at time t = 0.5s in the simulation for all the cases, where the loop 2 activates loop 3 in finding the global peak after eliminating the dummy peaks, which helps the P&O in tracking global maximum power. The results are displayed in Fig.A4.10 (*a*), (*b*) and (*c*) respectively for the three step changes applied. From Fig.A4.10, it can be observed that the proposed DPE MPPT scheme successfully tracks the PV panel power under the considered varying pattern condition with single step change. The convergence time is compared with [A4.20] and shown in Table-A4.7. Moreover, from Fig. A4.10, it is noticed that the convergence time for the DPE MPPT method is below 10ms compared to much larger time in [A4.15] and 250ms for [A4.20]. Thus, it can be concluded that the proposed DPE MPPT works faster than the existing MPPT schemes. In proposed MPPT scheme the tracking is smoother with considerable reduction of searching period for pattern-to-pattern variations.

A4.5.3 Multiple step change in patterns

In the next stage of simulation with the proposed system, an arbitrary multiple step change in patterns is applied e.g., Pa_2-Pa_3-Pa_1-Pa_3-Pa_2 to test the dynamic performance. In this case also, any other possible pattern can be applied for testing purpose. The step change is applied at each 0.5 sec time interval. The tracked power for considered step changes is shown in Fig. A4.11. From this, it can be observed that, with the multiple variation in patterns, the proposed MPPT can perform smooth tracking with good dynamic behaviour.

A4.6. EXPERIMENTAL RESULTS AND DISCUSSION

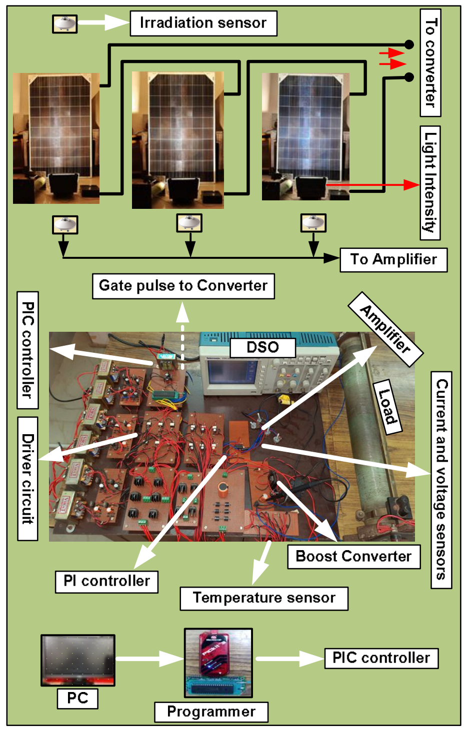

Fig.A4.12. Hardware setup for proposed system

The experimental verification is performed with three solar panels connected in 3S configuration along with anti-parallel diode protection as shown in Fig. A4.12. In the proposed scheme, artificial insolation is created using incandescent lamps in the test room, where each solar panel is employed with incandescent lamp as shown in Fig. A4.12.

Scale : X-axis : 100ms/div
Y-axis : 200W/div

a

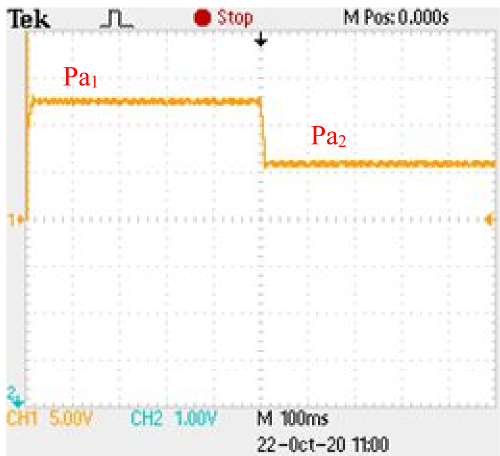

Scale : X-axis : 100ms/div
Y-axis : 200W/div

b

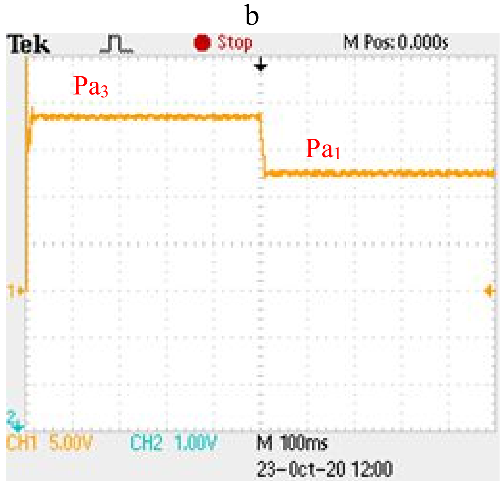

Scale : X-axis : 100ms/div
Y-axis : 200W/div

c

Fig.A4.13. Experimental results (a. Pa_3-Pa_2, b. Pa_1-Pa_2, c. Pa_3-Pa_1)

Moreover, the lamps can be switched on and off instantly and by this way the solar panels tend to operate with sudden changes in irradiation.

The system can supply generated power to load through boost converter. The PV panel current and voltage are driven as input to PIC 18F452 controller using sensors. LM35 is used for sensing temperature in which the temperature is converted to equivalent voltage. Pyranometer is used for sensing irradiance of each panel, as an equivalent voltage with precision. These input signals are passed through suitable low pass filters to remove the signal noises. The entire schematic diagram for the experimental set-up is shown in Fig.A4.12.

The red line indicates the flow of inputs given to PIC controller which is programmed using a programmer with PC interface. The output pulses generated by PIC are in the range of 5V with low driving capability with no isolation. Thus, in order to enhance the voltage to 12V, the driver circuit with TLP250H with isolation is employed. The pulses are given to gate of the power MOSFET K2611 of the boost converter.

For practical validation of the proposed concept, initially a step change in shading patterns e.g., Pa_3-Pa_2, Pa_1-Pa_2 and Pa_3-Pa_1 are applied. The proposed MPPT has been employed and the results are displayed in Fig. A4.13 (*a*), (*b*) and (*c*). Similarly, for the case of, partial shading within the panel for 3S-configuration, of 50-50% shading, with irradiation levels of G_{11}= 150 W/m^2, G_{12} = 250 W/m^2, G_{21}= 350 W/m^2 and G_{22} = 750 W/m^2, the tracked maximum power 143.29W is shown in Fig. A4.14, where the actual power is 144.62W and same is represented in Table-A4.6. From this, it can be observed that the proposed MPPT can efficiently track the maximum power with good dynamic behaviour and low convergence time.

The proposed Dummy Peak Elimination Based MPPT Technique, is based on perturb and observe algorithm for tracking. It is known fact that, P&O efficiency is depends on steady state oscillation and drift due to change in irradiation. Since, the initial point is estimated near to the global maximum, the time required for tracking maximum power is reduced. In proposed system, PI controller is employed to make the steady state error near to zero. Moreover, the P&O is assisted with irradiation sensors, making it drift free with improved efficiency. So, the P&O shows the similar tracking properties as of [A4.25], with a major advantage of tracking global maximum under partial shading condition. For the considered scenarios the experimentally obtained efficiency for different irradiations on panel and for partial shading with in panel case is represented in Table-A4.6.

Scale: X-axis: 100ms/div
Y-axis: 50W/div

Fig.A4.14. Experimental results (3S configuration :50-50% case)

Table A4.6. Efficiency of proposed DPE MPPT for different patterns and partial shading within panel

Patterns	P_m (actual)	P_m (tracked)	Efficiency (%)
Pa1	492.67	488.33	99.12
Pa2	235.69	233.38	99.02
Pa3	747.23	741.25	99.2
50-50%	144.62	143.29	99.08

Table A4.7. Comparison of existing MPPT techniques with DPE MPPT under PS condition

Properties	**EA-P&O [4.20]**	**[4.15]**	**Proposed DPE**
Complexity	Medium	High	Low
Tracking accuracy	High	High	High
Converging time	High	High	low
Scanning requirement	Yes	No	No
Irradiation sensor	No	No	Yes
Temperature sensor	No	Yes	Yes

Table-A4.7 represents the comparison between the existing EA-P&O [A4.20], the recent method described in [A4.15] and with proposed DPE based MPPT. Even though the proposed MPPT requires irradiation sensors unlike the other two, it has the major advantage of requiring almost negligible scanning time and low complexity. Besides, the proposed technique does not require high-end devices like scanner etc., which require high computational facility for the processor along with commercial impact. The proposed DPE based MPPT is easier to implement with less mathematical burden in its structure.

A4.7. CONCLUSION

An improved MPPT method under PS condition has been described in this research work. The major drawbacks of the existing popular techniques e.g., EA-P&O [A4.20] or ANN based [A4.15] MPPT has been removed in the proposed method. The EA- P&O requires larger scanning time when there is a change in shading pattern resulting in low dynamic performance. Moreover, achievement of high accuracy can increase the complexity of this system for real time implementation. Method in [A4.15], has good tracking efficiency with better dynamic response, but requires ANN for PS detection making it highly computation intensive with choice proper initialization algorithm for real time implementation.

The proposed dummy peak elimination based MPPT can compute all the nearest points to the power peaks of the cascaded PV panel configuration under PS condition. The dummy peaks are cancelled and the point nearest to the global peak is estimated, which becomes the start point for P&O. The Proposed DPE MPPT has low computational requirement for the processor with very good dynamic properties. Due to the absence of metaheuristic methods in the proposed algorithm it is easier to implement with processors having low computational facility and thus can be cost-effective. The proposed system is compared with the existing methods which showed encouraging results. The proposed system is simple and effectively implementable with already accessible drive compatible setup. As a future work, the proposed scheme must be expanded for series-parallel configurations.

Related publication:

- **BSV Sai**, D. Chatterjee et al., "A dummy peak elimination based MPPT technique for PV generation under partial shading condition," **IET Renew. Power Gener.**, 2021, 15:2438–2451.

References:

[A4.1] Ku Ding, XinGao Bian, HaiHao Liu, and Tao Peng.: 'A MATLAB-Simulink-Based PV Module Model and Its Application under Conditions of Non uniform Irradiance', IEEE Trans. On ENERGY Conv. vol. 27, no. 4, Dec.2012.

[A4.2] Hitesh K. Mehta, Himanshu Warke, Kaushik Kukadiya and Ashish K. Panchal.: 'Accurate Expressions for Single-Diode-Model Solar Cell Parameterization', *IEEE journal of Photovolt*., vol. 9, no. 3, May 2019.

[A4.3] H. Patel and V. Agarwal.: 'MATLAB-based modeling to study the effects of partial shading on PV array characteristics', *IEEE Trans. Energy Con.* vol. 23, no. 1, pp. 302–310, Mar. 2008.

[A4.4] Jieming Ma, Xinyu Pan, Ka Lok Man, Xingshuo Li, Huiqing Wen and Tiew On Ting.: 'Detection and Assessment of Partial Shading Scenarios on Photovoltaic Strings', *IEEE Trans. on Ind. Applications*, VOL. 54, NO. 6, NOV./DEC. 2018.

[A4.5] Sanjeev Kumar Pandey, Sanjaykumar Limaji Patil and Shrivijay B. Phadke.: 'PWM-Based Adaptive Sliding-Mode Control for Boost DC–DC Converters', *IEEE Trans. on Ind. Electron*., vol. 65, no. 6, June 2018.

[A4.6] Mohamad Reza Banaei and Sajad Ghabeli Sani.: 'Analysis and Implementation of a New SEPIC-Based Single-Switch Buck–Boost DC–DC Converter with Continuous Input Current', *IEEE Trans. on Power Electron*., vol. 33, no. 12, Dec. 2018.

[A4.7] Indu Rani Balasubramanian, Saravana Ilango Ganesan and Nagamani Chilakapati.: 'Impact of partial shading on the output power of PV systems under partial shading conditions', *IET Power Electron*., 2014, Vol. 7, Iss. 3, pp. 657–666

[A4.8] Amit Kumer Podder, Naruttam Kumar Roy and Hemanshu Roy Pota.: 'MPPT methods for solar PV systems: a critical review based on tracking nature', *IET Renew. Power Gener*., 2019, Vol. 13 Iss. 10, pp. 1615-1632.

[A4.9] Adeel Feroz Mirza, Qiang Ling, M. Yaqoob Javed and Majad Mansoor.: 'Novel MPPT techniques for photovoltaic systems under uniform irradiance and Partial shading', *Solar Energy* 184 (2019) 628–648.

[A4.10] Majad Mansoor, Adeel Feroz Mirza, Qiang Ling and M. Yaqoob Javed.: 'Novel Grass Hopper optimization based MPPT of PV systems for complex partial shading conditions', *Solar Energy 198 (2020) 499–518.*

[A4.11] Aranzazu D. Martin, Jesus R. Vazquez and J.M. Cano.: 'MPPT in PV systems under partial shading conditions using artificial vision', *Electric Power Systems Research* 162 (2018) 89–98.

[A4.12] B. Y. Lin, L. Wang and Q. H. Wu.: 'Maximum Power Point Scanning for PV Systems under Various Partial Shading Conditions', *IEEE Trans. on Sustainable Energy*, 2020.

[A4.13] Yu-Pei Huang, Ming-Yi Huang and Cheng-En Ye.: 'A Fusion Firefly Algorithm with Simplified Propagation for Photovoltaic MPPT under Partial Shading Conditions', *IEEE Trans. on Sustainable Energy*, 2020.

[A4.14] Ali F. Murtaza and Riaz Ahmad.: 'Optical isolation mechanism based MPPT for PV array under partial shading condition', *Solar Energy* 185 (2019) 516–524.

[A4.15] Venkata Reddy Kota and Muralidhar Nayak Bhukya.: 'A novel global MPP tracking scheme based on shading pattern identification using artificial neural networks for photovoltaic power generation during partial shaded condition', *IET Renew. Power Gener., 2019, Vol. 13 Iss. 10, pp. 1647-1659.*

[A4.16] Hong Li, Duo Yang, Wenzhe Su, Jinhu Lu and Xinghuo Yu.: 'An Overall Distribution Particle Swarm Optimization MPPT Algorithm for Photovoltaic System Under Partial Shading', *IEEE Trans. on Ind. Electron*., VOL. 66, NO. 1, JAN 2019.

[A4.17] Neeraj Priyadarshi, Sanjeevikumar Padmanaban, Jens Bo Holm-Nielsen, Frede Blaabjerg and Mahajan Sagar Bhaskar.: 'An Experimental Estimation of Hybrid ANFIS–PSO-Based MPPT for PV Grid Integration Under Fluctuating Sun Irradiance', *IEEE Systems Journal*, 2019.

[A4.18] Thanikanti Sudhakar Babu, J. Prasanth Ram, Tomislav Dragicevic, Masafumi Miyatake, Frede Blaabjerg and Natarajan Rajasekar.: 'Particle Swarm Optimization Based Solar PV Array Reconfiguration of the Maximum Power Extraction Under Partial Shading Conditions', *IEEE Trans. on Sustainable Energy*, VOL. 9, NO. 1, JAN 2018.

[A4.19] Dimas AjiNugraha, K. L. Lian and Suwarno.: 'A Novel MPPT Method Based on Cuckoo Search Algorithm and Golden Section Search Algorithm for Partially Shaded PV System', *canadian journal of electrical and computer engineering, vol. 42, no. 3, summer 2019.*

[A4.20] Jubaer Ahmed and Zainal Salam.: 'An Enhanced Adaptive P&O MPPT for Fast and Efficient Tracking Under Varying Environmental Conditions', *IEEE Trans. ON SUSTAINABLE ENERGY*, VOL. 9, NO. 3, JULY 2018.

[A4.21] Jubaer Ahmed and Zainal Salam.: 'An Accurate Method for MPPT to Detect the Partial Shading Occurrence in a PV System', *IEEE Trans. ON INDUSTRIAL INFORMATICS*, VOL. 13, NO. 5, OCTOBER 2017.

[A4.22] Ariya Sangwongwonich, Yongheng Yang, Dezso sera, Hamid Soltni and Frede Blaabjerg.: 'Analysis and Modelling of Interharmonics from Grid-connected Photovoltaic Systems', *IEEE Trans. Power electron*, VOL. PP, NO. 99, 2017.

[A4.23] Hadi M. El-Helw, Ahmed Magdy, And Mostafa I. Marei.: 'A Hybrid Maximum Power Point Tracking Technique for Partially Shaded Photovoltaic Arrays', *IEEE Access, VOL. 5, 2017.*

[A4.24] Mohamed Lasheen, Ali Kamel Abdel Rahman, Mazen Abdel-Salam and Shinichi Ookawara.: 'Adaptive reference voltage-based MPPT technique for PV applications', *IET Renew. Power Gener., 2017, Vol. 11 Iss. 5, pp. 715-722.*

[A4.25] Mazen Abdel-Salama, Mohamed-Tharwat El-Mohandes and Mohamed Goda.: 'An improved perturb-and-observe based MPPT method for PV systems under varying irradiation levels', Solar Energy 171 (2018) 547–561.

B. Using Operating point (Series-Parallel)

B4.1. INTRODUCTION

The non-renewable energy sources are facing a severe threat of extinction, due to their over utilization to satisfy the needs of exponentially raising population [B4.1-B4.2]. By considering all these facts, it can be noted that, there is a void for the requirement of alternate power source in exchange of the non-renewable sources.

In most cases, a boost converter is used in MPPT, owing to its simple construction and non-inverted output nature [B4.3-B4.5]. Due to the multiple peak nature in the output characteristics, MPP tracking is a vital encounter during PS conditions [B4.6-B4.8]. Under PS condition, conventional MPPT schemes like CV based MPPT scheme, MP&O method and ARV based MPPT etc., fails in tracking the MPP efficiently. Many optimization-based schemes are developed for the global maximum tracking under PS situation [B4.9-B4.10].

Even though, artificial vision-based scheme, is capable of tracking the peak point effectively, it has the major disadvantage of requiring higher cost camera for the accurate detection of shading pattern. If low-cost camera is employed for detecting shading pattern, as mentioned in [B4.11], it leads to the precision error. For peak point detection, ANN based MPPT scheme is employed, where ANN is used in detecting shading pattern, for estimating the nearest voltage reference to global maximum [B4.12]. Even though, [B4.12] is advantageous, it requires higher initial work and is harder to implement while coming to real time situation. EA-P&O algorithm is the modified version of conventional P&O scheme, which can track the MPP effectively under PS condition [B4.13]. Since [B4.13] requires scanning in its topology, it leads to higher settling time, resulting in poor dynamic characteristics. The peak point detection scheme in [B4.14] is projected to track the global maximum successfully, but this scheme deals with only series configurations and there is no proper structure mentioned for series-parallel constructions.

CS and PSO methods are the wide-ranging MPPT schemes for tracking global maximum under multiple peaks situation [B4.15-B4.16]. Coming to the dynamic operation, CS displays healthier operating characteristics compared to PSO [B4.17]. A hybrid particle swarm optimization (PSO) and P&O based MPPT scheme has been proposed in [B4.18], where irradiation sensors are employed for shading pattern detection using ANN. Under uniform shading pattern P&O comes into action, PSO operates under partial shading condition. Usage of ANN and PSO, makes the system complex under hardware implementation. The modified butterfly optimization algorithm [B4.19], improved bat algorithm [B4.20], modified maximum power trapezium methods in [B4.21], [B4.22] and [B4.23] have the common disadvantage of complexity in construction, while coming to hardware implementation. Overall, it can be observed that almost all the optimization-based schemes have the major disadvantage of requiring high end hardware and considerable time in tracking maximum power.

In this research work, an FGPE based MPPT has been presented, where the shading pattern detection for series-parallel panels is done using sensors. The FGPE MPPT has lower settling time and negligible power oscillations while adjusting to new operating point, thereby overcoming the drawbacks in the existing methods. The limitation of DPE MPPT described in [B4.24] is that, it is only applicable with series configurations and no direction was shown for series-parallel combinations.

In the proposed FGPE based tracking scheme, the series-parallel configurations of PV-array has been considered, with other focuses on,

- Good tracking efficiency
- Smooth tracking under sudden changes in irradiation patterns and
- Better dynamic characteristics

B4.2. SOLAR PANEL MODELLING

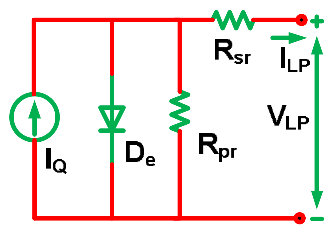

Fig. B4.1. Power electronic circuit for PV cell

In this work, a single diode model [B4.1], is employed for solar cell modelling, as a result of its accuracy in producing solar panel characteristics. The power electronic circuit for single diode model is represented in Fig. B4.1. By using KVL and diode characteristics, the relation between current and voltage for PV cell is represented in (B4.1). Moreover, V_{ov} and I_{sc} are expressed in terms of G and T as (B4.2) and (B4.3) [B4.1].

Using (B4.1)-(B4.3), the I-V and P-V curves of a PV panel as represented in Table-B4.1, is displayed in Fig. B4.2a. The MPP values for the respective I-V and P-V characteristics are represented in Fig. B4.2b.

$$I_{LP} = I_Q - I_{sa}\left[e^{\frac{Q(V_{LP}+R_{sr}I_{LP})}{N_S AK\times T}} - 1 \right] - \frac{V_{LP}+R_{sr}I_{LP}}{R_{pr}} \tag{B4.1}$$

$$I_{sc} = I_{sc,r}\left[1+\alpha\left(T-T_r\right)\right]\frac{G}{G_r} \tag{B4.2}$$

$$V_{ov} = V_{ov,r}\left[1 + a\times\ln\frac{G}{G_r} + \beta\left(T-T_r\right)\right] \tag{B4.3}$$

Table B4.1. Manufacturer Data for PV Panel (TP250MBZ)

Variables	Quantity
MPP power	249W
MPP voltage	30V
MPP current	8.3A
SCC	8.83A
OCC	36.8V
Temperature coefficient of I_{sc}	0.064%/^{0}C
Temperature coefficient of V_{ov}	-0.33%/^{0}C

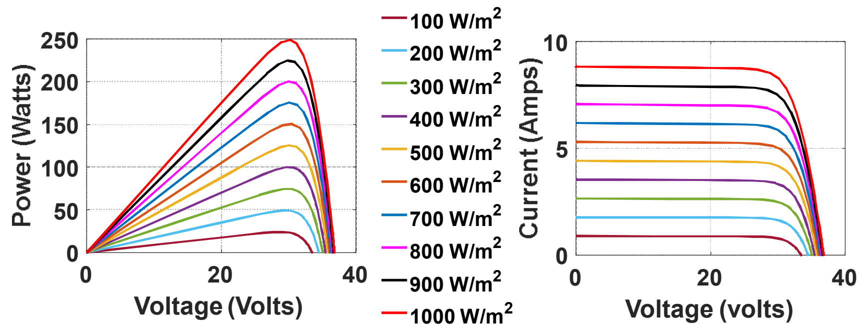

(a)

Irradiation (W/m^2)	100	200	300	400	500
MPP current (Amps)	0.83	1.68	2.54	3.37	4.18
MPP voltage (Volts)	28.98	29.2	29.27	29.6	29.99
MPP power (Watts)	23.93	49.1	74.34	99.9	125.4
Irradiation (W/m^2)	600	700	800	900	1000
MPP current (Amps)	4.95	5.85	6.69	7.54	8.3
MPP voltage (Volts)	30.44	30	29.97	29.8	30.01
MPP power (Watts)	150.5	176	200.4	225	249.1

(b)

Fig. B4.2. (a) Output curves (b) MPP values of single solar module

B4.3. PROPOSED FGPE TECHNIQUE FOR GLOBAL MAXIMUM DETECTION

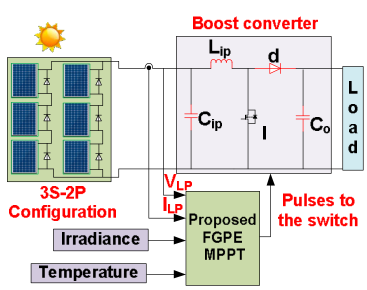

Fig. B4.3. Proposed FGPE scheme

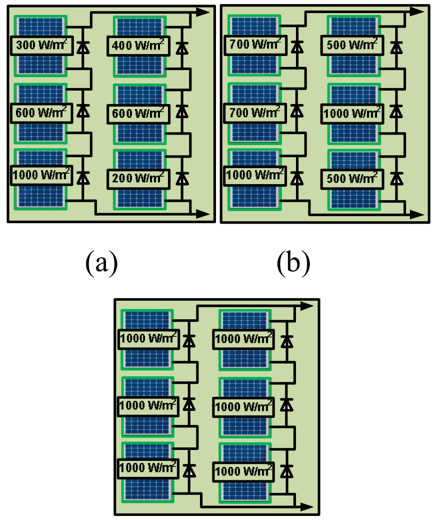

(c)

Fig. B4.4. Different shading patterns for 3S-2P (a) Pattern 1 (b) Pattern 2 and (c) Pattern

Fig. B4.3 denotes the block diagram of the PV connected boost converter using proposed FGPE scheme for MPPT. The proposed MPPT method can be used for any number of series-parallel configurations of solar panels. For simulation and experimental verification, the 3S-2P configuration is considered, for which the typical shading patterns used are represented in Fig. B4.4.

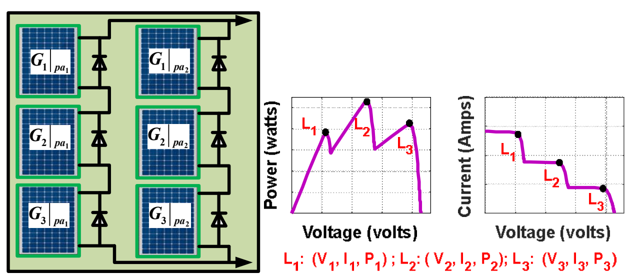

(a) (b)

Fig. B4.5. Assumed 3S-2P configuration (a) Pattern (b) P-V and I-V curves

B4.3.1 Proposed FGPE Scheme

For the considered 3S-2P configuration, the proposed algorithm shall require the irradiation values of each panels coming from respective sensors. For developing the mathematical modelling, the configuration is divided into three sets for 3S configuration. Each set will have two elements for 2P configuration. Thus, the sets for irradiation pattern can be defined as,

$$\textbf{Set 1: } \{\left[G_1|_{pa_1}\right] \text{and } \left[G_1|_{pa_2}\right]\} \tag{B4.4}$$

$$\textbf{Set 2: } \{\left[G_2|_{pa_1}\right] \text{and } \left[G_2|_{pa_2}\right]\} \tag{B4.5}$$

$$\textbf{Set 3: } \{ \left[G_3|_{pa_1} \right] \text{and } \left[G_3|_{pa_2} \right] \} \quad \text{(B4.6)}$$

The typical arrangement of 3S-2P configuration is shown in Fig. B4.5a. If the irradiation values are in the order of $G_1|_{pa_1} > G_3|_{pa_1} > G_2|_{pa_1}$ for first parallel string and $G_1|_{pa_2} > G_2|_{pa_2} > G_3|_{pa_2}$ for second parallel string, the respective sets can be modified as,

$$\textbf{Set 1: } \{ \left[G_1|_{pa_1} \right] \text{and } \left[G_1|_{pa_2} \right] \} \quad \text{(B4.7)}$$

$$\textbf{Set 2: } \{ \left[G_3|_{pa_1} \right] \text{and } \left[G_2|_{pa_2} \right] \} \quad \text{(B4.8)}$$

$$\textbf{Set 3: } \{ \left[G_2|_{pa_1} \right] \text{and } \left[G_3|_{pa_2} \right] \} \quad \text{(B4.9)}$$

The P-V and I-V curves obtained for Fig. B4.5a configuration assuming a three peak situation can be as shown in Fig. B4.5b. At peak point L_1, the MPP values for voltage, current and power are assumed to be V_1, I_1 and P_1 respectively. The same can be observed at L_2 and L_3 locations.

Fig. B4.6, denotes the proposed algorithm for FGPE MPPT method. The loop 1 consists of traditional perturb and observe (P&O) scheme and loop 2 is meant for Pattern detection where ε is in the range of 0 to 1. The loop 3 of the algorithm does the operation of reaching the point very close to the global maximum power. The determined near global maximum point in loop 3 is used as a reference point for P&O to track exact maximum power.

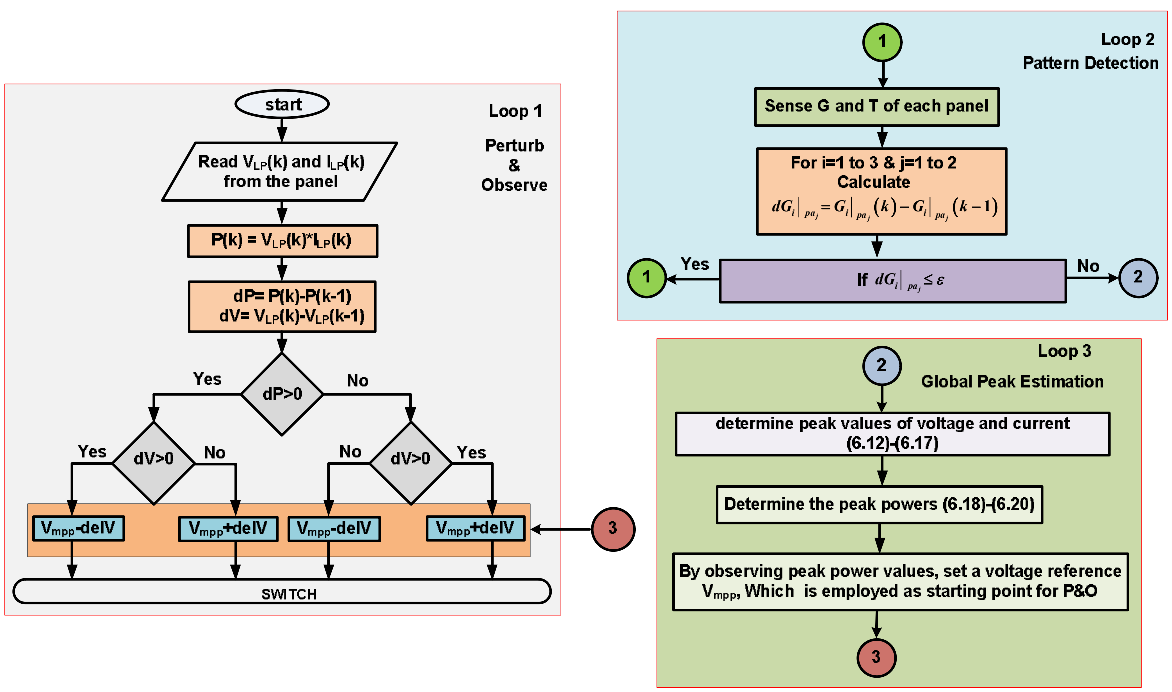

Fig. B4.6. Flow chart for the proposed FGPE algorithm

The proposed model assumes the first local peak voltage corresponding to maximum irradiation values for the first set. Whereas, the current considered at this local peak is equal to the sum of the

MPP currents at each of the irradiation in the set. For the next set, the voltage considered is the sum of the first local peak voltage and the voltage corresponding to the maximum irradiation of set 2. The MPP current at the second local peak can be calculated as for set 1. For next any sets, this same process can follow. The two coefficients K_1 and K_2 for the panels can be calculated as,

$$K_1 = \left.\frac{I_{mpp}}{I_{sc}}\right|_{STC} \tag{B4.10}$$

$$K_2 = \left.\frac{V_{mpp}}{V_{ov}}\right|_{STC} \tag{B4.11}$$

For any irradiance and temperature, the I_{sc} and V_{ov} values can be determined using (B4.2) and (B4.3) [B4.2]. Using I_{sc} and V_{ov} of individual panels with any irradiation pattern, the respective V_1, V_2 and V_3 for PV array can be obtained as (B4.12)-(B4.14),

$$V_1 \approx K_2 \times \left[\left.(V_{ov})\right|_{Max(set1)} \right] \tag{B4.12}$$

$$V_2 \approx K_2 \times \left[\left.(V_{ov})\right|_{Max(set1)} + \left.(V_{ov})\right|_{Max(set\,2)} \right] \tag{B4.13}$$

$$V_3 \approx K_2 \times \left[\left.(V_{ov})\right|_{Max(set1)} + \left.(V_{ov})\right|_{Max(set\,2)} + \left.(V_{ov})\right|_{Max(set\,3)} \right] \tag{B4.14}$$

Similarly, for MPP currents I_1, I_2 and I_3, the expressions are,

$$I_1 \approx K_1 \times \left[\sum_{i=1}^{2} \left. I_{sc} \right|_{G_1|_{pa_i}} \right] \tag{B4.15}$$

$$I_2 \approx K_1 \times \left[\sum_{i=1}^{2} \left. I_{sc} \right|_{G_2|_{pa_i}} \right] \tag{B4.16}$$

$$I_3 \approx K_1 \times \left[\sum_{i=1}^{2} \left. I_{sc} \right|_{G_3|_{pa_i}} \right] \tag{B4.17}$$

Employing (B4.12)-(B4.17), the values of power at all the dummy peak points can be calculated as,

$$P_1 = V_1 \times I_1 \tag{B4.18}$$

$$P_2 = V_2 \times I_2 \tag{B4.19}$$

$$P_3 = V_3 \times I_3 \tag{B4.20}$$

The global maximum power point is the maximum value of power obtained using (B4.18)-(B4.20). This maximum power point is employed as a starting location for P&O in determining the exact MPP. Irrespective of configurations and shading patterns, these modelling equations are applicable in finding global MPP.

B4.3.2 Verification of the Proposed FGPE Scheme for 3S-2P configuration through simulation

For simulation, the Fig. B4.4(a), B4.4(b) and B4.4(c) represent different irradiation values with 3S-2P configuration. Moreover, three different shading patterns e.g. pattern 1, 2 and 3 are considered for verification. In Pattern 1, the first parallel string has the irradiation levels of 300 W/m^2, 600 W/m^2 and 1000 W/m^2 for its three panels. The second parallel string has irradiation levels of 400 W/m^2, 600 W/m^2 and 200 W/m^2. Similarly, for other patterns the respective irradiation levels are as displayed in Fig. B4.4(b) and B4.4(c) respectively. The patterns 1, 2 and 3 result in the three peaks, two peaks and single peak in the output P-V characteristics as shown in Fig B4.7a, B4.7b and B4.7c. From Fig. B4.6a, the three sets can be obtained following (B4.4)-(B4.6) as,

Set 1: {1000 W/m^2 and 600 W/m^2}.

Set 2: {600 W/m^2 and 400 W/m^2}.

Set 3: {300 W/m^2 and 200 W/m^2}.

For pattern 1, by considering the MPP values of individual panels as shown in Fig. B4.2b, voltage, current and power values at dummy peaks are determined using (B4.12)-(B4.20). Thus V_1= 30.01V, I_1= 13.25A, P_1= 397.63W, at first peak, V_2= 60.45V, I_2= 8.32A, P_2= 502.94W at second peak and V_3=89.72V, I_3= 4.22A, P_3= 378.62W at third peak. Thus, the global peak point is at L_2. Fig. B4.7a shows the actual plot for pattern 1. From Fig.B4.7a, it can be noted that, the voltage, current and power values at first peak L_1 are, V_1 = 28.43V, I_1=13.33A and P_1=378.86W respectively. Similarly, at location L_2, V_2 = 61.64V, I_2=8.6A and P_2=529.28W and at L_3, V_3 = 94.94V, I_3=4.33A and P_3=419.3W. Thus, it can be observed that, the proposed method tracks the voltage reference very near to the actual global maximum point which occurs at second peak, the same is represented in Table-B4.2.

Further, in proposed scheme, the 3S-2P configurations are experiencing the patterns 2 and 3 as represented in Fig. B4.6(b) and B4.6(c). The patterns 2 and 3 results in the P-V and I-V curves as displayed in Fig. B4.7b and B4.7c. By following process similar to that of pattern 1, the actual and measured MPPT values for pattern 2 and pattern 3 are represented in Table-B4.2. From Table-B4.2, the measured MPP values using proposed scheme are nearer to that of actual MPP values. The measured V_{mpp} value is used in the proposed FGPE scheme for successful tracking of global maximum power. In the proposed algorithm PI controller with proper tuning is employed for improving dynamic characteristics.

Table B4.2. MPP Values Comparison for Different Patterns

Patterns	Comparison	V_{mpp} (V)	I_{mpp} (A)	P_{mpp} (W)
Pattern 1	Calculated	61.64	8.6	502.94
	Actual	60.45	8.32	529.28
Pattern 2	Calculated	93.1	10.14	943.8
	Actual	90.09	10.03	903.6
Pattern 3	Calculated	90.26	16.56	1495.1
	Actual	90.03	16.6	1494.5

B4.3.3 Proposed FGPE MPPT Scheme for mS-nP system

The proposed system can be expanded for a complex mS-nP system, as considered in Fig. B4.8 with *m* and *n* can be any integer. The considered irradiation levels are in the order of $G_1|_{pa_1} \geq G_2|_{pa_1} \geq .... \geq G_m|_{pa_1}$ for first parallel string and $G_1|_{pa_N} \geq G_2|_{pa_N} \geq .... \geq G_m|_{pa_n}$ for nth parallel string. Similar kind of irradiation pattern is seen in remaining parallel strings. The set formation can be obtained as,

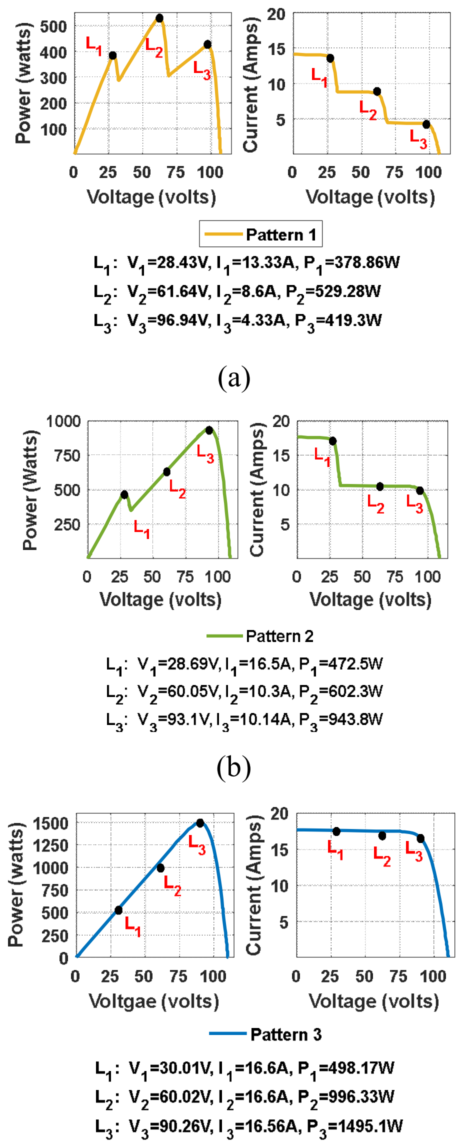

(c)

Fig. B4.7. P-V and I-V curves (a) pattern 1 (b) pattern 2 and (c) pattern 3

Set 1: $\{ \left[G_1|_{pa_1}\right], \left[G_1|_{pa_2}\right], ..., \left[G_1|_{pa_n}\right] \}.$

Set 2: $\{ \left[G_2|_{pa_1}\right], \left[G_2|_{pa_2}\right], ..., \left[G_2|_{pa_n}\right] \}.$

…………………………………………………………...

Set M: $\{[G_m|_{pa_1}],[G_m|_{pa_2}]..............,[G_m|_{pa_n}]\}$.

By using proposed method, the MPP voltage values can be calculated as,

$$V_1 \approx K_2 \times \left[(V_{ov})\big|_{Max(set1)} \right] \tag{B4.21}$$

$$V_2 \approx K_2 \times \left[(V_{ov})\big|_{Max(set1)} + (V_{ov})\big|_{Max(set\ 2)} \right] \tag{B4.22}$$

$$\cdots\cdots\cdots\cdots\cdots\cdots\cdots\cdots\cdots\cdots\cdots\cdots$$

$$V_m \approx K_2 \times \left[(V_{ov})\big|_{Max(set1)} + (V_{ov})\big|_{Max(set\ 2)} + .. + (V_{ov})\big|_{Max(set\ m)} \right] \tag{B4.23}$$

Similarly, for MPP currents I_1, I_2 and I_3, the expressions are,

$$I_1 \approx K_1 \times \left[\sum_{i=1}^{n} I_{sc}\big|_{G_1|_{pa_i}} \right] \tag{B4.24}$$

$$I_2 \approx K_1 \times \left[\sum_{i=1}^{n} I_{sc}\big|_{G_2|_{pa_i}} \right] \tag{B4.25}$$

$$\cdots\cdots\cdots\cdots\cdots\cdots\cdots\cdots\cdots\cdots\cdots\cdots\cdots\cdots\cdots\cdots$$

$$I_m \approx K_1 \times \left[\sum_{i=1}^{n} I_{sc}\big|_{G_3|_{pa_i}} \right] \tag{B4.26}$$

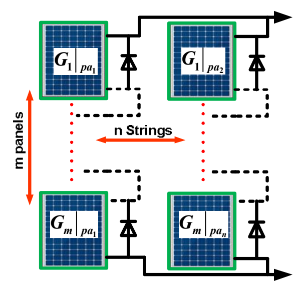

Fig. B4.8. Complex mS-nP configurations

Table B4.3. MPP Values at Different Peaks For 10S-10P System

Peak	V_{mpp}(V)	I_{mpp}(A)	P_{mpp}(kW)
1	30.01	83	2.491
2	60.02	83	4.982
3	90.03	83	7.472
4	120.04	83	9.99
5	150.05	83	12.45
6	180.49	49.5	8.934
7	210.93	49.5	10.441
8	241.37	49.5	11.948
9	271.81	49.5	13.455
10	302.25	49.5	14.961

The proposed system is operated for the complex 10S-10P configuration as displayed in Fig. B4.9. The respective P-V and I-V characteristics for considered configuration is represented in Fig. B4.10. From Fig. B4.10, the actual MPP values at local and global peak points are represented using red dots, where local peak is at 12.41kW and 150.1182V, global peak is at 14.164kW and 314.7083V. Using proposed global peak estimation scheme, the 10 peak points are placed over output curves. By using (B4.21)-(B4.26), where m=n=10, MPP values at peaks are listed in Table-B4.3. From Table-B4.3, it can be found that, peak 10 is nearer to global maximum, the respective peak point is employed as an initial point for P&O in tracking MPP.

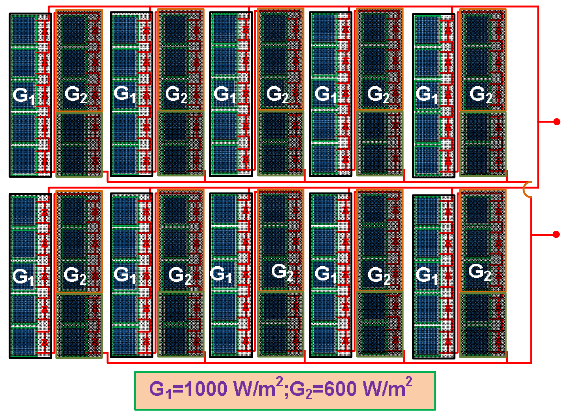

Fig. B4.9. Complex 10S-10P configurations

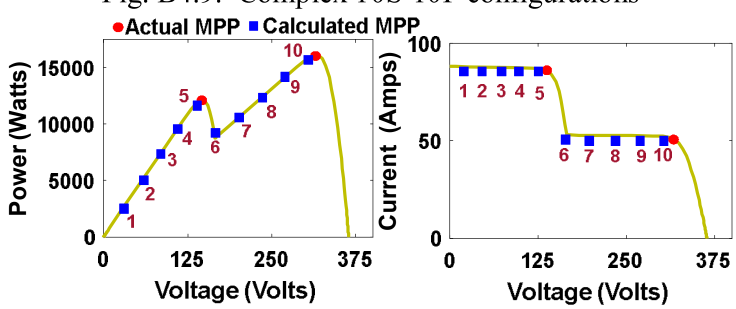

Fig. B4.10. Dummy peak placement on output characteristics

B4.3.4 Real Time Placement of Irradiation Sensors

In this section, the real time placement of sensors is demonstrated in Fig. B4.11 and B4.12.

Case 1. For simple configurations considering Fig. B4.11,

$$\left.\begin{array}{ll} G_1\big|_{pa_1} = \dfrac{G_{11}+G_{21}}{2} & G_1\big|_{pa_2} = \dfrac{G_{31}+G_{21}}{2} \\ G_2\big|_{pa_1} = \dfrac{G_{21}+G_{12}}{2} & G_2\big|_{pa_2} = \dfrac{G_{21}+G_{32}}{2} \\ G_3\big|_{pa_1} = \dfrac{G_{12}+G_{22}}{2} & G_3\big|_{pa_3} = \dfrac{G_{32}+G_{22}}{2} \end{array}\right\} \tag{B4.27}$$

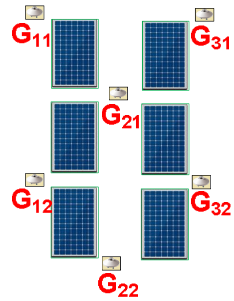

Fig. B4.11. Zig-Zag type sensor placement

As it is known that, there is a case of shading with in a panel, where it cannot be assumed that, panel is experiencing uniform shading over its surface. So, the real time implementation of FGPE MPPT scheme is similar to that of DPE scheme [B4.24], where the sensors are placed as a zig-zag pattern as shown in Fig. B4.11.

By using the zig-zag arrangement, the panel is assumed to be irradiated uniformly by an average value of sensors, which are placed near to the individual solar panel. So, the individual panel irradiation can be determined from (B4.27).

Case 2. For complex configurations considering Fig. B4.12,

In real time situation with large number of panels, the number of sensors can be greatly increased if placements are considered like Fig. B4.12. In such cases, the uniform irradiations can be assumed within small areas e.g., 25m^2 typically. The placement of sensors in such situations is shown in Fig. B4.12. The modified expressions for calculating irradiation levels are as,

$$\left.\begin{array}{ll} G_1\big|_{Area1}=\dfrac{G_{11}+G_{21}}{2} & G_1\big|_{Area2}=\dfrac{G_{31}+G_{21}}{2} \\ G_2\big|_{Area3}=\dfrac{G_{21}+G_{12}}{2} & G_2\big|_{Area4}=\dfrac{G_{21}+G_{32}}{2} \end{array}\right\} \tag{B4.28}$$

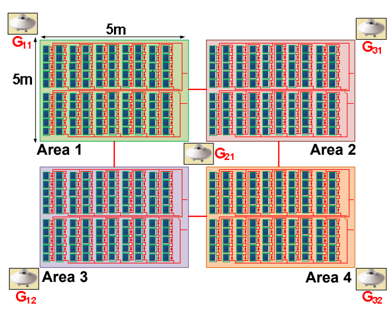

Fig. B4.12. Placement of sensors for complex systems

B4.4. SIMULATION AND HARDWARE RESULTS

The proposed FGPE MPPT has been simulated in MATLAB simulink atmosphere and also verified through real time experiments. Fig. B4.13, represents the hardware implementation of proposed system, where it consists of six solar panels arranged in 3S-2P configuration. Boost converter with IGBT switch GT50JR22 has been employed in the proposed system, where, inductance and capacitance values are designed according to load requirement. PIC18F452 controller is employed to provide switching pulses along with TLP250H as isolated gate driver. Artificial insolation is created in lab atmosphere, in which the level of irradiation can be varied using a rheostat. The panels are arranged so that, each panel is associated with varying irradiation source, where, the panel experiences uniform irradiation over its surface.

The proposed system has been studied for three pattern variations as indicated in Fig. B4.4. For the first case, the pattern is shifted from pattern 3 to pattern 1 at 0.5 sec. The respective simulation and hardware results are displayed in Fig. B4.14a and B4.14b respectively. The same pattern shifting situation have been applied for methods used in [B4.13], [B4.12] and [B4.25]. The corresponding power tracking plots are shown in Fig B4.15a, B4.15b and B4.15c respectively.

The settling times from Fig. B4.15a, B4.15b and B4.15c are 150ms, 200 ms and >500ms respectively. Therefore, the proposed FGPE scheme is displaying faster response (<10ms) compared to [B4.13], [B4.12] and [B4.25].

For the second case, the pattern is shifted from pattern 3 to pattern 2 also at 0.5s. The respective simulation and hardware results are displayed in Fig. B4.16a and B4.16b respectively.

For the third case, the pattern is shifted from pattern 2 to pattern 1 at 0.5 sec. The respective simulation and hardware results are displayed in Fig. B4.17a and B4.17b respectively. Fig. B4.18, represents the tracked PV panel power for the considered 10S-10P configuration.

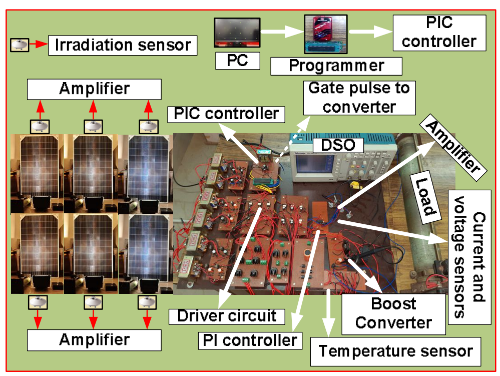

Fig. B4.13. Hardware setup for proposed MPPT scheme

From Fig. B4.14, B4.16, B4.17 and B4.18, it can be observed that, the tracking follows smooth path, along with near zero steady state oscillations. Since there is no requirement of optimization scheme, the tracking time for global maximum is lesser. Also, the proposed FGPE MPPT scheme is irradiation sensitive, power output displays lower drift under sudden change in irradiation. For the considered patterns and configurations, the tracked efficiency of the proposed FGPE scheme has been represented in Table-B4.4, by employing the ratio between tracked steady state power to actual power.

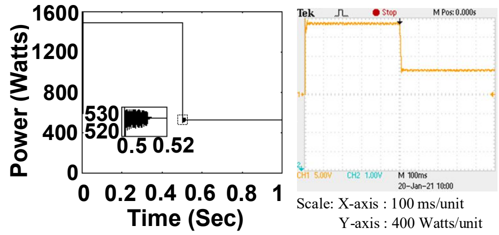

(a) (b)

Fig. B4.14. PV panel power for first case (a) Simulation and (b) Hardware

Table-B4.5, represents the overall comparison of proposed scheme with few existing MPPT schemes. Because of the simple shading pattern detection unlike [B4.12], proposed scheme can be implemented very easily, while coming to real time situation. In the proposed scheme, near global maximum is faster, due to its simple algorithm, resulting in faster tracking compared to [B4.13]. Even though, [B4.25] has the better tracking efficiency at different load variations [B4.25], it has the major disadvantage of its incapability in differentiating between uniform and partial shaded patterns. Unlike [B4.24], the FGPE scheme is able to operate successfully in tracking MPP for any type of series-parallel configuration.

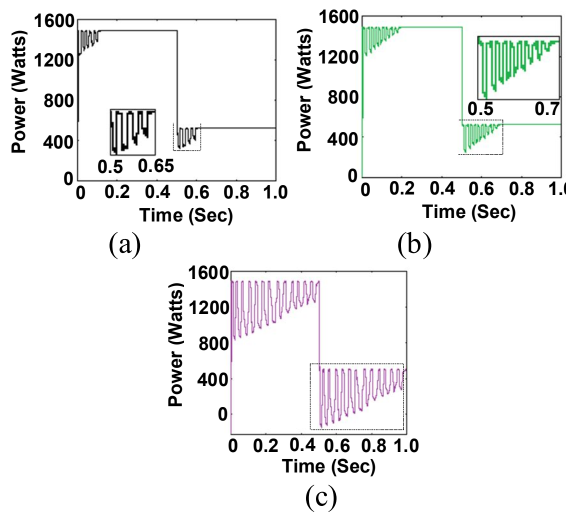

Fig. B4.15. PV panel power for first case using (a) [B4.13] (b) [B4.12] and (c) [B4.25]

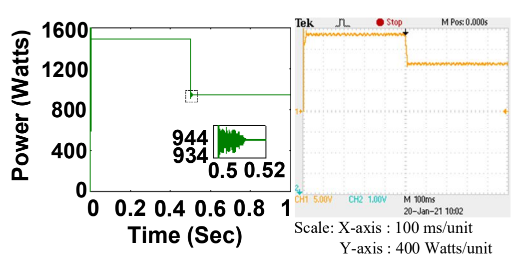

(a) (b)

Fig. B4.16. PV panel power for second case (a) Simulation and (b) Hardware

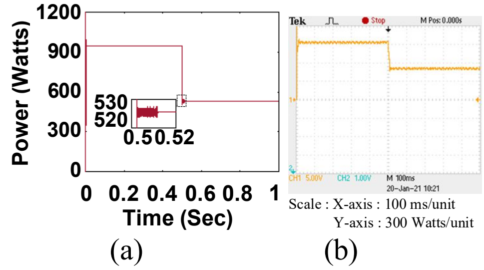

Fig. B4.17. PV panel power for third case (a) Simulation and (b) Hardware

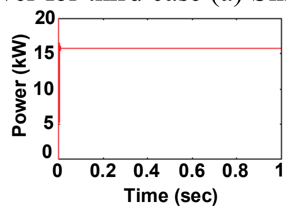

Fig. B4.18. PV panel power for the considered 10S-10P configuration

Table B4.4. Efficiency of Proposed FGPE Scheme for The Considered Patterns and Configurations

Patterns and Configurations	**P_{mpp}(W) (Actual)**	**P_{mpp}(W) (Tracked)**	**Efficiency (%)**
Pattern 1	529.28	524.68	99.13
Pattern 2	943.8	935.21	99.09
Pattern 3	1495.1	1483.3	99.21
10S-10P	16164	16039.5	99.23

Table B4.5. Comparison of FGPE Scheme With Few Existing Schemes

Properties	**[B4.13]**	**[B4.12]**	**[B4.25]**	**[B4.24]**	**FGPE**
Difficulty	Medium	High	High	Low	Low
Efficiency	High	High	High	High	High
Settling time	High	High	High	low	low
necessity of Scanning	Yes	No	No	No	No
Irradiation sensor	No	No	No	Yes	Yes
Temperature sensor	No	Yes	No	Yes	Yes
Operated for series-parallel configuration	Yes	Yes	Yes	No	Yes

B4.5. CONCLUSION

In this work, a fast-global peak estimation based MPPT scheme has been implemented for tracking global maximum under PS situation. The proposed FGPE technique has the major advantage of low complexity in real time implementation. Moreover, proposed scheme is faster responsive compared to exiting EA-P&O algorithm, since it does not require any scanning in tracking global MPP. Also, the proposed scheme is able to differentiate between the uniform and partial shaded patterns.

In this proposed work, a fast-global peak estimation based MPPT method is presented, which is able to address the series parallel configuration of any nature. It has the dynamic characteristics similar to that of DPE MPPT scheme. Since, the proposed system is irradiation sensitive, it avoids fluctuation in output, under sudden change in shading patterns. The proposed FGPE scheme is able to detect the nearest location to global maximum by sensing irradiation and temperature levels of individual solar panels, resulting in low settling time. The proposed FGPE MPPT scheme is simple and can be implemented easily with already available hardware. As a future work, the proposed scheme must be implemented wit reduced irradiation sensors.

Related publication:

- **BSV Sai**, D. Chatterjee, "A Fast-Global Peak Estimation Technique for Photovoltaic System Under Partial Shading Situation," **IEEE**, 2022. (Submitted to journal)

References:

[B4.1]Ku Ding, XinGao Bian, HaiHao Liu, and Tao Peng.: 'A MATLAB-Simulink-Based PV Module Model and Its Application under Conditions of Non uniform Irradiance', IEEE Trans. On ENERGY Conv. vol. 27, no. 4, Dec.2012.

[B4.2]Hitesh K. Mehta, Himanshu Warke, Kaushik Kukadiya and Ashish K. Panchal, "Accurate Expressions for Single-Diode-Model Solar Cell Parameterization," *IEEE journal of Photovolt*., vol. 9, no. 3, May 2019.

[B4.3]Sanjeev Kumar Pandey, Sanjaykumar Limaji Patil and Shrivijay B. Phadke, "PWM-Based Adaptive Sliding-Mode Control for Boost DC–DC Converters," IEEE Trans. on Ind. Electron., vol. 65, no. 6, June 2018.

[B4.4]B. Lekshmi Sree and M.G. Umamaheswari, "A Hankel matrix reduced order SEPIC model for simplified voltage control optimization and MPPT," Solar Energy, Vol. 170, Aug. 2018, Page no. 280-292.

[B4.5]R.B.A.Cunha, R.S.Inomoto, J.A.T.Altuna, F.F.Costa, S.G.Di Santo and A.J.Sguarezi Filho, "Constant switching frequency finite control set model predictive control applied to the boost converter of a photovoltaic system," Solar Energy, Vol. 189, 1 Sept. 2019, Page no. 57-64.

[B4.6]H. Patel and V. Agarwal, "MATLAB-based modeling to study the effects of partial shading on PV array characteristics," *IEEE Trans. Energy Con.* vol. 23, no. 1, pp. 302–310, Mar. 2008.

[B4.7]Indu Rani Balasubramanian, Saravana Ilango Ganesan and Nagamani Chilakapati, "Impact of partial shading on the output power of PV systems under partial shading conditions," *IET Power Electron*., 2014, Vol. 7, Iss. 3, pp. 657–664.

[B4.8]Jieming Ma, Xinyu Pan, Ka Lok Man, Xingshuo Li, Huiqing Wen and Tiew On Ting, "Detection and Assessment of Partial Shading Scenarios on Photovoltaic Strings," *IEEE Trans. on Ind. Applications*, VOL. 54, NO. 6, NOV./DEC. 2018.

[B4.9]Muralidhar Killi and Susovon samanta, "Modified Perturb and Observe MPPT Algorithm for Drift Avoidance in Photovoltaic Systems," *IEEE Tans. Ind. Electron*, VOL. 62, NO. 9, Sep.2015.

[B4.10] Mohamed Lasheen, Ali Kamel Abdel Rahman, Mazen Abdel-Salam and Shinichi Ookawara, "Adaptive reference voltage-based MPPT technique for PV applications," *IET Renew. Power Gener., 2017, Vol. 11 Iss. 5, pp. 715-722.*

[B4.11] Aranzazu D. Martin, Jesus R. Vazquez and J.M. Cano, "MPPT in PV systems under partial shading conditions using artificial vision," *Electric Power Systems Research* 162 (2018) 89–98.

[B4.12] Venkata Reddy Kota and Muralidhar Nayak Bhukya, "A novel global MPP tracking scheme based on shading pattern identification using artificial neural networks for photovoltaic power generation during partial shaded condition," *IET Renew. Power Gener., 2019, Vol. 13 Iss. 10, pp. 1647-1659.*

[B4.13] Jubaer Ahmed and Zainal Salam, "An Enhanced Adaptive P&O MPPT for Fast and Efficient Tracking Under Varying Environmental Conditions," *IEEE Trans. ON SUSTAINABLE ENERGY*, VOL. 9, NO. 3, JULY 2018.

[B4.14] Ziqiang Bi, JiemingMa, Ka LokMan, Jeremy S. Smith, Yong Yue and Huiqing Wen, "An Enhanced 0.8V_{OC}-Model-Based Global Maximum Power Point Tracking Method for Photovoltaic Systems," *IEEE Trans. Ind. Appl.*, Vol. 56, No. 6, Nov./Dec. 2020.

[B4.15] Hong Li, Duo Yang, Wenzhe Su, Jinhu Lu and Xinghuo Yu, "An Overall Distribution Particle Swarm Optimization MPPT Algorithm for Photovoltaic System Under Partial Shading," *IEEE Trans. on Ind. Electron*., VOL. 66, NO. 1, JAN 2019.

[B4.16] Thanikanti Sudhakar Babu, J. Prasanth Ram, Tomislav Dragicevic, Masafumi Miyatake, Frede Blaabjerg and Natarajan Rajasekar, "Particle Swarm Optimization Based Solar PV Array Reconfiguration of the Maximum Power Extraction Under Partial Shading Conditions," *IEEE Trans. on Sustainable Energy*, VOL. 9, NO. 1, JAN 2018.

[B4.17] Dimas AjiNugraha, K. L. Lian and Suwarno, "A Novel MPPT Method Based on Cuckoo Search Algorithm and Golden Section Search Algorithm for Partially Shaded PV System," *canadian journal of electrical and computer engineering, vol. 42, no. 3, summer 2019.*

[B4.18] Hadi M. El-Helw, Ahmed Magdy, And Mostafa I. Marei, "A Hybrid Maximum Power Point Tracking Technique for Partially Shaded Photovoltaic Arrays," *IEEE Access, VOL. 5, 2017.*

[B4.19] Immad Shams, Saad Mekhilef and Kok Soon Tey, "Maximum Power Point Tracking Using Modified Butterfly Optimization Algorithm for Partial Shading, Uniform Shading, and Fast Varying Load Conditions," *IEEE Trans. Power Electron.*, Vol. 36, No. 5, May 2021.

[B4.20] Chih Yu Liao, Ramadhani Kurniawan Subroto, Ibrahim Saiful Millah, Kuo Lung Lian And Wei-Tzer Huang, "An Improved Bat Algorithm for More Efficient and Faster Maximum Power Point Tracking for a Photovoltaic System Under Partial Shading Conditions," *IEEE Access*, Jun. 2020.

[B4.21] Shungang Xu, Yuan Gao, Guohua Zhou and Guihua Mao, "A Global Maximum Power Point Tracking Algorithm for Photovoltaic Systems Under Partially Shaded Conditions Using Modified Maximum Power Trapezium Method," *IEEE Trans. on Ind. Electron.*, Vol. 68, No. 1, Jan. 2021.

[B4.22] Chao Huang, Long Wang, Zijun Zhang, Ryan Shun-cheung Yeung, Alain Bensoussan and Henry Shu-hung Chung, "A Novel Spline Model Guided Maximum Power Point Tracking Method for Photovoltaic Systems," *IEEE Trans. Sustain. Energy*, vol. 11, no. 3, Jul. 2020.

[B4.23] J. Prasanth Ram, Dhanup S. Pillai, N. Rajasekar and Scott M. Strachan, "Detection and Identification of Global Maximum Power Point Operation in Solar PV Applications Using a Hybrid ELPSO-P&O Tracking Technique," *IEEE J. of Emer. and Selected Topics in Power Electron.*, VOL. 8, NO. 2, Jun. 2020.

[B4.24] Boni Satya Varun Sai, Sarang A. Khadtare and Debashis Chatterjee, "A dummy peak elimination based MPPT technique for PV generation under partial shading condition," *IET Renewable Power Generation*. 2021;1–14.

[B4.25] Immad Shams, Saad Mekhilef and Kok Soon Tey, "Improved-Team-Game-Optimization-Algorithm-Based Solar MPPT With Fast Convergence Speed and Fast Response to Load Variations," *IEEE Trans. on Ind. Electron*., Vol. 68, No. 8, Aug. 2021.

C. Using Operating Characteristics

C4.1 INTRODUCTION

The non-renewable energy sources are almost near extinction, due to their over consumption in meeting the needs of enlarged world population. The non-renewable energy sources generate wastage and greenhouse gases along with energy, leads to the pollution of land, air and water [C4.1]. Therefore, there is a high requirement of alternate energy production to avoid the exploitation of the non-renewable sources. Amongst renewable energy sources, solar energy displays high flexibility in power generation due to its easy installation and noise free operation. In spite of many advantages, the solar energy has also a major drawback due to its non-uniform distribution of irradiance over panels resulting from several factors. This leads to high complexity for maximum power extraction methods. Several literatures are already available to address this major issue [C4.2].

Amongst various configurations, the series-parallel models are advantageous due to their capability to address both the load voltage and current characteristics. Boost converter is the most commonly employed DC-DC converter in PV system, due to its simple structure and non-inverted output nature [C4.3-C4.5]. The multiple peak nature of P-V and I-V characteristics, under PS condition, creates a major problem in tracking MPP [C4.6-C4.8]. Under, PS condition, the conventional MPPT schemes like ARV based MPPT, CV based MPPT scheme and MP&O method etc., fails in tracking the MPP successfully. The global maximum detection under PS situation is successfully executed by many optimization-based methods [C4.9-C4.10].

Artificial vision-based scheme [C4.11] is able to track the global maximum efficiently, but it requires high cost camera to detect the shading pattern. Even though low-cost camera can be employed as mentioned in [C4.11] for pattern detection, it can lead to the precision error. ANN based MPPT scheme is used for global maximum point tracking, in which shading pattern is detected by employing ANN. The estimated global maximum point is employed to detect the nearest voltage reference to global maximum [C4.12]. This method is difficult to execute in real time situation as it requires complex initialization method for tracking purpose. In [C4.13], the adapted version of conventional P&O scheme is introduced for tracking MPP effectively under PS condition. But the requirement of scanning in EA-P&O topology leads to higher settling time and poor dynamic characteristics. The $0.8V_{oc}$ is method discussed in [C4.13] is easy to implement but it results in higher settling time in reaching steady sate. Moreover, this method undergoes huge fluctuations under sudden change in irradiation. The tracking of global maximum is successfully done by employing the peak point detection scheme [C4.14]. But this method deals only with series configurations and no proper structure has been proposed for series-parallel configurations. CS and PSO methods are the most commonly used MPPT schemes for global maximum detection by overcoming the local maximum barrier [C4.15-C4.17]. A hybrid PSO and P&O based MPPT scheme has been projected for tracking global maximum power in [C4.18], where ANN along with irradiation sensors has been established to detect the pattern. The PSO comes into operation during partial shading, while P&O works for uniform shading case. The hardware implementation of [C4.18] is difficult due to the usage of both ANN and PSO in its architecture. The Modified Butterfly Optimization Algorithm [C4.19], Improved Bat Algorithm [C4.20], Modified Maximum Power Trapezium Methods in [C4.21], [C4.22] and [C4.23] have the major disadvantage of complexity in implementation, while coming to real time condition. Although, optimization-based schemes are able to track the global maximum with good operating characteristics, they have the major disadvantage of requiring high end equipment and more settling time in tracking maximum power.

A SB MPPT has been discussed in this research work, where the sensors are employed to detect the shading pattern for series-parallel PV configurations. The proposed method uses the operating characteristics of the PV panels. The modified characteristics under any operating conditions e.g. temperature and irradiation etc. can be obtained from the initially stored characteristics at STC following the proposed method. The proposed SB MPPT displays better operating characteristics compared to the existing methods e.g., lower settling time and near zero power oscillation while adjusting to new operating point. The proposed system is verified for three series-two parallel (3S-2P) configuration through both MATLAB simulation and suitable hardware implementation.

C4.2 SOLAR PANEL MODELLING

A single diode model [C4.1], is used in solar cell modelling, because of its ability to generate accurate solar panel characteristics. Fig. C4.1, denotes the power electronic circuit for single diode model.

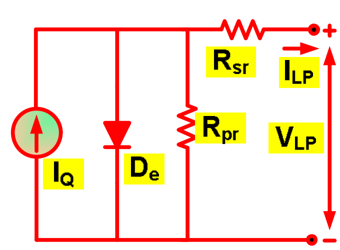

Fig. C4.1. Single diode model for solar cell

Table C4.1. Manufacturer Data for Solar Panel (TP250MBZ)

Variables	Quantity
MPP power	249W
MPP voltage	30V
MPP current	8.3A
SCC	8.83A
OCC	36.8V
Temperature coefficient of I_{sc}	$0.064\%/^0C$
Temperature coefficient of V_{ov}	$-0.33\%/^0C$

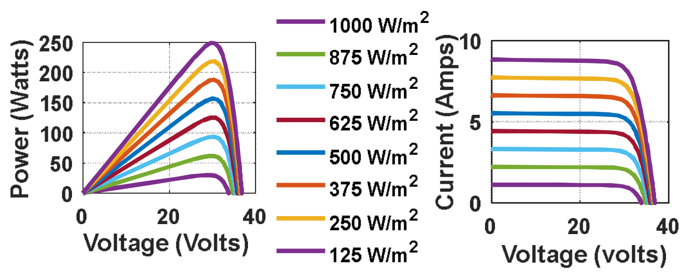

(a)

Irradiation	125	250	375	500
MPP Voltage	28.502	29.1402	30.3505	29.99
MPP Current	1.0566	2.1159	3.0833	4.18
MPP Power	30.1143	61.6574	93.5812	125.41
Irradiation	625	750	875	1000
MPP Voltage	30.0267	30.203	30.4042	30.01
MPP Current	5.2249	6.2277	7.1927	8.3
MPP Power	156.8873	188.0963	218.6885	249.1

(b)

Fig. C4.2. (a) Output curves (b) MPP values of single solar module

The relation between R_{sr}, R_{pr}, I_{LP} and V_{LP} is given by,

$$I_{LP} = I_Q - I_{sa}\left[e^{\frac{Q(V_{LP}+R_{sr}I_{LP})}{N_S AK\times T}} - 1\right] - \frac{V_{LP}+R_{sr}I_{LP}}{R_{pr}} \qquad \text{(C4.1)}$$

The V_{ov} and I_{sc} are expressed in terms of G and T as [C4.1],

$$I_{sc} = I_{sc,r}\left[1+\alpha\left(T-T_r\right)\right]\frac{G}{G_r} \qquad \text{(C4.2)}$$

$$V_{ov} = V_{ov,r}\left[1 + a\times\ln\frac{G}{G_r} + \beta\left(T-T_r\right)\right] \qquad \text{(C4.3)}$$

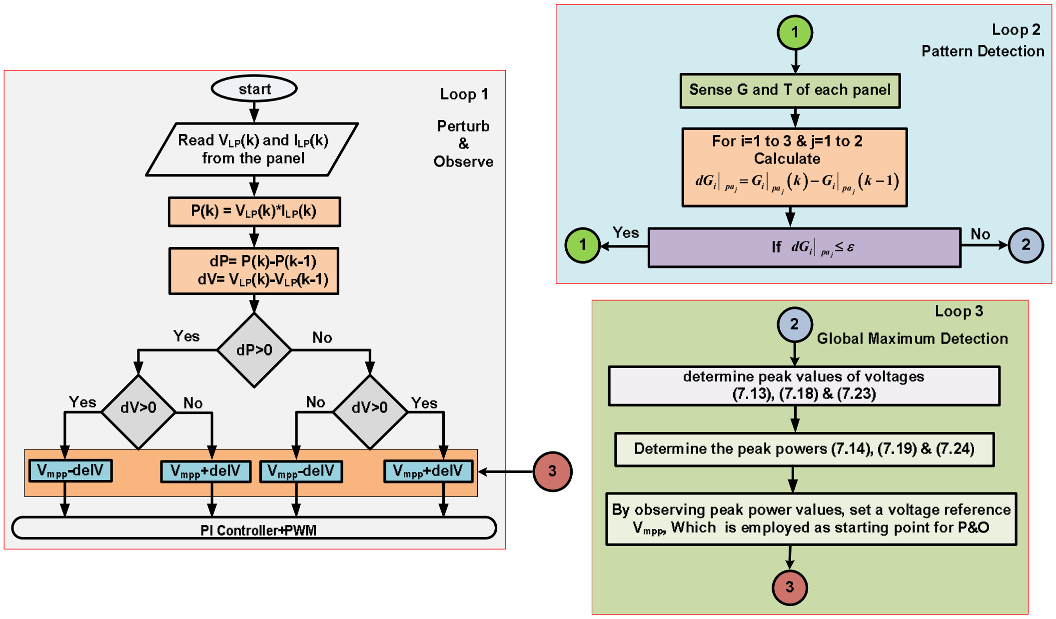

Fig. C4.3. Flowchart of the proposed SB algorithm

The manufacturer details for a typical panel TP250MBZ are shown in Table-C4.1. The respective I-V and P-V curves of the considered PV panel are represented in Fig. C4.2a. and Fig. C4.2b, represents the MPP values for the respective I-V and P-V characteristics.

C4.3 PROPOSED SB TECHNIQUE FOR GLOBAL MAXIMUM DETECTION

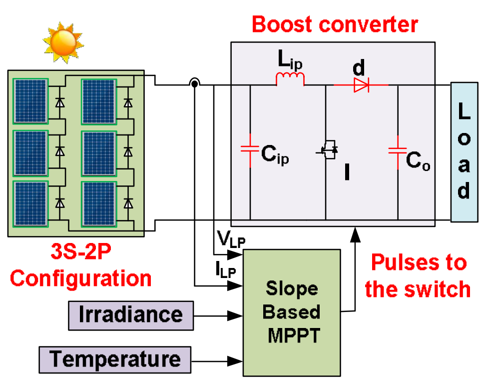

Fig. C4.4. Proposed SB scheme

The proposed SB scheme along with DC-DC converter is represented in Fig. C4.4. The proposed MPPT method is verified through simulation in MATLAB and with proto type hardware setup with different shading patterns for 3S-2P configuration. However, the proposed scheme can work successfully for any number of series parallel configurations.

C4.3.1 Determination of first peak point on P-V Curve

The proposed SB algorithm is represented in Fig. C4.3. It consists of three loops, where loop 1 does the operation of traditional P&O scheme and loop 2 is meant for Pattern detection. The nearest point to global maximum detection is done by employing the loop 3. The estimated global maximum point is used as a reference point in P&O MPPT for tracking global maximum power.

The first peak determination in proposed SB scheme is explained with a complex MS-NP system as shown in Fig. C4.6.

The irradiation levels for each parallel string are to be arranged in descending order for the proposed method. For the present case, it is assumed that the irradiation levels for the first parallel string are in the order of $G_1|_{pa_1} \geq G_2|_{pa_1} \geq .... \geq G_M|_{pa_1}$ and $G_1|_{pa_N} \geq G_2|_{pa_N} \geq .... \geq G_M|_{pa_N}$ for Nth parallel string. Similar kind of irradiation pattern can be assumed in remaining parallel strings. In the proposed model, the sets for irradiation levels of individual panels with MS-NP configuration can be formed as,

Set 1: $\{\left[G_1|_{pa_1}\right], \left[G_1|_{pa_2}\right], ..., \left[G_1|_{pa_N}\right]\}$.

Set 2: $\{\left[G_2|_{pa_1}\right], \left[G_2|_{pa_2}\right], ..., \left[G_2|_{pa_N}\right]\}$.

……………………………………………….

Set M: $\{\left[G_M|_{pa_1}\right], \left[G_M|_{pa_2}\right] ...., \left[G_M|_{pa_N}\right]\}$.

After the set formation as above, the next task is to find out the open circuit voltage and short circuit current levels for each panel with given irradiations using (C4.2) and (C4.3). Therefore, the MPP voltage and current values for individual solar panels in the MS-NP configuration can be determined as,

$$(V_{\max})_{ij} \approx K_2 \times \left[(V_{ov})\Big|_{G_i|_{pa_j}} \right] \tag{C4.4}$$

$$(I_{\max})_{ij} \approx K_1 \times \left[(I_{sc})\Big|_{G_i|_{pa_j}} \right] \tag{C4.5}$$

Where i=1, 2, ………, M and j=1, 2………., N. The factors K_1 and K_2 can be calculated as,

$$K_1 = \left. \frac{I_{mpp}}{I_{sc}} \right|_{STC} \tag{C4.6}$$

$$K_2 = \left. \frac{V_{mpp}}{V_{ov}} \right|_{STC} \tag{C4.7}$$

Using (C4.4) and (C4.5), the MPP power for individual panels can be calculated as,

$$(P_{\max})_{ij} = (V_{\max})_{ij} \cdot (I_{\max})_{ij} \tag{C4.8}$$

Further, the positive slope of P-V graph to reach P_{max} for individual panels can be calculated using (C4.4), (C4.5) and (C4.8) as,

$$(m)_{ij} \approx \frac{(P_{\max})_{ij}}{(V_{\max})_{ij}} \tag{C4.9}$$

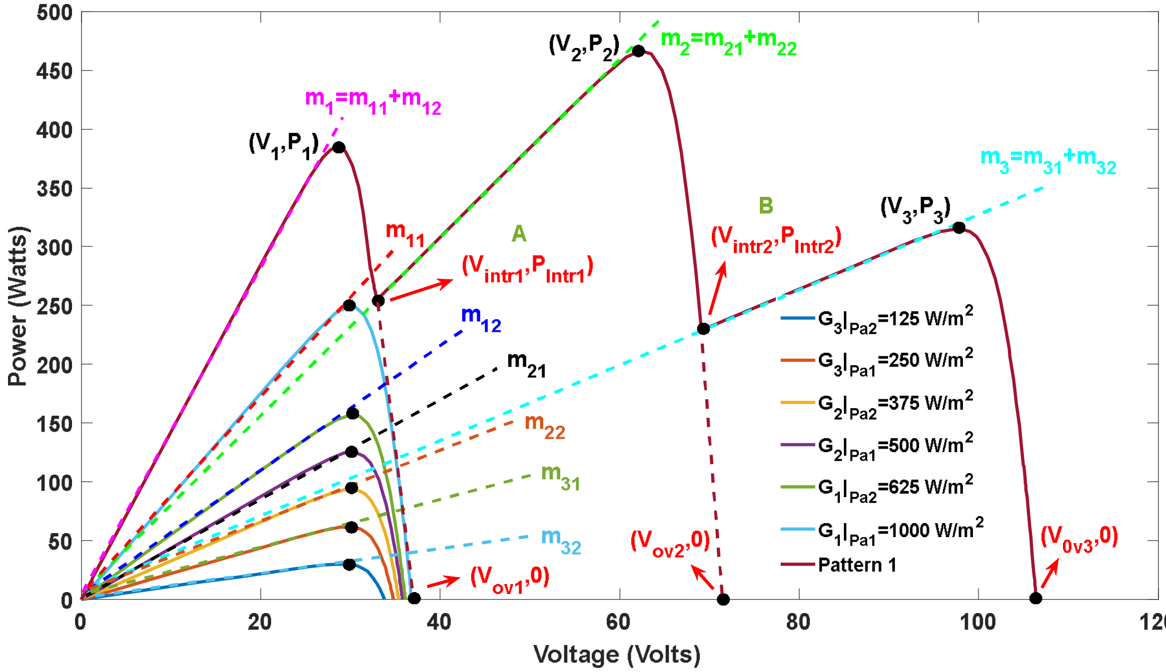

Fig. C4.5. P-V curves for the individual solar panels and pattern 1

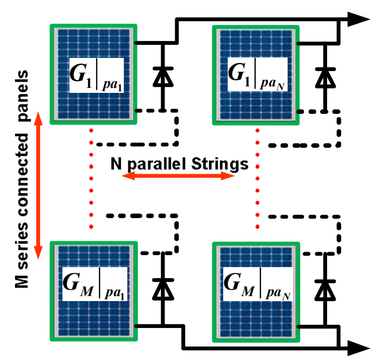

Fig. C4.6. Complex MS-NP configurations

The real and virtual open circuit voltage points in the P-V curve with multiple peaks can be calculated as,

$$V_{ov1} \approx \left(V_{ov}\right)\Big|_{Max(set1)} \tag{C4.10}$$

$$V_{ov2} \approx \sum_{k=1}^{2}\left[\left(V_{ov}\right)\Big|_{\max(set\,k)}\right] \tag{C4.11}$$

....

$$V_{ovM} \approx \sum_{k=1}^{M}\left[\left(V_{ov}\right)\Big|_{\max(set\,k)}\right] \tag{C4.12}$$

By using the available data of individual solar panels, the voltage and power at the first peak of P-V curve can be determined as,

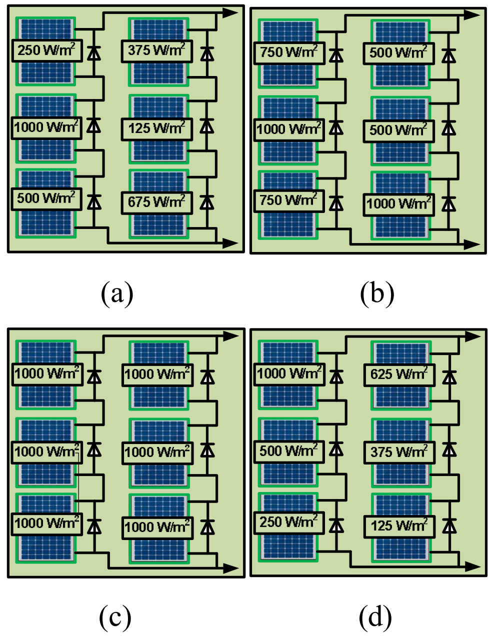

Fig. C4.7. Different shading patterns for 3S-2P (a) Pattern 1 (b) Pattern 2 (c) Pattern 3 and (d) Panel rearrangement of (a) by using the proposed SB scheme

$$V_1 \approx K_2 \times V_{ov1} \tag{C4.13}$$

$$P_1 = V_1 \times \left[\sum_{i=1}^{N} m_{1j} \right] \tag{C4.14}$$

C4.3.2 Implementing SB scheme for 3S-2P Configuration

For 3S-2P configuration, different irradiation patterns considered are shown in Fig. C4.7. The patterns 1, 2 and 3, results in the three, two and single peaks in the P-V characteristics respectively. Based on the irradiation values of individual solar panels, the 3S-2P configuration of Fig. C4.7a, can be rearranged as Fig. C4.7d. Same method can be followed for other patterns. Based on earlier discussion, for the pattern rearrangement shown in Fig. C4.7d, the set formation can be obtained as,

Set 1: {1000 W/m^2 and 625 W/m^2}.

Set 2: {500 W/m^2 and 375 W/m^2}.

Set 3: {250 W/m^2 and 125 W/m^2}.

By following the proposed first peak calculation part as shown in preceding section, the unknown points (V_1, P_1), (V_{ov1}, 0), (V_{ov2}, 0) and (V_{ov3}, 0) on the combined P-V curve of Fig. C4.5, has been determined for pattern 1. By using these points, the intercept points A and B can be calculated as represented below. The point A is formed due to the intersection of lines with negative slope at first peak and positive slope of second peak. From Fig. C4.6, the equation for negative slope line with first peak can be expressed as,

$$P = P_1 - \frac{P_1 \times V}{V_{ov1} - V_1} + \frac{P_1 \times V_1}{V_{ov1} - V_1} \tag{C4.15}$$

Similarly, the positive slope line equation for second peak can be formulated as,

$$P = m_2 \times V = (m_{21} + m_{22}) \times V \tag{C4.16}$$

The voltage at the intercept point A can be calculated by substituting (C4.16) in (C4.15) as,

$$V_{intr1} = \frac{P_1 \times V_{ov1}}{\left[(m_{21} + m_{22}) \times (V_{ov1} - V_1)\right] + P_1} \tag{C4.17}$$

All the parameters of (C4.17) has been already calculated through SB first peak calculation. From this intercept point A, the voltage V_2 at second peak can be calculated as,

$$V_2 \approx V_{intr1} + (K_2 \times V_{ov2}) \tag{C4.18}$$

By using (C4.17), the second power peak P_2 can be calculated as,

$$P_2 = (m_{21} + m_{22}) \times V_2 \tag{C4.19}$$

Using points (V_2, P_2) and (V_{ov2}, 0) in Fig. C4.5, the second interception point B can be calculated similar to point A. The equation for negative slope line for second peak can be formulated as,

$$P = P_2 - \frac{P_2 \times V}{V_{ov2} - V_2} + \frac{P_2 \times V_2}{V_{ov2} - V_2} \tag{C4.20}$$

The expression for the positive slope line of third peak can be formulated as,

$$P = m_3 \times V = (m_{31} + m_{32}) \times V \tag{C4.21}$$

The voltage for the interception point B can be obtained by substituting (C4.21) in (C4.20) as,

$$V_{intr2} = \frac{P_2 \times V_{ov2}}{\left[(m_{31} + m_{32}) \times (V_{ov2} - V_2)\right] + P_2} \tag{C4.22}$$

All the parameters of (C4.22) has been already calculated during SB first peak calculation and intercept A estimation. From this intercept point B, the V_3 can be calculated as,

$$V_3 \approx V_{intr2} + (K_2 \times V_{ov3}) \tag{C4.23}$$

By using (C4.23), the third peak power P_3 can be calculated as,

$$P_3 = (m_{31} + m_{32}) \times V_3 \tag{C4.24}$$

By comparing (C4.14), (C4.19) and (C4.24), the peak at which the global maximum power occurs can be determined. By employing proposed SB scheme for pattern-1, the calculated global maximum is located at P_{max}=456.286W and V_{max}=62.806V. The comparison of actual and calculated global maximum MPP values of global maximum for all patterns considered is shown in Table-C4.2. From Table-C4.2, it can be observed that, the proposed SB scheme is able to predict the global maximum peak with high accuracy. The respective predicted peak voltage value is used as a reference for P&O scheme, in tracking global maximum. Also, PI controller with proper tuning is employed in the proposed scheme.

Table C4.2. MPP Values Comparison for Different Patterns

Patterns	Comparison	V_{mpp} (V)	P_{mpp} (W)
Pattern 1	Calculated	62.806	456.286
	Actual	62.401	466.703
Pattern 2	Calculated	92.634	964.274
	Actual	92.555	979.918
Pattern 3	Calculated	90.27	1494.87
	Actual	90.03	1494.5

C4.3.3 Sensor Placement

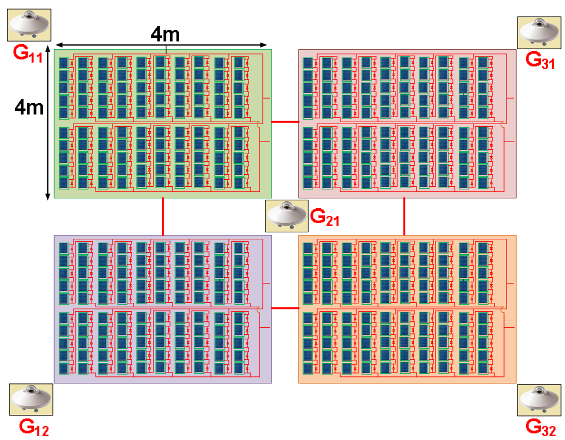

Fig. C4.8. Sensor placement for large number of panels

The simplified sensor placement for the PV farm with large number of panels are represented in Fig. C4.8. For the large plants with large number of panels, the proposed arrangement of the irradiation sensors is as shown in Fig. C4.8. This can avoid the requirement of higher number of irradiation sensors. It is assumed that the irradiation level can remain almost same for a larger area compared to individual panel. In the proposed configuration an area equal to 16m^2 are considered to be experiencing uniform irradiation over solar panels. The modified expressions for calculating irradiation levels are as (C4.26).

$$\left.\begin{array}{ll} G_1\big|_{Area1}=\dfrac{G_{11}+G_{21}}{2} & G_1\big|_{Area2}=\dfrac{G_{31}+G_{21}}{2} \\ G_2\big|_{Area3}=\dfrac{G_{21}+G_{12}}{2} & G_2\big|_{Area4}=\dfrac{G_{21}+G_{32}}{2} \end{array}\right\} \tag{C4.26}$$

C4.4 SIMULATION AND HARDWARE RESULTS

The proposed SB MPPT has been simulated in MATLAB & Simulink atmosphere and also verified through real time experiments. Fig. C4.9, represents the hardware implementation of proposed system, where it consists of six solar panels arranged in 3S-2P configuration. Boost converter with IGBT switch GT50JR22 has been employed in the proposed system. The inductance and capacitance values are designed according to load requirement. PIC18F452 controller is employed to provide switching pulses along with TLP250H as isolated gate driver. Artificial insolation is created in lab atmosphere, in which the level of irradiation can be varied using a rheostat. The panels are arranged so that, each panel is associated with varying irradiation source, where, the panel experiences uniform irradiation over its surface.

The proposed system has been studied for three pattern variations as indicated in Fig. C4.7. For the first case, the pattern is shifted from pattern 3 to pattern 1 at 0.5 sec. The respective simulation and hardware results are displayed in Fig. C4.11a and C4.11b respectively. The same pattern shifting situation have been applied for methods used in [C4.13], [C4.12] and [C4.25]. The corresponding power tracking plots are shown in Fig C4.12a, C4.12b and C4.12c respectively. The settling times observed from Fig. C4.11a, C4.11b and C4.11c are 150ms, 200 ms and >500ms respectively. Therefore, the proposed SB scheme is displaying faster response (<10ms) compared to [C4.13], [C4.12] and [C4.25].

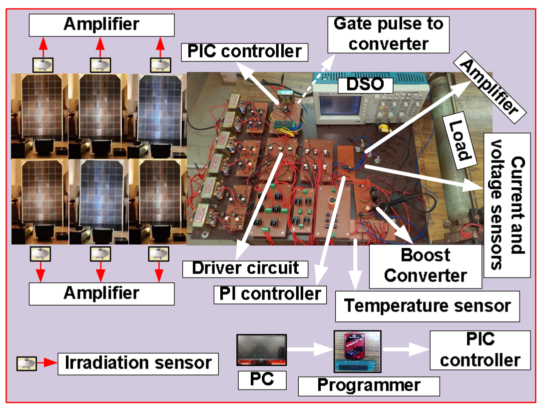

Fig. C4.9. Hardware setup for proposed MPPT scheme

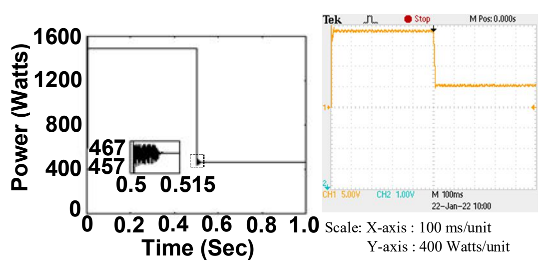

(a) (b)

Fig. C4.10. PV panel power for first case (a) Simulation and (b) Hardware

Table C4.3. Efficiency of Proposed SB Scheme For The Considered Patterns And Configurations

Patterns and Configurations	P_{mpp}(W) (Actual)	P_{mpp}(W) (Tracked)	Efficiency (%)
Pattern 1	466.703	462.59	99.12
Pattern 2	979.918	971.099	99.1
Pattern 3	1495.1	1482.99	99.19

For the second case, the pattern is shifted from pattern 3 to pattern 2 also at 0.5s. The respective simulation and hardware results are displayed in Fig. C4.12a and C4.12b respectively. For the third case, the pattern is shifted from pattern 2 to pattern 1 at 0.5 sec. The respective simulation and hardware results are displayed in Fig. C4.13a and C4.13b respectively.

From Fig. C4.12 and C4.13, it can be observed that, the tracking follows smooth path, along with near zero steady state oscillations. Since there is no requirement of optimization scheme, the tracking time for global maximum is lesser. Also, the proposed SB MPPT scheme is irradiation sensitive, power output displays lower drift under sudden change in irradiation. For the considered patterns and configurations, the tracked efficiency of the proposed SB scheme has been represented in Table-C4.3.

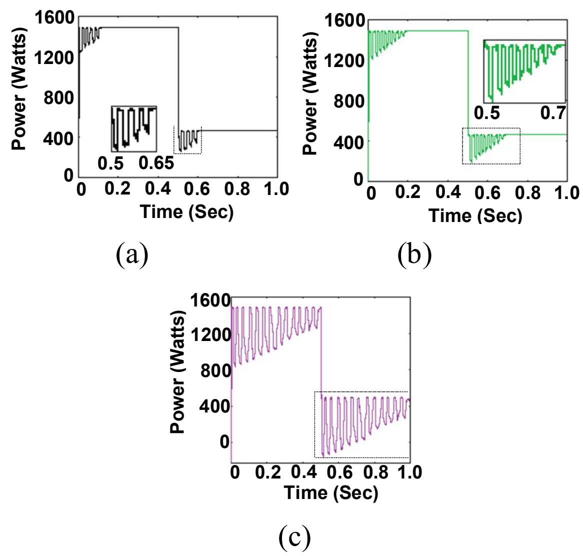

Fig. C4.11. PV panel power for first case using (a) [C4.13] (b) [C4.12] and (c) [C4.25]

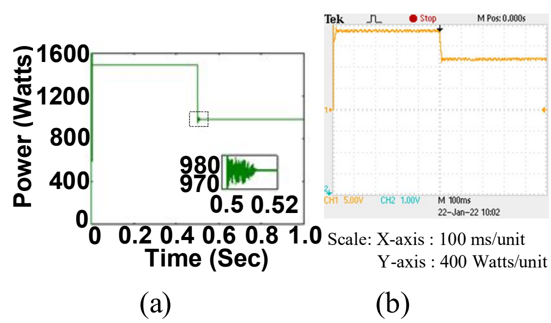

Fig. C4.12. PV panel power for second case (a) Simulation and (b) Hardware

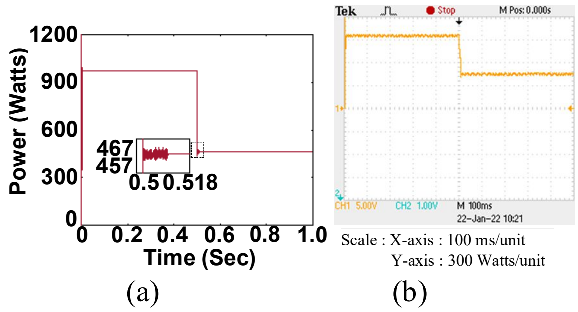

Fig. C4.13. PV panel power for third case (a) Simulation and (b) Hardware

Table-C4.4, represents the overall comparison of proposed scheme with few existing MPPT schemes. Because of the simple shading pattern detection unlike [C4.12], proposed scheme can be implemented very easily, while coming to real time situation. In the proposed scheme, near global maximum is faster, due to its simple algorithm, resulting in faster tracking compared to [C4.13]. Even though, [C4.25] has the better tracking efficiency at different load variations, it has the major disadvantage of its incapability in differentiating between uniform and partial shaded patterns. Unlike [C4.24], the SB scheme is able to operate successfully in tracking MPP for any type of series-parallel configurations.

Table C4.4. Comparison of SB Scheme With Few Exiting Schemes

Properties	[C4.13]	[C4.12]	[C4.25]	[C4.24]	SB
Difficulty	Medium	High	High	Low	Low
Efficiency	High	High	High	High	High
Settling time	High	High	High	low	low
necessity of Scanning	Yes	No	No	No	No
Irradiation sensor	No	No	No	Yes	Yes
Temperature sensor	No	Yes	No	Yes	Yes
Operated for series-parallel configuration	Yes	Yes	Yes	No	Yes

C4.5 CONCLUSION

In this work, a slope based accurate MPPT scheme has been implemented for tracking global maximum under PS situation. The proposed SB technique has the major advantage of low complexity in real time implementation. Moreover, the proposed scheme is faster responsive compared to exiting EA-P&O algorithm, since it does not require any scanning in tracking global MPP. Also, it is able to differentiate between the uniform and partial shaded patterns.

The proposed SB MPPT scheme is able to address the series parallel configuration of any nature. Since, the proposed system is irradiation sensitive, it avoids fluctuation in output, under sudden change in shading patterns. The proposed SB scheme is able to detect the nearest location to global maximum by sensing irradiation levels of individual solar panels, resulting in low settling time. Moreover, the proposed SB MPPT scheme is simple and can be implemented easily with already available hardware. As a future work, the proposed scheme must be implemented wit reduced irradiation sensors.

Related Publication:

- **BSV Sai**, D. Chatterjee, "An Accurate MPPT Technique under Partial Shading Conditions Using PV Panel Operating Characteristics," **IEEE**, 2022. (Submitted to journal)

References:

[C4.1]Ku Ding, XinGao Bian, HaiHao Liu, and Tao Peng.: 'A MATLAB-Simulink-Based PV Module Model and Its Application under Conditions of Non uniform Irradiance', IEEE Trans. On ENERGY Conv. vol. 27, no. 4, Dec.2012.

[C4.2]Linta Eliya Mathew and Ashish K. Panchal, "A Complete Numerical Investigation on Implicit and Explicit PV Single-Diode-Models Using I- and V-Approaches," *IEEE journal of Photovolt.*, Vol. 11, No. 3, May 2021.

[C4.3]Singh, K. A., Prajapati, A., and Chaudhary, K., "High gain compact interleaved boost converter with reduced voltage stress for PV application," *IEEE Journal of Emerging and Selected Topics in Power Electronics*, Oct. 2021.

[C4.4]Sara Hasanpour, Tohid Nouri, Frede Blaabjerg and Yam P. Siwakoti, "High Step-Up SEPIC-Based Trans-Inverse DC-DC Converter with Quasi-Resonance Operation for Renewable Energy Applications," *IEEE Transactions on Industrial Electronics*, Feb. 2022.

[C4.5]Seneke Chamith Chandrarathna and Jong-Wook Lee, "A Self-Resonant Boost Converter for Photovoltaic Energy Harvesting With a Tracking Efficiency >90% Over an Ultra-Wide Source Range," *IEEE Journal of Solid-State Circuits*, Nov. 2021.

[C4.6]Kais Abdulmawjood, Samer Alsadi, Shady S. Refaat and Walid G. Morsi, "Characteristic Study of Solar Photovoltaic Array Under Different Partial Shading Conditions," *IEEE Access*, Page No. 6856 – 6866, Jan. 2022.

[C4.7]G. M. Madhu, S. Member, and C. Vyjayanthi, "Investigation on Effect of Irradiance Change in Maximum Power Extraction From PV Array Interconnection Schemes During Partial Shading Conditions," *IEEE Access*, vol. 9, pp. 96995–97009, July. 2021.

[C4.8]Ali Bidram, Ali Davoudi and Robert S. Balog, "Control and Circuit Techniques to Mitigate Partial Shading Effects in Photovoltaic Arrays," *IEEE Journal of Photovoltaics*, Vol. 2, Issue: 4, Oct. 2012.

[C4.9]Muralidhar Killi and Susovon samanta, "Modified Perturb and Observe MPPT Algorithm for Drift Avoidance in Photovoltaic Systems," *IEEE Tans. Ind. Electron*, VOL. 62, NO. 9, Sep.2015.

[C4.10] Mohamed Lasheen, Ali Kamel Abdel Rahman, Mazen Abdel-Salam and Shinichi Ookawara, “Adaptive reference voltage-based MPPT technique for PV applications,” *IET Renew. Power Gener., 2017, Vol. 11 Iss. 5, pp. 715-722.*

[C4.11] Aranzazu D. Martin, Jesus R. Vazquez and J.M. Cano, “MPPT in PV systems under partial shading conditions using artificial vision,” *Electric Power Systems Research* 162 (2018) 89–98.

[C4.12] Venkata Reddy Kota and Muralidhar Nayak Bhukya, “A novel global MPP tracking scheme based on shading pattern identification using artificial neural networks for photovoltaic power generation during partial shaded condition,” *IET Renew. Power Gener., 2019, Vol. 13 Iss. 10, pp. 1647-1659.*

[C4.13] Jubaer Ahmed and Zainal Salam, “An Enhanced Adaptive P&O MPPT for Fast and Efficient Tracking Under Varying Environmental Conditions,” *IEEE Trans. ON SUSTAINABLE ENERGY*, VOL. 9, NO. 3, JULY 2018.

[C4.14] Ziqiang Bi, JiemingMa, Ka LokMan, Jeremy S. Smith, Yong Yue and Huiqing Wen, “An Enhanced 0.8V_{OC}-Model-Based Global Maximum Power Point Tracking Method for Photovoltaic Systems,” *IEEE Trans. Ind. Appl.*, Vol. 56, No. 6, Nov./Dec. 2020.

[C4.15] Ramdan B. A. Koad, Ahmed Faheem Zobaa and Adel El-Shahat, “A Novel MPPT Algorithm Based on Particle Swarm Optimization for Photovoltaic Systems,” *IEEE Transactions on Sustainable Energy*, Volume: 8, Issue: 2, April 2017.

[C4.16] Neeraj Priyadarshi, Sanjeevikumar Padmanaban, Jens Bo Holm-Nielsen, Frede Blaabjerg and Mahajan Sagar Bhaskar, “An Experimental Estimation of Hybrid ANFIS–PSO-Based MPPT for PV Grid Integration Under Fluctuating Sun Irradiance,” IEEE Systems Journal, Vol. 14, No. 1, March 2020.

[C4.17] Jubaer Ahmed and Zainal Salam, “A Maximum Power Point Tracking (MPPT) for PV system using Cuckoo Search with partial shading capability,” *Applied Energy*, 119, (2014), 118–130.

[C4.18] Hadi M. El-Helw, Ahmed Magdy, And Mostafa I. Marei, “A Hybrid Maximum Power Point Tracking Technique for Partially Shaded Photovoltaic Arrays,” *IEEE Access, VOL. 5, 2017.*

[C4.19] Immad Shams, Saad Mekhilef and Kok Soon Tey, “Maximum Power Point Tracking Using Modified Butterfly Optimization Algorithm for Partial Shading, Uniform Shading, and Fast Varying Load Conditions,” *IEEE Trans. Power Electron.*, Vol. 36, No. 5, May 2021.

[C4.20] Chih Yu Liao, Ramadhani Kurniawan Subroto, Ibrahim Saiful Millah, Kuo Lung Lian And Wei-Tzer Huang, "An Improved Bat Algorithm for More Efficient and Faster Maximum Power Point Tracking for a Photovoltaic System Under Partial Shading Conditions," *IEEE Access*, Jun. 2020.

[C4.21] Shungang Xu, Yuan Gao, Guohua Zhou and Guihua Mao, "A Global Maximum Power Point Tracking Algorithm for Photovoltaic Systems Under Partially Shaded Conditions Using Modified Maximum Power Trapezium Method," *IEEE Trans. on Ind. Electron.*, Vol. 68, No. 1, Jan. 2021.

[C4.22] Chao Huang, Long Wang, Zijun Zhang, Ryan Shun-cheung Yeung, Alain Bensoussan and Henry Shu-hung Chung, "A Novel Spline Model Guided Maximum Power Point Tracking Method for Photovoltaic Systems," *IEEE Trans. Sustain. Energy*, vol. 11, no. 3, Jul. 2020.

[C4.23] J. Prasanth Ram, Dhanup S. Pillai, N. Rajasekar and Scott M. Strachan, "Detection and Identification of Global Maximum Power Point Operation in Solar PV Applications Using a Hybrid ELPSO-P&O Tracking Technique," *IEEE J. of Emer. and Selected Topics in Power Electron.*, VOL. 8, NO. 2, Jun. 2020.

[C4.24] Boni Satya Varun Sai, Sarang A. Khadtare and Debashis Chatterjee, "A dummy peak elimination based MPPT technique for PV generation under partial shading condition," *IET Renewable Power Generation*. 2021;1–14.

[C4.25] Immad Shams, Saad Mekhilef and Kok Soon Tey, "Improved-Team-Game-Optimization-Algorithm-Based Solar MPPT With Fast Convergence Speed and Fast Response to Load Variations," *IEEE Trans. on Ind. Electron.*, Vol. 68, No. 8, Aug. 2021.

MPPT SCHEME FOR WIND DRIVEN DFIG SYSTEM

5.1 INTRODUCTION

Wind power is most promising because of its abundant accessibility and pollution less nature compared to the other available renewable sources. The usage of wind energy for the residential purpose, leads to energy independence [5.1-5.2].

DFIG has the advantages of variable speed and constant frequency operation, low mechanical tension, maximum power capturing ability, decoupled active or reactive power governance, etc. [5.3-5.4]. These advantages in DFIG are due to the control schemes used in the back-to-back converters [5.5].

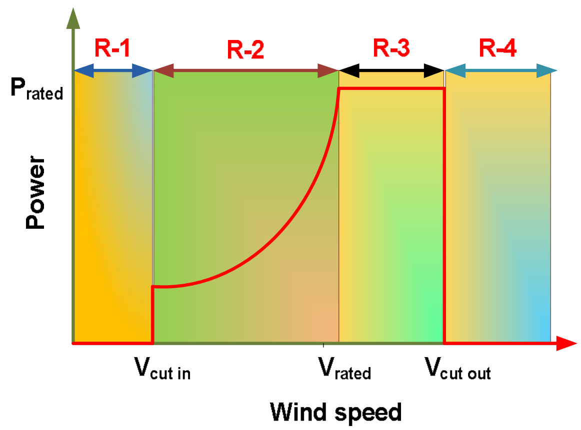

Fig. 5.1. Different operating areas for wind turbine

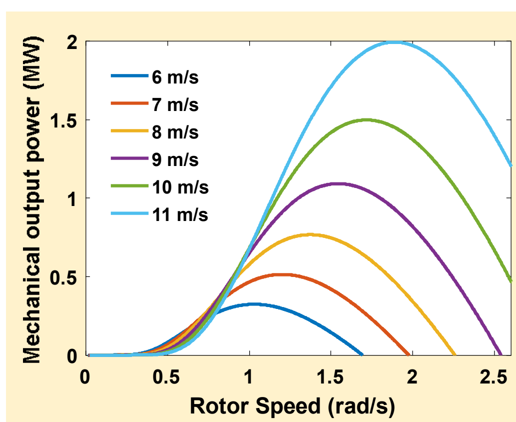

Fig. 5.2. Power-speed characteristics at various wind speeds

The working range for variable speed WECS is primarily divided into four regions, Region-1 (R-1), R-2, R-3, and R-4, as represented in Fig. 5.1. In R-1 and R-4, DFIG is not in the operating state, owing to safety measurements. In R-2, DFIG operates in MPP tracking zone, where the system is operated under below rated speeds. In R-3, DFIG operates in pitch controlling region, where the pitch controller is employed to reduce the stress over the wind turbines for above rated speeds [5.6]. As shown in Fig. 5.2, DFIG displays non-linear mechanical power and rotor speed characteristics. So, in DFIG, MPPT methods are employed for the efficient operation of the system [5.7].

Many optimization-based schemes are used for tracking MPP in WECS [5.8-5.19]. Even though optimization-based schemes display better-operating characteristics, the settling time is longer. PSO and cuckoo search (CS) algorithms are the most commonly used approaches for MPPT in wind and PV generation [5.20-5.23]. Even though CS shows -operating properties than PSO, the latter is simpler while coming to real-time implementation [5.24-5.25].

In this research work, an SSM-PSO scheme has been proposed as a modified version of the PSO scheme. The anemometer is used for tracking MPP in proposed scheme like [5.28-5.32]. The speed sensor is employed to minimize the searching space area, leading to improved dynamic characteristics and better accuracy. The proposed SSM-PSO scheme has been implemented for a 2MW DFIG-wind system in MATLAB-Simulink atmosphere. The proposed scheme is able to address the drawbacks of existing schemes and the major outcomes of SSM-PSO method are,

- Provides lower settling time compared to existing SS-P&O scheme.
- Results in lower steady state oscillations compared to existing LS-P&O scheme.
- Under sudden change in wind speeds, proposed SSM-PSO displays lower oscillations in output characteristics compared to LS and SS P&O schemes.
- The proposed scheme is flexible and can be easily implemented with existing drive-compatible hardware.

5.2 SYSTEM CONFIGURATION

The wind-turbine-based DFIG system transforms wind power into electrical power. Fig. 5.3, displays the block diagram for a 2 MW DFIG system, where the energy is transferred over a direct connection and back-to-back converter topology to the grid. The grid side converter (GSC) controlling has a major purpose of maintaining a constant DC-link voltage in the proposed topology, irrespective of the direction and quantity of the rotor power. The independent controlling of reactive power and rotor speed is the major objective of the rotor side controller. As the proposed work is more related to MPPT, only Rotor side converter (RSC) controller design is considered in the present research work, as displayed in Fig. 5.4. In the proposed scheme, the estimation of the rotor position and speed is done by employing the model reference adaptive system (MRAS) control technique [5.27].

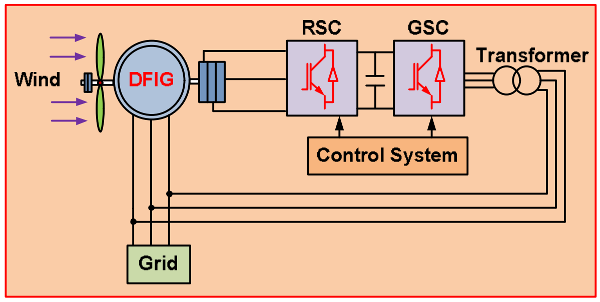

Fig. 5.3 Schematic circuit for DFIG system

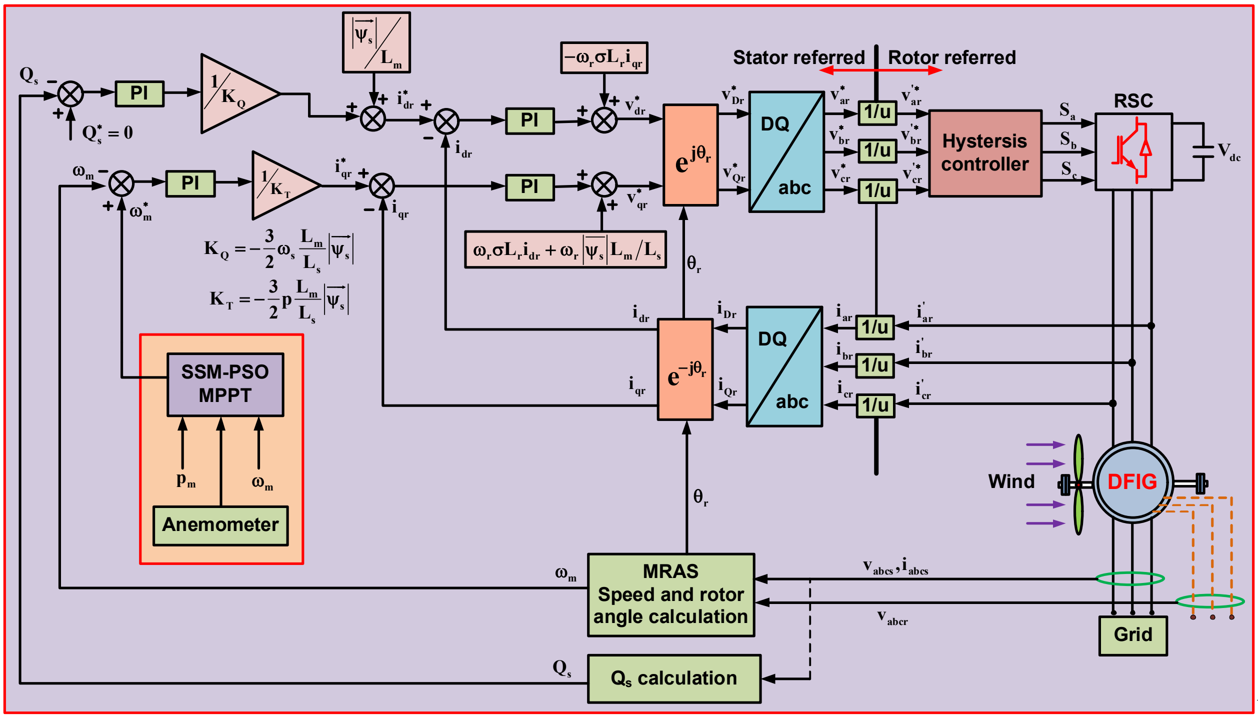

Fig. 5.4. The control scheme for the proposed system

5.2.1 Wind turbine modelling

The mechanical power developed in the wind turbine is represented as (5.1), where β is pitch angle, ρ is air density (kg/m^3), C_p is power coefficient of a wind turbine, A is the swept area (m^2), V_w is wind velocity $(m/\sec)$, and λ is tip speed ratio. The C_p is calculated using (5.2), where C_1 to C_7 values are as represented in Table-5.1. From (5.2), λ_i is calculated in terms of β and λ as (5.3). For a known value of wind speed, λ is calculated as a function of rotor speed (ω_m) as shown in (5.4). At the optimum power case, (5.4) can be formulated as (5.5).

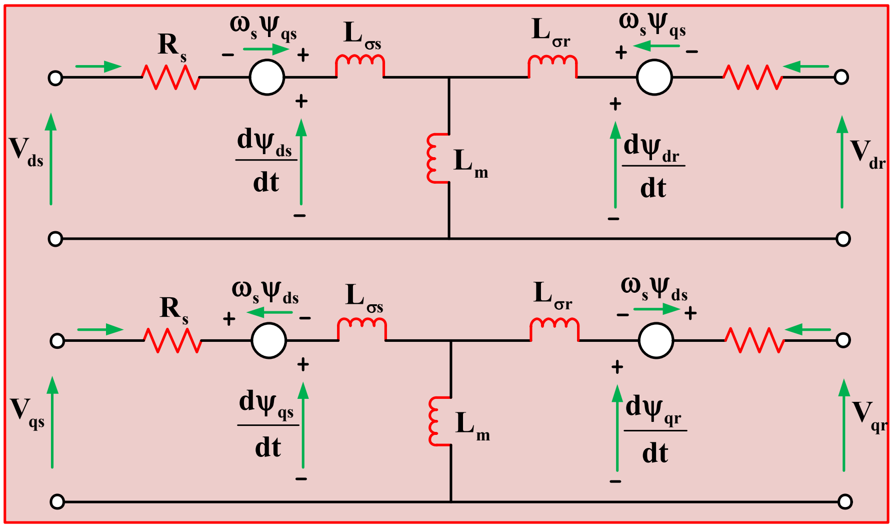

Fig. 5.5. DFIG modelling in dq-reference frame

$$P_m = \frac{1}{2}\rho A C_p(\beta,\lambda) V_w^3 \tag{5.1}$$

$$C_p = C_1\left(\frac{C_2}{\lambda_i} - C_3\beta - C_4\beta^{C_5} - C_6\right)\left(e^{C_7/\lambda_i}\right) \tag{5.2}$$

$$\lambda_i = \frac{1}{\lambda + 0.02\beta} - \frac{0.003}{1+\beta^3} \tag{5.3}$$

$$\lambda = \frac{\omega_m R}{V_w} \tag{5.4}$$

$$\lambda_{opt} = \frac{\omega_{opt} R}{V_w} \tag{5.5}$$

5.2.2 DFIG Modelling

In Fig.5.5, DFIG modelling using a dq-reference frame is represented. The equations for stator and rotor voltages in dq components are represented in (5.6)-(5.9), where V_{ds}, V_{qs}, V_{dr} and V_{qr} are dq components of stator voltages and rotor voltages, ψ_{ds}, ψ_{qs}, ψ_{dr} and ψ_{qr} are dq components of stator flux and rotor flux, i_r is rotor current, ω_r is rotor speed, ω_s is synchronous speed, i_{ds}, i_{qs}, i_{dr} and i_{qr} are dq components of stator and rotor currents, ψ_s is stator flux and ψ_r is rotor flux.

$$v_{ds} = R_s i_{ds} + \frac{d\psi_{ds}}{dt} - \omega_s \psi_{ds} \tag{5.6}$$

$$v_{qs} = R_s i_{qs} + \frac{d\psi_{qs}}{dt} - \omega_s \psi_{qs} \tag{5.7}$$

$$v_{dr} = R_r i_{dr} + \frac{d\psi_{dr}}{dt} - \omega_r \psi_{dr} \tag{5.8}$$

$$v_{qr} = R_r i_{qr} + \frac{d\psi_{qr}}{dt} - \omega_r \psi_{qr} \tag{5.9}$$

In the same manner, the flux developed in DFIG system are represented using (5.10)-(5.13).

$$\psi_{ds} = L_s i_{ds} + L_m i_{dr} \tag{5.10}$$

$$\psi_{qs} = L_s i_{qs} + L_m i_{qr} \tag{5.11}$$
$$\psi_{dr} = L_m i_{ds} + L_r i_{dr} \tag{5.12}$$
$$\psi_{qr} = L_m i_{qs} + L_r i_{qr} \tag{5.13}$$

Where the electromagnetic torque T_{em} is represented as,

$$T_{em} = \frac{3}{2} p \frac{L_m}{L_s} \left(\psi_{qs} i_{dr} - \psi_{ds} i_{qr} \right) \tag{5.14}$$

5.3 CONTROL STRATEGIES IN THE DFIG SYSTEM

Since the proposed scheme focuses mainly on maximum power point tracking, RSC controlling is mainly discussed in this research work compared to GSC controlling. While, in the proposed scheme, the DC-link voltage is voltage is maintained constant by employing the scheme same as [5.11] at GSC.

5.3.1 Rotor current control loops

Out of available controlling schemes in DFIG, the proposed system has been operated with the vector control. The control structure has been explained in steps for better understanding, where the first step is about examining the current loops. As shown in Fig. 5.6, vector control is performed in a synchronous revolving dq frame, where the stator flux is aligned with the dq frame [5.1]. Due to this, it can be represented that the rotor current and torque or active stator power are proportional to the reactive power and quadrature rotor current, respectively.

$$v_{dr} = R_r i_{dr} + \sigma L_r \frac{di_{dr}}{dt} - \omega_r \sigma L_r i_{qr} + \frac{L_m}{L_s} \frac{d\left|\overrightarrow{\psi_s}\right|}{dt} \tag{5.15}$$
$$v_{qr} = R_r i_{qr} + \sigma L_r \frac{di_{qr}}{dt} + \omega_r \sigma L_r i_{dr} + \omega_r \frac{d\left|\overrightarrow{\psi_s}\right|}{dt} \tag{5.16}$$

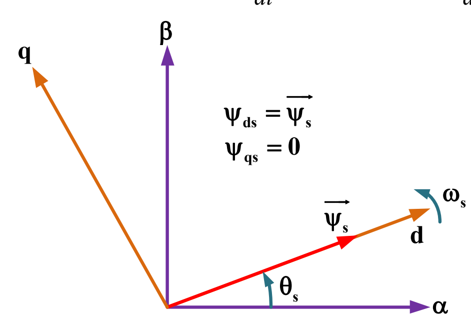

Fig. 5.6 The stator flux space vector alignment with synchronous rotating dq frame

By substituting (5.10)-(5.13) in (5.6)-(5.9), rotor voltage can be represented in terms of stator flux (note that $\psi_{qs} = 0$) and rotor currents (5.15)-(5.16). In (5.15) and (5.16), leakage factor, $\sigma = 1 - L_m / L_s \, L_r$. Since, the grid and stator are directly connected, stator flux is considered to be constant $\left\{ \left(d\left|\overrightarrow{\psi_s}\right| / dt \right) = 0 \right\}$ in (5.15) and (5.16). From (5.15) and (5.16), it can be noted that d-q rotor currents can be controlled by simply employing the PI controller for individual current components, as shown in Fig. 5.4. If DFIG displays a different stator to rotor turns ratio, it should be employed in the control scheme. The current reference values in Fig. 5.4, are generated with speed and power control loops. In Fig. 5.4, stator side referred rotor currents are employed in current loops working, while the rotor-referred quantities conversion is executed at the currents and before the creation of the pulses for the converter for the voltages. The corresponding closed-loop transfer function displays a second-order system with one zero, where the appropriate gain values for the PI controller can be designed using classic control theory [5.1].

5.3.2 Speed and power control loops

Since the stator flux space vector is in phase with the d-axis in the reference frame, (5.14) can be modified as,

$$T_{em} = -\frac{3}{2} p \frac{L_m}{L_s} \left| \overrightarrow{\psi_s} \right| i_{qr} \approx K_T i_{qr} \tag{5.17}$$

From (5.17), it can be observed that, electromagnetic torque is proportional to the q-axis rotor current. Therefore, electro-magnetic torque can be controlled by employing rotor current. Also, it can be used in controlling the speed of the DFIG, if the application needs it. From (5.18), it can be noted that, the d-axis rotor current has its effect on stator reactive power.

Therefore, from the axis orientation employed, it can be observed that the dq components of rotor currents can be employed in controlling reactive power and torque autonomously. The same has been employed in the complete control scheme, as shown in Fig. 5.4. In Fig. 5.4, speed and power control loops are employed for the overall controlling scheme along with current controlling loops. Moreover, by using Q_s loop, the magnetization of the machine can be controlled. The magnitude of stator flux is considered to be constant, as the grid and stator are directly associated, and can be calculated by employing grid voltage. The stator flux equations can be represented as (5.19).

$$\left.\begin{aligned} Q_s &= \frac{3}{2}\left(v_{qs} i_{ds} - v_{ds} i_{qs}\right) \\ Q_s &= -\frac{3}{2}\omega_s \frac{L_m}{L_s}\left|\overrightarrow{\psi_s}\right|\left[i_{dr} - \frac{\left|\overrightarrow{\psi_s}\right|}{L_m}\right] \\ Q_s &= K_Q\left[i_{dr} - \frac{\left|\overrightarrow{\psi_s}\right|}{L_m}\right] \end{aligned}\right\} \tag{5.18}$$

$$\left|\overrightarrow{\psi_s}\right| = \psi_{ds} = L_s i_{ds} + L_m i_{dr},\ \psi_{qs} = 0 = L_s i_{qs} + L_m i_{qr} \tag{5.19}$$

For real-time applications, different Q_s values are required based on grid codes. Thus, the grid system operator can set the Q_s reference directly. From Fig. 5.4, it is assumed that internal current control loops execute faster than the external speed and power control loops to avoid the computation delay. The speed and power control loops can be modeled as first and second-order systems, where the tuning is done to fix the PI controller gain values. The proposed scheme generates the speed reference by the SSM-PSO technique for tracking maximum power. Fig. 5.4 represents the overall vector scheme with proposed SSM-PSO scheme, where the system results in constant torque at varying speed. The stator voltage can be assumed constant because of the direct linkage between stator and grid. As T_{em} and Q_s are constants, the stator currents are also maintained at constant values.

5.4 THE DFIG SYSTEM THE PROPOSED SSM-PSO BASED MPPT FOR DFIG

The P&O method is widely employed to track MPP for WECS [5.7]. Fig. 5.7, represents the flowchart for existing P&O, where the sensed mechanical power (P_m) and rotor speed (ω) are used for tracking maximum power [5.9]. The P&O scheme operates in two types of steps they are, large steps (LS) and small steps (SS). The larger step change in rotor speed $(\Delta\omega)$ value in the P&O scheme results in the faster system response, but it results in the large fluctuations over the steady-state operation. Moreover, due to its weather-insensitive nature, the P&O scheme displays higher fluctuations in the output characteristics under an abrupt variation in wind speed. P&O scheme with a smaller $\Delta\omega$ value results in the slower response, but it results in lower fluctuations over the steady-state operation. Moreover, the smaller step value results in the lower efficiency during maximum power point (MPP) tracking.

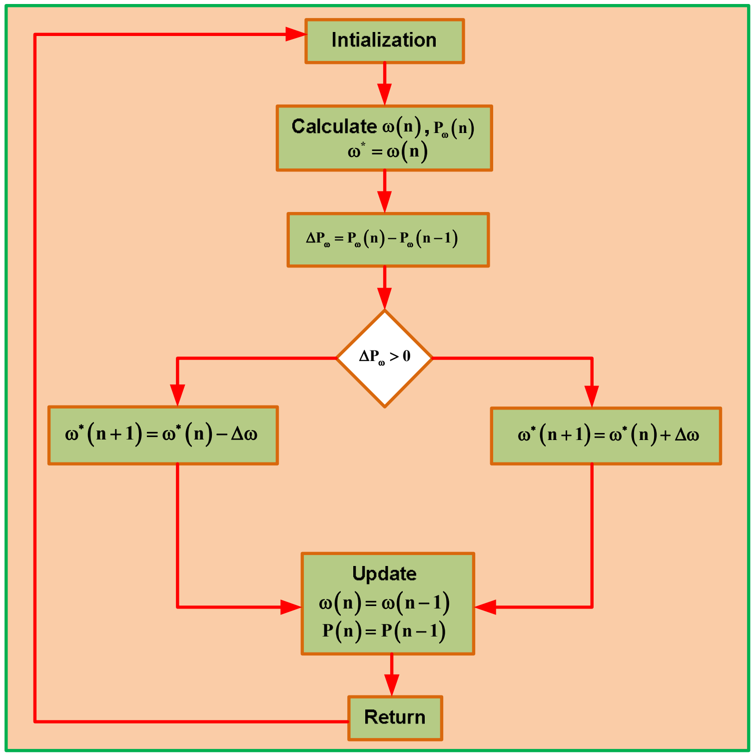

Fig. 5.7. Perturb and observe MPPT scheme

PSO is most famously utilized advancement framework for discovering global maximum under non-linear operation. PSO has been modelled based on bird flock's behavior, it is a speculative and population-based evolutionary algorithm (EA) search technique. A Swarm of individuals is maintained by the PSO algorithm in which each particle signifies a candidate solution. Particles track a basic conduct in which they mime the accomplishment of neighboring particles and their own accomplished victories. Therefore, best particle (P_{best}) in neighborhood affects the particle's position, along with the best solution (G_{best}) discovered by the particle itself. Particle location, x_i, is updated by employing [5.24],

$$x_i^{k+1} = x_i^k + v_i^{k+1} \tag{5.20}$$

Where step size is represented by velocity component, v_i. The velocity is formulated by,

$$v_i^{k+1} = \omega v_i^k + c_1 r_1 \left\{P_{besti} - x_i^k\right\} + c_2 r_2 \left\{G_{best} - x_i^k\right\} \tag{5.21}$$

Where random numbers $r_1, r_2 \in u(0,1)$, c_1 and c_2 are coefficient of acceleration and ω is inertia weight. The personal best position of particle i is P_{besti} and the best position of the particles is G_{best}. In Fig. 5.8, the particles in optimization practice with distinctive movement are represented. If the original rotor speed defines the position, then rotor speed perturbation is displayed by the velocity. Therefore, (5.20) is further formulated as,

$$\omega_i^{k+1} = \omega_i^k + v_i^{k+1} \tag{5.22}$$

From Fig. 5.7 and (5.22), it can be observed that, the overall operating structure in the P&O scheme and PSO scheme are similar. But, in PSO perturbation in present, the rotor speed is based on the P_{besti} and G_{best}. If the rotor speed is nowhere near the other two rotor speeds, then the subsequent variation in rotor speed is higher and vice-versa. In P&O, perturbation in rotor speed is constant, while in PSO, the perturbation varies with position of the particles.

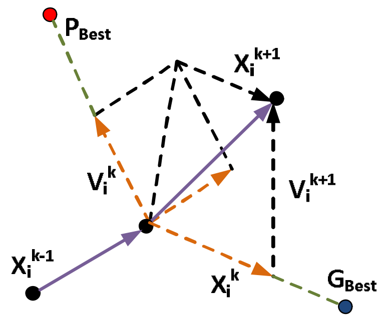

Fig. 5.8. Particle movement in particle swarm optimization

5.4.1 SSM-PSO formulation in DFIG MPPT

Before describing PSO implementation in MPP tracking, a solution vector of rotor speeds with Np particles has been considered as,

$$\begin{aligned} x_i^k &= \omega_g = \left[\omega_1, \omega_2, \omega_3, ..., \omega_j\right] \\ j &= 1,2,3,4, ...N_P \end{aligned} \tag{5.23}$$

The objective function is formed with the idea of comparing the power of updated power with the former one as a function of rotor speed. So, the objective function can be defined as,

$$P\left(\omega_i^k\right) - P\left(\omega_i^{k-1}\right) = f_k \tag{5.24}$$

The function f_k can be calculated subjected to $P\left(\omega_i^k\right) > P\left(\omega_i^{k-1}\right)$, where $P(\omega_i)$ can be obtained using (5.1)-(5.4).

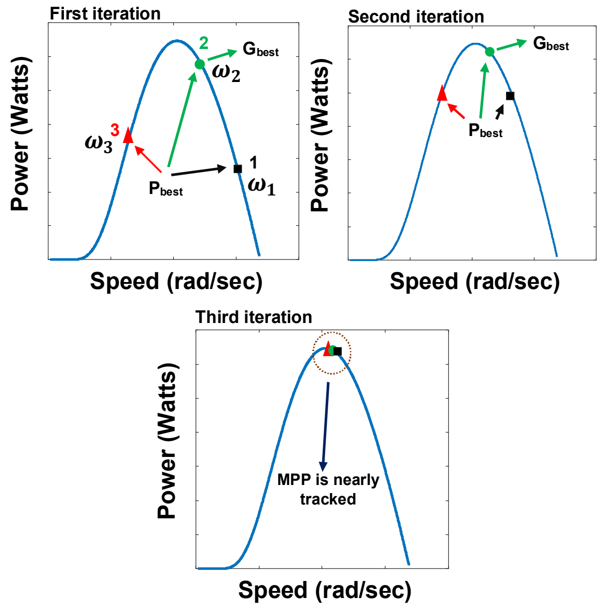

Fig. 5.9. Particle movement for MPPT process in PSO scheme

To initialize the optimization procedure, assume that the flowchart communicates three-rotor reference speeds, as shown in Fig. 5.4. In Fig. 5.9, three different rotor speeds ω_1, ω_2 and ω_3 are represented using square, circular and triangular notations, respectively. These rotor speeds are used as P_{besti} in the first iteration. Of these three particles, particle 2 is said to be G_{best}, as it can be noted that, particle 2 is nearer to the maximum power. In the second iteration, the resultant velocity is only because of the G_{best} parameter. Since, the $(P_{besti} - \omega(2))$ is zero in (5.21), the velocity of G_{best} particle $(\omega(2))$ becomes zero. So, it can be observed that, the velocity of particles becomes zero and there is no use of this particle in further exploration of MPP.

To avoid this, perturbations in particles are allowed, as shown in the second iteration of Fig. 5.9. Since the previous rotor speeds in the system operate at better fitness values, the particles are driven towards G_{best} with low velocity [5.26]. In the third iteration of Fig. 5.9, it can be noted that all three particles arrive at an MPP. Due to the very low velocity, all three particles are arriving a constant value, avoiding the oscillation over steady-state, unlike P&O.

5.4.2 Proposed SSM-PSO for searching space optimization

$$\omega_{opt} = \frac{\lambda_{opt} V_w}{R} \tag{5.25}$$

In the proposed SSM-PSO, the actual improvement is made to reduce the searching space. Fig. 5.11, represents the proposed SSM-PSO mechanism for MPP tracking in DFIG. Using the anemometer, the optimum rotor speed value can be obtained using (5.25). The searching space can be minimized by employing a constant, as represented in Fig. 5.10. The particles at different positions are initialized using (5.26), where $\omega_{\max}$ and $\omega_{\min}$ are calculated using (5.27) and (5.28) in the proposed system.

$$x_i = \omega_{\min} + \frac{(i-1)[\omega_{\max} - \omega_{\min}]}{N_p - 1} \tag{5.26}$$

$$i = 1, 2, 3, 4, ..., N_p$$

$$\omega_{\max} = \omega_{opt} + \in \tag{5.27}$$

$$\omega_{\min} = \omega_{opt} - \in \tag{5.28}$$

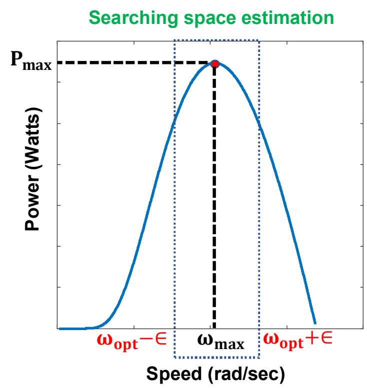

Fig. 5.10. Searching space mechanism in the proposed system

By employing the searching space estimation mechanism, the particle's placement area over $P{-}\omega$ is minimized. The derived reference rotor speed from SSM-PSO has been compared with the actual rotor speed, as shown in Fig. 5.4, for tracking maximum power. The SSM-PSO results in better tracking efficiency and near-zero steady oscillations.

Moreover, the proposed SSM-PSO scheme displays better dynamic characteristics compared to the P&O scheme with a low step and large step operations. The searching space minimization mechanism used in proposed scheme is independent of generator type. It depends mainly on the wind speed, sensed by anemometer. So, SSM-PSO scheme can be implemented for the generators other than DFIG.

5.5 SIMULATION RESULTS AND DISCUSSIONS

The proposed SSM-PSO scheme has been simulated for a DFIG-Wind Turbine system in a MATLAB-simulink environment. The DFIG-wind system is implemented in MATLAB with design parameters as given in Table-5.1. The proposed scheme has been tested for step and random variations of wind speeds. Moreover, the existing LS-P&O and SS-P&O [5.7] schemes are compared with the proposed scheme for the same changes in the wind speed to prove the proposed scheme's usefulness.

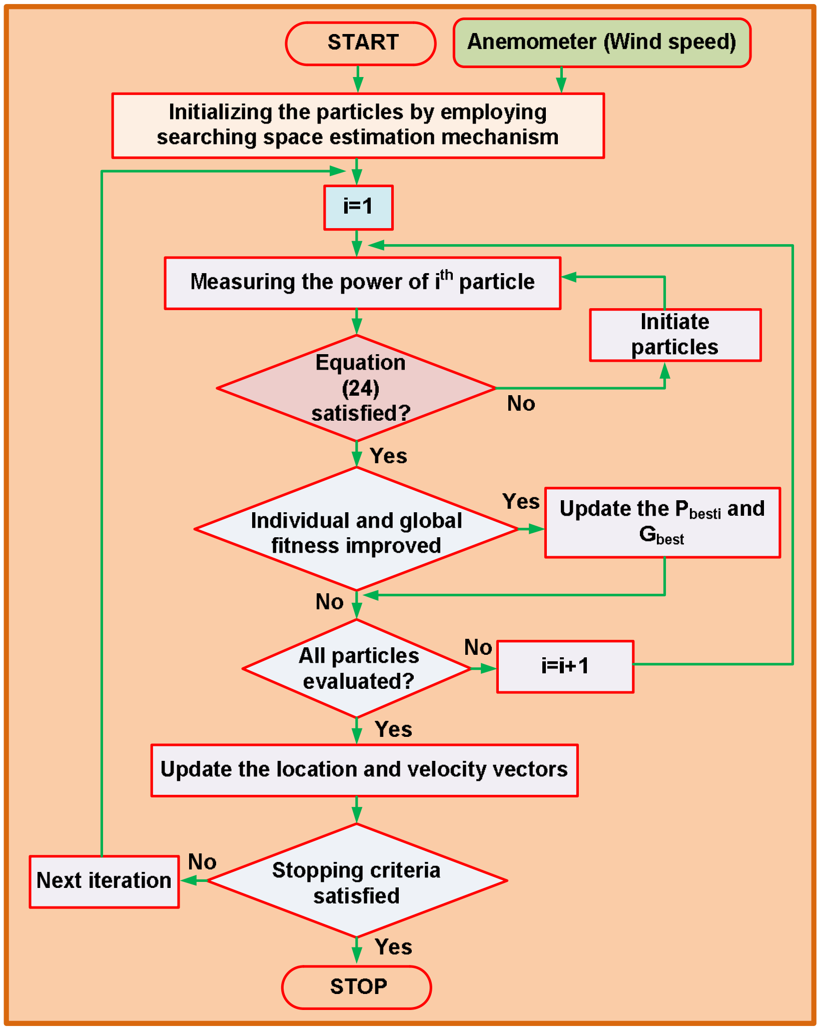

Fig.5.11. Proposed SSM-PSO algorithm

5.5.1 Single step variations in wind speed

The proposed SSM-PSO, SS-P&O and LS-P&O are operated for a step-up variation in wind speed from 6 m/s to 8 m/s, as represented in Fig. 5.12a. The rotor side characteristics such as tip speed ratio, power coefficient, rotor speed and mechanical power are represented as shown in Fig. 5.13a, 5.13b, 5.13c and 5.13d, respectively.

Also, the proposed SSM-PSO, SS-P&O, and LS-P&O are operated for a step-down variation in wind speed from 8 m/s to 6 m/s, as represented in Fig. 5.12b. The rotor side characteristics with step-down variation are represented as shown in Fig. 5.14a, 5.14b, 5.14c, and 5.14d, respectively.

Overall, from Fig. 5.13 and 5.14, it can be observed that, the LS-P&O scheme settles faster compared to SS-P&O and SSM-PSO schemes. But it is noted that, LS-P&O exhibits higher oscillations over a steady-state, leads to the inefficiency of the system. Coming to LS-P&O, from Fig. 5.13 and 5.14, it is noted that, LS-P&O leads to lower steady-state oscillations. On the other hand, the LS-P&O has a major disadvantage of higher settling time or slower response. The proposed SSM-PSO scheme displays both the advantages of faster response and lower steady-state error.

Table 5.1. System parameters

Wind turbine	
Number of blades	3
Gear Ratio (N)	100
Blade radius (R)	42 m
Air density (ρ)	1.225 kg/m^3
Optimal Tip speed ration (λ_{opt})	7.2
Maximum power coefficient (C_{p_max})	0.44
Unknown coefficients (C_1-C_7)	C_1=0.73, C_2=151, C_3=0.58, C_4=0.002 C_5=2.14, C_6=13.2, C_7=-18.4
DFIG parameters	
Peak power	2 MW
Pole pair (p)	2
Rated torque	12.7 K-Nm
Stator connection	Star
Stator resistance (R_s)	2.6 $m\Omega$
Stator leakage inductance $(L_{\sigma s})$	87 μH
Magnetizing inductance (L_m)	2.5 mH
Turns ratio (u)	0.34
Rotor resistance (R_r)	26.1 $m\Omega$
Rotor leakage inductance $(L_{\sigma r})$	783 μH
Rated stator voltage (V_s)	690 V_{rms}
Rated stator current (i_s)	1760 A_{rms}
Rated rotor voltage (V_r)	2070 V_{rms}
Stator inductance (L_s)	2.587 mH
Rotor inductance (L_r)	2.587 mH

From Fig. 5.13 and 5.14, it can be observed that, the settling time of LS-P&O is around 80 ms, for SS-P&O, settling time is around 1300 ms and finally, for proposed SSM-PSO, it is around 350ms. From Fig 5.13a and 5.14a, it can be observed that, the proposed SSM-PSO method preserves the C_{p_max} successfully related to LS-P&O and SS-P&O schemes. From 5.13c and 5.14c, it is noted that the proposed SSM-PSO method tracks the mechanical power efficiently related to LS-P&O and SS-P&O schemes. The comparison of tracked maximum power with actual maximum power at wind speeds of 6 m/s and 8 m/s are represented in Fig. 5.20. From, Fig.

5.13d and 5.14d, it is noted that, the peak to peak oscillation in LS-P&O is higher compared to SS-P&O and SSM-PSO schemes.

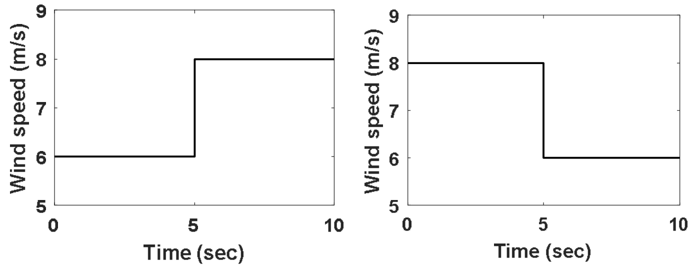

a b

Fig. 5.12 Single Step changes in wind-speed (a) Step-up (b) Step-down

5.5.2 Two-step variations in wind speed

The proposed SSM-PSO SS-P&O and LS-P&O are operated for a two-step-up variation in wind velocity from 7 m/s to 9 m/s to 11 m/s as shown in Fig. 5.15a. The rotor side characteristics with two step-up variations in wind velocity are represented as shown in Fig. 5.16a, 5.16b, 5.16c and 5.16d, respectively.

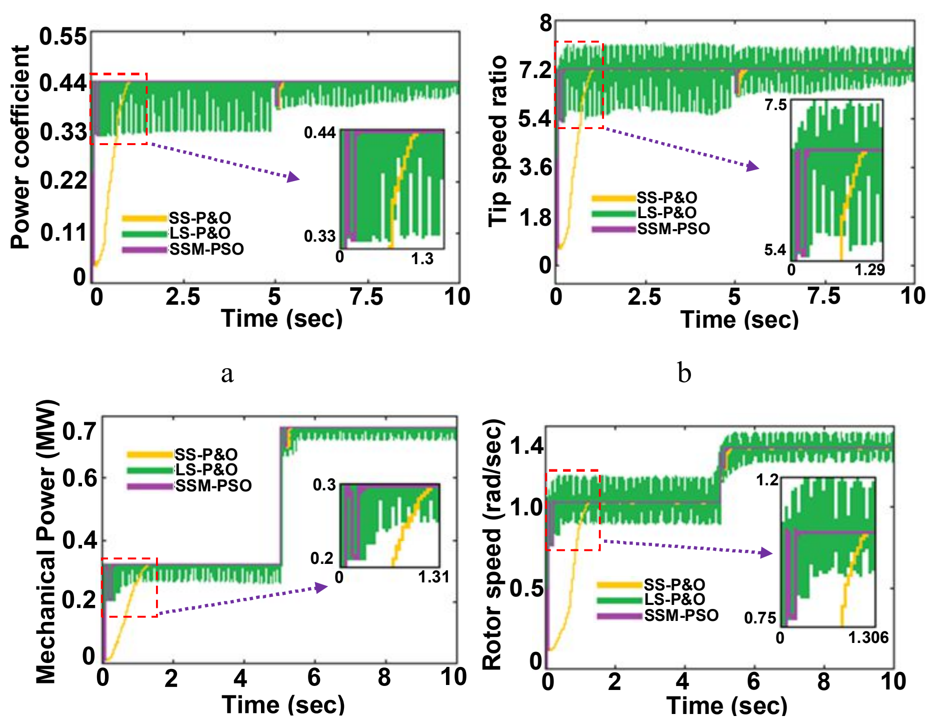

Fig. 5.13. Rotor side characteristics for single step-up variation in wind speed (a) Power coefficient (b) Tip speed ratio (c) Mechanical power (d) Rotor speed

As displayed in Fig. 5.15b, the proposed SSM-PSO, SS-P&O and LS-P&O are operated for a two-step-down variation in wind speed from 11 m/s to 9 m/s to 7 m/s. The rotor side characteristics with two-step-down variation are represented as shown in Fig. 5.17a, 5.17b, 5.17c and 5.17d, respectively.

From Fig. 5.16 and 5.17, it can be observed that the proposed SSM-PSO scheme displays better dynamic characteristics compared to LS-P&O and SS-P&O schemes under multiple wind speed step variations.

Even in the sudden speed variations, the proposed scheme does not divert its tracking path and tracks the maximum power efficiency. The tracked power is related with the actual power in Fig. 5.20. From this, it is observed that the proposed SSM-PSO displays average efficiency of 92.01%.

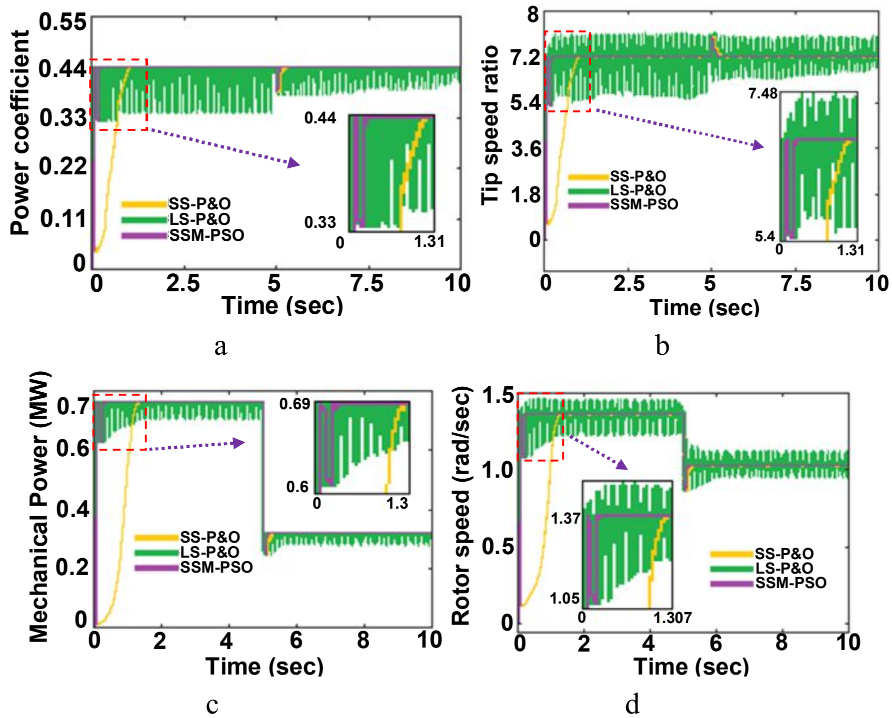

Fig. 5.14. Rotor side characteristics for single step-down variation in wind speed (a) Power coefficient (b) Tip speed ratio (c) Mechanical power (d) Rotor speed

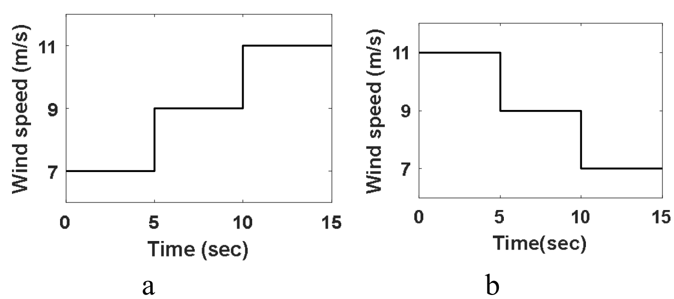

Fig. 5.15. Two Step changes in wind-speed (a) Step-up (b) Step-down

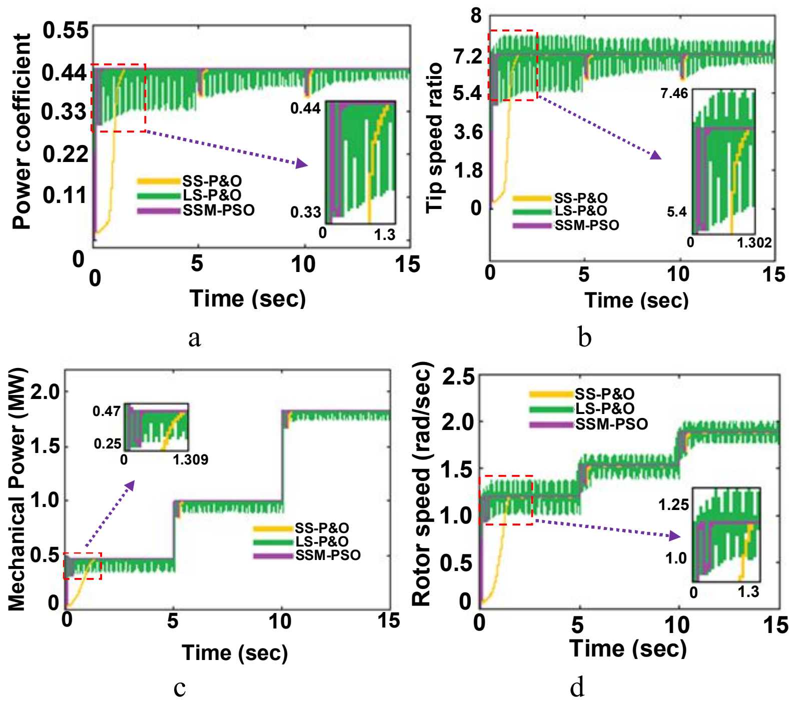

Fig. 5.16. Rotor side characteristics for two step-up variation in wind speed (a) Power coefficient (b) Tip speed ratio (c) Mechanical power (d) Rotor speed

5.5.3 Random variation in wind speed

The proposed SSM-PSO scheme has been operated for random wind speed variation, as shown in Fig. 5.18. The respective rotor side characteristics are represented in Fig. 5.19a, 5.19b, 5.19c & 5.19d, respectively. From Fig. 5.19, it is noted that the proposed SSM-PSO tracks maximum power more efficiently compared to LS-P&O and SS-P&O. Moreover, due to its weather-sensitive nature, the SSM-PSO displays no drift under variation of wind speed along with near-zero steady-state oscillation.

5.5.4 Overall comparison between SSM-P&O and existing MPPT schemes

Table. 5.2. Comparison of SSM-PSO with existing MPPT schemes

Algorithms	Settling time	Oscillations	Efficiency
LS-P&O [5.7]	77 ms	1.2	--
SS-P&O [5.7]	>1300 ms	0.05	87.11%
MP&O [5.7]	930 ms	0.3	88.23%
RA-P&O [5.7]	<600 ms	0.001	91.39%
Proposed SSM-PSO	<350 ms	0.001	92.01%

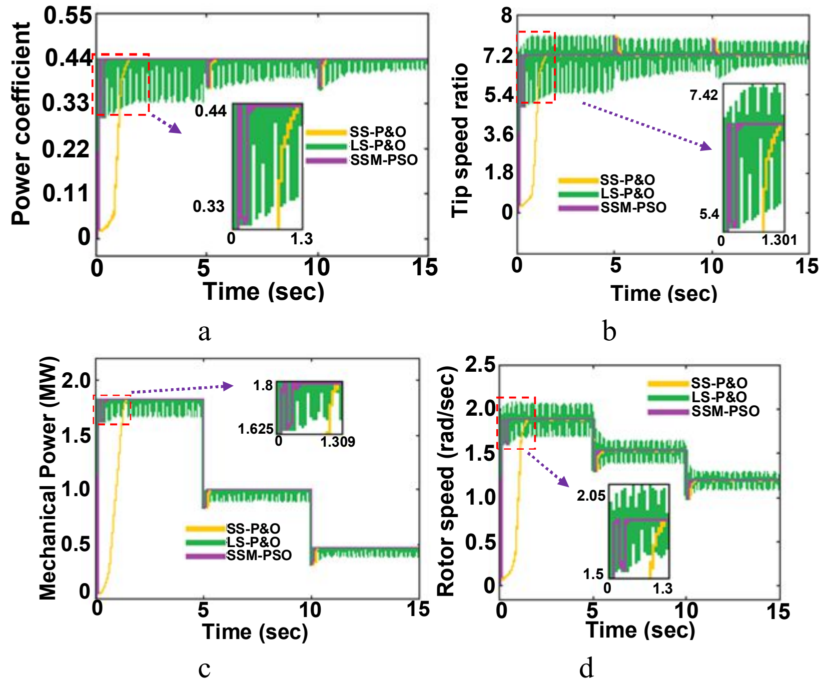

Fig. 5.17. Rotor side characteristics for two step-down variation in wind speed (a) Power coefficient (b) Tip speed ratio (c) Mechanical power (d) Rotor speed

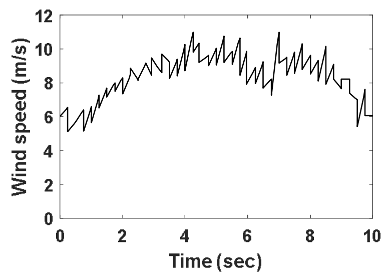

Fig. 5.18. Random changes in wind-speed

To justify the advantage of the proposed SSM-P&O technique, it is related to the traditional P&O scheme. SS-P&O scheme results in the larger settling time (>1300 ms) and lower oscillations (0.05 rad/s). LS-P&O scheme results in larger oscillations (1.2 rad/s) and faster response (< 77 ms), can affect the larger inertia machines. By employing modified P&O (MP&O) scheme [5.7], the settling time and oscillations can be controlled.

Even though in MP&O, settling time can be reduced to 930 ms, it displays a larger oscillation of 0.3 rad/s. The recently introduced robust adaptive step-sizes P&O (RA-P&O) MPPT scheme in [5.7], displays the reduction in both settling time and oscillations to 600 ms and 0.001 rad/s, respectively. Moreover, the RA-P&O scheme displays an improvement in the tracking efficiency of 91.39%.

The proposed SSM-PSO scheme displays much lower settling time (<350 ms) compared to RA-P&O scheme. Also, the proposed SSM-PSO scheme results in the lesser oscillations of 0.001

rad/s. Moreover, the proposed SSM-PSO scheme displays an improved efficiency of 92.01%. Table-5.2 represents the comparison of the proposed SSM-PSO scheme with existing MPPT schemes, which also reflects the superiority of the SSM-PSO over other existing schemes.

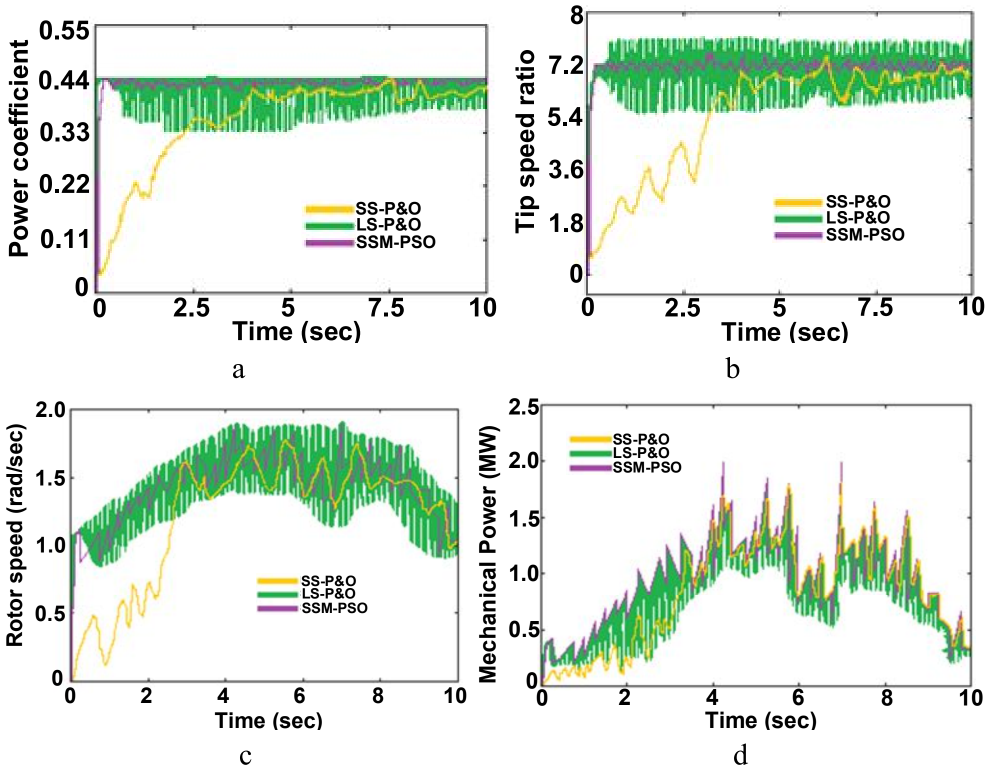

Fig. 5.19. Rotor side characteristics for random variation in wind speed (a) Power coefficient (b) Tip speed ratio (c) Rotor speed (d) Mechanical power

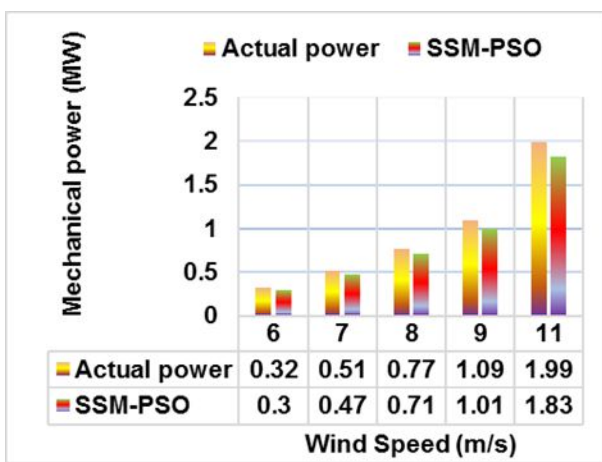

Fig. 5. 20. Efficiency of proposed SSM-PSO at different wind speeds

5.6 CONCLUSION

DFIG has the significant advantage of flexible operation at wide speed ranges. But, the non-linear $P-\omega$ characteristics result in the difficulty of tracking maximum power point. Already few conventional and optimization-based schemes are available in research platforms for tracking MPP. The optimization-based schemes avoid the oscillation behaviour over a steady state; same time, they result in more settling time. Compared with optimization-based schemes, conventional schemes are simpler and easily implementable in real-time situations. P&O method is the most generally employed conventional topology for tracking MPP. P&O method is normally operated with small and large step changes.

The P&O with smaller step-change results in the low oscillation of 0.05 rad/s over steady-state but results in the low tracking efficiency. Further, the P&O with large step changes results in lesser tracking of 77ms, but leads to higher oscillations. Since, the P&O is weather insensitive; it leads to fluctuation in output characteristics under a sudden change in wind speeds. The optimization-based schemes can avoid the -insensitive nature, but they result in complexity in execution during real-time.

PSO is the most commonly used and simply executable among existing optimization-based schemes. But, PSO results in a higher settling time, leading to a slower response. In this research work SSM-PSO scheme has been introduced to avoid the disadvantages of PSO. In the proposed system, an anemometer has been employed to decide the space for placing particles in tracking MPP. The SSM-PSO scheme is successful in minimizing the searching space, leading to lesser MPP tracking time (<350ms). Also, the proposed SSM-PSO leads to the lesser oscillation of 0.001 rad/s. Moreover, the proposed SSM-PSO scheme is easily implementable due to its simple searching mechanism. The proposed SSM-PSO scheme has been implemented for 2MW DFIG system in MATLAB Simulink atmosphere, which displayed satisfactory results. The proposed work can be implemented using a hardware prototype as a future work.

Related publication:

- **BSV Sai**, D. Chatterjee et al., “An SSM-PSO Based MPPT Scheme for Wind driven DFIG system,” **IEEE Access**, 2022.

References:

[5.1] Ku Ding, XinGao Bian, HaiHao Liu, and Tao Peng.: ‘A MATLAB-Simulink-Based PV Module Model and Its Application under Conditions of Non uniform Irradiance’, IEEE Trans. On ENERGY Conv. vol. 27, no. 4, Dec.2012.

[5.2] Haitham Abu-Rub, Mariusz Malinowski and Kamal Al-Haddad, “Power Electronics for Renewable Energy Systems, Transportation and Industrial Applications,” *IEEE Press and John Wiley & Sons Ltd,* 2014.

[5.3] Abdellatif Kasbi and Abderrafii Rahali, "Adaptive FOPI Controller Based on The Fuzzy Supervisory for Wind Power Conversion System Equipped by A Doubly Fed Induction Generator," Int Trans Electr Energ Syst. 2021, e12923.

[5.4] Gonzalo Abad, Jesu´s Lo´pez, Miguel A. Rodrı´guez, Luis Marroyo and Grzegorz Iwanski, "Doubly Fed Induction Machine Modeling and Control for Wind Energy Generation," *IEEE Press and John Wiley & Sons Ltd,* 2011.

[5.5] Nishad Mendis, Kashem M. Muttaqi, Saad Sayeef and Sarath Perera, "Standalone Operation of Wind Turbine-Based Variable Speed Generators with Maximum Power Extraction Capability," *IEEE Trans. Energy Convers.*, Vol. 27, No. 4, Dec.2012.

[5.6] Krishna S. Patel & Vijay H. Makwana, "Modified Control Technique of DFIG for Power Quality Improvement," *IETE Journal of Education*, 2021, 62:1,44-54.

[5.7] Fariba Fateh, Warren N. White and Don Gruenbacher, "A Maximum Power Tracking Technique for Grid-Connected DFIG-Based Wind Turbines," *IEEE J Emerg Select Top Power Electron*, VOL. 3, NO. 4, DEC. 2015.

[5.8] Mousa HHH, Youssef A-R, Mohamed EEM, "Study of robust adaptive step-sizes P&O MPPT algorithm for high-inertia WT with direct-driven multiphase PMSG," *Int Trans Electr Energ Syst*., 2019, 29: e12090.

[5.9] Ali Darvish Falehi, "An innovative optimal RPO-FOSMC based on multi-objective grasshopper optimization algorithm for DFIG-based wind turbine to augment MPPT and FRT capabilities," *Chaos, Solitons and Fractals* 130, 2020, 109407.

[5.10] Abdel-Raheem Youssef, Ahmed I.M. Ali, Mahmoud S.R. Saeed and Essam E.M. Mohamed, "Advanced multi-sector P&O maximum power point tracking technique for wind energy conversion system," *Electrical Power and Energy Systems*, 107, 2019, 89–97.

[5.11] Jie Wang and Didi Bo, "Adaptive fixed-time sensorless maximum power point tracking control scheme for DFIG wind energy conversion system," *Int J Electr Power Energy Syst.,* 135, 2022, 107424.

[5.12] Bo Yang, Xiaoshun Zhang, Tao Yu, Hongchun Shu and Zihao Fang, "Grouped grey wolf optimizer for maximum power point tracking of doubly-fed induction generator-based wind turbine," *Energy Conversion and Management,* 133, 2017, 427–443.

[5.13] Hamid Chojaa, Aziz Derouich, Seif Eddine Chehaidia, Othmane Zamzoum, Mohammed Taoussi and Hasnae Elouatouat, "Integral sliding mode control for DFIG based WECS with MPPT based on artificial neural network under a real wind profile," *Energy Reports*, 7, 2021, 4809–4824.

[5.14] K. Belmokhtar, M.L. Doumbia and K. Agbossou, “Novel fuzzy logic based sensorless maximum power point tracking strategy for wind turbine systems driven DFIG (doubly-fed induction generator),” *Energy*, 76, 2014, 679e693.

[5.15] Kunlun Han, Tianwei Huang and Linfei Yin, “Quantum parallel multi-layer Monte Carlo optimization algorithm for controller parameters optimization of doubly-fed induction generator-based wind turbines,” *Applied Soft Computing*, 112, 2021, 107813.

[5.16] Ahmed Fathy, Abdullah G. Alharbi, Sulaiman Alshammari and Hany M. Hasanien, “Archimedes optimization algorithm based maximum power point tracker for wind energy generation system,” *Ain Shams Engineering Journal*, 2021.

[5.17] Jeroen D.M. De Kooning, Arash E. Samani, Simon De Zutter, Jeroen De Maeyer and Lieven Vandevelde, “Techno-economic optimisation of small wind turbines using co-design on a parametrised model,” *Sustainable Energy Technologies and Assessments*, 45, 2021, 101165.

[5.18] Mohammad Mahdi Rezaei, “A nonlinear maximum power point tracking technique for DFIG-based wind energy conversion systems,” *Engineering Science and Technology*, *an International Journal*, 21, 2018, 901–908.

[5.19] Ganesh P. Prajapat, N. Senroy and I.N. Kar, “Estimation based enhanced maximum energy extraction scheme for DFIG-wind turbine systems,” *Sustainable Energy, Grids and Networks*, 26, 2021, 100419.

[5.20] Yuliang Sun, Shaomin Yan, Bin Cai, YuqiangWu and Zhongcai Zhang, “MPPT Adaptive Controller of DC-based DFIG in Resistances Uncertainty,” *International Journal of Control, Automation and Systems*, 19(8), 2021, 2734-2746.

[5.21] James Kennedy and Russell Eberhart, “Particle Swarm Optimization,” *IEEE*, 1995.

[5.22] Salmi Hassan, Badri Abdelmajid, Zegrari Mourad, Sahel Aicha and Baghdad Abdennaceur, “PSO-Backstepping controller of a grid connected DFIG based wind turbine,” International Journal of Electrical and Computer Engineering (IJECE), Vol. 10, No. 1, Feb. 2020, pp. 856-867.

[5.23] Masafumi Miyatake, Mummadi Veerachary, Fuhito Toriumi, Nobuhiko Fujii and Hideyoshi Ko, “Maximum Power Point Tracking of Multiple Photovoltaic Arrays: A PSO Approach,” *IEEE Trans On Aerospace and Electronic Systems,* Vol. 47, No. 1, Jan. 2011.

[5.24] B. Srikanth Goud, P. Srinivasa Varma, B. Loveswara Rao, M. Sai Krishna Reddy, A. Pandian and Ch. Rami Reddy, “Cuckoo Search Optimization based MPPT for Integrated DFIG-Wind Energy System,” *IEEE International Conference on Decision Aid Sciences and Application (DASA)*, 2020.

[5.25] Kashif Ishaque, Zainal Salam, Muhammad Amjad, and Saad Mekhilef, "An Improved Particle Swarm Optimization (PSO)–Based MPPT for PV With Reduced Steady-State Oscillation," *IEEE Trans. Power Electron*., Vol. 27, No. 8, Aug. 2012.

[5.26] Kinattingal Sundareswaran, Peddapati Sankar, P. S. R. Nayak, Sishaj P. Simon, and Sankaran Palani, "Enhanced Energy Output from a PV System Under Partial Shaded Conditions Through Artificial Bee Colony," *IEEE Trans. Sustain. Energy*, Vol. 6, No. 1, Jan. 2015.

[5.27] Mohammadmehdi Seyedmahmoudian, Saad Mekhilef, Rasoul Rahmani, Rubiyah Yusof and Ali Asghar Shojaei, "Maximum power point tracking of partial shaded photovoltaic array using an evolutionary algorithm: A particle swarm optimization technique," *Journal of Renewable and Sustainable Energy*, 6, 023102, 2014.

[5.28] P.K. Gayen, D. Chatterjee and S.K. Goswami, "Stator side active and reactive power control with improved rotor position and speed estimator of a grid connected DFIG (doubly-fed induction generator)," *Energy (2015) 461-472*.

[5.29] Linus RM, Damodharan P, "Maximum power point tracking method using a modified perturb and observe algorithm for grid connected wind energy conversion systems. IET Renew Power Gener. 2015; 9:682-689.

[5.30] Youssef A-R, Ali AI, Saeed MS, Mohamed EE, "Advanced multi-sector P&O maximum power point tracking technique for wind energy conversion system," Int J Electr Power Energy Syst. 2019; 107:89-97.

[5.31] Fathabadi Hassan, "Novel highly accurate universal maximum power point tracker for maximum power extraction from hybrid fuel cell/photovoltaic/wind power generation systems," Energy 2016; 116:402–16es.

[5.32] Rajin M. Linus and Perumal Damodharan, "Maximum power point tracking method using a modified perturb and observe algorithm for grid connected wind energy conversion systems," IET Renew. Power Gener., 2015, Vol. 9, Iss. 6, pp. 682–689.

MPPT TECHNIQUE FOR GRID INTEGRATION OF HYBRID PHOTOVOLTAIC-BATTERY- DFIG BASED WECS

6.1 INTRODUCTION

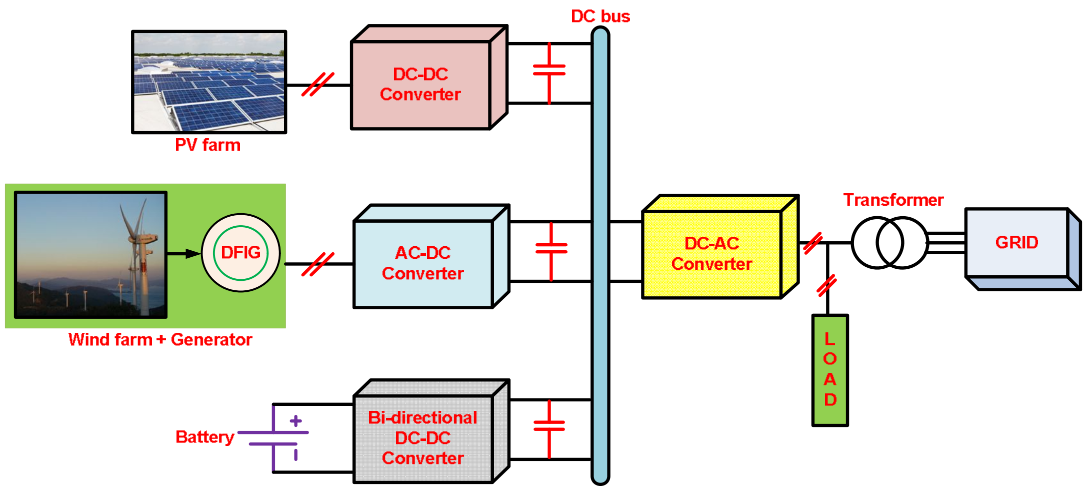

Fig. 6.1. DC coupled HRES system

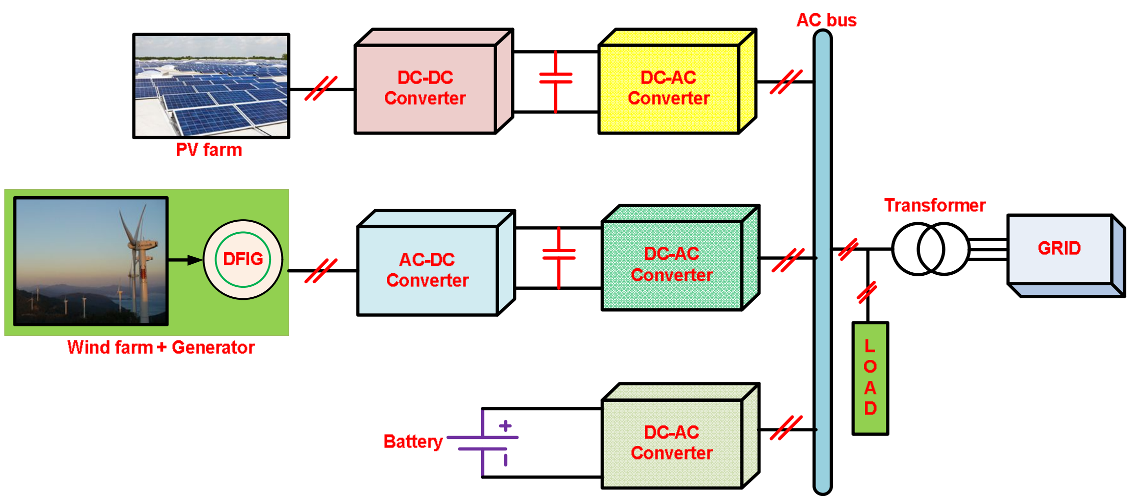

Fig. 6.2. AC coupled HRES system

The WECS and PV systems shares the major share of renewable energy production in modern world [6.1-6.2]. Also, the combined energy from these sources can supply the power to large number of loads. The PV-wind system is further integrated with energy storage systems like the battery, fuel cell etc., in delivering the efficient power supply to the customers [6.3-6.5]. Therefore, proper control strategies are required for tracking the maximum power for PV and wind systems [6.6].

The classifications and architecture of HRES are represented in Fig. 6.1 & 6.2 [6.7-6.9]. There is mixed HRES, in which displays advantages of the both AC and DC coupled schemes [6.10]. A PSO-BPSO Technique, Particle Swarm Optimization Algorithm and Two-Stage Optimization are employed in sizing of the HRES [6.11-6.19]. Along with the sizing, the economic assessment of the HRES implementation is defined in [6.14]. The wind/PV along with battery/supercapacitor-based systems are defined in [6.15,6.16]. The HRES can be operated in grid connected and standalone modes. It is observed that most of the HRES are operated in the standalone mode. In [6.17], there is system established for the standalone microgrid operation. The power quality improvement of the standalone hybrid energy system is proposed in [6.18]. Sensitivity analysis of a standalone hybrid system for the rural healthcare facility is represented in [6.19]. The grid connected HRES are discussed in [6.20]. From [6.21-6.24], it can be observed that the MPPT schemes plays a key role in the operating characteristics of the system.

Different MPPT schemes are employed for tracking maximum power in PV system. For the optimum usage of available PV panel power, different MPPT schemes has been proposed [6.25-6.34]. In this research work, IARV MPPT scheme is discussed for detecting maximum power. IARV displays improved MPPT characteristics compared to P&O based schemes. Unlike CV scheme, it displays better tracking efficiency at lower irradiation cases. The IARV scheme does not require any memory unit for tracking MPP. So, the proposed method is economical and easy real time implementable compared to ARV scheme.

DFIG has the major advantages of variable speed and constant frequency operation, low mechanical tension, maximum power capturing ability, decoupled active or reactive power governance, etc., [6.35-6.36]. Different optimization based MPPT schemes have been developed for tracking MPP in DFIG system [6.37-6.50]. In this research work, an SSM-ABC is proposed as an improved version of ABC. In proposed scheme the tracking time is considerably decreased by employing searching space minimization mechanism.

Overall, HRES along with proposed IARV and SSM-ABC schemes has been implemented for a PV system of 12KW, DFIG of 10KW and battery of 5KW in MATLAB & Simulink atmosphere and OPAL-RT. Moreover, the system with proposed MPPT schemes displayed improved dynamic characteristics and lower inter-harmonic content compared to the system with P&O scheme.

6.2 SYSTEM CONFIGURATION

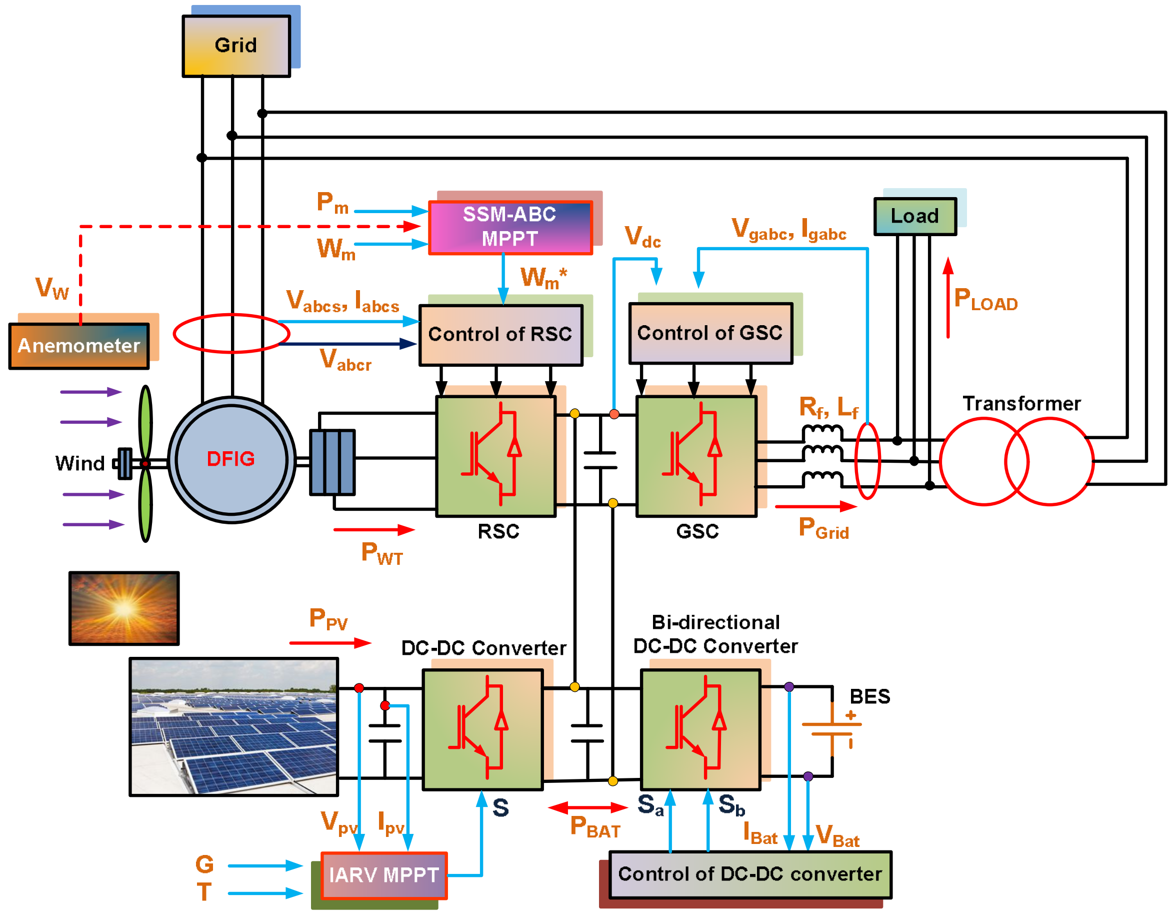

Fig. 6.3. Block diagram for proposed HRES system

The DC-coupled HRES system is taken into consideration for developing the proposed system. Fig. 6.3, represents the overall block diagram for the proposed scheme. The DFIG, PV and battery system are operated together to supply the continuous supply to the load. The proposed system consists of DFIG system with RSC, PV configuration with DC-DC converter and Battery with bi-directional DC-DC converter. These all-coupled systems are connected to GSC through a DC link capacitor. The values of the system parameters are represented in Table-6.1.

6.2.1 PV modelling

Single diode model is mostly considered for PV cell modelling due to its accuracy in producing the output characteristics [6.29]. Fig. 6.4 represents the solar cell circuit employing single diode model. Using Fig. 6.4, the mathematical relation amongst I_{PV} and V_{PV} can be formulated as (6.1).

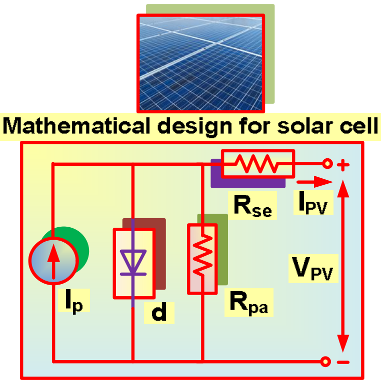

Fig. 6.4. Solar cell representation

Table 6.1. System Parameters

WT driven DFIG parameters	
Peak power	10 KW
Pole pair	4
Peak voltage	400V
Stator resistance	0.2147 Ω
Rotor resistance	0.2205 Ω
Stator leakage inductance	0.991 mH
Magnetizing inductance	64.19 mH
Rotor leakage inductance	0.991 mH
Turns ratio	0.34
Blade radius	3.45 m
Air density	1.225 kg/m^3
Damping Coefficient	0.01 Nm.s/rad
Inertia constant	2 s
Optimal Tip speed ration	7.2
Maximum power coefficient	0.44
Unknown coefficients (C_1-C_7)	C_1=0.5176, C_2=116, C_3=0.4, C_4=5 C_5=21, C_6=0.0068, C_7=0.08
Solar panel characteristics (TP250MBZ)	
MPP Power	249 watts
MPP Voltage	30 volts
MPP Current	8.3 amps
Short Circuit Current	8.83 amps
Open Circuit Voltage	36.8 volts
Temperature coefficient of I_{sho}	0.064%/^{0}C
Temperature coefficient of V_{ope}	-0.33%/^{0}C
Storage system	
Rated battery capacity	75 Ah
Rated battery Voltage	12 V

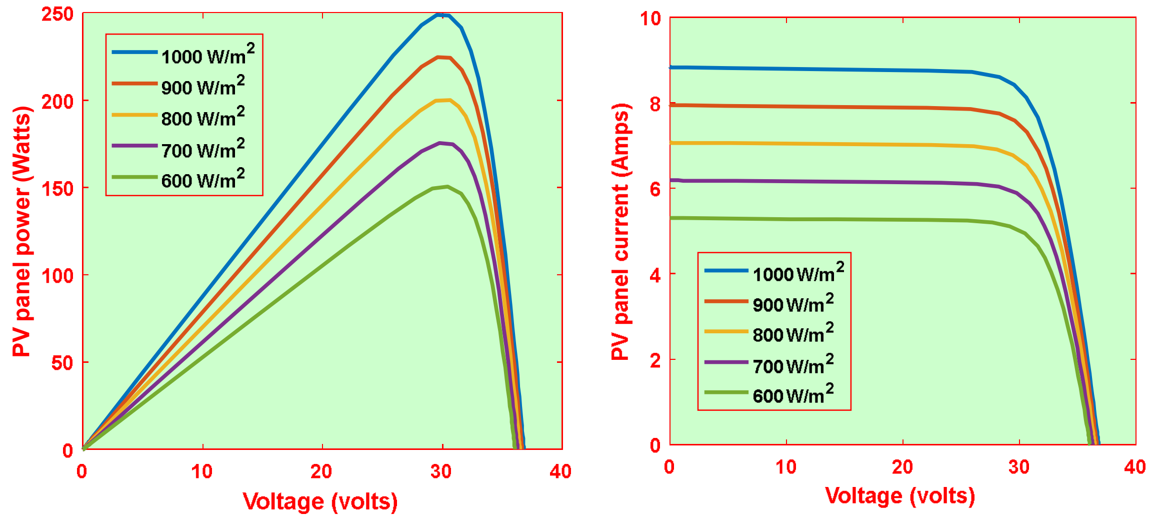

(a) (b)

Fig. 6.5. Output characteristics of 24S-2P configuration. (a) P-V characteristics (b) I-V characteristics

Table 6.2. P_m, V_m, I_m, V_{ope} And I_s for 24S-24P Configuration

G (W/m^2)	P_M (KW)	V_M (Volts)	I_M (Amps)	V_{ope} (Volts)	I_{sho} (Amps)
600	150.54	30.44	4.95	36.05	5.30
700	175.64	30.04	5.85	36.28	6.19
800	200.40	29.97	6.69	36.47	7.07
900	224.84	29.82	7.54	36.64	7.95
1000	249.1	30.01	8.3	36.79	8.83

$$I_{PV} = I_{PV} - I_o\left(e^{\frac{q(V_{PV}+R_{se}I_{PV})}{AkT}} - 1\right) - \frac{V_{PV}+R_{se}I_{PV}}{R_{pa}} \tag{6.1}$$

The I_{sho} and V_{ope} are expressed in terms of irradiation and temperature as,

$$I_{sho} = I_{sho,ref}\left[1+\alpha\left(T-T_{ref}\right)\right]\frac{G}{G_{ref}} \tag{6.2}$$

$$V_{ope} = V_{ope,ref}\left[1 + a\times\ln\frac{G}{G_{ref}} + T_{\beta}\left(T-T_{ref}\right)\right] \tag{6.3}$$

Table-6.1, represents the manufacturer data for solar panel. For the considered solar panel, P-V and I-V characteristics are represented in Fig. 6.5. Using Fig. 6.5, the V_{ope}, I_{sho}, MPP voltage, MPP current and MPP power values are represented in Table-6.2.

6.2.2 Wind turbine modelling

The mechanical power generated by WT is defined as (6.4). The λ_i can be evaluated by employing β and λ as (6.6). The λ can be measured using rotor speed as shown in (6.7). At the MPP, (6.7) can be modified as (6.8). The wind turbine characteristics are represented in Table-6.1.

For the considered turbine parameters, the power-rotor speed characteristics at various wind speeds are represented in Fig. 6.6.

$$P_m = \frac{1}{2}\rho A_r C_p(\beta,\lambda)V_w^3 \tag{6.4}$$

$$C_p = C_1\left(\frac{C_2}{\lambda_i} - C_3\beta - C_4\beta^{C_5} - C_6\right)\left(e^{C_7/\lambda_i}\right) \tag{6.5}$$

$$\lambda_i = \frac{1}{\lambda + 0.02\beta} - \frac{0.003}{1+\beta^3} \tag{6.6}$$

$$\lambda = \frac{\omega_m R}{V_w} \tag{6.7}$$

$$\lambda_{opt} = \frac{\omega_{opt} R}{V_w} \tag{6.8}$$

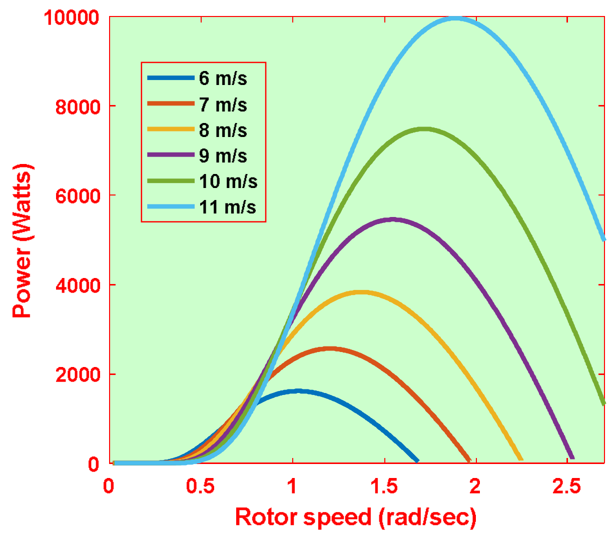

Fig. 6.6. Power vs rotor speed characteristics at various wind speed levels

6.2.3 DFIG modelling

The DFIG modelling by employing dq-reference frame is represented in Fig.6.7. The rotor and stator voltage equations in dq components are represented in (6.9)-(6.12).

$$v_{ds} = R_s i_{ds} + \frac{d\psi_{ds}}{dt} - \omega_s \psi_{ds} \tag{6.9}$$

$$v_{qs} = R_s i_{qs} + \frac{d\psi_{qs}}{dt} - \omega_s \psi_{qs} \tag{6.10}$$

$$v_{dr} = R_r i_{dr} + \frac{d\psi_{dr}}{dt} - \omega_r \psi_{dr} \tag{6.11}$$

$$v_{qr} = R_r i_{qr} + \frac{d\psi_{qr}}{dt} - \omega_r \psi_{qr} \tag{6.12}$$

The flux generated in DFIG are denoted by employing (6.13)-(6.16).

$$\psi_{ds} = L_s i_{ds} + L_m i_{dr} \tag{6.13}$$

$$\psi_{qs} = L_s i_{qs} + L_m i_{qr} \tag{6.14}$$
$$\psi_{dr} = L_m i_{ds} + L_r i_{dr} \tag{6.15}$$
$$\psi_{qr} = L_m i_{qs} + L_r i_{qr} \tag{6.16}$$

The T_{em} is denoted as,

$$T_{em} = \frac{3}{2} p \frac{L_m}{L_s} \left(\psi_{qs} i_{dr} - \psi_{ds} i_{qr} \right) \tag{6.17}$$

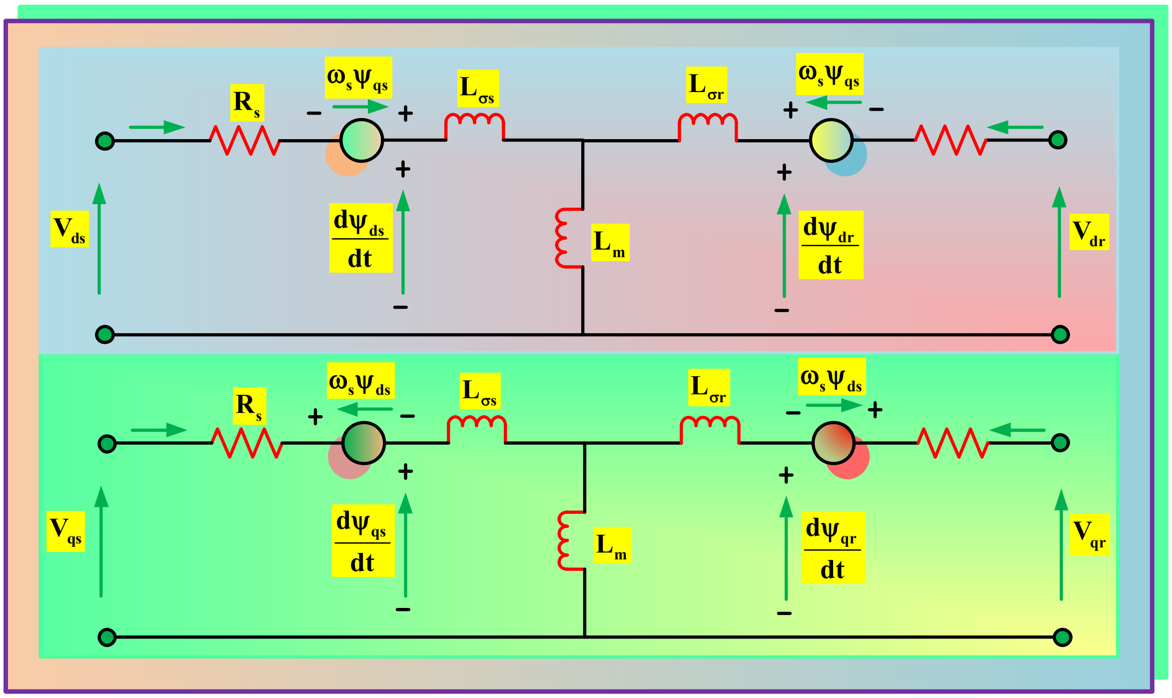

Fig. 6.7. dq-reference frame for DFIG design

6.3 PROPOSED MPPT CONTROL STRATEGIES FOR HRES

In this section, the proposed MPPT schemes for PV and wind systems are thoroughly discussed. Also, the idea behind the development of proposed schemes is properly defined.

6.3.1 Proposed IARV MPPT scheme for PV system

The algorithm for proposed IARV scheme has been represented in the Fig. 6.8. In the proposed scheme, the nearest point to MPP is estimated by employing proposed peak detection criteria. This nearest point is employed as the starting point for tracking in incremental conductance algorithm. The proposed scheme does not require any memory unit for tracking MPP like ARV MPPT scheme.

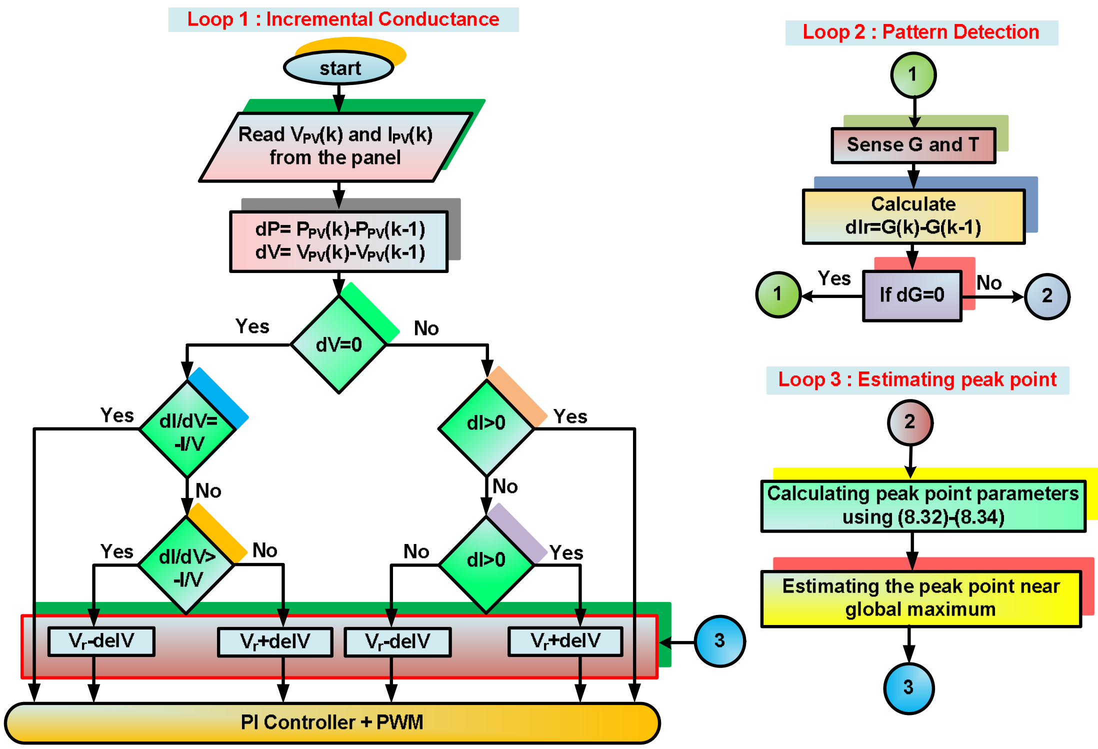

Fig. 6.8. Proposed IARV MPPT scheme

6.3.1.1 Relation between MPP values for single panel and aS-bP configuration

For finding the relation between MPP values, aS-bP configuration is considered in the proposed system, where a=24 and b=2. The P-V and I-V characteristics for the considered configuration is represented in Fig. 6.9. Using Fig. 6.9, the V_{ope}, I_{sho}, MPP voltage, MPP current and MPP power values are represented in Table-6.3.

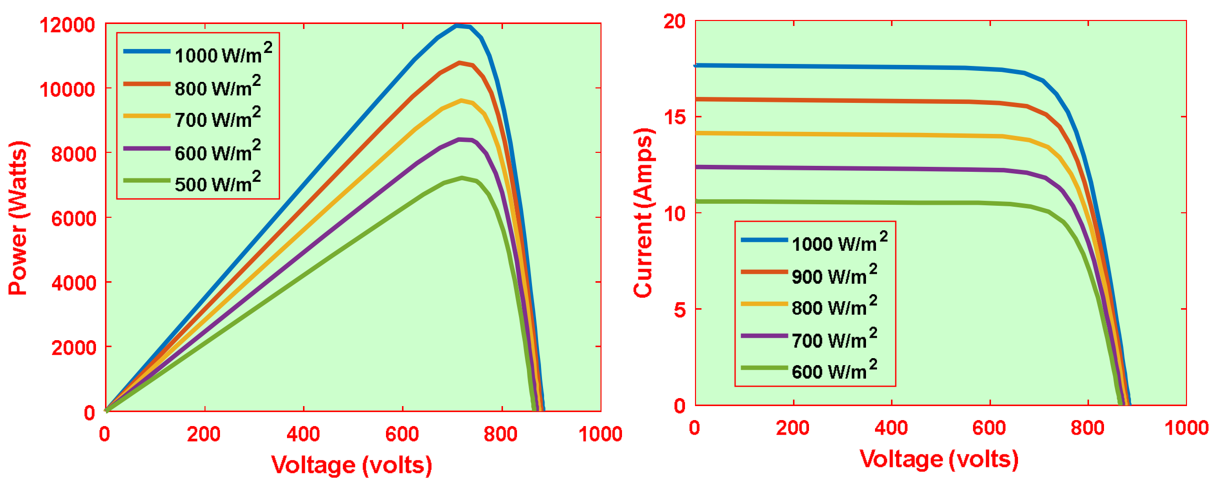

(a) (b)

Fig. 6.9. Output characteristics of 24S-24P configuration. (a) P-V characteristics (b) I-V characteristics

Table 6.3. P_m, V_m, I_m, V_{ope} And I_s for 24S-2P Configuration

G (W/m²)	P_M (KW)	V_M (Volts)	I_M (Amps)	V_{ope} (Volts)	I_{sho} (Amps)
600	7.23	730.56	9.9	865.2	10.6
700	8.43	720.96	11.7	870.72	12.38
800	9.62	719.28	13.38	875.28	14.14
900	10.79	715.68	15.08	879.36	15.9
1000	11.96	720.24	16.6	882.96	17.66

By observing Table-6.2 and Table-6.3, the relation between the MPP voltage values for single panel and 24S-2P configuration ca be obtained as,

$$\left(V_M\big|_{24S-2P}\right)_{600} \approx 24\times\left(V_M\big|_{1S}\right)_{600} \tag{6.18}$$

$$\left(V_M\big|_{24S-2P}\right)_{700} \approx 24\times\left(V_M\big|_{1S}\right)_{700} \tag{6.19}$$

$$\left(V_M\big|_{24S-2P}\right)_{800} \approx 24\times\left(V_M\big|_{1S}\right)_{800} \tag{6.20}$$

$$\left(V_M\big|_{24S-2P}\right)_{900} \approx 24\times\left(V_M\big|_{1S}\right)_{900} \tag{6.21}$$

$$\left(V_M\big|_{24S-2P}\right)_{1000} \approx 24\times\left(V_M\big|_{1S}\right)_{1000} \tag{6.22}$$

Similarly, the relation between the MPP current values for 1S and 24S-2P configurations can be obtained as,

$$\left(I_M\big|_{24S-2P}\right)_{600} \approx 2\times\left(I_M\big|_{1S}\right)_{600} \tag{6.23}$$

$$\left(I_M\big|_{24S-2P}\right)_{700} \approx 2\times\left(I_M\big|_{1S}\right)_{700} \tag{6.24}$$

$$\left(I_M\big|_{24S-2P}\right)_{800} \approx 2\times\left(I_M\big|_{1S}\right)_{800} \tag{6.25}$$

$$\left(I_M\big|_{24S-2P}\right)_{900} \approx 2\times\left(I_M\big|_{1S}\right)_{900} \tag{6.26}$$

$$\left(I_M\big|_{24S-2P}\right)_{1000} \approx 2\times\left(I_M\big|_{1S}\right)_{1000} \tag{6.27}$$

6.3.1.2 Proposed peak point detection for aS-bP configuration

By observing (6.18)-(6.27), it can be noted that the MPP values of series-parallel configurations can be founded by employing MPP values of single solar panel. The proposed peak point detection can be explained further using three steps.

Step-1: For the sensed irradiation and temperature values, calculate the I_{sho} and V_{ope} using (6.2) and (6.3).

Step-2: Using the I_{sho} and V_{ope}, the MPP current values of individual solar panels can be calculated as,

$$\left(V_M\big|_{1S}\right)_G \approx K_1\times\left(V_{ope}\big|_{1S}\right)_G \tag{6.28}$$

$$\left(I_M\big|_{1S}\right)_G \approx K_2\times\left(I_{sho}\big|_{1S}\right)_G \tag{6.29}$$

Where K_1 and K_2 are calculated as,

$$K_1 \approx \frac{\left(V_M\big|_{1S}\right)_{STC}}{\left(V_{ope}\big|_{1S}\right)_{STC}} \tag{6.30}$$

$$K_2 \approx \frac{\left(I_M\big|_{1S}\right)_{STC}}{\left(I_{sho}\big|_{1S}\right)_{STC}} \tag{6.31}$$

Step-3: By employing (6.28)-(6.31), the MPP values for aS-bP configuration can be calculated as,

$$\left(V_M\big|_{24S-2P}\right)_G \approx a \times \left(V_M\big|_{1S}\right)_G \tag{6.32}$$

$$\left(I_M\big|_{24S-2P}\right)_G \approx b \times \left(I_M\big|_{1S}\right)_G \tag{6.33}$$

$$\left(P_M\big|_{24S-2P}\right)_G \approx \left(V_M\big|_{1S}\right)_G \times \left(I_M\big|_{1S}\right)_G \tag{6.34}$$

By using (6.32)-(6.34), the nearest point to MPP is measured. This point is employed in setting the initial point of searching for incremental conductance method. The estimating peak mechanism helps IARV scheme to settle faster compared to P&O based schemes. Also, the proposed scheme displays lower fluctuations under sudden change in irradiation compared to P&O method.

6.3.2 Proposed SSM-ABC scheme for WECS

The proposed system mainly focuses on the improved MPPT methods. So, the proposed scheme is well addressed with RSC side, while GSC converter control is similar to that of [6.1]. Fig. 6.10 represents the overall RSC control scheme along with proposed SSM-ABC method. In this work, SSM-ABC scheme has been proposed for tracking maximum power in DFIG system. It mainly focuses on reducing the minimization of searching space in tracking MPP. As shown in Fig. 6.10, the position and speed estimation of rotor is done by employing MRAS control strategy [6.51].

The proposed SSM-ABC algorithm has been represented in Fig. 6.11. Before describing step wise SSM-ABC implementation in MPP tracking, a solution vector of rotor speeds with Np bees has been considered as,

$$\begin{aligned} x_i^k &= \omega_g = \left[\omega_1, \omega_2, \omega_3, \ldots\ldots, \omega_j\right] \\ j &= 1,2,3,4, \ldots\ldots\ldots\ldots\ldots\ldots\ldots N_P \end{aligned} \tag{6.35}$$

The objective function is formed with the idea of comparing the power of updated power with the former one as a function of rotor speed. So, the objective function can be defined as,

$$P\left(\omega_i^k\right) - P\left(\omega_i^{k-1}\right) = f_k \tag{6.36}$$

The function f_k can be calculated subjected to $P\left(\omega_i^k\right) > P\left(\omega_i^{k-1}\right)$, where $P(\omega_i)$ can be obtained using (6.4)-(6.7).

For SSM-ABC formulation, the output power of DFIG system is considered as nectar amount. Also, the rotor speeds are the decision variable that are termed as food source position in SSM-

ABC algorithm. In this proposed scheme, the tracking time is minimized by reducing the searching space. The step wise operation of SSM-ABC scheme in tracking MPP is denoted below.

Step-1: Proposed initialization

Initialize the NP, of which half of the bees are considered as employed bees and other half as onlooker bees. In the initial stage, all these bees are placed at different food source positions using (6.37).

$$x_i = \omega_{\min} + \frac{(i-1)[\omega_{\max} - \omega_{\min}]}{N_p - 1}$$
$$i = 1,2,3,4,......................,N_p \tag{6.37}$$

Where $\omega_{\max}$ and $\omega_{\min}$ are calculated by employing proposed initialization strategy. Anemometer is used to calculate the optimum rotor speed value as (6.38). Further, the measured optimum rotor speed value is used set $\omega_{\max}$ and $\omega_{\min}$ values by employing (6.39) and (6.40). This initialization part is helpful in placing the bees nearest to MPP.

$$\omega_{opt} = \frac{\lambda_{opt} V_w}{R} \tag{6.38}$$

$$\omega_{\max} = \omega_{opt} + \in \tag{6.39}$$

$$\omega_{\min} = \omega_{opt} - \in \tag{6.40}$$

Step-2: Estimating the Quantity of the Nectar

The amount of output power for each rotor speed reference is calcualted using mathematical formulation in simulation. The measured nectat amount is used to decide to assign the employer and onlooker bees.

Step-3: Finding new food source position

The process of searching MPP for DFIG system is done in two phases, where first phase is for employed bees and second phase is for onlooker bees. Employed bees update their positions by employing (6.41).

$$x_i^{k+1} = x_i^k + \gamma\left(x_i^k - x_j^k\right)$$
$$j \in \left(1,2,..............,\frac{N_P}{2}\right) \tag{6.41}$$

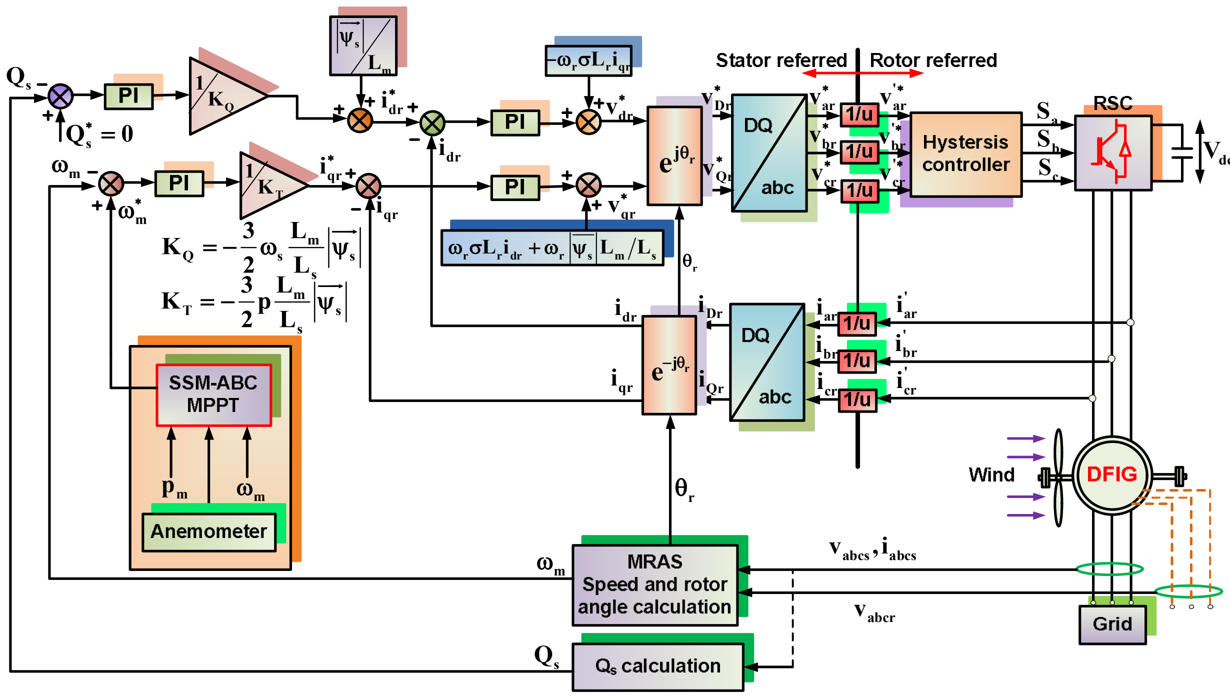

Fig.

6.10. Proposed control scheme for RSC in DFIG system

Where γ values are in the levels of [-1, 1]. The employed bees now verify the quantity of food source at new locations. If the quantity at new locations is higher, then the employed bees stays at the updated position. Otherwise, the employed bees return to the old position as (6.42).

$$x_i^{k+1} = x_i^k \tag{6.42}$$

The onlooker bees' dances towards the employed bee location where the quantity if food source is higher using (6.43).

$$x_i^{k+1} = x_{hi}^k + \frac{\gamma\left[\omega_{max} - \omega_{min}\right]}{\frac{N_p}{2} - 1} \tag{6.43}$$

Where X_{hi} denotes the food source position with high nectar amount.

Step-4: Termination Conditions:

If there is no further increase in the amount of DFIG output power after five consecutive iterations, termination of the process begins. The present position is employed as optimum rotor speed for tracking MPP. If termination condition is not reached, system will go to step-2.

Step-5: Reinitializing the process:

If there is a change in wind speed, the process will restart the bee initialization. This wind speed variation can be observed by anemometer.

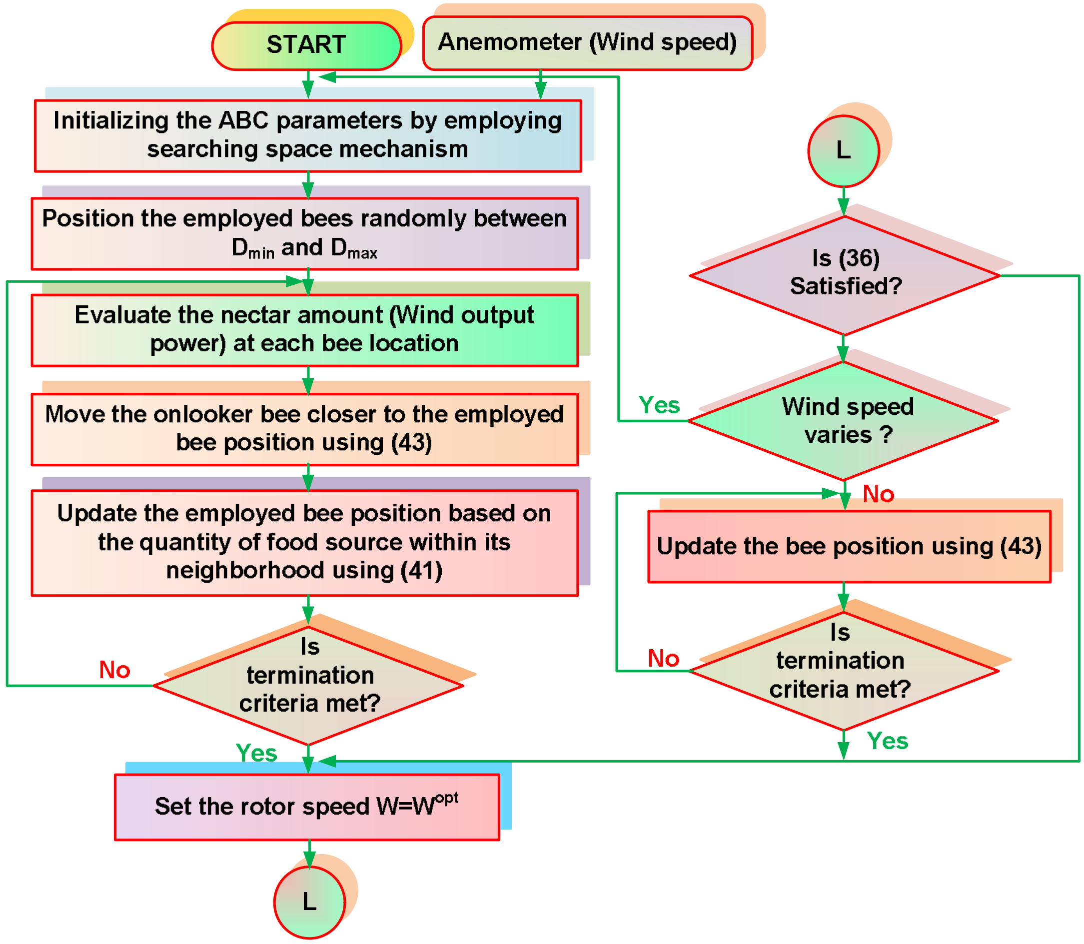

Fig. 6.11. Proposed SSM-ABC algorithm

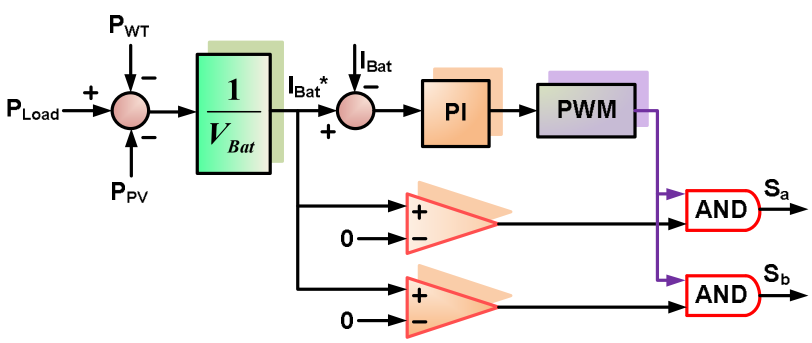

Fig. 6.12. Battery control strategy

The proposed SSM-ABC scheme is established to eliminate the disadvantages of the existing P&O scheme. The proposed scheme displays lower selling time compared SS-P&O scheme and it displays the lower steady state oscillation compared to LS-P&O scheme [6.36]. Also, the proposed scheme is easy to implement compared to other existing optimization-based schemes. The battery control strategy for the considered system is represented in Fig. 6.12. This control strategy is similar to that of the technique used in [6.1].

6.4 RESULTS AND DISCUSSIONS

The system with proposed IARV and SSM-ABC schemes are implemented in MATLAB & simulink atmosphere and OPAL-RT. The OPAL-RT setup in laboratory is represented in Fig. 6.13.

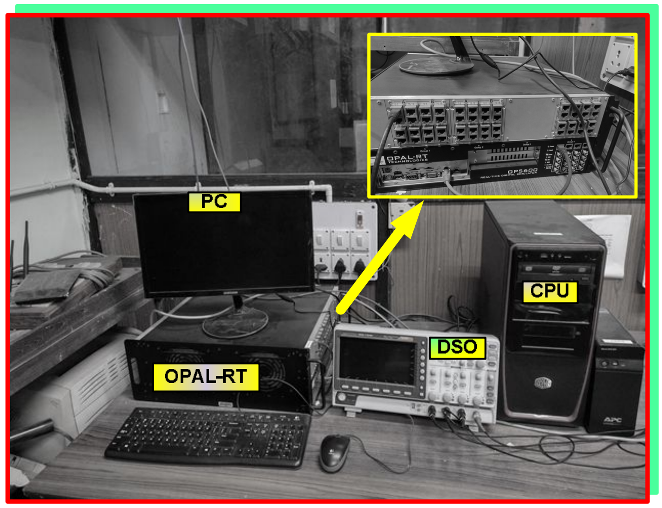

Fig. 6.13. OPAL-RT setup in laboratory

6.4.1 Analysis of proposed IARV scheme

The PV system is operated for the IARV MPPT scheme as shown in Fig. 6.8. Further, the proposed scheme is operated for the irradiation levels as shown in Fig. 6.14a. For the considered irradiation pattern, PV panel voltage, current and power are displayed in Fig. 6.14b, 6.14c & 6.14c respectively. From Fig. 6.14, it can be observed that the proposed IARV MPPT scheme able to detect the MPP efficiently. Due to its near MPP detection strategy, IARV method is able to track the MPP faster compared to P&O and MP&O schemes [6.29]. The IARV MPPT scheme shows the tracking time of 14.5ms. The proposed scheme does not display any drift under sudden change in irradiation like P&O. The proposed IARV MPPT scheme displays the improved MPPT efficiency of 99.09%.

Even though [6.33] reduces inter-harmonics, it has the major disadvantage of inefficiency in tracking under lower irradiation cases. Beside maintaining good dynamic characteristics, IARV scheme is able to display improved efficiency at all possible irradiation cases. The proposed scheme has been implemented in OPAL-RT. The respective PV panel voltage, current and power are represented in Fig 6.15a, 6.15b & 6.15c respectively.

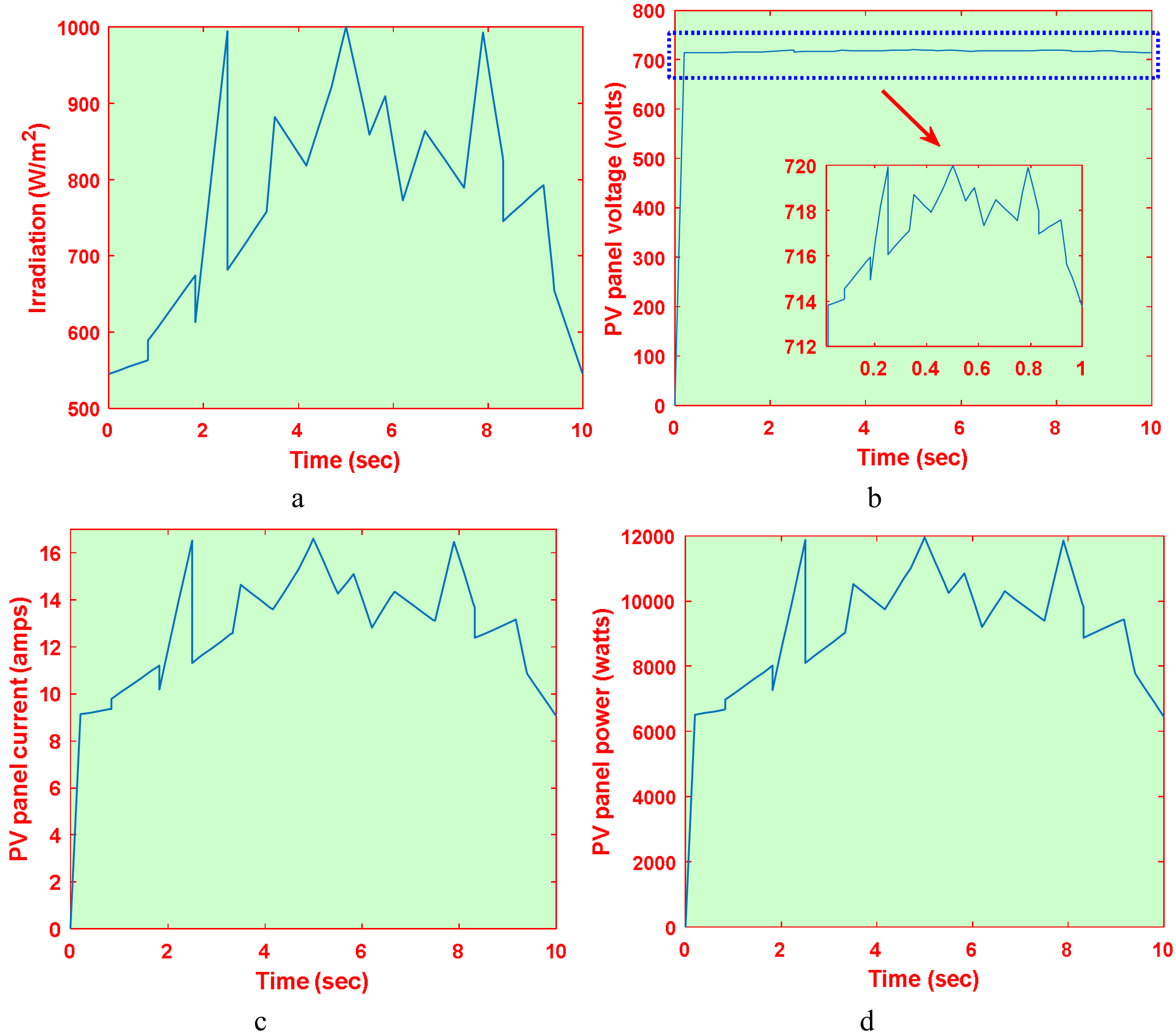

Fig. 6.14. PV system with proposed IARV MPPT (a) Irradiation, (b) Voltage, (c) Current and (d) Power

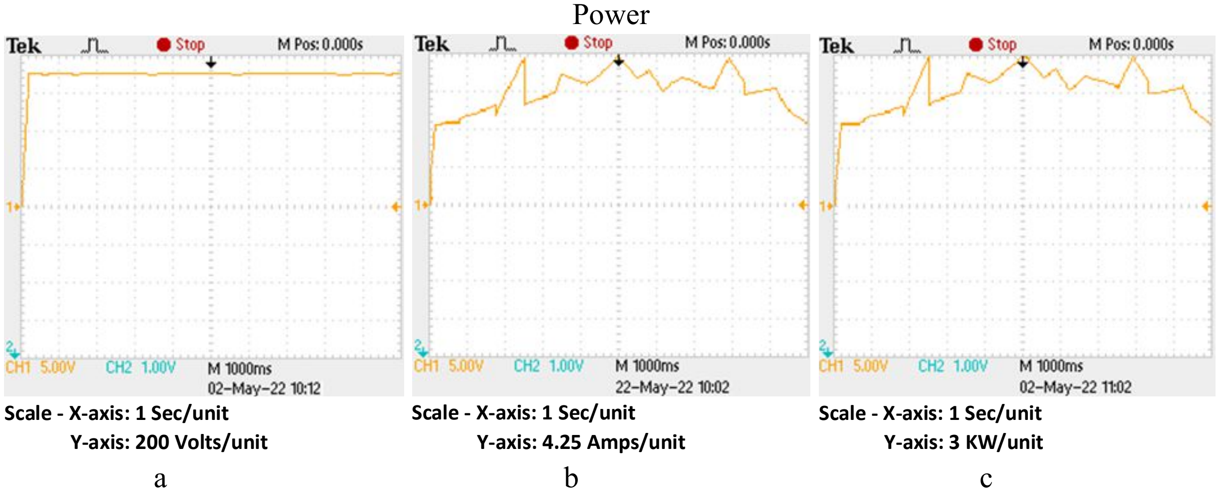

Fig. 6.15. Proposed IARV MPPT in OPAL-RT (a) Voltage, (b) Current and (c) Power

The comparison of tracking speed and efficiency between IARV and P&O based schemes are represented in Table-6.4. From this it can be observed that, leaving drift avoidance the operating characteristics of P&O and MP&O schemes are almost similar.

Table. 6.4. Tracking Time and Efficiency Comparison of IARV MPPT Scheme With P&O Based Schemes

Properties	P&O	MP&O	IARV
Efficiency (%)	98.14	98.37	99.09
Tracking time (ms)	26.2	26.18	14.5

6.4.2 Analysis of proposed SSM-ABC scheme

The DFIG system is operated with the proposed SSM-ABC scheme for MPPT. The system is operated for the wind speed profile as shown in Fig. 6.16a. The respective DFIG characteristics such as mechanical power, power coefficient, rotor speed and tip speed ratio are represented in Fig. 6.16b, 6.16c, 6.16d & 6.16e respectively. From this it can be observed that the proposed SSM-ABC scheme is able to detect the MPP effectively with low settling time. Also, it is noted that the SSM-ABC does not deviate or fluctuate under the random variation of wind speed.

The proposed scheme displays the faster settling time (<350ms) compared to SS-P&O (>1300ms). Also, the SSM-ABC displays lower steady state oscillations of 0.001 rad/s compared to LS-P&O. The proposed scheme has been implemented in OPAL-RT. The respective mechanical power, power coefficient, rotor speed and tip speed ratio are represented in Fig. 6.17a, 6.17b, 6.17c & 6.17c respectively. The proposed SSM-ABC scheme compared with the P&O based schemes in Table-6.5. The proposed scheme able to show the improved efficiency of 92.12% compared to P&O scheme.

6.4.3 Comparison of inter-harmonic content

The HRES is operated for the P&O scheme for both the wind and PV based systems. Also, the same system is operated for proposed IARV and SSM-PSO schemes for PV and wind systems respectively. The wind and PV profile are employed similar to Fig. 6.14a and Fig. 6.16a. The respective DC link voltage for HRES with IARV and SSM-PSO schemes is represented in Fig. 6.18a. Also, the grid voltage and current for proposed system are represented in Fig. 6.18b and 6.18c respectively. Using OPAL-RT, the grid characteristics for P&O based system are represented in Fig. 6.19.

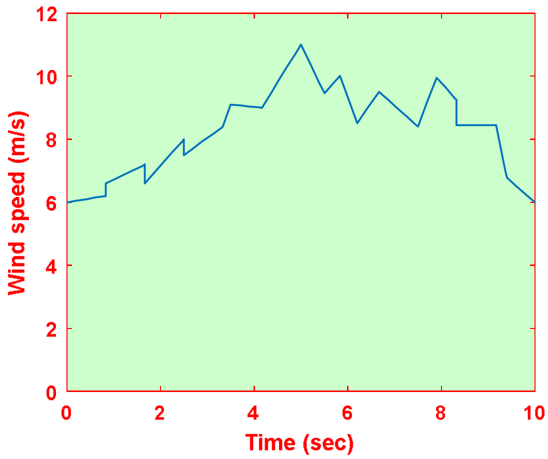

a

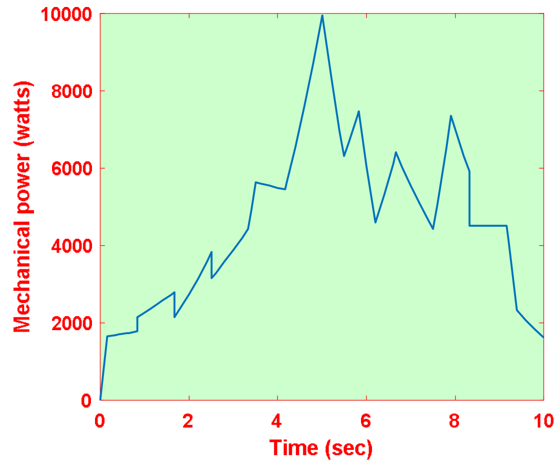

b

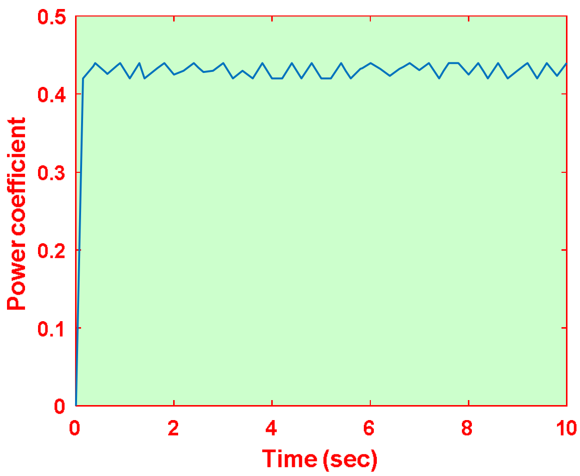

c

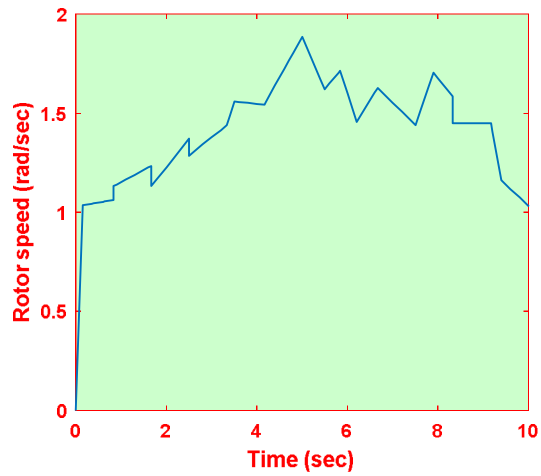

d

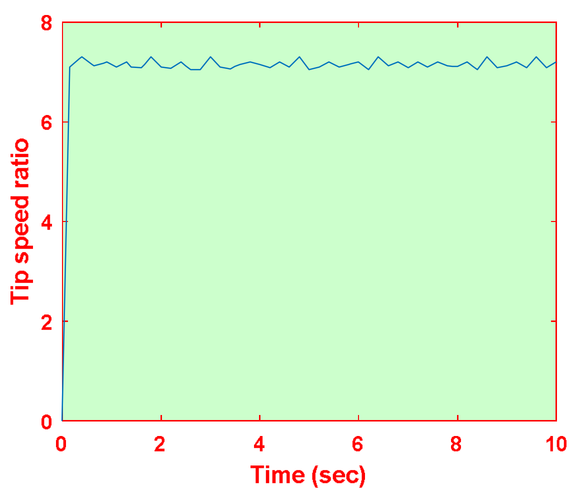

e

Fig. 6.16. DFIG system with proposed SSM-ABC MPPT (a) wind speed profile, (b) Power, (c) Power coefficient, (d) Rotor speed and (e) Tip speed ratio

Scale - X-axis: 1 Sec/unit
Y-axis: 2.5 KW/unit

a

Scale - X-axis: 1 Sec/unit
Y-axis: 0.1/unit

b

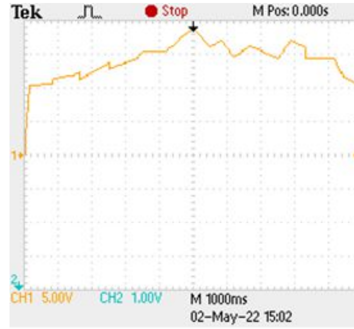

Scale - X-axis: 1 Sec/unit
Y-axis: 0.5 Rad/sec/unit

c

Scale - X-axis: 1 Sec/unit
Y-axis: 2/unit

d

Fig. 6.17. Proposed SSM-ABC in OPAL-RT (a) Power, (b) Power coefficient, (c) Rotor speed and (d) Tip speed ratio

Similarly, the DC link voltage, grid voltage and current parameter for P&O based system are represented in Fig. 6.20a, 6.20b and 6.20c respectively. Using OPAL-RT, the grid parameters with P&O scheme are represented in Fig. 6.21. Using the grid currents, the FFT analysis carried out for the considered system with P&O scheme and proposed schemes. The respective %fundamental components for frequency ranges from 0 to 100 Hz is represented in Table-6.6. The 50 Hz component is generally of 100%, it is opted out for better representation of inter-harmonics.

Table 6.5. Assessment of SSM-ABC with P&O Scheme

Algorithms	Settling time	Oscillations	Efficiency
LS-P&O [6.36]	77 ms	1.2	--
SS-P&O [6.36]	>1300 ms	0.05	87.11%
Proposed SSM-ABC	<350 ms	0.001	92.12%

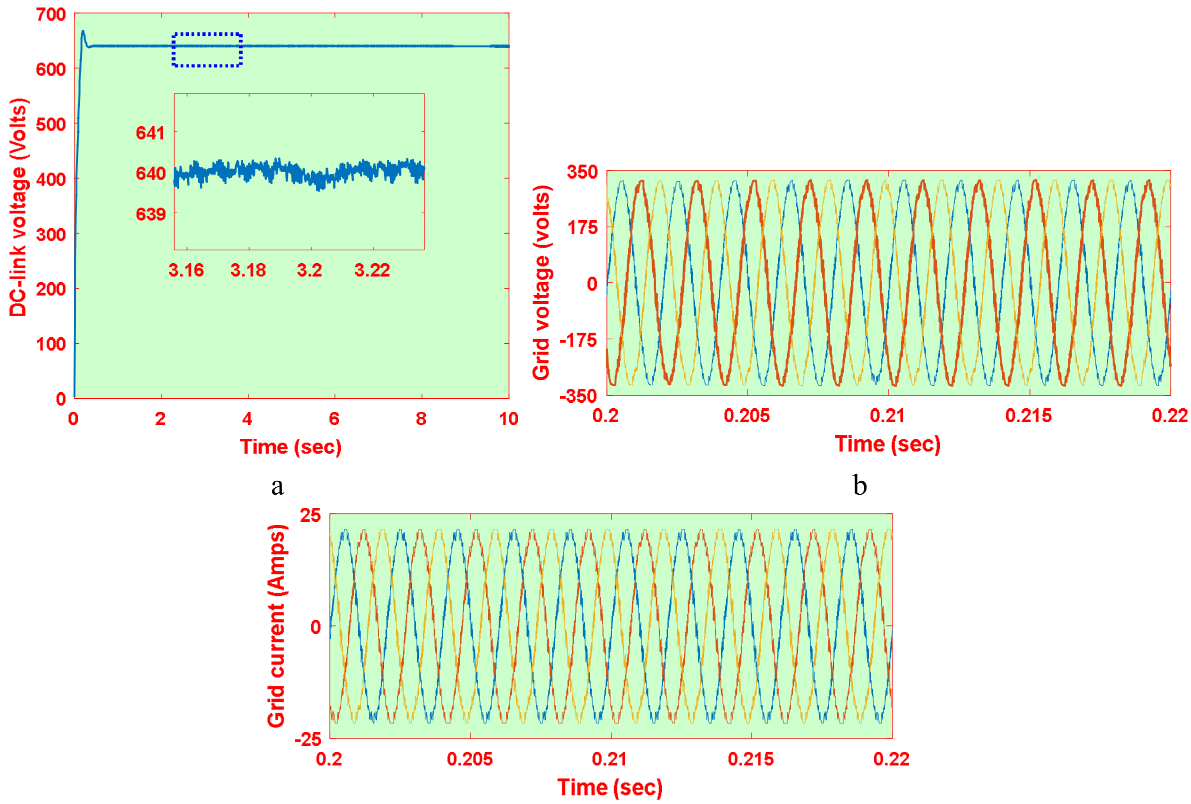

a b

c

Fig. 6.16. Grid parameters for proposed system (a) DC-link voltage, (b) Voltage and (c) Current

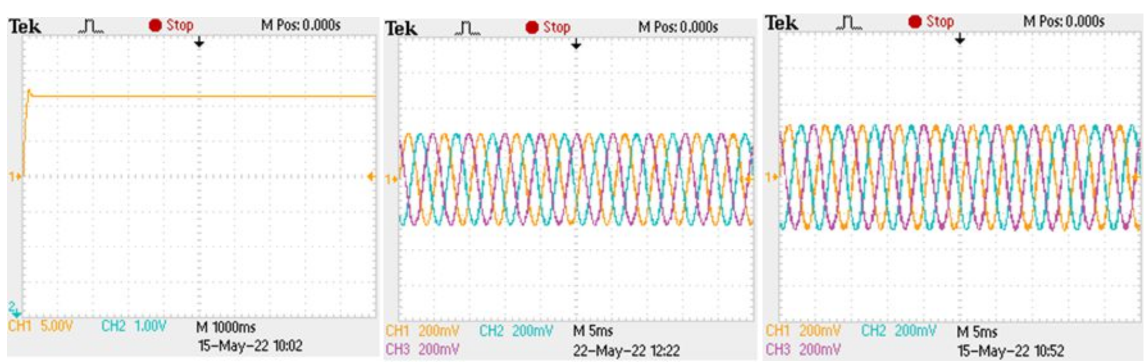

Scale - X-axis: 1 Sec/unit
Y-axis: 300 Volts/unit

Scale - X-axis: 5 ms/unit
Y-axis: 300 Volts/unit

Scale - X-axis: 5 ms/unit
Y-axis: 20 Amps/unit

a b c

Fig. 6.19. Grid parameters for proposed system in OPAL-RT (a) DC-link voltage, (b) Voltage and (c) Current

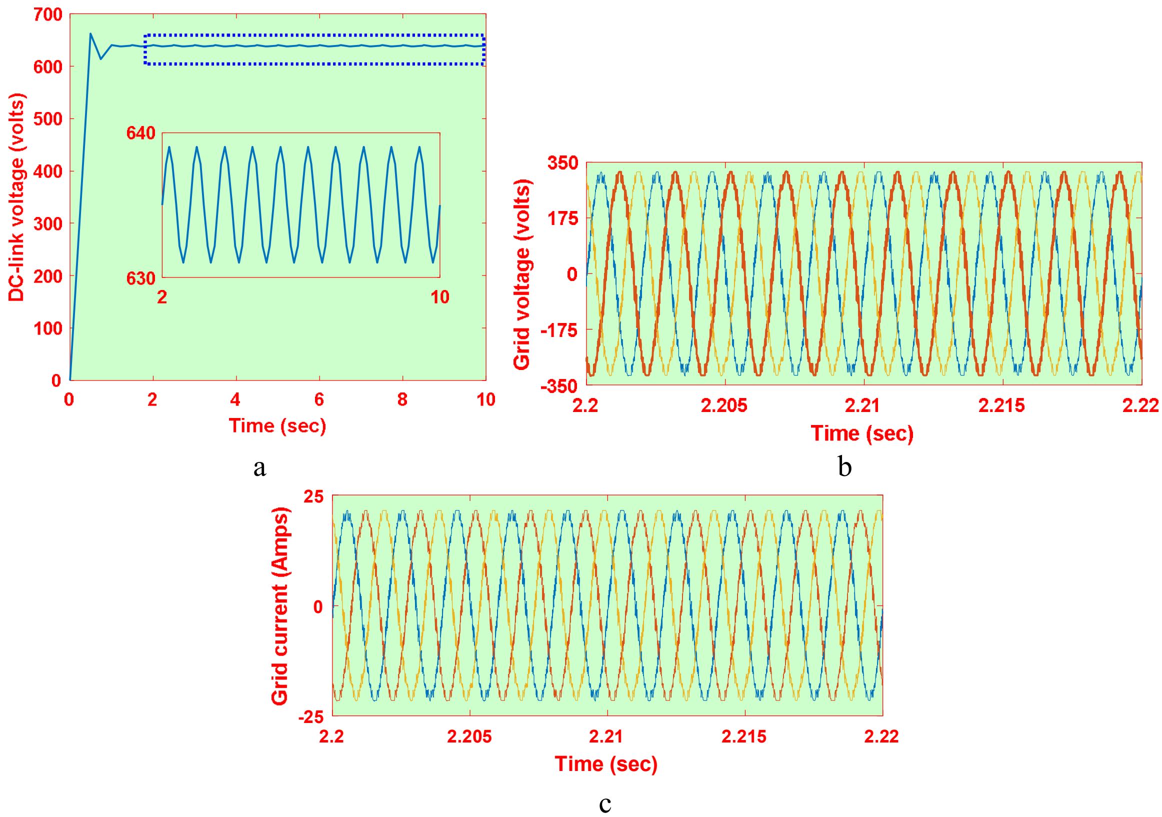

Fig. 6.20. Grid parameters for P&O based system (a) DC-link voltage, (b) Voltage and (c) Current

The frequency vs %Fundamental component for grid currents using P&O scheme and proposed MPPT schemes are represented in Fig. 6.22. The FFT results for system with P&O scheme in OPAL-RT are represented in Fig. 6.23a. Similarly, the OPAL-RT output for proposed system is represented in Fig. 6.23b.

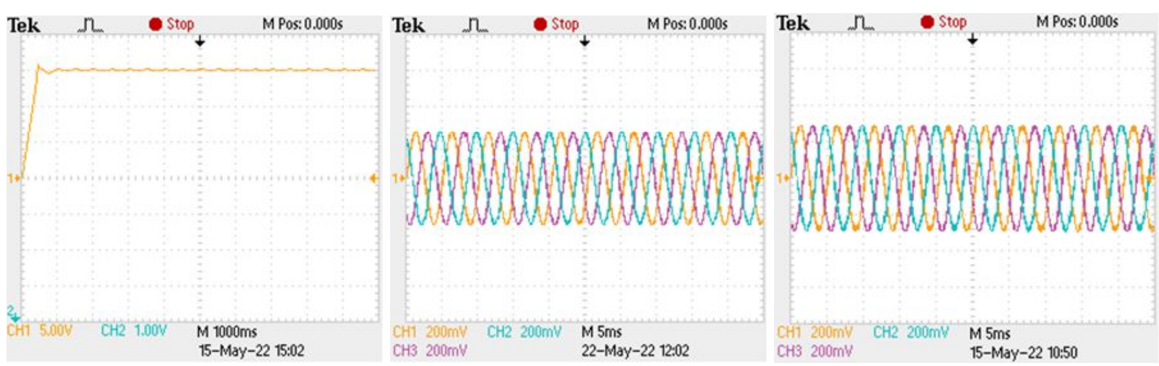

Scale - X-axis: 1 Sec/unit
Y-axis: 210 Volts/unit

a

Scale - X-axis: 5 ms/unit
Y-axis: 300 Volts/unit

b

Scale - X-axis: 5 ms/unit
Y-axis: 20 Amps/unit

c

Fig. 6.21. Grid parameters for P&O based system in OPAL-RT (a) DC-link voltage, (b) Voltage and (c) Current

From these is outputs, it can be observed that the system with proposed MPPT schemes display low inter-harmonic content compared to P&O based system. Overall, the proposed system displays the reduced average inter-harmonic content of 32.19% compared to P&O based system.

Table 6.6. Inter-harmonic Comparison Between P&O Based System and Proposed System

FREQUENCY (Hz)	P&O	Proposed system	FREQUENCY (Hz)	P&O	Proposed system
0	0.21	0.15	51.72	4.61	4.3
1.72	0.27	0.19	53.45	2.11	1.38
3.45	0.3	0.2	55.17	1.94	1.5
5.17	0.29	0.2	56.89	1.89	1.2
6.89	0.32	0.21	58.62	1.44	0.94
8.62	0.32	0.22	60.34	1.62	1.02
10.34	0.35	0.22	62.06	1.21	0.72
12.07	0.35	0.24	63.79	1.41	0.87
13.79	0.39	0.24	65.52	1.07	0.61
15.52	0.41	0.27	67.24	1.23	0.75
17.24	0.44	0.26	68.97	0.98	0.55
18.97	0.47	0.31	70.69	1.08	0.66
20.69	0.49	0.28	71.41	0.91	0.51
22.41	0.55	0.36	74.14	0.97	0.59
24.14	0.54	0.31	75.86	0.85	0.48
25.86	0.65	0.42	77.58	0.87	0.53
27.59	0.61	0.34	79.31	0.8	0.46
29.31	0.78	0.49	81.03	0.79	0.48
31.03	0.68	0.38	82.76	0.76	0.44
32.76	0.94	0.59	84.48	0.73	0.44
34.48	0.78	0.45	86.21	0.72	0.42
36.21	1.14	0.72	87.93	0.68	0.41
37.93	0.92	0.55	89.66	0.68	0.4
39.66	1.38	0.88	91.38	0.64	0.38
41.38	1.15	0.77	93.1	0.65	0.39
43.01	1.71	1.09	94.83	0.61	0.36
44.83	1.65	1.33	96.55	0.62	0.37
46.55	2.01	1.31	98.28	0.58	0.35
48.28	4.31	4.13	100	0.59	0.36
			AVERAGE	**0.991**	**0.672**

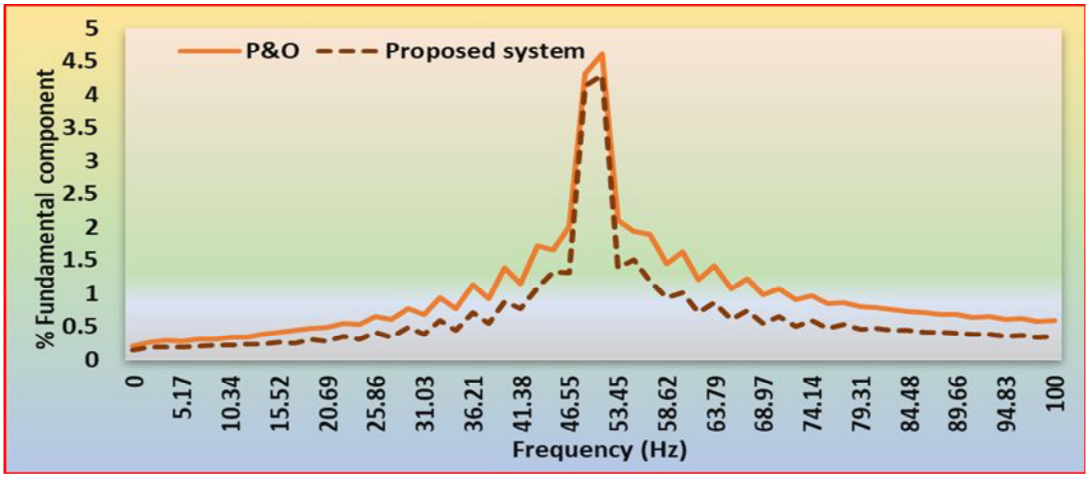

Fig. 6.22. Comparison of inter-harmonic content of between P&O based system and proposed system

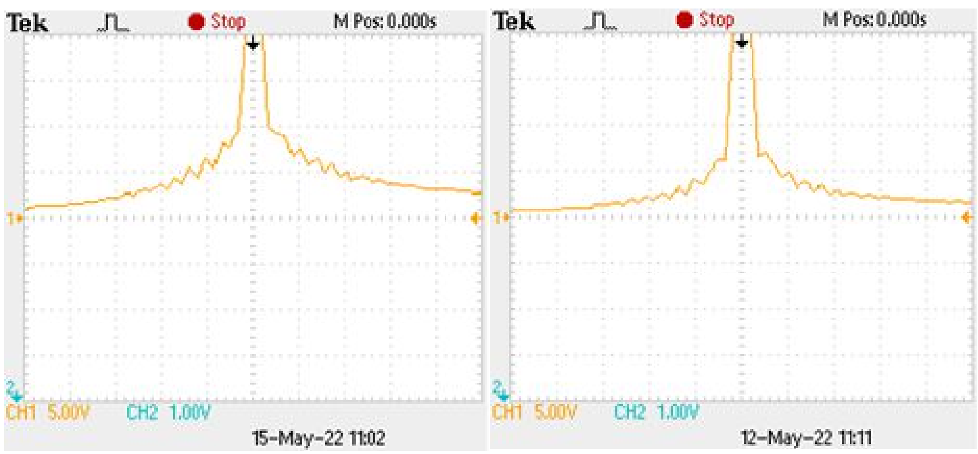

Scale - X-axis: 10 Hz/unit
Y-axis: 4%/unit

a

Scale - X-axis: 10 Hz/unit
Y-axis: 4%/unit

b

Fig. 6.23. Inter-harmonics in grid current using OPAL-RT (a) P&O based system and (b) Proposed system

6.5 CONCLUSION

In this research work, the DFIG, PV and BES are operated collectively to supply the reliable power to grid. Also, the proposed system is operated with proposed MPPT schemes for PV and WECS in generating improved dynamic characteristics. Further, the proposed MPPT schemes are operated to reduce the injection of inter-harmonics into the grid.

(1) In proposed system, an IARV MPPT scheme has been established for addressing the drawback of ARV method.

(2) The proposed IARV MPPT is able to the track the PV MPP power with better efficiency of 99.09% compared to P&O and MP&O schemes [6.29].

(3) The proposed IARV MPPT scheme do not undergo drift under sudden change in irradiation like P&O. Also, IARV MPPT scheme displays lower settling time of 14.5ms compared to MP&O.

(4) Also, the proposed IARV method displays better tracking efficiency at lower irradiation levels compared to CV MPPT.

(5) Moreover, IARV method does not require memory for tracking MPP. This leads to low processing cost compared to ARV scheme.

(6) The proposed SSM-PSO scheme able to display the lower tracking time (<350ms) compared to SS-P&O (>1300ms). Also, it displays low steady state error of (0.001 rad/s) compared to LS-P&O scheme (1.2 rad/s) [6.36].

(7) The SSM-PSO scheme displays the improved efficiency of 92.12% compared to P&O based schemes.

(8) The IARV and SSM-PSO schemes are employed in the proposed system, it is noted that the proposed system is able to display the lower inter-harmonic content compared to P&O based system.

(9) It is observed that the proposed system displays the reduced average inter-harmonic content of 32.19% compared to P&O scheme.

(10) As a future work, the solar panels under partial shading situation can be considered in the HRES.

Related publication:

- **BSV Sai**, D. Chatterjee, "An Improved MPPT Technique for Grid Integration of Hybrid Photovoltaic-Battery- DFIG based WECS," **Elsevier**, 2022. (Submitted to journal)

References:

[6.1] Gajewski, P and Krzysztof, P, "Control of the Hybrid Renewable Energy System with Wind Turbine," Photovoltaic Panels and Battery Energy Storage. Energies 2021, 14, 1595.

[6.2] G. B. Arjun Kumar and Shivashankar, "Optimal power point tracking of solar and wind energy in a hybrid wind solar energy system," International Journal of Energy and Environmental Engineering, 2021.

[6.3] Can Wan, Weiting Qian, Changfei Zhao, Yonghua Song and Guangya Yang, "Probabilistic Forecasting Based Sizing and Control of Hybrid Energy Storage for Wind Power Smoothing," IEEE transactions on sustainable energy, vol. 12, no. 4, october 2021.

[6.4] Unnikrishnan Raveendran Nair, Monika Sandelic, Ariya Sangwongwanich, Tomislav, D, IEEE, Ramon Costa-Castelló and Frede Blaabjerg, "Grid Congestion Mitigation and Battery Degradation

Minimisation Using Model Predictive Control in PV-Based Microgrid," IEEE transactions on energy conversion, vol. 36, no. 2, June, 2021.

[6.5] Pranoy Roy, Jiangbiao He, Tiefu Zhao and Yash Veer Singh, "Recent Advances of Wind-Solar Hybrid Renewable Energy Systems for Power Generation: A Review," IEEE open journal of the industrial electronics society, 2022.

[6.6] Boualam Benlahbib, Noureddine Bouarroudj, Saad Mekhilef, Dahbi Abdeldjalil, Thameur Abdelkrim, Farid Bouchafaa and Abelkader lakhdari, "Experimental investigation of power management and control of a PV/wind/fuel cell/battery hybrid energy system microgrid," international journal of hydrogen energy,45, 2020, 2911-29122.

[6.7] Rashid Al Badwawi, Mohammad Abusara and Tapas Mallick, "A Review of Hybrid Solar PV and Wind Energy System, Smart Science," 2015, 3:3, 127-138,

[6.8] Mohamed, H.A., Khattab, H.A., Mobarka, A., Morsy, G.A., "Design, control and performance analysis of DC-DC boost converter for stand-alone PV system," In Proceedings of the 2016 Eighteenth International Middle East Power Systems Conference (MEPCON), Cairo, Egypt, 27–29 December 2016; pp. 101–106.

[6.9] Liyong, Y.; Peie, Y.; Zhenguo, C.; Zhigang, C.; Zhengxi, L, "A novel control strategy of power converter used to direct driven permanent magnet wind power generation system," In Proceedings of the 2009 2nd International Conference on Power Electronics and Intelligent Transportation System (PEITS), Shenzhen, China, 19–20 December 2009; Volume 1, pp. 456–459.

[6.10] Villalva, M.G.; Gazoli, J.R.; Filho, E.R, "Comprehensive approach to modelling and simulation of photovoltaic arrays," IEEE Trans. Power Electron. 2009, 24, 1198–1208.

[6.11] O. Llerena-Pizarro, N. Proenza-Perez, C. Tuna and J. Luz, "A PSO-BPSO Technique for Hybrid Power Generation System Sizing," IEEE Latin America Transactions, Vol. 18, No. 8, August 2020.

[6.12] Jon Martinez-Rico, Ekaitz Zulueta, Ismael Ruiz de Argandoña, Unai Fernandez-Gamiz and Mikel Armendia, "Multi-objective Optimization of Production Scheduling Using Particle Swarm Optimization Algorithm for Hybrid Renewable Power Plants with Battery Energy Storage System," Journal of Modern Power Systems and Clean Energy, Vol. 9, No. 2, March 2021.

[6.13] Jonglak Pahasa and Issarachai Ngamroo, "Two-Stage Optimization Based on SOC Control of SMES Installed in Hybrid Wind/PV System for Stabilizing Voltage and Power Fluctuations," IEEE Transactions On Applied Superconductivity, Vol. 31, No. 8, November 2021.

[6.14] Kumar D and Tewary T., "Techno-economic assessment and optimization of a standalone residential hybrid energy system for sustainable energy utilization," Int J Energy Res. 2021;1–20.

[6.15] Tingna Shi1, Haitian Lu, Yanfei Cao, Xinmin Li, Changliang Xia, "Supercapacitor/battery hybrid energy storage unit for brushless DC motor operation," IET Electr. Power Appl., 2020, Vol. 14 Iss. 4, pp. 597-604.

[6.16] Tareq Salameh, Mohammad Ali Abdelkareem, A.G. Olabi, Enas Taha Sayed, Monadhil Al-Chaderchi and Hegazy Rezk, "Integrated standalone hybrid solar PV, fuel cell and diesel generator power system for battery or supercapacitor storage systems in Khorfakkan, United Arab Emirates," international journal of hydrogen energy, 46, 2021, 6014-6027.

[6.17] Juma, M.I., Mwinyiwiwa, B.M.M. Msigwa, C.J and Mushi, A.T., "Design of a Hybrid Energy System with Energy Storage for Standalone DC Microgrid Application," Energies, 2021, 14, 5994.

[6.18] Soufiane Marmouh, Mohamed Boutoubat and Lakhdar Mokrani, "Performance and power quality improvement based on DC-bus voltage regulation of a stand-alone hybrid energy system," Electric Power Systems Research 163 (2018) 73–84.

[6.19] Jamiu O. Oladigbolu, Yusuf A. Al-Turki and Lanre Olatomiwa, "Comparative study and sensitivity analysis of a standalone hybrid energy system for electrification of rural healthcare facility in Nigeria," Alexandria Engineering Journal (2021) 60, 5547–5565.

[6.20] Sudip Bhattacharyya, S. Puchalapalli and Bhim Singh, "Operation of Grid Connected PV-Battery-Wind Driven DFIG Based System," IEEE Transactions on Industry Applications, 2022.

[6.21] Simone Vanti, Prabhat Ranjan Bana, Salvatore D'Arco and Mohammad Amin, "Single-Stage Grid-Connected PV System with Finite Control Set Model Predictive Control and an Improved Maximum Power Point Tracking," IEEE Transactions on Sustainable Energy, Vol. 13, No. 2, April 2022.

[6.22] Priyadarshi N, Padmanaban S, Bhaskar MS, Blaabjerg F and Holm-Nielsen JB, "An improved hybrid PV-wind power system with MPPT for water pumping applications," Int Trans Electr Energ Syst. 2020, 30, e12210.

[6.23] Ratnakar Babu Bollipo, Suresh Mikkili, and Praveen Kumar Bonthagorla, "Hybrid, Optimal, Intelligent and Classical PV MPPT Techniques: A Review," CSEE Journal of Power and Energy Systems, Vol. 7, No. 1, January 2021.

[6.24] Ariya Sangwongwanich, Yongheng Yang, Dezso Sera, Hamid Soltani, and Frede Blaabjerg, "Analysis and Modeling of Interharmonics From Grid-Connected Photovoltaic Systems," IEEE Transactions on Power Electronics, Vol. 33, No. 10, October 2018.

[6.25] M.A. Danandeh and S.M. Mousavi G, "Comparative and comprehensive review of maximum power point tracking methods for PV cells," Renewable and Sustainable Energy Reviews, Vol. 82, Part 3, Feb. 2018, Pages 2743-2767.

[6.26] Mingxuan Mao, Lichuang Cui, Qianjin Zhang, Ke Guo, Lin Zhou and Han Huang, "Classification and summarization of solar photovoltaic MPPT techniques: A review based on traditional and intelligent control strategies," Energy Reports Volume 6, Nov. 2020, Pages 1312-1327.

[6.27] Hafsa Abouadane, Abderrahim Fakkar, Dezso Sera, Abderezak Lashab, Sergiu Spataru and Tamas Kerekes, "Multiple-Power-Sample Based P&O MPPT for Fast-Changing Irradiance

Conditions for a Simple Implementation," IEEE Journal of Photovoltaics, Vol.10, Iss. 5, Sept. 2020.

[6.28] Shun-Chung Wang, Hung-Yu Pai, Guan-Jhu Chen, and Yi-Hwa Liu, "A Fast and Efficient Maximum Power Tracking Combining Simplified State Estimation with Adaptive Perturb and Observe," IEEE Access, Vol. 8, 2020.

[6.29] Muralidhar Killi and Susovon samanta, "Modified Perturb and Observe MPPT Algorithm for Drift Avoidance in Photovoltaic Systems," IEEE Tans. Ind. Electron, VOL. 62, NO. 9, Sep.2015.

[6.30] Vibhu Jately, Somesh Bhattacharya, Brian Azzopardi, Antoine Montgareuil, Jyoti Joshi, and Sudha Arora, "Voltage and Current Reference Based MPPT Under Rapidly Changing Irradiance and Load Resistance," IEEE Trans. On Energy Conv., Vol. 36, No. 3, Sept. 2021.

[6.31] Shengqing, L., Fujun, L., Jian, Z. et al., "An improved MPPT control strategy based on incremental conductance method," Soft Comput 24, 6039–6046, 2020.

[6.32] Mohamed Lasheen, Ali Kamel Abdel Rahman, Mazen Abdel-Salam and Shinichi Ookawara, "Adaptive reference voltage-based MPPT technique for PV application," IET Renew, Power Gener., 2017, Vol. 11 lss. 5, PP. 715-722.

[6.33] Ariya Sangwongwonich, Yongheng Yang, Dezso sera, Hamid Soltni and Frede Blaabjerg, "Interharmonics from grid connected PV systems: Mechanism and Mitigation," IEEE 3rd international future energy electronics conference and ECCE Asia (IFEEC 2017-ECCE).

[6.34] Ariya Sangwongwonich and Frede Blaabjerg, "Mitigation of Interharmonics in PV Systems with Maximum Power Point Tracking Modification," IEEE Trans. Power electron, VOL.34, NO. 9, 2019.

[6.35] Nishad Mendis, Kashem M. Muttaqi, Saad Sayeef and Sarath Perera, "Standalone Operation of Wind Turbine-Based Variable Speed Generators with Maximum Power Extraction Capability," IEEE Trans. Energy Convers., Vol. 27, No. 4, Dec.2012.

[6.36] Mousa HHH, Youssef A-R, Mohamed EEM, "Study of robust adaptive step-sizes P&O MPPT algorithm for high-inertia WT with direct-driven multiphase PMSG," Int Trans Electr Energ Syst., 2019, 29: e12090.

[6.37] Ali Darvish Falehi, "An innovative optimal RPO-FOSMC based on multi-objective grasshopper optimization algorithm for DFIG-based wind turbine to augment MPPT and FRT capabilities," Chaos, Solitons and Fractals 130, 2020, 109407.

[6.38] Abdel-Raheem Youssef, Ahmed I.M. Ali, Mahmoud S.R. Saeed and Essam E.M. Mohamed, "Advanced multi-sector P&O maximum power point tracking technique for wind energy conversion system," Electrical Power and Energy Systems, 107, 2019, 89–97.

[6.39] Jie Wang and Didi Bo, "Adaptive fixed-time sensorless maximum power point tracking control scheme for DFIG wind energy conversion system," Int J Electr Power Energy Syst., 135, 2022, 107424.

[6.40] Bo Yang, Xiaoshun Zhang, Tao Yu, Hongchun Shu and Zihao Fang, "Grouped grey wolf optimizer for maximum power point tracking of doubly-fed induction generator based wind turbine," Energy Conversion and Management, 133, 2017, 427–443.

[6.41] Kunlun Han, Tianwei Huang and Linfei Yin, "Quantum parallel multi-layer Monte Carlo optimization algorithm for controller parameters optimization of doubly-fed induction generator-based wind turbines," Applied Soft Computing, 112, 2021, 107813.

[6.42] Ahmed Fathy, Abdullah G. Alharbi, Sulaiman Alshammari and Hany M. Hasanien, "Archimedes optimization algorithm based maximum power point tracker for wind energy generation system," Ain Shams Engineering Journal, 2021.

[6.43] Jeroen D.M. De Kooning, Arash E. Samani, Simon De Zutter, Jeroen De Maeyer and Lieven Vandevelde, "Techno-economic optimisation of small wind turbines using co-design on a parametrised model," Sustainable Energy Technologies and Assessments, 45, 2021.

[6.44] Mohammad Mahdi Rezaei, "A nonlinear maximum power point tracking technique for DFIG-based wind energy conversion systems," Engineering Science and Technology, an International Journal, 21, 2018, 901–908.

[6.45] Ganesh P. Prajapat, N. Senroy and I.N. Kar, "Estimation based enhanced maximum energy extraction scheme for DFIG-wind turbine systems," Sustainable Energy, Grids and Networks, 26, 2021, 100419.

[6.46] Yuliang Sun, Shaomin Yan, Bin Cai, YuqiangWu and Zhongcai Zhang, "MPPT Adaptive Controller of DC-based DFIG in Resistances Uncertainty," International Journal of Control, Automation and Systems, 19(8), 2021, 2734-2746.

[6.47] James Kennedy and Russell Eberhart, "Particle Swarm Optimization," IEEE, 1995.

[6.48] Salmi Hassan, Badri Abdelmajid, Zegrari Mourad, Sahel Aicha and Baghdad Abdennaceur, "PSO-Backstepping controller of a grid connected DFIG based wind turbine," International Journal of Electrical and Computer Engineering (IJECE), Vol. 10, No. 1, Feb. 2020, pp. 856-867.

[6.49] Kashif Ishaque, Zainal Salam, Muhammad Amjad, and Saad Mekhilef, "An Improved Particle Swarm Optimization (PSO)–Based MPPT for PV With Reduced Steady-State Oscillation," IEEE Trans. Power Electron., Vol. 27, No. 8, Aug. 2012.

[6.50] Kinattingal Sundareswaran, Peddapati Sankar, P. S. R. Nayak, Sishaj P. Simon, and Sankaran Palani, "Enhanced Energy Output from a PV System Under Partial Shaded Conditions Through Artificial Bee Colony," IEEE Trans. Sustain. Energy, Vol. 6, No. 1, Jan. 2015.

[6.51] P.K. Gayen, D. Chatterjee and S.K. Goswami, "Stator side active and reactive power control with improved rotor position and speed estimator of a grid connected DFIG (doubly-fed induction generator)," Energy (2015) 461-472.

CONCLUSION AND FUTURE WORK

In this research work, different MPPT schemes are developed to improve the dynamic characteristics of the PV and wind systems. The outcomes of the individual proposed schemes are displayed below.

(Chapter.2) The proposed INHARE MPPT scheme displays better tracking efficiency comparing to CV MPPT under lower irradiation levels. Also, it displays interharmonic-elimination similar to that of CV MPPT. Also, compared to P&O-based MPPT schemes, the proposed INHARE MPPT scheme displays effective interharmonic elimination irrespective of the step up/down changes with different voltage steps and sampling frequency changes.

(Chapter.3) The proposed improved WA-P&O scheme has improved characteristics over existing commonly used P&O based MPPT schemes in terms of lower settling time, negligible steady state error and avoidance of drift under sudden change in irradiation. Moreover, the adaptive PI controller mechanism improves the overall dynamics characteristics compared to existing schemes. In this research work an improved WA-P&O scheme is suggested to avoid the disadvantages of existing conventional MPPT algorithms. As a future work, the proposed WA-P&O scheme can be applied for any complex series-parallel configuration of PV panels to justify its usefulness.

(Chapter.4) **A.** The proposed dummy peak elimination based MPPT introduced can compute all the nearest points to the power peaks of the cascaded PV panel configuration under PS condition. The dummy peaks are cancelled and the point nearest to the global peak is estimated, which becomes the start point for P&O. The Proposed DPE MPPT has low computational requirement for the processor with very good dynamic properties. Due to the absence of metaheuristic methods in the proposed algorithm it is easier to implement with processors having low computational facility and thus can be cost-effective.

B. In this work, a fast-global peak estimation based MPPT scheme has been implemented for tracking global maximum under PS situation. The proposed FGPE technique has the major advantage of low complexity in real time implementation. Moreover, proposed scheme is faster responsive compared to exiting EA-P&O algorithm, since it does not require any scanning in tracking global MPP. In this proposed work, a fast-global peak estimation based MPPT method is presented, which is able to address the series parallel configuration of any nature. It has the dynamic characteristics similar to that of DPE MPPT scheme.

C. In this work, a slope based accurate MPPT scheme has been implemented for tracking global maximum under PS situation. The proposed SB technique has the major advantage of low complexity in real time implementation. Moreover, the proposed scheme is faster responsive compared to exiting EA-P&O algorithm, since it does not require any scanning in tracking global MPP. In this research work, the DFIG, PV and BES are operated collectively to supply the reliable power to grid. Also, the proposed system is operated with proposed MPPT schemes for PV and WECS in generating improved dynamic characteristics. Further, the proposed MPPT schemes are operated to reduce the injection of inter-harmonics into the grid.

(Chapter.5) The SSM-PSO scheme has been introduced to avoid the disadvantages of PSO. In the proposed system, an anemometer has been employed to decide the space for placing particles in tracking MPP. The SSM-PSO scheme is successful in minimizing the searching space, leading to lesser MPP tracking time. Also, the proposed SSM-PSO leads to the lesser oscillation over steady state. Moreover, the proposed SSM-PSO scheme is easily implementable due to its simple searching mechanism.

(Chapter.6) In this research work, the DFIG, PV and BES are operated collectively to supply the reliable power to grid. Also, the proposed system is operated with proposed MPPT schemes for PV and WECS in generating improved dynamic characteristics. Further, the proposed MPPT schemes are operated to reduce the injection of inter-harmonics into the grid.

Coming to the future work, MPPT schemes must be developed for more complex series-parallel PV systems. Also, the usage of number of sensors for wind and PV MPPT cases must be reduced. In case of hybrid energy generation, the partial shading case of PV system must be considered as an improvement.